SOIL-PILE, PILE GROUP FOUNDATIONS AND PIPELINE SYSTEMS INTERACTION BEHAVIOR EXTENDING SATURATED AND UNSATURATED SOIL MECHANICS

MOHAMMED AL-KHAZAALI

A thesis submitted in partial fulfillment of the requirements for the
Doctorate in Philosophy degree in Civil Engineering

Department of Civil Engineering
Faculty of Engineering
University of Ottawa

ABSTRACT

Rapid growth in population along with positive trends in global economy over the past several decades has significantly contributed to an increased demand for various infrastructure needs worldwide. For this reason, the focus of this thesis has been directed towards extending the mechanics of unsaturated soils, which is an emerging geotechnical engineering field to investigate the behavior of two key infrastructure systems, namely pile foundations and energy pipeline systems. The mechanism of soil-pile foundations and soil-pipeline systems interaction behavior has several similarities.

Both these infrastructure facilities require comprehensive understanding of the soil-structure interaction mechanism. Reliable estimation of mechanical properties of both the soil and the soil-structure interface is required for the rational interpretation the load-displacement behavior of pile foundations and pipeline systems. Currently, the design of systems is predominantly based on design codes and guidelines that use empirical procedures or employ the principles of saturated soil mechanics. In many scenarios, pile foundations extend either totally or partly in unsaturated soils as the groundwater table level in many regions is at a greater depth. Such scenarios are commonly encountered in semi-arid and arid regions of the world. In addition, pipeline systems are typically buried at shallow depths in unsaturated soil strata, which are susceptible to wetting and drying, freezing and thawing cycles or both, due to seasonal environmental changes. Capillary stress or matric suction in the unsaturated zone increases the effective stress contribution towards the shear strength and stiffness of soil and soil-structure interface. Extending saturated soil mechanics to design or analyze such structures may lead to erroneous estimation of pile foundation carrying capacity or loads transferred on pipeline body from the surrounding unsaturated soil.

Experimental, analytical and numerical investigations were undertaken to study the behavior of single pile, pile group, and pipeline systems in saturated and unsaturated sands under static loading. The experimental program includes 40 single model pile and 2×2 pile group, and six prototype pipeline tests under saturated and unsaturated condition. The results of the experimental studies suggest that matric suction has significant contribution towards the mechanical behavior of both pile foundation and pipeline system.

The axial load carrying capacity of single pile and pile group increased approximately 2 to 2.5 times and the settlement reduced significantly compared to saturated condition. The influence of matric suction towards a single pile is significantly different in comparison to pile group behavior. The cumulative influence of matric suction and stress overlap of pile group behavior in sandy soils result in erroneous estimation of pile group capacity, if principles of saturated soil mechanics are extended. Group action plays major role in changing the moisture regime under the pile group leading to incompatible stress state condition in comparison to single pile behavior.

On the other hand, the peak axial load on the pipe is almost 2.5 folds greater in unsaturated sand that undergoes much less displacement in comparison to saturated condition. Such an increase in the external axial forces may jeopardize the integrity of energy pipeline systems and requires careful reevaluation of existing design models extending the principles of unsaturated soil mechanics. Two analytical design models to estimate the axial force exerted on pipeline body were proposed. The proposed models take account of matric suction effect and soil dilatancy and provide smooth transition from unsaturated to saturated condition. These models were developed since measurement of the unsaturated soil and interface shear strength and stiffness properties need extensive equipment that require services of trained professional, which are expensive and time consuming. The models utilize the saturated soil shear strength parameters and soil-water characteristic curve (SWCC) to predict the mechanical behavior of the structure in saturated and unsaturated cohesionless soils. The prototype pipeline experimental results were used to verify the proposed models. The predicted axial force on pipeline using the proposed models agrees well with the measured behavior under both saturated and unsaturated conditions.

Moreover, numerical techniques were proposed to investigate the behavior of pile foundation and pipeline system in saturated and unsaturated sand. The proposed methodology can be used with different commercially available software programs. Two finite element analysis programs were used in this study; namely, PLAXIS 2D (2012) to simulate soil-pile foundation behavior and SIGMA/W (2012) to simulate soil-pipeline system behavior. The proposed techniques require the information of unsaturated shear strength and stiffness, which can be derived from saturated soil properties and the SWCC. The model was verified using pile and pipeline test results from this study and other research studies from the published literature. There is a good agreement between the measured behavior and the predicted behavior for both the saturated and unsaturated conditions. The methodology was further extended to investigate the

behavior of rigid and flexible pipelines buried in Indian Head till (IHT) during nearby soil excavation activity. The simulation results suggest that excavation can be extended safely without excessive deformation to several meters without the need for supporting system under unsaturated condition.

The studies summarized in the thesis provide evidence that the principles of saturated soil mechanics underestimate the pile foundations carrying capacity as well as the axial force exerted on pipelines in unsaturated soils. Such approaches lead to both uneconomical pile foundation and unsafe pipeline systems designs. For this reason, the pile and pile group carrying capacity and pipeline axial force should be estimated taking into account the influence of matric suction as well as the dilatancy of the compacted sand. The experimental studies, testing techniques along with the analyses of test results and the proposed analytical and numerical models are useful for better understanding the pile foundation and buried pipeline behaviors under both saturated and unsaturated conditions. The proposed analytical and finite element models are promising for applying the mechanics of unsaturated soils into conventional geotechnical engineering practice using simple methods.

DEDICATION

To my beloved family, the soul of my father Abdulzahra Al-Khazaali, the soul of my mother Ibtisam Hagoug, wife Zaman and children, Hasan, Ahmed and Batool.

ACKNOWLEDGMENTS

Research studies presented in this dissertation were perform at the Department of Civil Engineering at the University of Ottawa under the supervision of Prof. Sai K. Vanapalli. I would like to express my deepest gratitude and appreciation to Dr. Vanapalli for his continuous encouragement, guidance and supports throughout the course of my Ph.D. research study. I am honored and am proud for that Dr. Vanapalli is not only my supervisor, but also a lifetime truthful friend.

My sincere gratitude is also extended to the evaluation committee members of my Ph.D. thesis, Dr. Gerald A. Miller (University of Oklahoma), Dr. Mohammad Rayhani (Carleton University), Dr. Magdi Mohareb (University of Ottawa), and Dr. Jules-Angel Infante Sedano (University of Ottawa), for their time and valuable comments that helped improving this dissertation.

I gratefully express my appreciation to the Iraqi Ministry of Higher Education and Scientific Research for funding my Ph.D. research program.

My appreciations extend to my colleagues at the University of Ottawa for their friendship, company and support. They include; Muslim Majeed, Imad Alainachi, Zhong, Celestin, Mohammad Hyder, Won, Shunchao, Yunlong, Ping, Hongyu, Junping, Penghai, Jiaying, Xiuhan, Xiaokun, N'eem, Mohammad Salah. Special thanks go to Dr. Mohammed Fattah, Professor at University of Technology, and Mr. Saad Noori, Associated Professor at University of Technology, Iraq for their kind help and support throughout the course of my Ph.D. research study.

I am extremely thankful for my family, who supported me wholeheartedly and selfishly through turbulent times and calm, through creative periods and fallow. This accomplishment would not have been possible without their love, support and inspiration. I humbly dedicate this thesis to my family, Abdulzahra, Ibtisam, Zaman, Hasan, Ahmed and Batool.

LIST OF CONTENTS

LIST OF FIGURES

CHAPTER ONE

INTRODUCTION

1.1 Background

Rapid growth in world population, in addition to improved overall global economy over the past few decades has contributed to a significant increase in the urbanization of many countries. This growth has a significant impact in construction of new or expanding the existing civil infrastructure systems to meet the increased needs. Some of key infrastructure systems include pile foundations and energy pipeline systems. Piles are widely used foundations because of its excellent performance in different types of soils carrying loads from superstructures safely and alleviating settlement or heave associated problems. Pipeline systems, on the other hand, is a lifeline network that is constructed using different kinds of materials which include polyethylene, plastic, reinforced concrete or steel pipes to collect, transport, and distribute vital energy resources.

Most of the standards, design codes, guidelines extend the limit state approaches to assure safety and serviceability of structures (Allen 1975). The widely used limit state approaches are classified into two categories: Ultimate Limit States (ULS) and Serviceability Limit States (SLS). Meyerhof (1995) listed the problems associated with soil stability and elasticity, respectively, under ULS and SLS. The ULS takes into account of safety considering factors such as collapse due to crushing, buckling, yielding, instability including the fracture. The SLS takes account of functional performance and behavior under load including excessive deflection, vibration, cracking, permanent deformation, and corrosion (Allen 1975, Griffis 1993). Canadian Foundation Engineering Manual (2006) utilizes the limit state approaches and recommended that foundation design should satisfy two requirements; i) to be able to support the superstructure and carry the applied loads safely (i.e. ULS), and ii) to prevent excessive settlement of the structure (i.e. SLS). The key parameters that control the soil-structure mechanical behavior (i.e. stability and serviceability) under static loads are the soil and interface shear strength, τ and modulus of elasticity, E.

Shear strength parameters (i.e. cohesion, c, and angle of internal friction, ϕ) and E are conventionally determined using triaxial or direct shear testing equipment. Typical stress-strain relationship of soil in conventional triaxial test is shown in Figure (1.1). The E is defined as the ratio of the deviator stress to the corresponding axial strain, ε_a. Three moduli of elasticity can be recognized from this figure; namely, the initial modulus of elasticity, E_0, secant modulus, E_{50}, and unloading/reloading modulus, E_{ur}. These moduli control the elastic behavior of the soil under different loading stages.

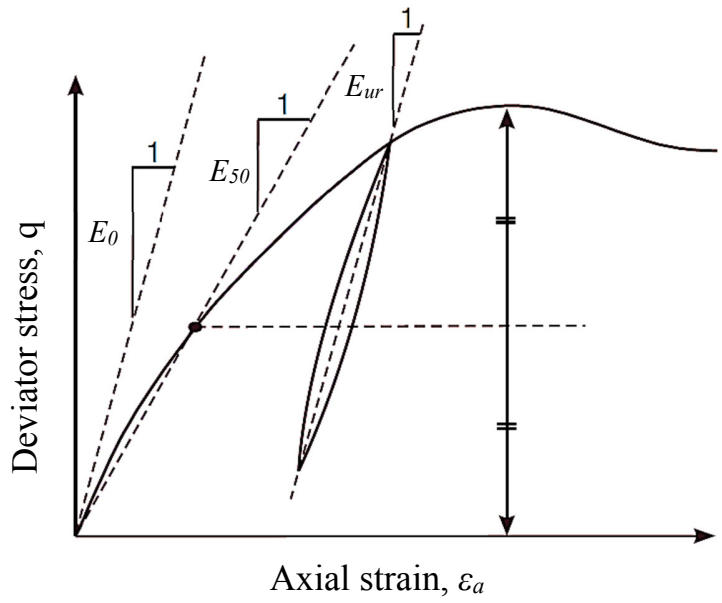

Figure 1.1 Typical stress-strain behavior in triaxial test (modified after Schanz et al. 1999).

Pile foundation usually consists of a group of piles that are joined at the head with a pile cap. The purpose of the pile cap is to ensure uniform load distribution on the piles and uniform settlement of the structure. The maximum pile group capacity is widely determined as: i) a ratio of the summation of individual piles capacities in the group, or ii) block failure, whichever is the lower. The maximum pile capacity consists of the summation of two parts, the shaft and the end bearing resistance. The load carrying contribution is derived majorly from shaft resistance in cohesive soils. However, the end bearing resistance predominantly contributes to load carrying capacity of pile foundations in coarse-grained soils. The mechanical behavior of single pile and

pile group foundation is highly dependent on soil type and condition, which is discussed in Chapter Two.

Typical load-settlement, $P - \delta$ behavior of a pile foundation consists of two zones; elastic and plastic zones of loading. In the elastic zone of loading, deformation or settlement is recoverable and the soil-pile behavior is governed by the soil stiffness. Poulos (1989) stated that pile settlement is governed by: i) the ratio of the modulus of elasticity of the pile section, E_P to modulus of elasticity of the soil, E, ii) the ratio of modulus of elasticity of the bearing stratum, E_b to modulus of elasticity of the soil, E, and iii) the pile length to diameter ratio L/d. However, pile stiffness is relatively high in comparison to soil stiffness. Therefore, in a homogeneous soil layer, modulus of elasticity of the soil, E would be the major factor that controls the elastic settlement of pile foundations. Once the soil is loaded, soil stiffness decreases and irreversible plastic strains start developing (Schanz et al. 1999) and the $P - \delta$ behavior of pile moves to plastic zone of loading. In this zone, the $P - \delta$ is governed by the soil shear strength (i.e. c, ϕ, and dilation angle, ψ) (Potts and Zdravković 2001) and the peak or maximum carrying capacity is mobilized. Figure 1.2 shows the effect of varying the initial modulus of elasticity and shear strength parameters on pile foundation behavior.

The study also investigates soil-pipeline interaction extending both saturated and unsaturated soil mechanics. Pipeline systems are usually buried at shallow depth and subjected to variety of external loads such as construction, traffic loading, earthquake, trenching and soil subsidence (Ng, 1994). These loads exert shear and normal stresses on the pipeline body, induce internal forces (i.e. internal axial, F_A and shear, F_V force and bending moment, M (Figure 1.3)) and can cause excessive damages to the pipeline. Failure of pipeline systems can lead to loss of expensive resources such as gas or oil due to leaking; in addition, they can contribute to failures such as slopes, sink holes, and more importantly cause irreparable damages to the environment in certain scenarios.

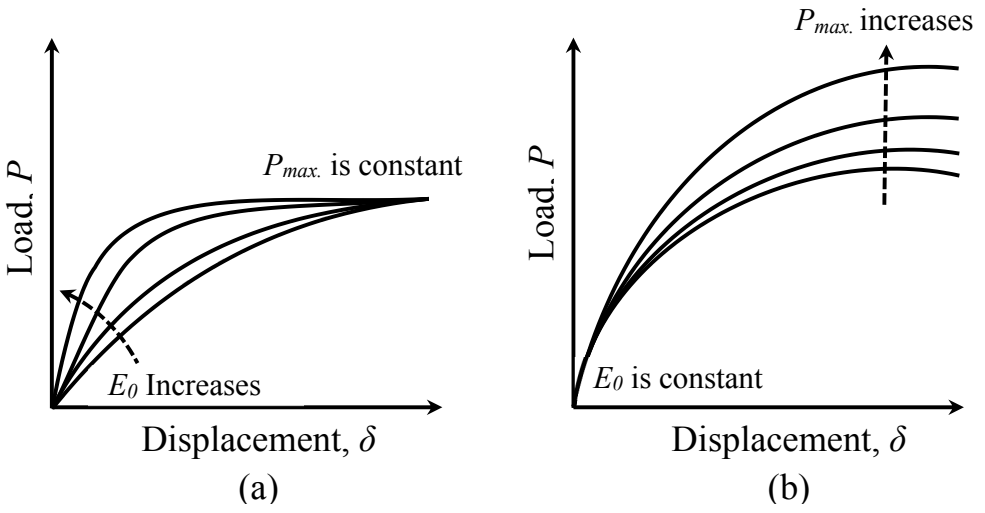

Figure 1.2 Variation of the load-settlement behavior of a pile foundation due to; (a) Varying of E_0, for the same shear strength parameters, and (b) Varying of shear strength parameters for the same E_0.

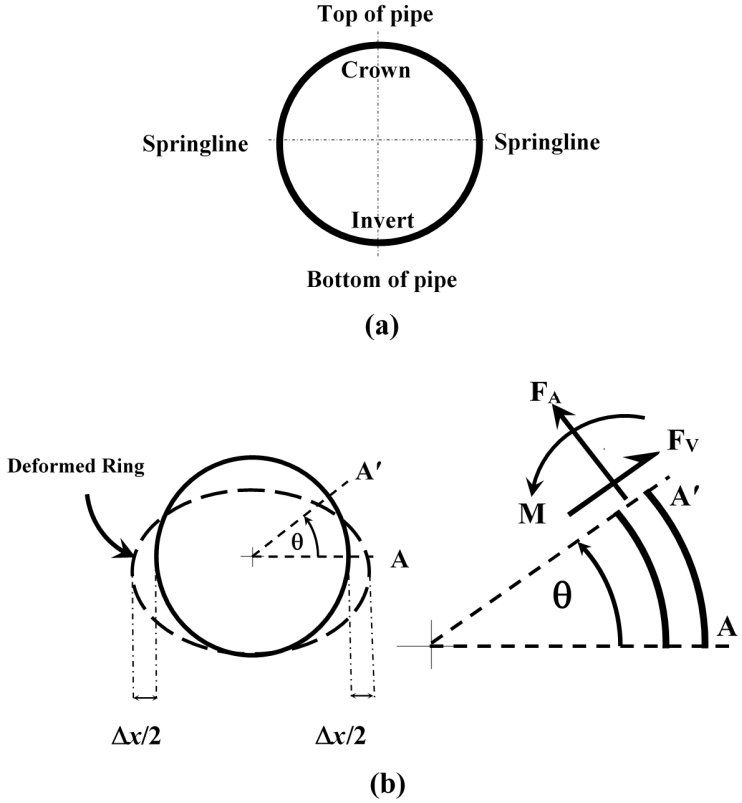

Figure 1.3 Pipeline hoop (a) Terminology as per ASTM F1668-08, and (b) Ring elastic deflection and internal forces.

Therefore, BS EN 14161:2003 (BSI, 2003) recommends that the minimum pipeline burial depth from the soil surface to the top of the pipeline shall not fall behind 0.8 to 1.2m to avoid any direct interference with human activities.

Rational design and analysis of soil-pipeline systems require comprehensive understanding of external (Figure 1.4) and internal stresses from traffic, soil overburden pressure, internal pressure of the transported fluid (i.e. gas, oil, and water), and pipeline material. Environmental factors such as freezing and thawing, drying and wetting cycles also have significant effects on the mechanical behavior of buried pipelines especially in the active zone (i.e. shallow depth 2-3 m), which is in many scenarios located above the groundwater table GWT (i.e. unsaturated zone).

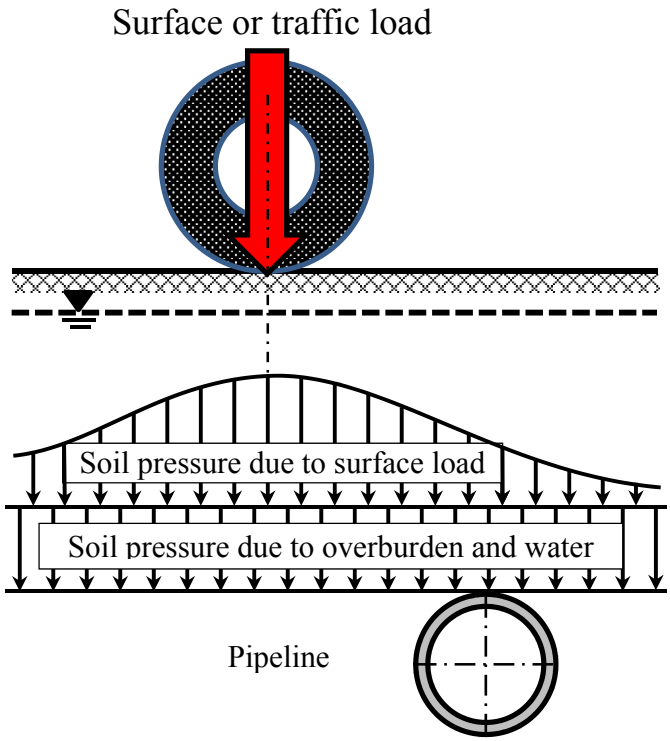

Figure 1.4 Vertical soil pressure due to surface loads and soil overburden and water pressures at the top of the pipe (modified after Watkins and Anderson 2000).

Design codes, guidelines and recommended practice procedure manuals extend principles of conventional soil mechanics in the design and analysis of subsurface structures (American Society of Civil Engineers (ASCE) 1984, ALA 2005, Indian Institute of Technology Kanpur

Guidelines for Seismic Design of Buried Pipelines (IITK-GSDMA) 2007, and Pipeline Research Council International (PRCI) 2009). The BS EN 1997-1:2004 (BSI, 2004) recommends that the most unfavorable groundwater condition that could occur during the design lifetime of the structure for ULS or in normal circumstances for SLS should be considered. In other words, the design and analysis assumptions should consider the GWT is at the natural ground surface and the soil is in a state of saturation condition. However, assuming the presence of GWT at the natural ground surface to satisfy conservative design requirements is not necessarily conservative.

Arid and semi-arid regions cover 66.5 million km^2 (Figure 1.5) (Achten et al. 2013) out of 135.2 million km^2 of the total land area available on our planet (Holmgren 2006). In these regions, the natural ground water table is typically at a greater depth because there is significant water evaporation in comparison to infiltration. Due to this reason, using the principles of saturated soil mechanics is not reliable for neither pile foundations nor pipeline systems, in these regions. The soils in these regions are typically in a state of unsaturated condition and hence their soil mechanical and the associated soil-structure interaction behaviors are significantly influenced by the capillary stress or matric suction, $(u_a - u_w)$ (Al-Khazaali and Vanapalli 2017). Georgiadis et al. (2003) numerically investigated the influence of the variation of groundwater table (GWT) depth on the behavior of pile foundation that is constructed totally or partially above GWT. From this study, they concluded that under a constant load, the settlement of the foundation is sensitive to the variation of GWT due to associated changes in $(u_a - u_w)$.

During the past six decades, the mechanical properties of unsaturated soils, such as the shear strength and stiffness, were interpreted considering the influences of soil suction and net normal stress (Bishop 1959, Burland 1964 and 1965, Fredlund et al. 1978, Edil et al. 1981, Wu et al. 1984, Alonso et al. 1990, Vanapalli et al. 1996, Khalili and Khabbaz 1998, Ng and Yung 2008, Hamid and Miller 2008 and 2009, Sawangsuriya et al. 2009, Khosravi and McCartney 2012, Oh and Vanapalli 2013, Lu and Kaya 2014, Hoyos et al. 2015). Therefore, both of the stress state variables, the matric suction and the net normal stress are essential for rational and reasonable interpretation and analysis of the mechanical behavior of soil-structure interaction problems in unsaturated soils.

Experimental and numerical research studies have been extensively undertaken to investigated the $P - \delta$ behavior of shallow and deep foundation in unsaturated soil during the last two decades

(Oloo et al. 1997, Georgiadis et al. 2003, Mohamed and Vanapalli 2006, Rojas et al 2007, Vanapalli and Mohamed 2007, Vanapalli et al 2007, Vanapalli et al 2010, Vanapalli and Taylan 2012, Wuttke et al. 2013, Sheikhtaheri 2014, Al-Khazaali and Vanapalli 2015, AL-Khazaali et al. 2016, Han et al.2016). Most of these studies related the $P - \delta$ behavior to soil-water characteristic curve (SWCC), which is defined as a relationship between the degree of saturation (S), gravimetric water content (w), or volumetric water content (θ) and soil suction. The studies suggest that matric suction significantly contributes to the carrying capacity of shallow and deep foundations and decrease the corresponding settlement. However, there are limited research studies addressed the pile group behavior in unsaturated soils to the best of the author's knowledge.

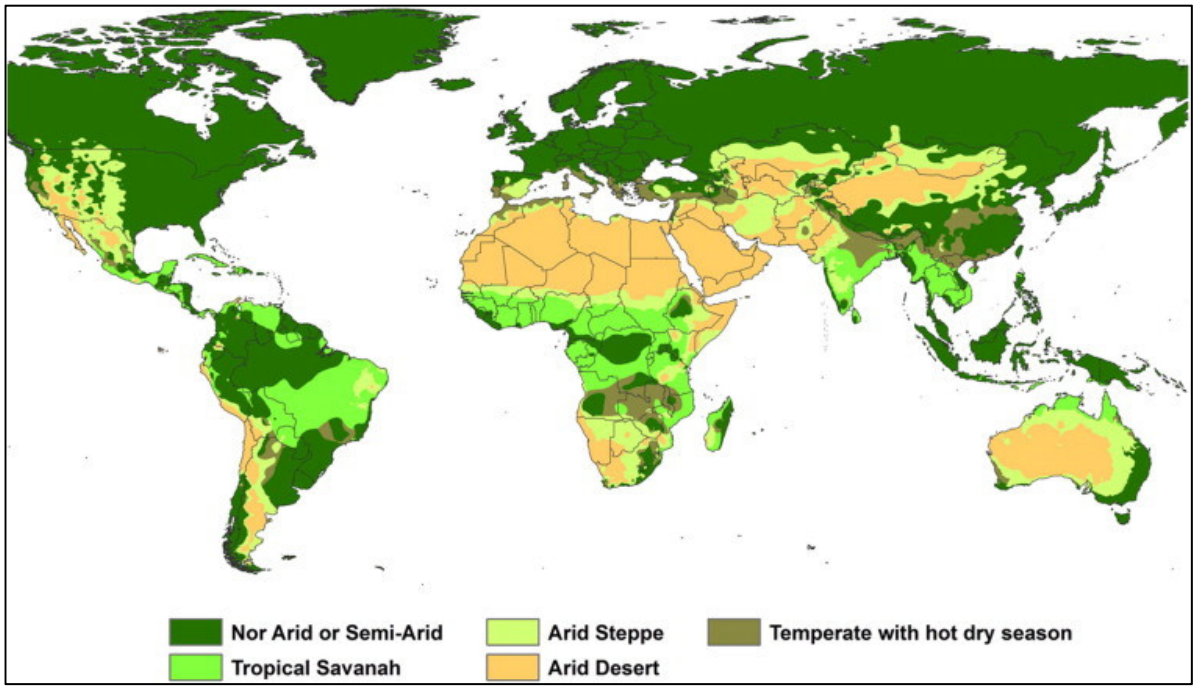

Figure 1.5 Map of globe climate zoning (modified after Achten et al. 2013).

On the other hand, limited research studies were devoted to understand the behavior of soil-pipeline system taking account of the influence of unsaturated condition; it is only in the recent decade there has been some interest (O'Rourke et al. 2008, Olson 2009, O'Rourke 2010, Jung et al. 2013, Saadeldin et al 2015, Robert et al. 2016). These studies have shown that the mechanical behavior of pipeline system in unsaturated soils is significantly influenced by the soil suction.

Pipeline systems buried in a typical unsaturated soil may experience higher stress and damages in comparison to a soil that is in a state of saturated condition (Al-Khazaali et al. 2016).

1.2 Key Objectives

This study aims at evaluation the mechanical behavior of pile, pile group and pipeline systems constructed in saturated and unsaturated soils. The study objectives are:

i) Developing a comprehensive experimental setup and standardized test methodology to investigate different soil-structure interaction problems under saturated and unsaturated conditions in coarse-grained soils. The setup and methodology should be able to produce different soil-matric suction profiles and create reliable saturated and unsaturated test conditions for coarse-grained soils.

ii) Evaluating the presently used design methods and provide a more generic pile foundation design procedure that can be extended for both saturated and unsaturated soils. More importantly, focus has been directed towards understating the cumulative influence of matric suction and stress overlap, and utilize this understanding in rational evaluation of pile group efficiency under unsaturated condition.

iii) Reassessing the available design procedures for pipeline systems and suggesting more comprehensive analytical design procedures extending both, saturated and unsaturated soil mechanics. The suggested analytical models take account of matric suction and dilation behavior of coarse-grained soils towards the mechanical behavior pipeline systems and provide smooth transition from unsaturated to saturated condition. Suggesting simple numerical modelling methodology extending the principles of saturated and unsaturated soil mechanics and utilizing the experimental results to validate the methodology. The proposed methodology utilizes the most widely used Mohr-Coulomb (MC) constitutive model that available in different commercial finite element software programs to encourage implementing unsaturated soil mechanics into conventional engineering practice.

1.3 Novelty

There are no published studies on comprehensive behavior of pile group in unsaturated soils to the best of the author's knowledge. The $P - \delta$ behavior of pile group foundation is significantly different if the influence of matric suction contribution is taken into account. In addition, pipeline studies have ignored or not duly acknowledged the close relationship between the soil-pipeline system behavior in unsaturated soils and the SWCC behavior.

Measuring reliable soil-structure system behavior requires comprehensive experimental program that consider and control important factors, which may contribute to the mechanical behavior. In this study, a comprehensive experimental setup able to duplicate different soil-matric suction profiles utilizing the hanging column technique is introduced. The system and test methodology can be used to investigate the behavior of different soil-structure interaction problems; for example: pile foundation, shallow foundation, pipeline system, soil nail, cone penetration, etc. in saturated and unsaturated condition. The setup was used to perform extensive experimental program with a total of six prototype pipeline axial force-displacement tests, and 40 single model pile and pile group load tests. The number of tests produced significant amount of data that can be used to develop mathematical, numerical, and analytical models extending the principles of unsaturated soil mechanics.

In addition, two semi-empirical models extending effective stress analysis to estimate the maximum and ultimate axial force exerted on pipeline of unsaturated sandy soil are introduced. The proposed model requires limited input data including the SWCC to predict the axial force in unsaturated soil. Interface effective angle of internal friction, δ' and dilation angle are required in addition to SWCC. The proposed model requires only one fitting parameter, which is found to be equal to 0.1 for coarse-grained soils. The proposed model was validated using results of experimental results from current study. The proposed model can be implemented in addressing geotechnical engineering problems.

Numerical analysis is considered as a valuable tool in conventional geotechnical engineering practice. One of most difficult tasks in numerical analysis is choosing a suitable constitutive model and obtaining the required input parameters. The parameters that are typically required in the numerical models include the unsaturated shear strength and stiffness; measurement

of these parameters is time consuming, expensive and requires elaborate testing equipment. Designers and practicing engineers typically prefer simple methods. Introducing complex parameters and variables such as soil suction will add more complexity to the conventionally followed design procedures in practice. For this reason, the present study aims to provide simple techniques to encourage the designers to use the principles of unsaturated soil mechanics into practice. The proposed numerical methodology utilizes the most widely used Mohr-Coulomb (MC) constitutive, which requires limited number of input parameters, to simulate unsaturated soil-structure behavior. The methodology utilizes the available features of PLAXIS 2D and SIGMA/W software to implement the unsaturated soil and interface parameters, which can be measured or derived from saturated parameters with the aid of SWCC. The proposed finite element techniques are validated using the experimental results from the present study and from other literature.

This study suggests that the combined effect of matric suction and stress overlap from adjacent piles can contribute to the complexity of the problem resulting in misleading estimation of group efficiency factor and hence the pile group capacity. In addition, erroneous results are likely if conventional soil mechanics principles are extended in the estimation of pile group capacity and group efficiency factor for unsaturated cohesionless soils. Such evidence highlight the need for rigorous interpretation of pile load tests results taking account of the influence of matric suction while evaluating pile group capacity and group efficiency factor in engineering practice for unsaturated sandy soils.

The comprehensive experimental model, analytical models, and numerical methodology are applicable in real practice and are promising to implement in design codes, guidelines and foundation design manuals.

1.4 Layout

This thesis is laid out in two parts: i) Part I is dedicated to understand the soil-pipeline system behavior using unsaturated soil mechanics and ii) Part II focuses on pile and pile group behavior extending the unsaturated soil mechanics.

- Chapter One presents the background, objective, novelty, and the layout of this thesis;

- Chapter Two includes literature review of the recent studies on pile foundation and soil-pipeline system in unsaturated soil;
- Chapter Three discusses a comprehensive experimental program to investigate axial force-displacement behavior of a rough surface prototype pipeline in saturated and unsaturated soil. In this chapter, the design of the test box and fabrication of the prototype pipe is presented. A simple numerical modelling methodology to investigate soil-structure interaction problems in saturated and unsaturated soil utilizing MC constitutive model and SWCC is introduced. The initial results of elastic axial force-displacement behavior of three tests were modeled using SIGMA/W software extending the principles of unsaturated soil mechanics;
- Chapter Four presents experimental results of six prototype pipeline axial force-displacement tests in saturated and unsaturated sand. Two analytical design models with one fitting parameter that take into account of matric suction and dilation behavior are introduced. Extensive discussion on dilation behavior of coarse-grained soils is summarized. In addition, theoretical formulation of the proposed models is presented along with justifications of choosing the used fitting parameter;
- Chapter Five discusses the deformations of soil-pipeline systems nearby unsupported trenches excavated in unsaturated Indian Head till (IHT) soil. The soil-pipeline system behavior is numerical investigated using SIGMA/W utilizing coupled effective stress analysis approach. In this chapter, the proposed numerical methodology was extended to investigate the behavior of buried pipeline in the proximity of unsupported excavation in saturated and unsaturated glacial till. Internal force in the pipe hope (i.e. shear force, axial force, and bending moment) were investigated and related to soil suction. Design charts are proposed to estimate the maximum allowable excavation depth based on maximum allowed deformation in pipeline as per several codes of practice;
- Chapter Six presents the fabrication and test results of two sets of model pile and 2×2 pile group. In this chapter, two approaches were considered in the design of the model piles utilizing previous recommendations available in the literature and numerical analysis using the commercial software PLAXIS 2D. The $P-\delta$ results of single model pile and 2×2 pile group foundation (smooth and rough surfaces) in coarse-grained soil under saturated and unsaturated conditions are presented and discussed. The influence of matric suction, soil dilatancy, and

group action on pile group behavior is evaluated extending the principles of saturated and unsaturated mechanics.

- Chapter Seven provides the summary and conclusions of the research undertaken in this thesis.

CHAPTER TWO

LITERATURE REVIEW

2.1 Introduction

Since the early 1900s, soil-structure interaction problems received significant attention from both research scholars and practicing engineers (Moser 2001). Soil-structure interaction is a field of study that comprehensively involves soil and structural mechanics, soil and structural dynamics, earthquake engineering, geophysics and geomechanics, material science, and computational and numerical methods to interpret the soil-structure system behavior (Kausel 2010). Pile foundations and pipeline systems, which are the focus of investigation in the present thesis, are typical geotechnical infrastructure that require fundamental understanding of the hydro-mechanical behavior of the soil as well as the structure.

Typically, in semi-arid and arid regions and in certain other regions of the world, the groundwater table (GWT) is at a greater depth and the soil above is in a state of unsaturated condition. The capillary zone above the groundwater table has been found to significantly influence the underground structures such as the shallow and deep foundations (Oloo et al. 1997, Georgiadis et al. 2003, Mohamed and Vanapalli 2006, Rojas et al 2007, Vanapalli and Mohamed 2007, Vanapalli et al 2007, Vanapalli et al 2010, Vanapalli and Taylan 2012, Wuttke et al. 2013, Sheikhtaheri 2014, Han et al.2016). Capillary stress or matric suction in the unsaturated zone contributes to the shear strength and stiffness of soil and soil-structure interface. Reliable estimation of the mechanical behavior of unsaturated soils can be achieved by extending the principles of unsaturated soils mechanics (Bishop 1959, Burland 1964 and 1965, Fredlund et al. 1978, Edil et al. 1981, Wu et al. 1984, Alonso et al. 1990, Vanapalli et al. 1996, Khalili and Khabbaz 1998, Ng and Yung 2008, Hamid and Miller 2008 and 2009, Sawangsuriya et al. 2009, Khosravi and McCartney 2012, Oh and Vanapalli 2013, Lu and Kaya 2014, Hoyos et al. 2015). In this chapter, the key concepts of unsaturated soils that are useful for the interpretation of pile foundations and pipeline systems are succinctly reviewed.

2.2 Unsaturated Soils

2.2.1 Stress State Variables for Interpretation of Unsaturated Soils Behavior

Conventional soil mechanics principles are typically extended in geotechnical engineering practice for interpretation of saturated soils and fully dry soils (i.e. two phase material, solid and water or air) using effective stress, ($\sigma - u_w$) concept, which is the stress differential between the total stress, σ and pore-water pressure, u_w. The effective stress concept introduced by Terzaghi (1925 and 1936) can be considered to be a single stress state variable that has been successfully used in the interpretation of the mechanical behavior (i.e. volume change and shear strength) of the saturated soils (Fredlund and Rahardjo 1993). Unsaturated soils are three phase materials that consists of solid, water and air phases. Bishop's (1959) extended the concept of the effective stress for saturated soils to explain the changes in volume and shear strength for unsaturated soils.

$$\sigma' = (\sigma - u_a) + \chi(u_a - u_w) \tag{2.1}$$

where, σ' = effective stress, σ = total normal stress, u_a = air pore pressure, u_w = pore water pressure, and χ = a parameter related to the degree of saturation, *S*, where the χ parameter is unity for saturated soil and zero for dry soil.

According to the principles of continuum mechanics, stress state variables should be defined as the non-material variables for the characterization of the stress condition. However, Bishop's equation has the χ parameter, which is dependent on the degree of saturation. To be consistent with principles of continuum mechanics, Burland (1964 and 1965) suggested that the mechanical behavior of unsaturated soil should be independently related to net normal stress, ($\sigma - u_a$), and the matric suction, ($u_a - u_w$).

Fredlund and Morgenstern (1977) introduced the air-water interface or contractile skin as a fourth phase of unsaturated soils (Figure 2.1). Based on multiphase continuum mechanics, force equilibrium equations for the individual phases of an unsaturated soil were formulated. These equations were set in such manner that the stresses associated with each phase were written in terms of physically measurable stresses (normal stress, σ, pore-air pressure, u_a, and pore-water pressure, u_w). Three possible combinations of stress state variables were introduced: with reference

to the normal stress; $(\sigma - u_w)$ and $(\sigma - u_a)$, with reference to the pore-water pressure; $(\sigma - u_w)$ and $(u_a - u_w)$, and with reference to the air-pore pressure; $(\sigma - u_a)$ and $(u_a - u_w)$. Any set of these three possible combinations can be used to define the stress state variables of the unsaturated soils.

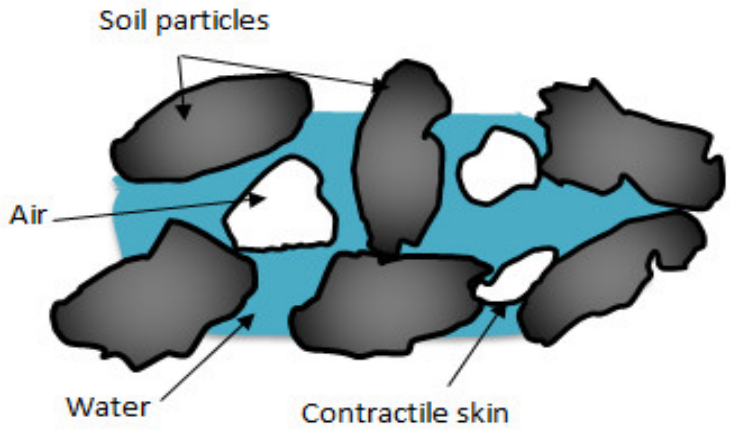

Figure 2.1 Typical structure in an unsaturated soil (modified after Taylan 2013).

Any of the three combinations can be used to describe the behavior of unsaturated soils. However, of the three independent stress state variables; the most practical and applicable are the net normal stress and matric suction (i.e. $(\sigma - u_a)$ and $(u_a - u_w)$). This combination separates the effect of the pore-water pressure, u_w from the effect of total stress, σ. In addition, pore air pressure, u_w is typically equal to the atmospheric pressure. In other words, the net normal stress, $(\sigma - u_a)$, can be easily determined. Whereas, in the first two combinations of stress variables, any change in pore water pressure will affect both of the independent stress state variables.

2.2.2 Shear Strength of Unsaturated Soils

Shear strength of a soil is the main property that is required in the prediction of the bearing capacity of foundations, slope stability and embankments, and lateral earth pressures against retaining walls. In saturated soils, the shear strength as given by a Mohr-Coulomb failure envelop can be expressed by the equation (2.2) using the effective normal stress, $(\sigma - u_w)$:

$$\tau = c' + (\sigma - u_w)\ tan\,\phi' \qquad (2.2)$$

where τ = shear stress at failure, c' = effective soil cohesion, ϕ' = effective angle of internal friction.

Figure (2.2) shows the failure envelope for a saturated soil; where this envelope represents possible combinations of shear stress and effective normal stress on the failure envelope at failure. The failure envelope is obtained by plotting a line tangent to a series of Mohr circles representing failure conditions. The slope of the failure envelope gives the effective angle of internal friction, ϕ', and the intercept of the failure envelope with the shear stress axis is called the effective cohesion, c', (Fredlund and Rahardjo 1993).

2.2.3 Linear Shear Strength of Unsaturated Soil

Fredlund et al. (1978), reanalysed shear strength test data of compacted shale and boulder clay from Bishop et al. (1960) and Potters flint and peerless clay (MIT) (1963), in terms of two independent set of stress variables. The theory of two independent stress state variables was introduced by Fredlund and Morgenstern (1977) to describe the behavior of unsaturated soils. Based on the analyzed data, Fredlund et al. (1978) introduced the shear strength equation for unsaturated soil in terms of these stress state variables (Eq. 2.3).

$$\tau_{unsat} = c' + (\sigma - u_a)\, tan\, \phi' + (u_a - u_w)\, tan\, \phi^b \qquad (2.3)$$

where τ_{unsat} = shear strength of an unsaturated soil, c' = cohesion intercept when the two stress variables $(\sigma - u_a)$, and $(u_a - u_w)$ are zero, ϕ' = friction angle with respect to changes in $(\sigma - u_a)$ when $(u_a - u_w)$ is held constant, and ϕ^b = friction angle due to the contribution of $(u_a - u_w)$ when $(\sigma - u_a)$ is held constant.

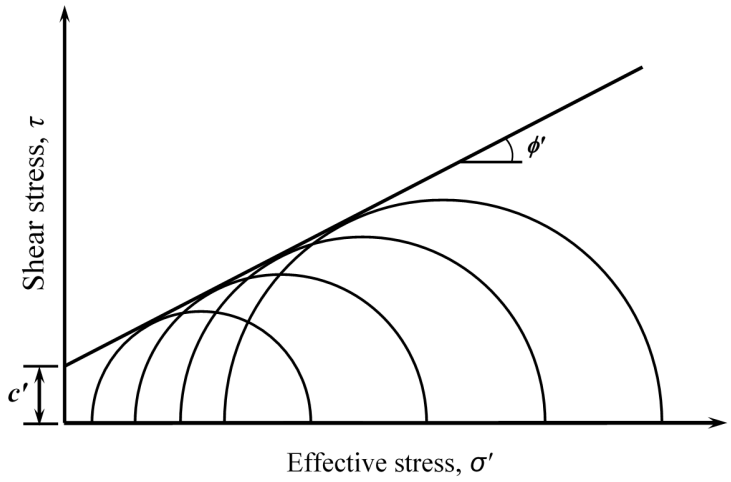

Figure 2.2 Mohr-Coulomb failure envelope for a saturated soil.

Eq. (2.3) resulting in a planer failure surface which is called the extended Mohr-Coulomb failure surface. Figure (2.3) shows that the contribution of matric suction towards the shear strength of unsaturated soil can be considered as contributing to cohesion of the soil (Ho and Fredlund 1982), (Eq. 2.4):

$$c = c' + (u_a - u_w)\, tan\, \phi^b \tag{2.4}$$

where c = total or apparent cohesion of unsaturated soil.

When the $(u_a - u_w)$ equals to zero, the apparent cohesion, c, becomes equal the effective cohesion, c'. Consequently, the Mohr-Coulomb failure envelope will be the same as for a saturated soil.

2.2.4 Non-Linear Shear Strength of Unsaturated Soil

Fredlund et al. (1978) proposed linear planar failure envelope based on the testing data of shear strength for unsaturated soils within a matric suction range of (0 to 200 kPa). Later studies by several investigators has shown that the failure envelope for unsaturated soil with respect to matric suction is typically non-linear. These conclusions were derived based on the shear strength behavior studied for a higher range of matric suction (i.e. 0 to 500 kPa) (Escario and Saez 1986, Gan 1986, Fredlund et al. 1987, Gan et al. 1988, Gan and Fredlund 1988, Vanapalli et al. 1996). A typical non-linear shear strength envelope tested by Gan (1986) on a glacial till is shown in Figure 2.4.

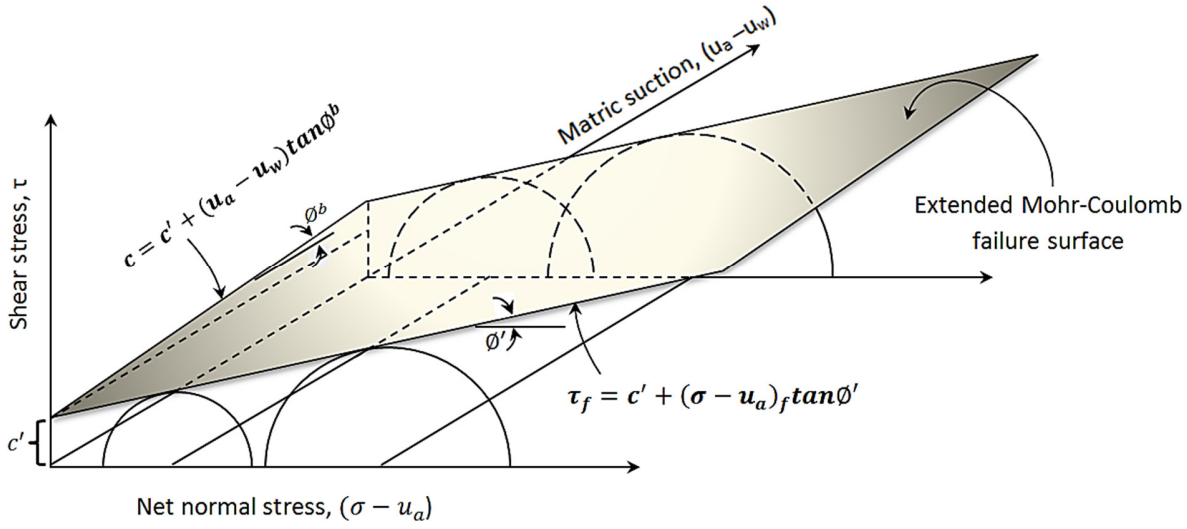

Figure 2.3 Extended Mohr-Coulomb failure surface (modified after Lu and Likos 2004).

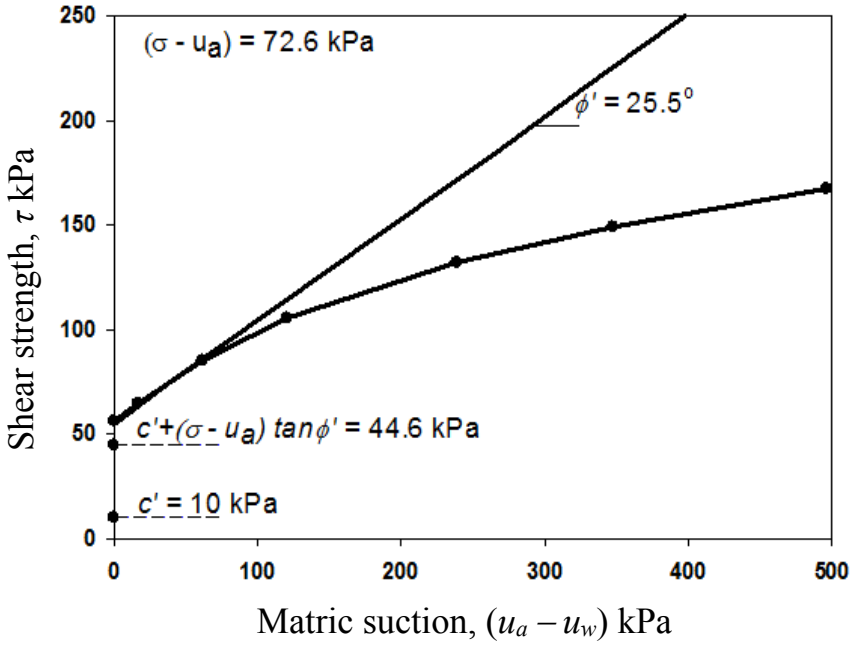

Figure 2.4 Curved failure envelope on the τ versus $(u_a - u_w)$ plane for a glacial till (modified after Fredlund et al. 1987).

Figure 2.5 highlights the strong correlation between the nonlinear variation of the shear strength with matric suction and the soil-water characteristic curve, which is a relationship between the degree of saturation and soil suction. Matric suction as a stress state contributes to the shear strength as an additional frictional parameter, ϕ^b. This is in addition to conventional angle of internal friction, ϕ'. The shear strength of unsaturated soils increases in a linear fashion up to the air-entry value (*AEV*) where $\phi^b = \phi'$. As the matric suction increases, the soil moves from a saturated condition to an unsaturated condition after (*AEV*). During the process of desaturation, the wetted area of contact between the soil particles decreases. Once the soil starts to desaturate, there is a nonlinear increase in shear strength and ϕ^b become less than ϕ' (Vanapalli 2010).

2.2.5 Modulus of Elasticity of Unsaturated Soil, E_{unsat}

The modulus of elasticity, *E* is the key parameter that has a strong relationship with the settlement behavior of soils. It is the response of a material to recoverable deformations and it can be defined as the ratio of the deviator stress in a conventional triaxial test to the corresponding normal strain (Lu and Kaya 2014). Duncan and Bursey (2013) stated that modulus of elasticity is required with suitable elastic solutions or finite element analysis for estimating soil settlement or soil masses movement in any soil-structure interaction, slope stability, expansive soil volume-change behavior problems to name some. Constitutive models relate soil deformation variables to changes in stress state variables by means of elastic modulus (Pereire and Fredlund 1997). Several scholars have utilized the modulus of elasticity to develop constitutive models (Duncan and Cheng 1970, Smith and Griffith 1982, Brinkgreve and Vermeer 1997, Schanz and Vermeer 1998), and semi-empirical and empirical models (Schmertmann 1970, Schmertmann et al. 1978, Bowles 1987, Berardi and Lancellotta 1991, Terzaghi et al 1996, Mayne and Poulos 1999, Mohamed et al. 2013) to simulate or estimate soil behavior.

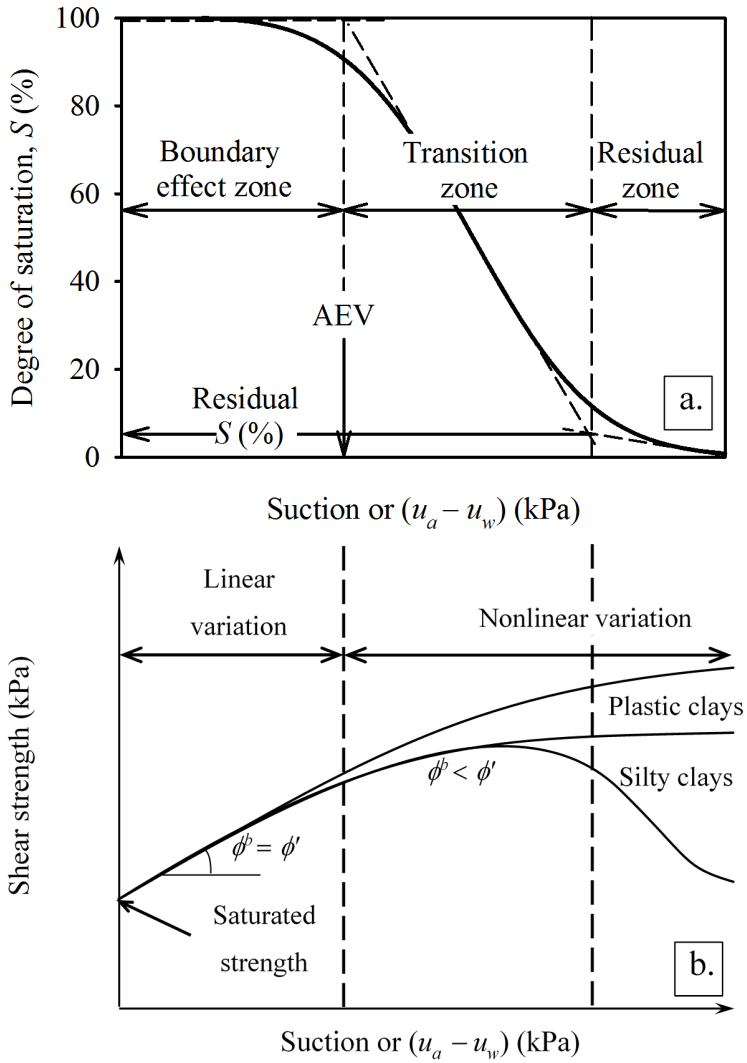

Figure 2.5 (a) SWCC showing different zones and (b) the variation of shear strength of unsaturated soils in various zones of unsaturation for different soils (modified after Vanapalli 2010).

For implementing conventional soil mechanics principles in practice, the soil is assumed to be saturated or in a state of dry conditions. The modulus of elasticity is related to the overburden and confining stresses, stress history, Soil type (Janbu 1963, Duncan and Cheng 1970, Schmertmann 1970, Schmertmann et al. 1978, Brinkgreve and Vermeer 1997, Schanz and Vermeer 1998). Janbu (1963) reported that modulus of elasticity values vary with respect to confining stress and suggested that this variation can be given by Eq. (2.5). In many scenarios,

however, the water table is at a greater depth due to the influence of environmental factors and therefore the soil is typically in a state of unsaturated condition. Barkan (1962) pointed out that in addition to the cohesion and friction forces, the presence friction and capillary forces (i.e. $(u_a - u_w)$) induced internal forces effect the soil elastic properties. Several researchers, since then, have studied the influence of capillary stress or soil suction on the modulus of elasticity of unsaturated soils (Barkan 1962, Edil 1973, Fredlund et al 1975, Edil et al. 1981, Miao et al. 2002, Liangtong 2003, Oh et al. 2009, Vanapalli and Oh 2010, Rahardjo et al. 2011, Lu and Kaya 2013, Lu and Kaya 2014, Adem and Vanapalli 2014). All these studies highlight the contribution of capillary stress or matric suction to the modulus of elasticity. Adem and Vanapalli (2014) stated that the modulus of elasticity of unsaturated soil is a function of initial soil condition (i.e. void ratio), initial state of hydration (i.e. water content or matric suction) and stress level (i.e. overburden and lateral stress).

$$E_{sat} = KP_a \left(\frac{\sigma_c}{P_a}\right)^n \tag{2.5}$$

where E_{sat} is the saturated modulus of elasticity, K is Janbu's dimensionless modulus number, P_a is the atmospheric pressure (i.e. P_a = 101.3 kPa), σ_c is the confining stress, and n is fitting parameter that control the rate of E_{sat} variation with σ_c. K and n are dimensionless numbers that can be obtained from log-log plotting of E_{sat} vs. σ_c results of series of triaxial tests (Duncan and Chang, 1970).

Measuring the modulus of elasticity of unsaturated soil is time consuming, expensive and requires elaborate testing equipment and highly trained staff. Several empirical and semi-empirical models have been proposed to predict and estimate the modulus of elasticity of unsaturated soils (Sawangsuriya et al., 2009, Oh et al. 2009, Vanapalli and Oh 2010, Lu and Kaya 2014, Adem and Vanapalli 2014, and Han and Vanapalli 2016).

Oh et al. (2009) analyzed load-settlement data of model footing tests for three different sands for different suction values. Their study showed that the modulus of elasticity linearly increases in the boundary effect zone (the zone in which the soil is in a state of saturated condition). In transition zone (in which the soil desaturates), the modulus of elasticity increases non-linearly up to a certain suction value and then starts decreasing. Finally, in the residual zone, the modulus

of elasticity converges to a constant value and is close to that of saturated condition. Oh et al. (2009) proposed a semi-empirical model to predict the variation of E_{unsat} with respect to $(u_a - u_w)$ for sandy soils (Eq. 2.6).

$$E_{unsat} = E_{sat}\left[1 + \alpha \frac{(u_a - u_w)}{(P_a/101.3)}(S^{\beta})\right] \tag{2.6}$$

where α and β are fitting parameters.

The β value was found to have a strong relationship to the soil plasticity index (I_p). For non-cohesive soils, β value equals 1 was found to provide good agreement with back calculated modulus of elasticity. On the other hand, α value was found to be a function of footing or foundation size and its value ranges between 0.5 and 2.5. The nonlinearity of the E_{unsat} variation with respect to matric suction is fitting parameters α and (S^{β}) dependent and it was explained by differentiating Eq. (2.6) as shown in Eq. (2.7).

$$\frac{dE_{unsat}}{d(u_a - u_w)} = \frac{E_{sat}.\alpha}{(P_a/101.3)}\left[S^{\beta} + (u_a - u_w)\frac{d(S^{\beta})}{d(u_a - u_w)}\right] \tag{2.7}$$

Lu and Kaya (2014) suggested that the modulus of elasticity versus volumetric water content relationship follows a power law decay and proposed a model as shown in Eq. (2.8).

$$E = E_d + (E_w - E_d)\left(\frac{\theta - \theta_d}{\theta_s - \theta_d}\right)^m \tag{2.8}$$

where E = modulus of elasticity, subscript d = dry state, w = wet state, and m = empirical fitting parameter

Eq. (2.8) does not consider the effect of confining stress on the modulus of elasticity, either. The effect of confining stress on the modulus of elasticity can be considered using another model proposed by Lu and Kaya (2014) Eq. (2.9); however, it requires four empirical parameters:

$$E = \frac{2A}{1+\mu}(\sigma - u_a) + \frac{2C}{1+\mu}\frac{1}{\alpha}\left[\left(\frac{\theta}{\theta_s}\right)^{n/n-1} - 1\right]^{1/n} \tag{2.9}$$

where μ = Poisson's ratio and A, C, α, and n = parameters

2.3 Pile Foundation

2.3.1 Stress Distribution under Pile Foundation

AASHTO (2002) defines two types of piles; i) Friction pile that derives its major capacity from soil resistance mobilized along the entire length of the embedded pile (i.e. skin resistance), and ii) End bearing pile that derives its major capacity from the resistance of the material on which the pile tip rests (i.e. tip resistance). The ultimate carrying capacity of a pile is a combination of shaft resistance and end bearing resistance.

Both friction and end bearing piles transfer a portion of the carried load to the surrounding soil through the shaft friction. Several approaches were introduced to interpret the load transfer mechanism. Seed and Reese (1957) proposed the distribution function approach in which the variation in the magnitude of axial force with depth along the pile is represented by a curve. The curve shows that the axial force in the pile varies with depth; at the head of the pile, the axial force in the pile will be equal to the total applied load and at the pile tip the load is equal to the axial force at the base of the pile. At any point in-between along the shaft, the axial load in the pile varies nonlinearly and equals to the arithmetic difference between the applied load and the side friction force acting along the pile shaft from the top of the pile to that point. The accumulated differences in shaft strain under the applied force and the soil strain caused by load transferred to the soil through skin resistance will result in relative slip between the pile and soil producing the ultimate skin friction (Bowles 1997). Coyle and Reese (1966) extended this approach utilizing the data of instrumented piles and model piles and proposed the load-transfer method. They suggested that the pile can be subdivided into several segments and used iteration and superposition techniques to calculate the load and the corresponding displacement for different segments starting from the tip of the pile to estimate the $P - \delta$ curve. Different load-transfer curves of slip versus shear strength of the soil can be generated using the $P - \delta$ results derived from the instrumented piles (Coyle and Sulaiman 1970).

When there is a strong (bearing) layer, piles transfer the major portion of the load from the structure to the bearing layer. Such piles are called bearing piles. Figures (2.6) shows different hypothetical failure patterns under pile foundation (Visec 1967). Unlike the friction piles, the

penetration of a bearing pile is typically small and the pile transfers the load to the soil in a small pressure bulb below the pile tip (Prakash and Sharma 1990).

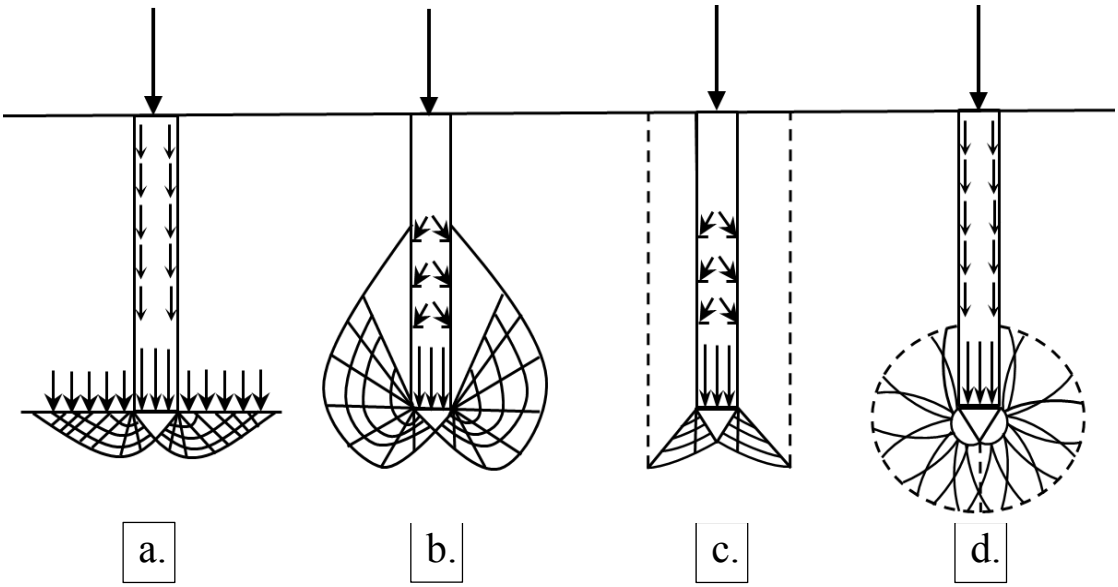

Figure 2.6 Assumed failure patterns under deep foundations (modified after Vesic 1967): (a) After Prandtl, Reissner, Caquot, Buisman, Terzaghi (b) After DeBeer, Jaky, Meyerhof (c) After Berezantsev and Yaroshenko, Vesic (d) After Bishop, Hill and Mott, Skemption, Yassin, and Gibson.

Pile foundation is typically constructed in a group consists of several bored or driven piles with a pile cap to distribute the loads from the superstructure on the piles underneath. When several piles constructed near to each other in a group, it is reasonable to expect that stresses from adjacent piles to overlap and affect the final carrying capacity of the pile group. This behavior is called group action. Figures (2.7) show the stresses overlap of adjacent end bearing and friction piles. The group action results in non-uniform stress overlap and load distribution to various piles (Prakash and Sharma 1990). For instance, Figure (2.8) shows two adjacent piles of a pile group (i.e., I and II) for interpreting different loading combinations. Soil elements *a* and *b* are assumed to represent reference elements of negligible weight when neither of the piles is loaded (Figure 2.8a). After pile I is loaded, the reference element *a* is distorted to the shape of element *a′*. The pile exerts shearing stress equal to τ_i on element *a′* (Figure 2.8b). The far element to the pile, *b* offers vertical support to element *a′* by the shearing stress τ_{iii}.

When two piles are loaded simultaneously, stresses overlap between them and more complex stress distribution occurs (Figure 2.8c). Element b'' symmetrically loaded by both piles; consequently, the distortion of element b' is not possible. Furthermore, it is not possible for shears on vertical planes to be transferred outward indefinitely, as for a single pile. Since element b'' must be symmetrical after distortion, the shearing stresses that element b'' takes on its sides are much smaller than those on b'. As a result, τ_i' must be smaller than τ_i. Therefore, to carry the pile load, the pile must settle further. This causes larger distortion on the outer side of the piles and increases the skin friction there. Therefore, in large groups of closely spaced friction piles the distribution of load to the piles is not uniform. For instance, the central piles could settle more on loading than the exterior piles because it is possible that exterior piles developed a slightly higher skin friction than if all piles settle equally. As all piles of a group settle equally, each exterior pile carries much higher load than interior piles.

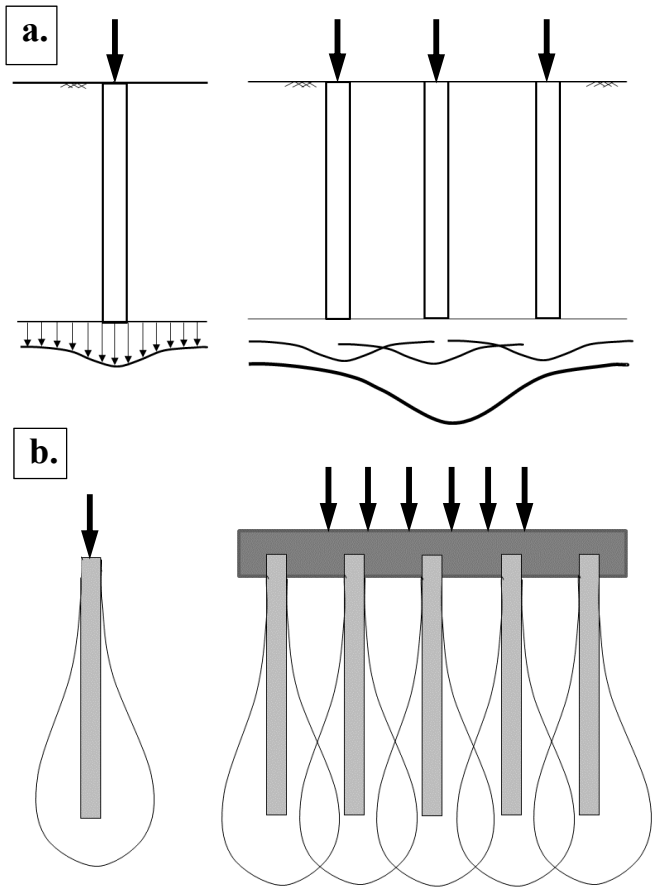

Figure 2.7 Stresses overlap of piles in a group; (a) end bearing piles, and (b) friction piles (modified after Prakash and Sharma 1990 and Bowles 1996).

O’Neill et al. (1977) extended the load-transfer approach to model the behavior of pile group by incorporating the pile-soil-pile interaction effects. Pile-soil-pile interaction is approximated using the single pile load-transfer curves with a multiplier taking into account the displacement of pile nodes and additional induced displacements at the nodes caused by soil reactions generated at the other nodes.

If the soil in which the piles are embedded and all bearing layers have sufficient capacity, each pile of the group is capable of carrying essentially the same load as that carried by single piles. If the bearing stratum is a compressible, the settlement of the pile group could be much higher than the settlement of individual piles, even though the bearing

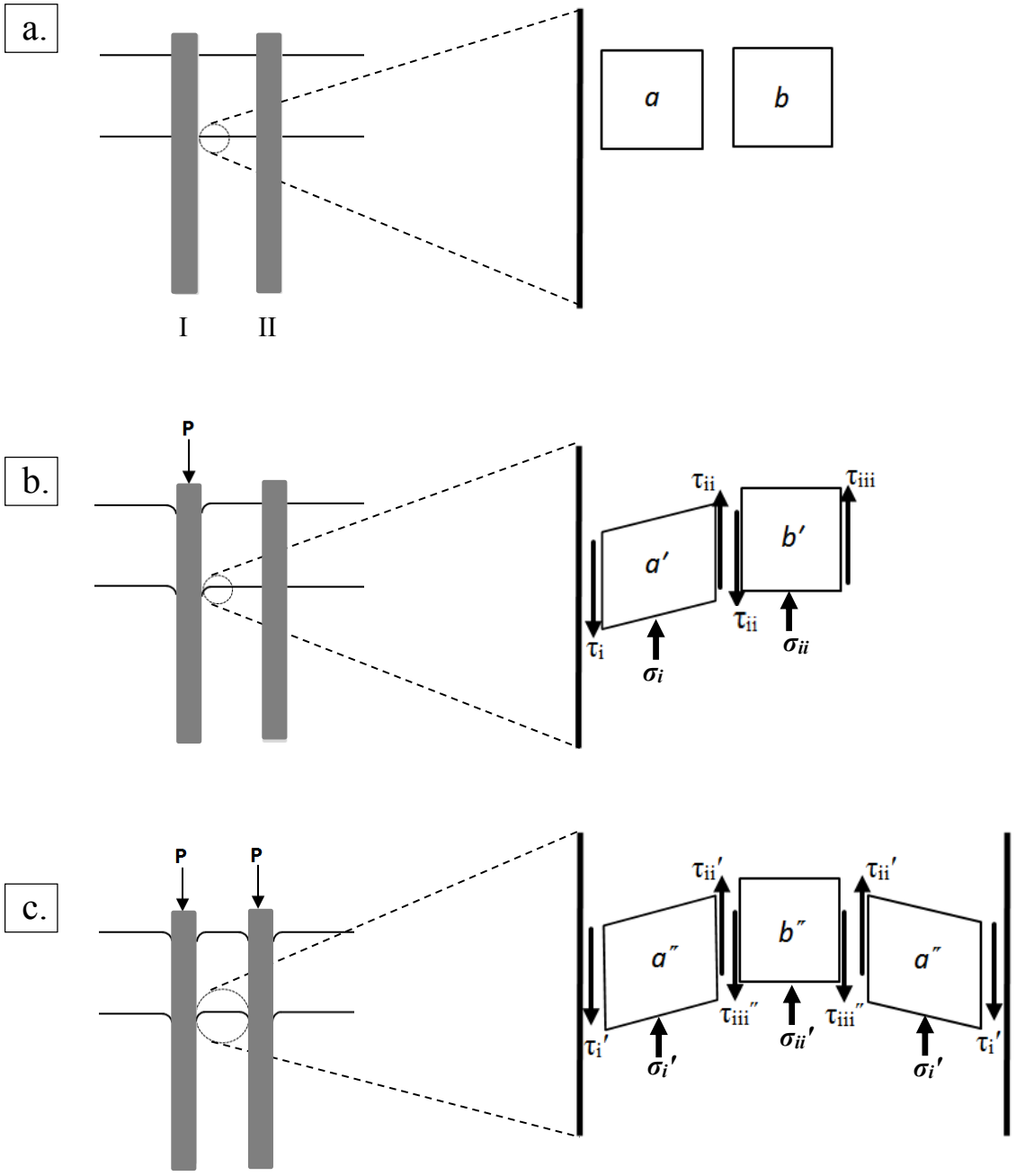

Figure 2.8 Shearing stresses and strains in the soil adjacent to loaded, single friction piles and pile groups (modified from Prakash and Sharma 1990).

pressure may be lower than the allowable value. The reason is that the stresses of the adjacent piles overlap below the tip of the bearing piles and the pile group will act as unit (Figure 2.7a). The bolded line represents total distribution stress under the pile group, which can be several times greater than that under single pile. Nevertheless, when the pile tip is supported by incompressible soil layer, the group settlement may essentially be equal to the settlement of the individual pile.

Consequently, the final pile group capacity will not be equal to the sum of the individual piles capacities due to stress interaction. The ratio of the pile group capacity to the summation of the individual pile capacities called the group efficiency factor, E_g. Canadian Foundation Engineering Manual (CFEM) (2006) suggests that pile driving in cohesionless will increase the lateral earth pressure and densify the surrounding soil resulting in larger individual pile capacity when installed as a group. Therefore, E_g for driven piles in cohesionless is greater than unity especially for close centre-to-centre spacing (i.e. 2D to 3D) (Kédzi 1957, Bowles 1997, Dia et al. 2012). For bored pile groups, however, the individual pile capacity in a group is reduced because of both the lateral earth pressure and sand density reduction due to boring process. A reduction factor of 0.67 was suggested by Meyerhof (1976) to be applied to the sum of individual pile capacities in clean sand.

2.3.2 Single Pile and Pile Group Ultimate Capacities

Pile group capacity can be defined as the contribution of the capacities of the individual piles of the group. The individual pile capacity, Q_p, is a function of the effective normal stress σ', the effective cohesion parameter, c', and the effective angle of internal friction ϕ'. In general, pile capacity is composed of two components; the shaft capacity, Q_s and the end bearing capacity, Q_b (Eq. 2.10).

$$Q_p = Q_b + Q_s \tag{2.10}$$

a. Bearing capacity

The ultimate capacity of a single pile is a combination of bearing and shaft capacities. The ultimate bearing capacity of a pile, Q_b in a saturated soil can be estimated using Tarzaghi's Eq. (2.11) can be used:

$$q_u = c'N_c + \sigma'_b N_q + 0.5\, B\, \gamma' N_\gamma \quad (2.11)$$

where q_u is ultimate bearing capacity (kN/m^2), c' is effective cohesion (kN/m^2), σ'_b is effective normal stress at the tip of the pile (kN/m^2), γ' is effective unit weight (kN/m^3), B is pile width or diameter (m), and N_c , N_q, N_γ are the bearing capacity factors which are function of the effective friction angle, ϕ'. Rajapakse (2008) stated that N_q value for sand depends on the sand state where N_q = 8 to 12 for loose sand, N_q = 12 to 40 for medium dense sand, and N_q = 40 for dense sand.

The end-bearing capacity is predominant in cohesionless soils. During the pile driving or soil drilling process, the surrounding soil gets disturbed due to installation up to distance of a few pile diameters. In drilled piles, the disturbance could arise due to loss of some of the surrounding soil. In contrast, in driven piles, the disturbance results from compaction and densification of the surrounding soil. Due to the difficulty in estimating the properties of the surrounding soils immediately after installation, the capacity of the piles is estimated based on initial strength parameters of the soil.

The end bearing capacity, Q_b in saturated cohesionless soils can be estimated by extending the Effective Stress Analysis (ESA) approach using Eq. (2.11). In sandy soils, there is no cohesion. Therefore, Eq. (2.11) can be re-written as (2.12):

$$Q_b = A_p[\sigma'_b N_q + \gamma' D_f N_q] \quad (2.12)$$

where A_p is the area of pile tip, γ' is soil unit weight (kN/m^3), and D_f is depth of pile (m).

Eq. (2.12) can be re-written as below since the width or diameter of pile is too small and can be neglected.

$$Q_b = A_p \sigma'_b N_q \quad (2.13)$$

In the Total Stress Analysis (TSA) approach, which is typically extended to the saturated clayey soils, the shear strength contribution arising from undrained friction, ϕ_u is zero. For this

reason, the shear strength of the bearing stratum arises from undrained shear strength parameter, c_u. For low to medium sensitivity, homogeneous clay bearing stratum, the undrained shear strength is assumed to remain unchanged during pile installation and can be used to determine the bearing resistance. For stiff and fissured clays, the undrained shear strength that is obtained from laboratory test, c_{ulab} depends on the size of the sample (Prakash and Sharma 1990). The c_{ulab} value decreases as the sample size increases which reflects significant influence of fissured material in controlling the strength of larger soil samples. Therefore, the undrained shear strength value has to be adjusted for scale effect (Meyerhof 1983, Prakash and Sharma 1990). A reduction factor, R_c can be used to reduce $c_{ulab.}$ value that can be used for determining the bearing capacity of piles in stiff, fissured clay as in Eq. (2.14).

$$c_u = R_c . c_{ulab.} \tag{2.14}$$

R_c can be estimated using the following empirical formulas that relate R_c to pile tip diameter, D (in meter) (Prakash and Sharma 1990).

1. For driven piles:

$$R_c = \frac{(D + 0.5)}{(2D)} \leq 1 \text{ for } D \geq 0.5 \tag{2.15}$$

2. For bored piles:

$$R_c = \frac{(D + 1)}{(2D + 1)} \leq 1 \tag{2.16}$$

Bearing capacity factors for TSA are $N_\gamma = 0$ and $N_q = 1$. In addition, the width of pile is too small and can be neglected. Consequently, the pile bearing capacity in saturated cohesive soils is given by Eq. (2.17):

$$Q_b = A_p c_u N_c \tag{2.17}$$

b. Shaft capacity

The second part of the Eq. (2.11) is the ultimate shaft capacity, Q_s. Two approaches can be used to determine the pile skin friction namely; ESA and TSA. Extending the ESA, the skin friction resistance, f_s is a function of effective cohesion, c', mean vertical effective stress, σ'_v and the effective angle of internal friction.

$$f_s = f(c', \sigma'_v, \phi') = c' + K_0 \sigma'_v tan\delta' \tag{2.18}$$

where K_0 is the mean lateral earth pressure at rest, and δ' is the angle of internal friction for the pile-soil interface and can be estimated as [(2/3)*ϕ'].

Burland (1973) extended the ESA and introduced the β-method Eq. (2.19) which is a modified form of Eq. (2.18) to determine the shaft capacity.

$$f_s = c' + \beta \sigma'_v \tag{2.19}$$

where, β is Burland-Bjerrum coefficient that is equal to [K_0 tan δ']. The β value ranges from 0.3 to 0.6 for both fine-grained and coarse-grained soils.

Vanapalli and Taylan (2012) stated that the soil remolding associated with pile installation results in significant reduction in soil cohesion leading to negligible contribution of cohesion towards the shaft capacity for coarse-grained soils and low percentage of fines soils such as silty sand soils.

In clayey soils, TSA is extended and the shaft capacity of a single pile, Q_s can be estimated by using Eq. (2.20), (Skempton 1959):

$$Q_s = \alpha A_s c_u \tag{2.20}$$

where A_s is area of the pile shaft, and α is adhesion factor between soil and pile. α value is not constant but decrease with increasing undrained shear strength, c_u, and varies from close to unity for low strength soft clays to 0.4 for stiff clay (Skempton 1959).

The ultimate single pile capacity in cohesionless soils can be obtained from Eq. (2.21) and in cohesive soils from Eq. (2.22):

$$Q_P = Q_b + Q_s = \sigma'_b N_q A_b + \beta \sigma'_v A_s \quad (2.21)$$

$$Q_P = Q_b + Q_s = A_p c_u N_c + \alpha A_s c_u \quad (2.22)$$

2.3.3 Pile Group Capacity

The ultimate pile group capacity in cohesionless and cohesive soils is not always equal to the sum of the capacities of the individual piles in the group. For most practical purposes, the ultimate load of a pile group, $(Q_G)_{ult}$, can be estimated from the smaller of the block failure (group action) and individual action. If there is no group action, individual action will dominate and pile group capacity can be estimated as the summation of individual pile capacities:

$$(Q_G)_{ult} = N_p * Q_p \quad (2.23)$$

where N_p is the piles number in the group.

If the piles are spaced closely enough, the stresses of the adjacent piles likely overlap and group action or block failure will be dominant; therefore, group efficiency factor, E_g should be used to estimate the ultimate group capacity (Eq. 2.24).

$$(Q_G)_{ult} = E_g * Q_p * N_p \quad (2.24)$$

The group efficiency of pile group driven in sandy soils is greater than unity, as explained earlier. It is conservative to assume an efficiency factor of unity for all practical purposes. The capacity of a pile in a group increases due to the densification of soil between neighboring piles at the narrow pile spacing up to 3D. The pile capacity increases due to the increase in pile shaft friction within the working load range of the pre-yield condition (Lee and Chung 2005).

On the other hand, bored piles do not compact the soil around the pile during the installation. In addition, when boring has to be done below water table, bentonite slurry is used to

stabilize bore and prevent water from filling the hole. Before pumping concrete, the bottom of the borehole has to be cleaned carefully which is not always possible. Consequently, the group efficiency factor will never be greater than one. However, efficiency factor can be taken as unity (Murthy 2003). Therefore, Eq. (2.23) can be used to estimate pile group capacity in cohesionless soils.

Group action is more predominant in cohesive soils. For engineering practice applications, Prakash and Sharma (1990) suggested E_g values for cohesive soils based on pile spacing from centre to centre (Table 2.1).

Table 2.1 Group efficiency value for pile spacing (Prakash and Sharma 1990).

Pile spacing (s)	3*D*	4*D*	5*D*	6*D*	8*D*
$\boldsymbol{E_g}$	0.7	0.75	0.85	0.9	1.0

2.3.4 Settlement of Single Pile and Pile Group in Cohesionless Soil

The settlement of pile foundation is complex because of the disturbance of the surrounding soil due to installation process. There are several factors that affect the settlement of pile: i) The length to diameter ratio *L/D*; ii) The ratio of Young's modulus of the equivalent pile section, E_P, to the modulus of elasticity of the soil, E_s; and iii) the ratio of the modulus of elasticity of the bearing stratum at the pile tip, E_b to E_s (Poulos, 1989). The most precise measurement of pile foundation load-settlement behavior can be obtained from a full-scale load test. The test procedures are described in the ASTM D1143. However, there are several empirical methods for estimating the settlement of piles in cohesionless soils; for example, Vesic (1970) introduced empirical formula to estimate the pile settlement:

$$S_t = B/100 + (Q_a L)/(A_P E_P) \quad (2.25)$$

where *St* = settlement of pile head, (inch), *B* = pile diameter (inch), Q_a = applied pile load (lb), *L* = pile length (inch), A_p = pile tip area (inch^2) , and E_P = modulus of elasticity of pile material (lb/inch^2).

In addition, the pile settlement can be estimated using the following semi-empirical method (Vesic 1977):

$$S_t = S_s + S_p + S_{ps} \tag{2.26}$$

$$S_s = (Q_b + \alpha_s Q_s)L / (A_P E_P) \tag{2.27}$$

$$S_p = C_p Q_b / (B q_p) \tag{2.28}$$

$$S_{ps} = C_s Q_s / (D_f q_p) \tag{2.29}$$

where S_t = total pile top settlement, S_s = settlement due to axial deformation of a pile shaft, S_p = settlement of pile base or point caused by load transmitted at the base, S_{ps} = settlement of pile caused by load transmitted along the pile shaft, C_p is an empirical coefficient that depends on soil density and type, and installation method (i.e. driven or bored) (Eq. 2.30), Q_b is the net point load (kN), Q_s is the pile shaft load, D_f is the embedded pile length, and q_p is the ultimate end (point)-bearing capacity (kN/m^2). α_s is a number that depends on distribution of skin friction along the pile shaft. α_s values are equal to 0.5 for the uniform or parabolic skin friction distribution and 0.67 for triangular shape distribution of skin friction.

$$Cs = 0.93 + 0.16\sqrt{D_f/D}\, C_p \tag{2.30}$$

From field observations, it has been found that the settlement of pile group is much higher than the settlement of a single pile under the corresponding working load. There are many factors that affect the settlement of a pile group, which include the shape, the size of the group, piles length, method of installation and many other possible factors (Murthy 2002). The settlement of a pile group, S_g, is a superposition of the displacement of the pile point, S_p, plus the elastic shortening of the pile shaft, S_s, between cap and pile tip as in Figure (2.9). For friction piles, the point displacement will be the significant quantity causing settlement.

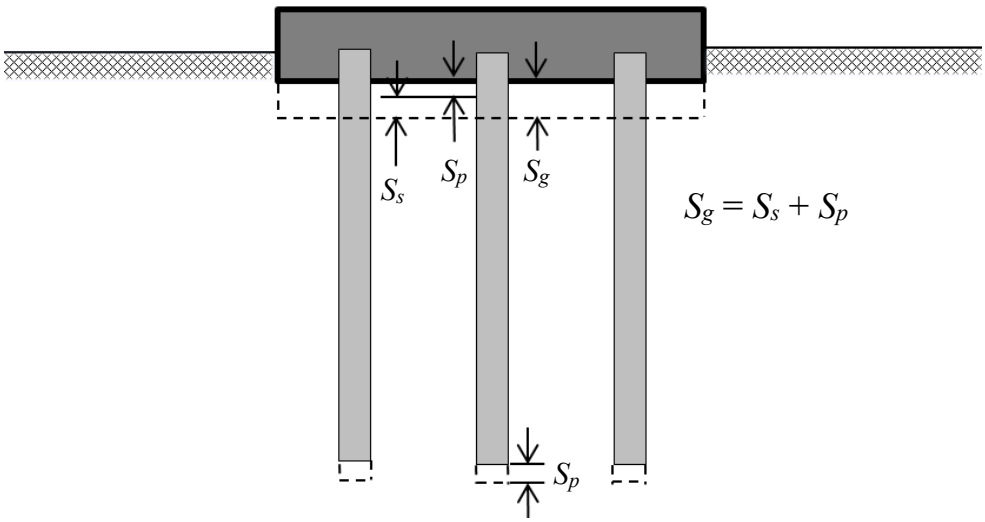

Figure 2.9 Pile group settlement (modified after Bowles 1997).

Eq. (2.31) gives group settlement factor, S_g, which is the ratio of a pile group settlement to a single pile settlement, S_t at corresponding working load.

$$F_g = \frac{S_g}{S_t} \tag{2.31}$$

Vesic (1967) introduced the relation between group settlement factor and relative width of the pile group, B_g to pile diameter, D (Figure 2.10a). Skempton et al. (1953) introduced a relation between group settlement factor and pile group width (Figure 2.10b). In recent years, several methods have been used to estimate settlement of single piles, such as load transfer method, elastic method and finite element method.

2.4 Pile Tests

2.4.1 Full Scale Pile Load Tests

The load-settlement, $P - \delta$ behavior of piles under service loads is a crucial factor in determining the stability and serviceability of superstructures. Full-scale pile load tests are used to estimate the real behavior of piles or pile groups under different load conditions. Several standards for full scale pile load tests under different loading conditions are available in ASTM, for example D 1143,

standard test method for piles under static axial compressive load, D 3966, standard test method for piles under axial tensile load, and D 4945, standard test method for high strain dynamic testing of piles. The full-scale tests provide reliable information about the pile behavior, capacity of the pile system and load distribution in the pile-soil system under field condition. The data from these tests are used to confirm the design assumptions or to provide information to modify the pile foundation design.

Dai et al. (2012) conducted full-scale pile load tests on single bored piles and pile groups installed in a soil profile with mixed layers of clay and silt in Nanjing, China. Two single piles and six pile groups of different pile arrangements; two, four and nine piles with different spacing and pile length were investigated. Based on the analysis of the field $P - \delta$ test results, the study concluded that based on conventional design methods, the single piles mobilized essentially only the shaft resistance while the base resistance to the ultimate design load was less than 5% (Figure 2.11). This study suggests that the shaft resistance is dominant in fine-grained soils. In addition, the general response of the individual piles in the two-pile groups was similar to the response of the single piles. Such a behavior is attributed to the small interaction between piles in the two-pile group. Meanwhile, 4- and 9-pile groups have substantial interaction and group effect. In addition, the researchers stated that pile spacing has greater impact on pile interaction (group effect) in comparison to pile length.

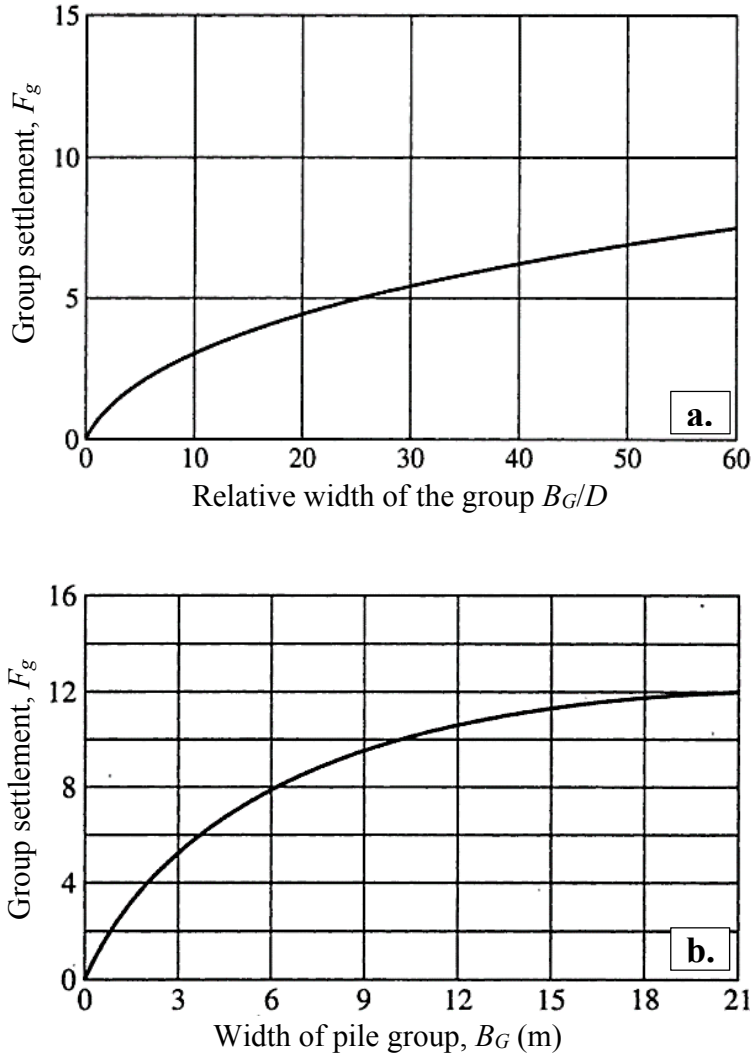

Figure 2.10 Group settlement factor, F_g variation with respect to; (a) width of pile in groups in sand (modified after Vesic 1967), and (b) pile group width (modified after Skempton et al. 1953).

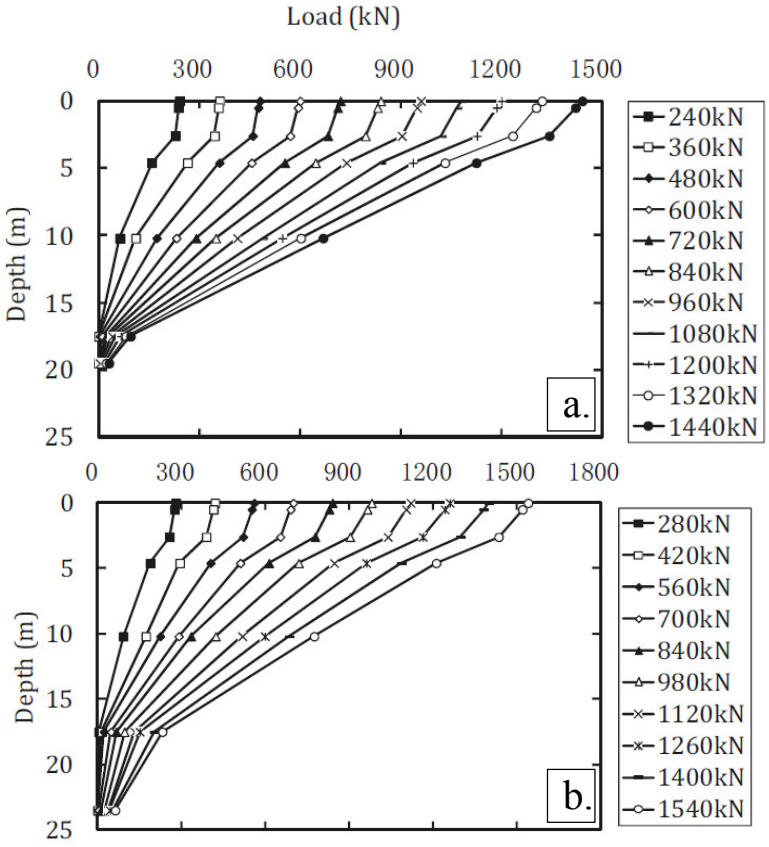

Figure 2.11 The axial load transfer distribution along the pile length; (a) pile length 20 m, and (b) pile length 24 m (modified after Dai et al. 2012).

The ultimate pile capacity in sand is a combination of shaft capacity and end bearing capacity, which is dominant in sandy soil. However, a field study of four steel pipe piles that were installed in dense sand in 1988 at Dunkirk, northern France of lengths between 11m to 22m revealed that the pile shaft capacities increased by 85% over five years period after construction (Chow et al., 1997). The piles were tested under compression and tension in in June 1989 (T89a) and September 1989 (T89b) and re-tested under tension in 1994 (T94). The variation of shear stress with depth in compression and tension for one of 11.1m in length piles is displayed in Figure (2.12). Chow et al., (1997) concluded that the increase was due to a change in the stress regime created during pile driving is the most possible reason for the observed situation. Creep may reduce arching effects around the pile shaft resulting in increasing the radial effective stress. In addition, the increase in radial stress during pile loading could be a result of strong dilation that was developed over years. Moreover, the upper 7m of the piles is passing through 4m unsaturated layer

and oxygenated sand was corroded and form up to 5mm strong adhering sand-rust-carbonate layer. Although the piles extended in unsaturated zone of about 25% of the short pile length and 12.5% of the longer ones, the study ignored the contribution of matric suction towards the pile shaft resistance. Figure (2.12) shows that shear stress distribution along the shaft increased under tension loads in the unsaturated zone.

Many other researchers used the field test data to derive empirical or semi-empirical pile design methods or to investigate the reliability of numerical models. Vijavergiya and Fotch (1972) introduced the conventional λ method for estimating the shaft capacity of driven piles in fine-grained soils based on field test data of 42 pile load tests. The λ method combines the total and effective stress approaches.

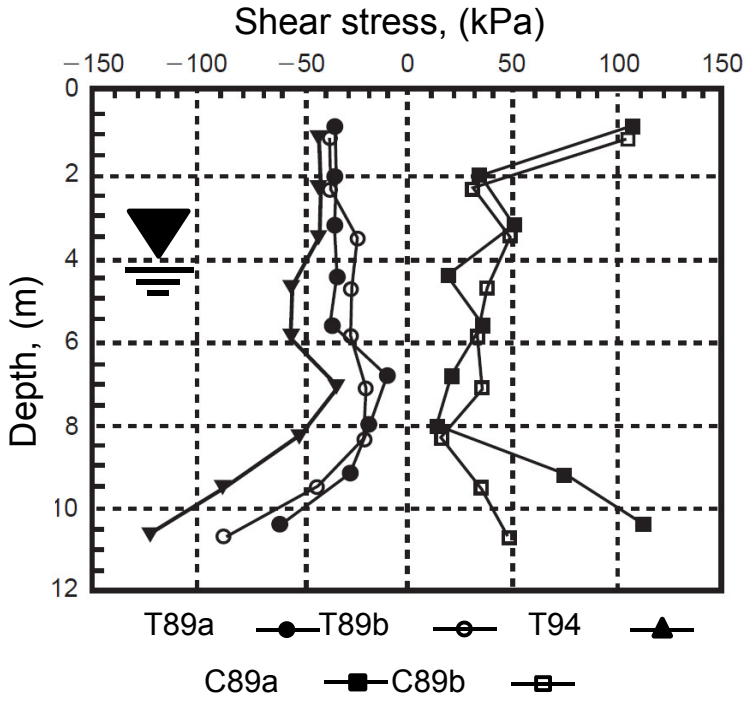

T: Tension, and C: Compression

Figure 2.12 Variation of shear stress with time along the embedded depth of 11.1 m length pipe pile in sand (modified after Chow et al. 1997).

The previous examples provide valuable information interpreting the behavior of pile foundation from in-situ pile load tests. The data obtained from the full-scale tests is valuable; however, these tests are elaborate, need-trained personnel to perform, time consuming and hence they are expensive. In order to elevate the drawbacks associated with full-scale tests, physical and numerical models have been extensively used to simulate different loading scenarios of pile foundations (i.e. static, and dynamic loads) (Beredugo 1966, Boominathan and Lakshmi 2000, Al-Mhaidib 2006, Lee and Chung 2005, Vanapalli et al. 2010, Vanapalli and Taylan 2011 and 2012, Gaaver 2013, Khari et al. 2013, Taylan, 2013, Sheikhtaheri 2014).

2.4.2 Scaled Pile Load Tests

Two types of physical models have been extensively used to investigate the pile foundation behavior in saturated and unsaturated soils. The first one is the traditional model, which requires of a soil container, a model pile or pile group, a loading system, different sensors and a controlling system. The second one is a centrifuge model.

Several parameters influence in obtaining reliable results from scaled (model) pile load tests, which include boundary effects, loading rate, stress level, soil properties, etc. The following paragraphs summarize some key details in order to understand the limitations of scaled pile load tests.

The pile length-to-diameter ratio, *L/d* and the stress interaction with testing tank boundaries are the main points that should be considered to model single pile or pile group. One of the major problems associated with pile modeling is the boundary and scale effects of the pile and the testing tank (Taylan 2013). Poulos (1989) stated that the behavior of a single pile (i.e. load-settlement relationship) is governed by the length-to-diameter ratio, *L/d* the pile stiffness factor (i.e. the ratio of Young's modulus of the pile section to the Young's modulus of the soil), E_P/E_S and the ratio of the modulus of elasticity of the bearing stratum to the modulus of elasticity of the soil, E_b/E_S. The geometry of the pile group is also a key factor that controls the load-settlement behavior as well as the factors governed the single pile behavior. The relative spacing between piles, *s/D*, and the number of pile in the group also influence the group settlement due to the interaction of the adjacent piles stresses.

The influence of size and boundary conditions should be eliminated. The stress interaction with the testing tank boundaries will increase the confining stress; and thus the pile capacity. Bolton (1999) and Gui et al. (1998) studied the influence of container/cone diameter ratio, *B/D* using different cone diameters in centrifuge test. This study results suggest that a *B/D* ratio greater than 22% would have no influence on the cone tip resistance. Moreover, a ratio of the distance of the test location from the nearest container side, *S/B* of 8% and 14% for dense and loose sand, respectively was found to have no influence on the cone tip resistance. Prakash and Sharma (1990) stated that pile transfers its load to the underneath bearing stratum in a small pressure bulb. The bulb pressure extends usually to a depth of (1.5 - 2*D*) under the pile tip or the pile group (Vanapalli and Mohamed 2007, Rajapakse 2008). Therefore, the stress bulb should be assured not to interact with the bottom boundary of the testing tank.

These studies provide valuable guidelines for performing reliable single model pile test. However, consistent guidelines are not available for conducting scaled pile group test. Several researchers used different container/pile group size, B/D_G ratio (Beredugo 1966, Vesić 1969, Boominathan and Lakshmi 2000, Al-Mhaidib 2006, Lee and Chung 2005, Gaaver 2013, Khari et al. 2013). Table (2.2) summarizes scale variation of the model pile and pile groups from the studies undertaken by various researchers.

Soil properties, for example grain size distribution, density, uniformity, degree of saturation, and repeatability of soil layers has significant effect on the scaled test results. Gui et al. (1998) suggested that the ratio of cone diameter, *D* to the mean grain size, D_{50} should be permitted not to fall below 20. Therefore, soil properties must be well defined and should be consistent during successive tests.

Several investigators studied the effect of loading rate on pile behavior in cohesive and cohesionless soils (Horvath 1995, Al-Mhaidib 1999 and 2006, Kong et al. 2008, Adejumo 2013, Adejumo et al. 2013). The studies showed that for both cohesive and cohesionless soils the pile capacity increases as loading rate increases. Moreover, in sandy soils, the effect of loading rate on pile capacity increases as the density increases (Al-Mhaidib 2006).

Table 2.2 Model pile and pile group in literature

Reference	*s*	Geometry	*B* (mm)	*D or* D_G (mm)	*L*/*D*	*B* / *D or* B/D_G
Boominathan and Aythiraman (2007)	Single	—	2000	5 – 20	10 – 40	100 – 400
Taylan (2013)	Single	—	300	20 – 45	4.44 – 10	6.66 – 15
Sheikhtaheri (2014)	Single	—	300	19.25 – 38.1	5.22 – 10	7.8 – 15
Beredugo (1966)	3 – 9*D*	3×4, and 3×5	762	9.52	28	1.6
Vesić (1969)	2 – 6*D*	2×2, and 3×3	2540	711	15	3.57
Boominathan and Lakshmi (2000)	3 - 7*D*	2×2, and 3×3	2000	19	30 - 50	4.38
Al-Mhaidib (2006)	3 - 9*D*	1×2, and 3×3	500	25	20	2.22
Lee and Chung (2005)	2 - 5*D*	3×3	1000	32	18	1.74
Gaaver (2013)	2.5*D*	1×2, 2×2, and 2×3	750	26	14, 20 and 26	3.85
Khari et al. (2013)	3 – 6*D*	1×2 and 3×3	900	15.88	32	3.15

D_G = Pile group width

The research objectives of the thesis were addressed based on scaled test results only. In other words, centrifuge models were beyond the scope of this study. However, they are discussed succinctly in the following paragraphs for their capability in controlling the stress level during the test. The most important feature in any centrifuge model is the simulation of self-weight to replicate full-scale test (Bolton et al. 1999). The main concept in centrifuge modelling is elevating the confining stress level within the model up to that in the field or the prototype. Figure (2.13a) shows that the soil stress of a prototype, σ_p at depth, l is equal to the (ρgl), where ρ is soil density, and g is earth gravitational acceleration. If a model was tested under centrifugal acceleration of 1g (Figure 2.13b) the soil stress of the model, σ_m at a model depth (l/N) is equal to ($\rho g(l/N)$), where N is scaling factor. Therefore, the stress within the model is not equal to that in the prototype. Consequently, only a centrifuge model with an acceleration of (Ng) (Figure 2.13c) can produce $\sigma_m = \sigma_p$.

Scaling laws for centrifuge models were discussed by Garnier et al. (2007) and a catalogue of scaling laws was prepared on behalf of the International Technical Committee, TC2. The goal of the catalogue is to provide a guide for modeling and scaling centrifuge models. The catalogue summarized the work of numerous scholars in different geotechnical study fields.

According to the catalogue, scaling factor for any quantity is marked with a star and define as the ratio of this quantity in the model to that in the prototype. These scaling laws were however derived from fundamental laws of statics. As discussed before, the main concept of the centrifuge model is to replicate the confining stress level of the field as in the following stress scaling law, σ^*:

$$\sigma^* = \frac{\sigma_m}{\sigma_p} = 1 \tag{2.32}$$

Eq. (2.32) can be re-written in as in Eq. (3.33):

$$\sigma^* = \rho^* g^* l^* \tag{2.33}$$

where ρ^* is density scaling law which is equal to (ρ_m/ρ_p), g^* is earth gravitational acceleration scaling law which is equal to (g_m/g_p), and l^* is dimension scaling law which is equal to (l_m/l_p). ρ_m, g_m, and l_m are density, earth gravity, and dimension of the model, respectively, ρ_p, g_p, and l_p are density, earth gravity, and dimension of the prototype, respectively.

The grain size effects also are considered when using centrifuge models. The following scaling laws are used when modeling (Garnier et al. 2007):

1. Bearing capacity of shallow footings:

$$\frac{B}{D_{50}} > 35 \tag{2.34}$$

where B is the diameter of circular footing or the width of strip footing, and D_{50} = mean grain size.

2. Response of piles to lateral loads:

$$\frac{B}{D_{50}} > 45 \text{ or } 60 \tag{2.35}$$

Frictional interface: In pullout loading tests, there is no significant effects on peak shear strength if the diameter of the model pile *B* satisfies:

$$\frac{B}{D_{50}} > 50 \text{ or } 100 \tag{2.36}$$

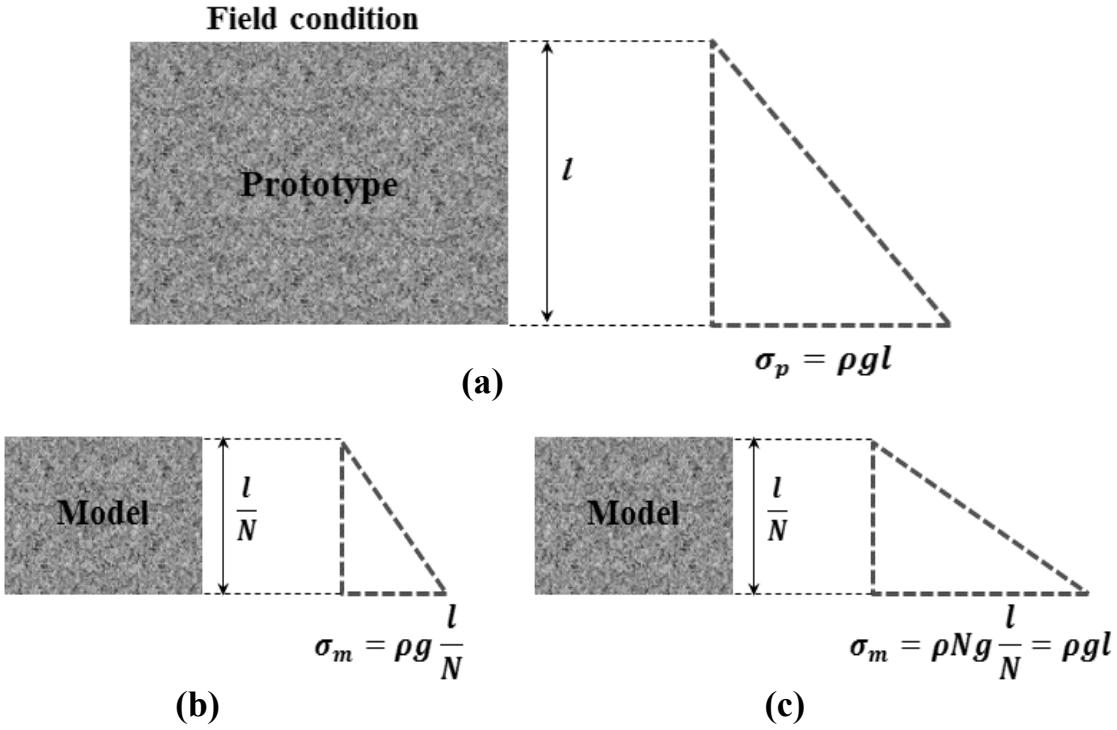

Figure 2.13 The effect of scaling on stresses of models; (a) Prototype (i.e., field condition), (b) a centrifuge model under 1*g* centrifugal acceleration, or traditional model, and (c) a centrifuge model under *Ng* centrifugal acceleration.

The interface roughness: The normalized roughness, R_n should be the same in the model and in the prototype.

$$\frac{B}{D_{50}} > 50 \text{ or } 100 \tag{2.36}$$

$$R_n = \frac{R_{max}}{D_{50}} \tag{2.37}$$

where R_{max} is maximum roughness. For perfectly rough interface, R_n is ranged from 0.1 to 1, and for perfectly smooth interface, R_n is less than 0.01.

The soil container should specify (H/2000) to keep the earth pressure coefficient at rest, K_o, close to its assumed value for no lateral strain, where H is height of wall model.

Table (2.3) gives the scale factor, N for centrifuge models that relate model to prototype quantities. These factors were derived based on assumption that both prototype and model have the same material characteristics. N is the ratio between prototype quantity to centrifuge model quantity (Avenzi and Zornberg 2002).

Centrifuge models have been extensively used to investigate the behavior of unsaturated soils as well. Such models are less cumbersome in comparison to the direct measurement of unsaturated transport properties such as the hydraulic conductivity, vapor diffusivity, retardation factors, thermal and electrical conductivities, and water potential to understand the soil-structure interaction which are recommended by ASTM D6527. Usually, long time is required to attain steady-state conditions and distributions of water because normal gravity does not provide large driving force relative to the low conductivity of unsaturated soil. In recent decades, rigorous constitutive, numerical and analytical models have also been suggested that are based on many model parameters. Obtaining these parameters is also time consuming and expensive. Centrifuge models greatly decrease the time required to reach the equilibrium condition due to magnifying the gravitational force, which acts as fluid driving force. The ASTM D6527, gives a standard test method for determining unsaturated and saturated hydraulic conductivity, k, by steady-state centrifugation. The centrifuge model is called *SSC-UFA* (steady-state centrifugation – unsaturated flow apparatus), by which flow of water or other fluid through a specimen is controlled while it is spinning in a centrifuge. The hydraulic conductivity of unsaturated soil, k of water flux, q under centripetal acceleration can be estimated using Darcy's law (Eq. 2.38).

$$q = -k\left[\frac{d\psi}{dr} - \rho_w \omega^2 r\right] \tag{2.38}$$

where r is distance from axis of rotation, ρ_w is water density, ω is rotation speed, ψ is matric potential, $d\psi/dr$ is the matric potential gradient, and ($\rho_w\omega^2 r$) is the centrifugal force per unit volume.

A rotational speed of 300 rad/min, typically assures that there is a sufficient water flux exists, the matric potential gradient can be much less than the acceleration (i.e. $d\psi/dr << \rho_w\omega^2 r$). Therefore, Darcy's law under these conditions can be rearranged to estimate the hydraulic conductivity (Eq. 2.39):

$$k = q/(\rho_w \omega^2 r) \tag{2.39}$$

Table 2.3 Scale factor for centrifuge modeling (Avenzi and Zornberg 2002).

Quantity	Prototype/Model
Length	*N*
Area	N^2
Volume	N^3
Velocity	*1*
Acceleration	*1/N*
Mass	N^3
Force	N^2
Energy	N^3
Stress	*1*
Strain	*1*
Mass density	*1*
Energy density	*1*
Time (dynamic)	*N*
Time (creep)	*1*
Time (diffusion)	N^2
Frequency	*1/N*
Pressure	*1*
Flow velocity	*1/N*
Flow quantity	*N*
Head	*N*
Capillary rise	*N*

Avanzi and Zornberg (2002) introduced four scale factors for centrifuge modeling of unsaturated soil as in Table (2.4).

Table 2.4 Scale factor for unsaturated water flow (Avanzi and Zornberg 2002).

Quantity	Prototype/Model
Suction, ψ	*1*
Unsaturated discharge velocity, *v*	*1/N*
Unsaturated flow rate, Q	*N*
Time, t	N^2

2.4.3 Pile Foundation in Unsaturated Soils

Behavior of single pile foundations in unsaturated soils have been investigated experimentally, analytically and numerically by several researchers (Georgiadis et al. 2003, Vanapalli et al 2010, Vanapalli and Taylan 2011 and 2012, Taylan 2013, Machmer 2012, Ravichandran et al. 2013, Shiekhtaheri 2014, Han et al. 2016) to name a few. However, there were very limited research studies addressed the pile group behavior in unsaturated soils to the best of the author knowledge.

Georgiadis et al. (2003) were the earliest investigators who numerically addressed the behavior of a single pile foundation in an unsaturated soil. A generalized constitutive model for unsaturated soils was suggested from this study. The model incorporates an equation for the yield and plastic potential surface, which allows simulating the behavior of piles in a wide variety of soils. The model more specifically focuses to simulate the behavior of a single pile foundation in an unsaturated layered soil upon wetting due to raising the GWT. The study concluded that that the principles of unsaturated soil mechanics provides reliable predictions in pile foundation behavior in comparison to analysis based on conventional soil mechanics principles.

Vanapalli et al. (2010) performed pile load test on Jacked mild steel open-end pipe piles embedded in saturated and unsaturated silty sand and clean concrete sand to evaluate the shaft capacity. The study concluded that the shaft capacity of the pile load tests increased under unsaturated condition for the silty sand by 35% -40% due to contribution of matric suction. The contribution of matric suction toward shaft capacity in the concrete clean sand; however, was

negligible. The result of the study were used to propose analytical model (Eq. 2.40) that takes account of matric suction contribution toward shaft capacity extending ESA.

Vanapalli and Taylan (2011) and (2012) proposed semi-empirical methods to estimate pile capacity in unsaturated Indian Head till (IHT) soil extending both ESA and TSA. The proposed methods were based on modifying the conventional β-method by Burland (1973), α-method by Skempton (1959), and λ-method by Vijayvergiya and Focht (1972). The studies included a series of single model pile load tests in a laboratory environment under saturated and unsaturated conditions to determine the influence of matric suction on the pile shaft capacity. The tests were conducted in a statically compacted fine-grained soil with different initial water contents (i.e. 13%, 16%, and 18%). A container of 300mm diameter and 300mm height was used to conduct these tests. A model pile of 20mm diameter was embedded down up to a depth of 200mm. The model pile was loaded using two rate of loading (i.e. 0.012mm/min for drained test, and 1.4 for undrained test). The tests were conducted under three different matric suction (i.e. 205, 110, and 55 kPa). The proposed models were modified by incorporating the matric suction into the original forms of β, α, and λ methods.

- Modified β-method (ESA):

$$Q_{f(us)} = Q_{fsat} + Q_{(u_a - u_w)} = [\beta \sigma'_v + (u_a - u_w) S^{\kappa} tan\, \delta'] A_s \quad (2.40)$$

where $Q_{f(us)}$ is the ultimate shaft capacity in unsaturated soil, Q_{fsat} is saturated shaft capacity, $Q_{(ua-uw)}$ is shaft capacity due the contribution of the matric suction, σ'_v is effective overburden pressure, β is Burland-Bjerrum coefficient, S is degree of saturation, and κ is fitting Parameter that is a function of plasticity index I_p, and A_s is the shaft surface area.

- Modified α-method (TSA):

$$Q_{f(us)} = \alpha c_{u(sat)} \left[1 + \frac{(u_a - u_w)}{(P_a/101.3)} (S^v)/\mu\right] A_s \quad (2.41)$$

where α is adhesion factor between soil and pile, $c_{u(sat)}$, and $c_{u(unsat)}$ are undrained shear strength under saturated and unsaturated conditions, respectively, P_a is atmospheric pressure, and v and μ are fitting parameters.

- Modified λ method (ESA and TSA):

$$Q_{f(us)} = \lambda \left[\sigma'_{v(avg)} + 2c_{u(sat)} \left[1 + \frac{(u_a - u_w)}{(P_a/101.3)} (S^v)/\mu \right] \right] A_s \quad (2.42)$$

where $\sigma'_{v(avg)}$ is the mean effective stress, and λ is frictional capacity coefficient which is a function of entire embedded depth of pile. Vijayvergiya and Focht (1972) suggested that the λ coefficient varies from 0.12 to 0.5 for pile penetration of 0 to 70 m based on 42 piles load test data.

Han et al. (2016) numerically investigated the behavior of a single friction pile in unsaturated IHT loaded under drained and undrained loading conditions. The finite element analysis (FEA) was performed considering axisymmetric model using the commercial software PLAXIS 2D to simulate the model pile behavior. The study considered the variation of shear strength and soil stiffness of soil and pile-soil interface with respect to matric suction. The results of the study were verified using model pile test results from Vanapalli and Taylan (2011) and (2012). Numerical modeling study results agreed reasonably with the measured load-settlement behavior.

The previous studies highlighted the following:

- The contribution of matric suction towards the shaft capacity is affected by the percentage of fine particles in a soil. The contribution of shaft capacity of a pile in a coarse-grained soil is limited. Such a behavior can be attributed to the rapid desaturation of coarse-grained soils since the coarse-grained soils reach the residual stage of desaturation under lower matric suction. However, if the percentage of fine particles in a soil increases, the contribution of matric suction towards pile shaft capacity increases. These observations are consistent with the shear strength behavior of unsaturated soils. According to Vanapalli et al. (1996) and Vanapalli et al. (1998), the shear strength of sand decrease in the residual stage due to low degree of saturation due to the availability of limited wetted contact area for suction transfer to the soil particles.
- The ultimate shaft capacity of a pile under unsaturated conditions is much higher in comparison to saturated conditions for both drained (i.e. ESA) and undrained (i.e. TSA) loading conditions.
- The numerical analysis showed that the conventional methods for estimating the load-settlement ($P - \delta$) behavior of pile foundations are conservative when they extended for

unsaturated fine-grained soils. In addition, the elastic-plastic Mohr-Coulomb model, which is available in the commercial software PLAXIS 2D and SIGMA/W, can be used to estimate the *p-δ* behavior of pile foundation in unsaturated soils.

Machmer (2012) conducted centrifuge pile load tests to investigate the pile behavior in unsaturated sandy soil under different degree of saturations profile (i.e. Unsat 1 and Unsat 2) (Figure 2.14), under two types of lateral loading, static cyclic loading and dynamic earthquake loading.

The tests were conducted at University of Colorado using centrifuge model and these results were simulated using finite element method. The model pile was made out of aluminum and had dimensions of 6.4mm diameter, 1.5mm thickness and 385mm length. The test container was a rigid aluminum box with inside dimensions of (30.5×122×43.5cm). Based on the type of centrifuge tests performed, they can be classified as either destructive or non-destructive. In the destructive tests, the original parameters of the soil continuously keep changing and hence is difficult to estimate or calculate them. Pile load tests are considered as destructive tests since the interaction of the soil with the pile creates a non-uniform and non-measureable soil profile around the pile. In addition, centrifuge tests are expensive and model construction is time consuming. Therefore, each centrifuge test setup was used to perform multiple tests by dividing the testing tank into three sections as follow: i) Section #1: to conduct a dynamic pile load test; ii) Section #2: to perform a static pile load test; and iii) Section #3: this section was prepared to measure the free field response of the soil under dynamic load. Ottawa sand, with a high relative density of 80% was used to perform these centrifuge tests.

The geotechnical centrifuge testing procedure in the previous study for investigating the pile behavior in unsaturated soil under static and dynamic loads was described in further detail in Ravichandran et al. (2013). The model dimensions were scaled using centrifuge scaling laws. The tests were conducted using Ottawa sand with an initial water content of 24% and degree of saturation of 28% at 50g centrifugal acceleration. The study proposed a method to control the soil moisture content during a centrifuge test, which consisted of several water sprayers that spray water from the top of the soil during the test. It was concluded from this study that the procedure adopted has limitations with the interpretation of results during long spinning duration time.

Several recommendations were suggested to overcome the limitations of associated with the testing procedures, which are summarized below:

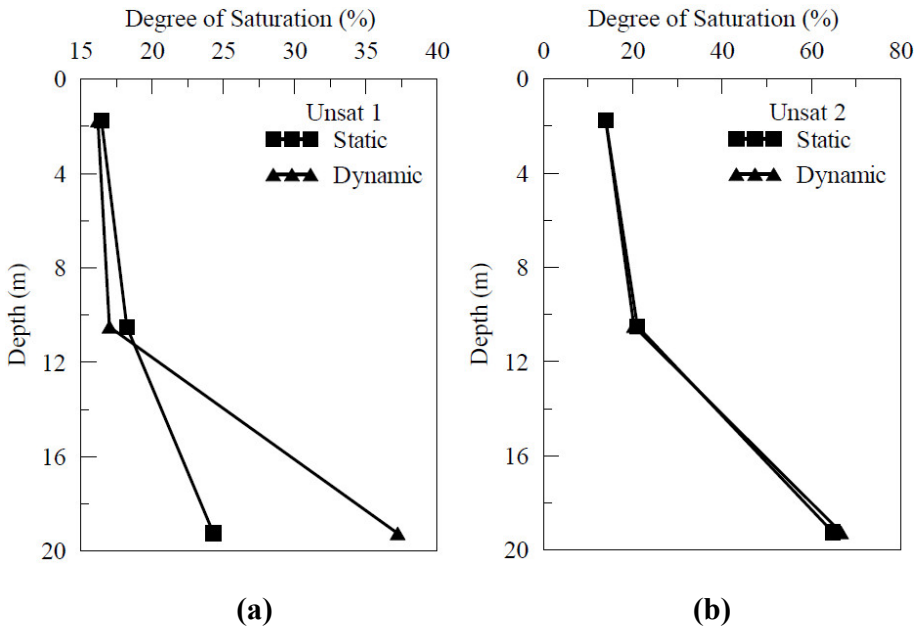

Figure 2.14 Variation of the degree of saturation with depth; (a) Unsat1, and (b) Unsat 2 (modified after Machmer 2012).

- The experimental results showed that the proposed method of water spraying from the top is relevant for obtaining reliable centrifuge test results for saturated soils. Such a technique alleviates desiccation associated with long duration of centrifuge spinning.
- A buffer layer should be applied between the drainage layer and the soil layer of interest to perform the centrifuge test under uniform degree of saturation. If such a measure is not introduced it is likely bottom of the soil which is being tested reaches saturated condition due to the capillary fringe from the drainage layer. The capillary rise can be reduced or neglect by using a gravel layer for drainage.
- The soil surface should be flattened carefully to avoid non-uniform water flow or infiltration through the weak soil-interfaces. Such a precautionary measure is useful to assure that the degree of saturation in the test sample is uniform.

Sheikhtaheri (2014) performed several single model pile load tests in two sandy soils under both saturated and unsaturated conditions. A tank, 300mm in diameter, 700mm in height, and 8mm

in thickness, was used as a soil container to perform the pile model test and determine the pile capacity in saturated and unsaturated conditions. The base of the tank has a plate with circular grooves to enable the gradual drainage of the soil. Three cylindrical solid stainless steel piles with base diameter of 38.1, 31.75, and 19.25mm and 350mm long were used in the testing program. In order to measure the pile shaft capacity, a hollow cylinder of 45mm diameter, 40mm height and 1mm thickness with holes in the bottom part was placed under the pile tip to provide free end bearing contact. In addition, the study proposed a semi-empirical model to estimate the end bearing capacity of individual piles in unsaturated soils considering the effect of matric suction (Eq. 2.43). The model was based on the conventional bearing capacity methods by Terzaghi (1943), Hansen (1970), and Janbu (1976).

$$Q_b = A_b\left(\left[c' + (u_a - u_w)_b\left(1 - S^{\psi_{BC}}\right)tan\phi' + (u_a - u_w)_{AVR}\, S^{\psi_{BC}} tan\phi'\right]N'_c\, d_c + \sigma'_{vb} N'_q d_q + \frac{1}{2} B\gamma N_\gamma\right) \quad (2.43)$$

where Q_b is pile bearing capacity, A_b is area of pile tip, $(u_a - u_w)_b$ = air-entry value (kPa), $(u_a - u_w)_{AVR}$ is average matric suction under the pile tip, N'_c, and N'_q and N'_γ, are bearing capacity factors, d_c, d_q are depth factors, σ'_{vb} is overburden pressure at the pile tip, B is pile diameter or width, and ψ_{BC} is bearing capacity fitting Parameter. A relationship between the bearing capacity fitting Parameter, ψ_{BC} and the plasticity index, I_p was proposed by Vanapalli and Mohamed (2007) based on test data results as given in eq. (2.44):

$$\psi_{BC} = 1.0 + 0.34\, I_p - 0.0031\, {I_p}^2 \quad (2.44)$$

The study concluded that the bearing capacity of single piles tested in unsaturated condition is much higher in comparison to saturated conditions due to the contribution of matric suction (Figure 2.15). In addition, the results showed that the contribution of the shaft capacity towards the pile capacity is relatively low in certain scenarios in comparison to the end pile capacity. However, the pile shaft capacity increased approximately five times under unsaturated conditions in comparison to saturated conditions.

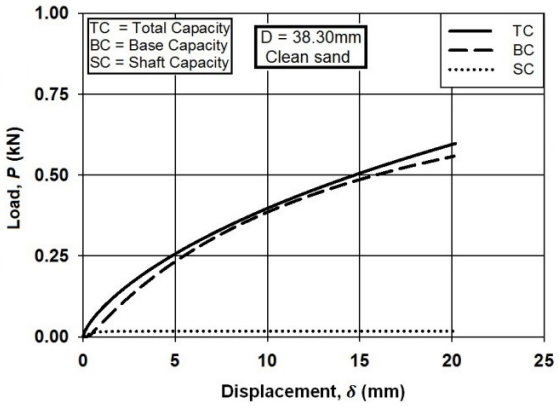

Sand #1: Sat. condition, $(u_a - u_w)_{AVR}$ = 0 kPa.

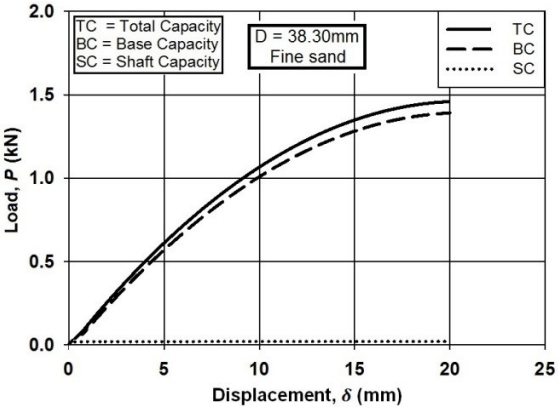

Sand #2: Sat. condition, $(u_a - u_w)_{AVR}$ = 0 kPa.

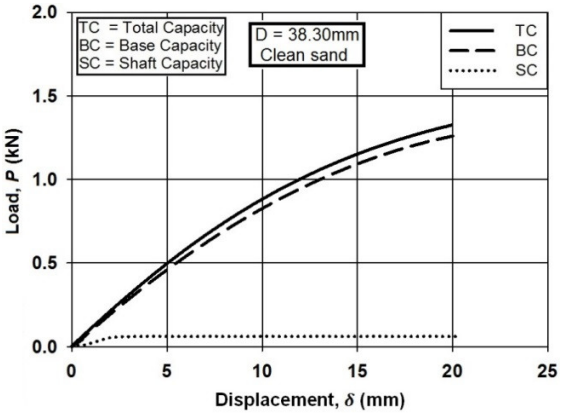

Sand #1: Unsat.condition, $(u_a - u_w)_{AVR}$ = 2 kPa.

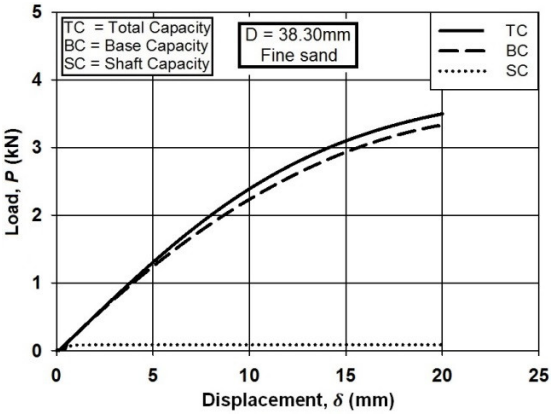

Sand #2: Unsat. condition, $(u_a - u_w)_{AVR}$ = 2 kPa.

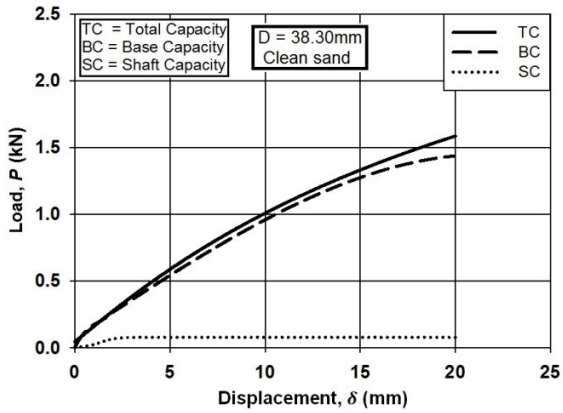

Sand #1: Unsat. condition, $(u_a - u_w)_{AVR}$ = 4 kPa.

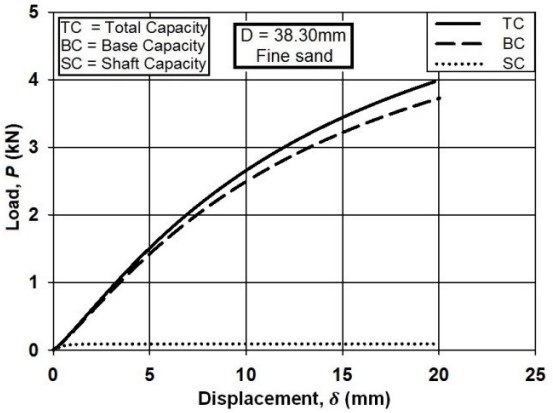

Sand #2: Unsat. condition, $(u_a - u_w)_{AVR}$ = 4 kPa.

Figure 2.15 Measured load-displacement of single model pile of diameter 38.1mm under saturated and unsaturated conditions (modified after Sheikhtaheri 2014).

2.5 Pipeline Systems

Pipeline systems are built out of polyethylene, plastic, or steel pipes that extend over several millions of kilometers to transport, distribute water, and petroleum products all over the world (Grigoryev 2006, Hopkins 2007, Gerard 2014). Pipeline systems form vital worldwide infrastructure that immensely benefit our present and future humankind energy needs. There is growing need for pipeline infrastructure to cater energy demands for all regions of the world. Stevens (2003) addressed two reasons for this need; i) Newer, more remote sources of oil and gas will be required since the presently available reserves that are close to traditional markets are gradually depleting; and ii) Changes in regulations decreased the constraints on gas markets and reinforced gas consumption in many areas. Table 2.5 summarizes some of the existing and prospective pipeline projects to highlight the key present and proposed pipeline infrastructure worldwide. Several thousands of kilometers of pipeline system will be constructed onshore all over the world in the next few decades investing several hundreds of billions of dollars. Energy piping systems generate several thousands of jobs opportunities and significantly contribute to the global economy.

Rational design of pipeline systems has been always a challenge to the structural and geotechnical engineers. For these type of systems, soil-structure interaction problems arise mainly due to the existence of two different materials next to each other (Leonards and Roy 1976).

2.5.1 Behavior of Buried Pipelines

There are two different types of pipelines: namely, rigid pipes (concrete, heavy walled cast iron pipes) and flexible pipes (polyvinyl chloride, polyethylene and steel pipes) (Moser 2001). There are fundamental differences between the behaviors of both these types of pipelines. Marston and Anderson (1913) were the first to highlight the differences between the behavior of rigid and flexible pipes by introducing a method to calculate the earth loads on buried pipes based on experimental data of testing a 36” (914.4mm) in diameter pipe. Zhao et al. (1998) stated that rigid pipelines are designed and installed to resist the applied

Table 2.5 Major present and prospective pipeline projects in different regions of the world: Investments and benefits.

Region	Investment and potential benefits	Reference
Africa	Africa is expected to become one of the most important natural gas production region in the near future to cater the needs of the world according to Energy Information Administration (EIA) (2007). There are several pipeline projects that connect North Africa to Europe. In addition, several projects are planned to transport natural gas within Africa, for example: • A 600 km pipeline project was planned by the Nigerian government to transport gas to Benin, Togo, and Ghana. The project is expected to save $500 billion in primary energy costs over a period of 20 years (Obadina 1999). • Chad-Cameroon pipeline project was constructed between 2000 and 2004 investing $3.5 billion. The pipeline project helped Chadian people to overcome poverty problems. • China invested $15 billion to construct 1500 km pipeline system in Sudan. This infrastructure facilitates to transport oil.	EIA (2007), Obadina (1999), and African Development Bank and African Union (2009).
Asia	Asian continent is the top consumer in global energy markets. According to International Energy Agency (IEA) (2008), the fast growing economy of China and India combined demand for energy will gradually increase to over 50% of the total world energy demands between 2006 and 2030. The new potential oil and gas suppliers in Central Asia (i.e. Kazakhstan, Turkmenistan, and Azerbaijan) in addition to Russia, will provide the needs for China and India by developing regional pipeline network (Chow 2010). Some of the proposed are listed below: • Eastern Siberia-Pacific Ocean oil pipeline will transport 300,000 barrels per day from Eastern Siberia, Russia to China and another 300,000 barrels per day to Japan and other Asian markets. • A pipeline project constructed by British petroleum (BP) and partners in Azerbaijan International Oil Consortium (AIOC) to transport oil from Azerbaijan to a marine terminal at Supsa in Georgia. BP and AIOC partners invested over $500 million in construction this pipeline. • Two pipeline projects transport the imported crude oil and natural gas from Middle East and Africa to Southwest China. The pipeline projects are 1,110 km (690 mile) crude oil pipeline starts from Kyaukphyu, Myanmar to China and 1807 km (1,123 mile) natural gas pipeline starts from the Bay of Bengal.	IEA (2008), and Chow et al. (2010)
Europe	For robust European Union energy market, new pipeline projects have been initiated to increase the import capacity from Africa, middle east, and Asia, and ensure stable supply of petroleum products. New pipeline projects were started by Turkey and Azerbaijan (TANAP) and Trans-Adriatic Pipeline project (TAP). Natural gas from Caspian Sea Shah Deniz fields in the east would be transported to Grecee via Turkey through TANAP. The project is expected to be completed in 2020 and will initially transport 16 billion cubic meter of gas per year with potential increase up to 31 billion cubic meter by 2026.The two projects, TANAP and TAP are to be connected in order to link Turkey with Italy through Greece and Albania. For EU, the new energy pipeline projects will provide safe routes and avoiding gas transit through Ukraine.	Bjørnmose et al. (2009), and DeMicco (2015)

Table 2.5 Continue

North America	Canada has extensive pipeline infrastructure; the value of energy transported over the Canadian pipeline system within Canada and to other export markets exceeded $100 billion annually during the period 2007 to 2012 while the annual cost of transport through the same pipelines averaged less than $5 billion. The exported energy by Canadian pipeline system contribute to approximately one fifth of Canada's total annual merchandise export revenues (Benoit, 2012). According to Canadian Energy Pipeline Association (CEPA) (2005), a hypothetical new natural gas pipeline investment of $1.52 billion, 1000 km located half in Alberta and half in British Columbia provinces would increase the Canadian gross domestic product (GDP) in the order of $1.2 billion. The new pipeline project would create several thousands of jobs in Alberta and British Columbia in addition to Ontario, Quebec, Saskatchewan, and Manitoba provinces. Furthermore, delaying the new pipeline construction would yield that the costs to the Canadian natural gas consumers could be as much as $57.5 billion over the period from 2006 to 2025 based on a constant 2005 dollar value. USA is the largest natural gas producer at 65 billion cubic feet per day. In addition, USA has achieved remarkable improvement in crude oil production capacity growth, adding 1.2 million barrels per day of capacity over the 2008-2012 period (Fullenbaum et al. 2013). The USA natural gas and oil pipeline system is the largest pipeline network with 4.18 million km (2.6 million miles) that carries 14 billion barrels of crude oil and about 25 trillion cubic feet of natural gas in 2012 (Gerard 2014). New pipeline projects are needed to support the large amounts of domestically produced energy and alleviate chokepoints that prevent efficient and timely delivery of energy resources. Keystone XL pipeline project, for example, between USA and Canada is a promising project. The proposed pipeline starts from Alberta and ends at Nebraska and pass through Saskatchewan in Canada and Montana, and South Dakota in USA. The Keystone XL pipeline will serve to transport up to 830,000 barrels of oil per day from Canada and America's Bakken Shale formation to USA (Gerard 2014). Keystone XL pipeline construction will create 42,000 job opportunities and provide $2 billion in workers pockets over two years.	Benoit (2012), CEPA (2005), Fullenbaum et al., (2013), Gerard (2014)
Middle East	Middle East region has significant oil and gas resources. According to the Organization of the Petroleum Exporting Countries (OPEC) (2015) around 23.5 million barrel per day (i.e. 20% of world oil production) is pumped from this region and around 800 billion barrels are reserved in this region out of around 1,493 billion barrels world proven crude oil reserves based on 2014 statistics. In addition, around 625,800 million cubic meters of natural gas were produced in 2014 and 80,109 billion cubic meter are reserved. The region suffered from several conflicts and political disturbances which threatened the flowing of petroleum products to the world markets. The vulnerability of the energy transportation systems in the region led to propose several new pipeline projects, for example (Mills 2016): • Ras Markaz pipeline project that is connected to export terminal and oil storage park near the port of Duqm in Oman. The project will offer an outlet to the Indian Ocean. • Haditha-Jordan pipeline project in Iraq. This project would help to reduce the dependence of Iraqi petroleum industry on the vulnerable Basra terminals and the Gulf and Strait of Hormuz. • Khurmala-Fishkhabour pipeline project in Iraq's Kurdistan region. • Another pipeline project in Iran is proposed to transport oil from Neka on the Caspian Sea to Jask on the Arabian Sea.	OPEC (2015), Mills (2016)

loads while flexible pipelines carry only a small portion and the major portion of the applied loads will be carried by the surrounding soil. Figure 2.16 shows the deformation in the soil cover or backfill above and around the pipeline. For a flexible pipe, the backfill settles and a dip would appear due to pipe deformation, while a hump or soil crack may be seen above and under undeformed rigid pipe.

The wall stresses for rigid pipes due to external and internal loads combination is a critical factor that controls the rigid pipeline behavior. Rigid pipe ring shows two distinct modes of deflection under the applied pressure; elastic and segmental deflection. The elastic deformation is very small and can be neglected for rigid pipes. On the other hand, the stiffness of flexible pipe to resist the ring deflection is more crucial (Moser 2001). Leonards and Roy (1976) stated that the behavior of commonly used materials for pipes such as steel, aluminum or concrete is linearly elastic in both compression and tension up to the yield point and it is reasonable to assume that material properties remain constant (i.e. Young's modulus and Poisson's ratio). In addition, they stated that concrete pipes (rigid pipes) developed cracks before collapse while steel pipes yield.

Almahakeri et al. (2012) investigated experimentally and numerically the flexural behavior of buried pipes in dense sand using three pipes (102mm nominal diameter and 1.83 m long) of different materials, steel and then glass-fiber reinforced polymers (GFRP). Fifteen tests were carried out with different burial depth-to-diameter ratio (H/D = 3, 5, and 7) considering commonly used shallow to deep burial depth in energy pipeline construction. The results of their study showed the GFRP pipes demonstrated higher flexibility in longitudinal bending in comparison to steel pipes. Such a behavior can be attributed to the variance in stiffness that yields limited failure zone in soil body for the GFRP pipes in comparison to steel pipes.

For better understanding the behavior of a buried flexible pipeline, different loading scenarios are shown in Figures 2.17 and 2.18 (Bickel et al. 2004). For unconfined or unburied pipelines with an adequate thickness under a uniform radial load, the pipeline shrinks slightly due to axial shortening but remain circular (Fig 2.17*a*). However, if the same pipeline is subjected to a concentrated load on the crown and invert, it will extensively

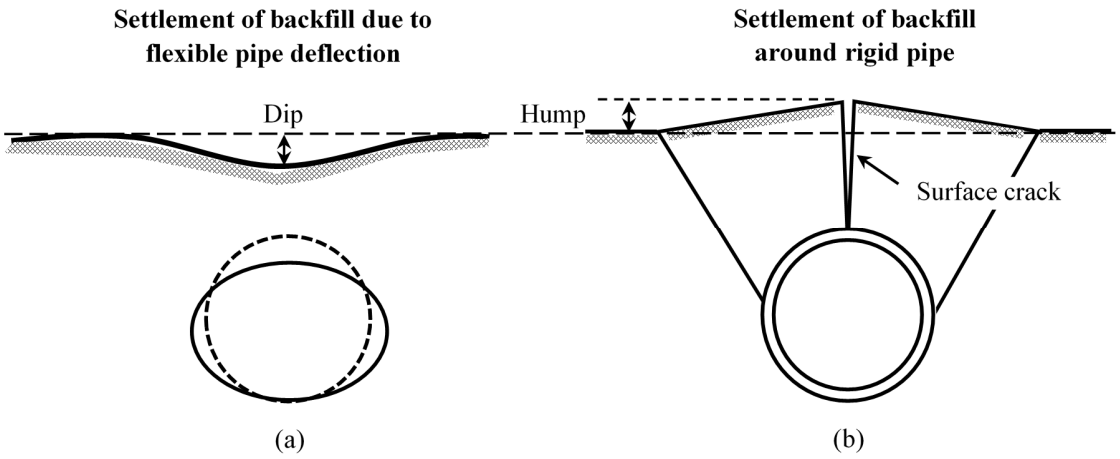

Figure 2.16 Backfill deformation; (a) Flexible pipe, and (b) Rigid pipe (modified after Watkins and Anderson, 2000).

bulge inward at these points and outward at the springline (Fig. 2.17*b*). If a partially confined pipeline, such as in case of partially buried pipes, is subjected to local active stress at crown and invert (Figure 2.18*a*), passive pressure is developed at the springline which reduces the outward and inward bulge of the pipeline greatly. The inward and outward bulging due to passive pressure further reduces around the perimeter in the confined pipelines (i.e. fully buried pipeline) (Figure 2.18*b*). For a general scenario, Figure (2.18*c*) shows a non-uniform active pressure acting on a fully confined pipeline. For this case, the passive pressure is distributed relatively uniformly and the pipeline distorted slightly and smoothly.

BS EN 1295-1(1998) and Canadian Standards Association (CSA), Z662-11(2012) summarize two different limit states for oil and gas pipeline systems: i) Ultimate Limit State (ULS) takes into account of in burst or collapse of pipeline systems leading to safety hazards which include rupture, yielding caused by primary loads, buckling resulting in collapse or rupture, and fatigue; and ii) Serviceability Limit State (SLS) relates to design and service requirements (i.e. restrict normal operation or affect durability) of pipeline systems without resulting in yielding caused by secondary loads, and buckling not resulting in collapse. In addition, CSA Z662-11(2012) defines Leakage Limit State (LLS) as a leak of less than 10mm in diameter that results in insignificant safety hazard due to limited loss of contaminant. Table (2.6) summarizes key information derived from several specifications, standards and design codes regarding the behavior of rigid and flexible pipes (i.e. The American Petroleum Institute (API), International Organization

for Standardization (ISO), American Society for Mechanical Engineering (ASME), American Standards for Testing Methods (ASTM), Ontario Provincial Standard Specification (OPSS), Det Norske Veritas Offshore Standards (DNV)).

Marston and Anderson (1913) introduced a theoretical framework to determine the earth pressure on a buried pipe in a trench extending the following assumptions: i) a prism of soil imposes a load on the pipe, ii) the settlement of backfill and pipe generates shearing or friction forces at the sides of the trench, and iii) cohesion is negligible since considerable time would have to pass before the backfill soil can develop cohesion which would cause the maximum load on pipe (Moser 2001). Spangler (1941) extended the theory of elasticity to propose a model to estimate elastic deflection of pipe ring considering elastic ring and elastic soil. Spanglar's Iowa equation (Eq. 2.45) was originally developed to estimate flexible pipe ring deflection. This equation is also applicable to estimate the elastic deflection of rigid pipes.

$$\Delta x = \frac{D_l K P}{\frac{\left(E_p I\right)_{eq}}{r^3} + 0.061 E'} \tag{2.45}$$

where Δx is horizontal ring deflection , P is vertical soil pressure, E_P is modulus of elasticity of pipe material, I is moment of inertia of pipe wall is $t^3/12$ for plain wall pipe, t is wall thickness of the pipe, r is radius is $D/2$, D is outer diameter, D_l is deflection lag factor, K is bedding constant, and E' is horizontal modulus of soil reaction. More information on these parameters can be found in literature (i.e. Zhao et al. 1998, Watkins and Anderson 2000, Moser 2001).

Table 2.6 Key specifications for rigid and flexible pipes summarized from different standards, specifications and design codes.

Pipe type	Standards, Specifications and Design codes	Specifications for flexible or rigid pipes
Flexible	API 17J, 2009, ISO 13628-2, 2006, and API 17k, 2002.	• Flexible pipe body is composed of a composite of layered materials that form a pressure-containing conduit and pipe structure allows large deflection without a significant increase in bending stress. Flexible pipes can be subdivided into: • Unbonded flexible pipes: the maximum allowable bending strain for polyethylene, PE and polyamide, PA 7.7%, for polyvinylidene flouoride, PVDF is 7% in static applications and for storage in dynamic applications, and 3.5% for operation in dynamic applications. For other polymer materials, the allowable strain will be as specified by the manufacturer. Refer to Table 6 in API 17J and ISO 13628-2. • Bonded flexible pipes, the maximum allowable strain for elastomer material is 50% of design maximum strain for aged material. Refer to Table 7 in API 17K.
	API 17B, 2002, and ISO 13628-11, 2007.	• This recommendation practice defines flexible pipe as a pipe with low bending stiffness and high axial tensile stiffness. These requirements can be achieved by using a composite pipe wall construction of helical armoring layers and polymer sealing. However, flexible pipes are designed to serve particular requirements for different projects and there is no specific or standard products. • Flexible pipe should be designed to prevent failure due to the combined effect of internal pressure, external pressure, torsional forces, axial forces, and bending. • Flexible pipes have internal diameters usually range from 0.05 to 0.5m (2 to 20inches). However, in some cases internal diameter can reach up to 0.914m (36inches) for low-pressure bonded flexible pipes such as oil suction and discharge hoses.
	ASTM F1668-08, 2016.	• Flexible pipes that are typically designed to rely on the stiffness of the soil surrounding them for support and transmit load on pipe to the soil at the side, such as thermoplastic and fiberglass. • Deflection of buried pipe may be expressed in general terms as : *Pipe deflection = load on pipe / (pipe stiffness + soil stiffness)* • The maximum deflection of buried flexible pipe is derived from both structural consideration include pipe cracking, yielding, strength, strain, and local deflection, and practical consideration include such factors as flow requirements, clearance for inspection and cleaning, and maintenance of joint seals.
	OPSS 401, 2013, and OPSS 421, 2013.	Flexible pipe diameter or span should not vary from the manufactured dimensions by more than 5% during cover and backfill placing operations.
Rigid	BS EN-1295-1, 1998.	Pipe types can be specified based on the relative pipe and surrounding soil stiffness which is useful in the evaluation of the backfill load, and the type of the material from which the pipe is made. For example, pipes that are fabricated of material fractured under small deformations are referred as rigid pipes.
	OPSS 401, 2013.	For rigid pipes, 2% deflection is the maximum deflection that rigid pipelines can sustain without cracks while flexible pipelines can deflect more than 2% safely.
	DNV-OS-F101, 2013, and DNV-RP-F116, 2009.	• Rigid pipes can be fabricated of carbons steel, stainless steel, clad-pipe. • The maximum accumulated nominal plastic strains should not exceed 2%. • The yield stress, YS of rigid steel pipe is defined as the stress at which the total strain is 0.5% (Figure 2.19). The tensile strains should not increase 0.4%.

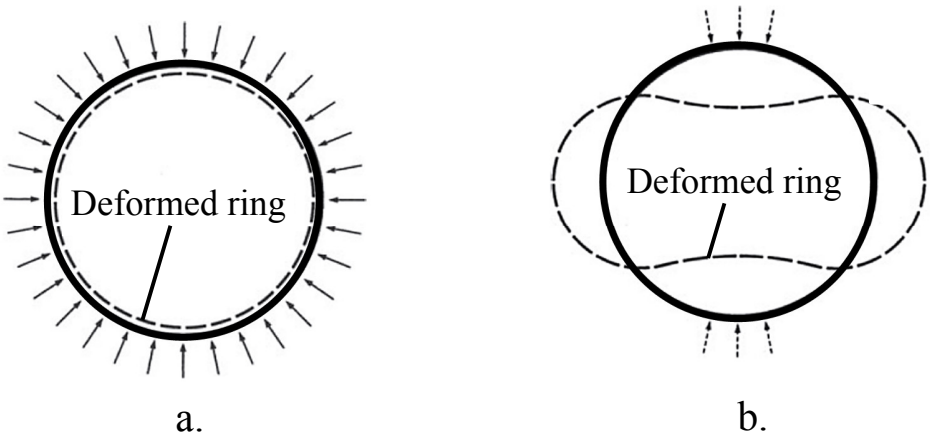

Figure 2.17 Unconfined pipeline deformation under; (a) uniform radial load, and (b) active load at crown and invert (modified after Bickel et al. 2004).

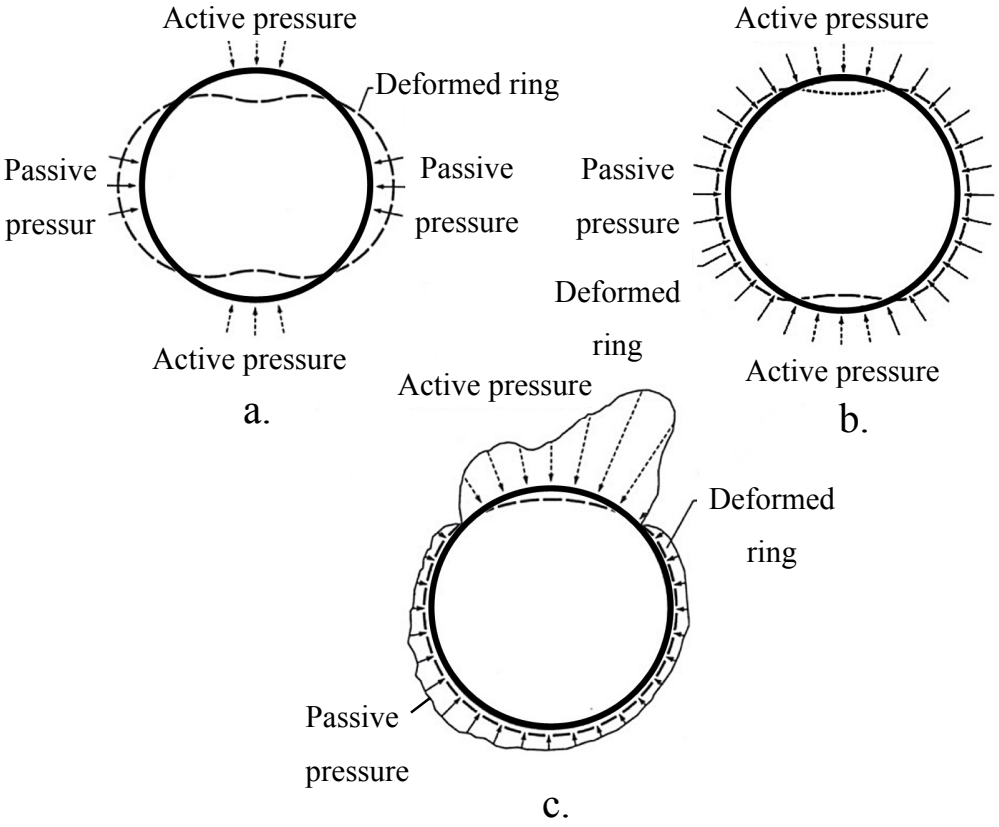

Figure 2.18 Pipeline deformation under; (a) partial confinement with local active pressure at the crown and the invert, (b) full confinement with local active pressure at the crown and the invert, and (c) full confinement with non-uniform active pressure (modified after Bickel et al. 2004).

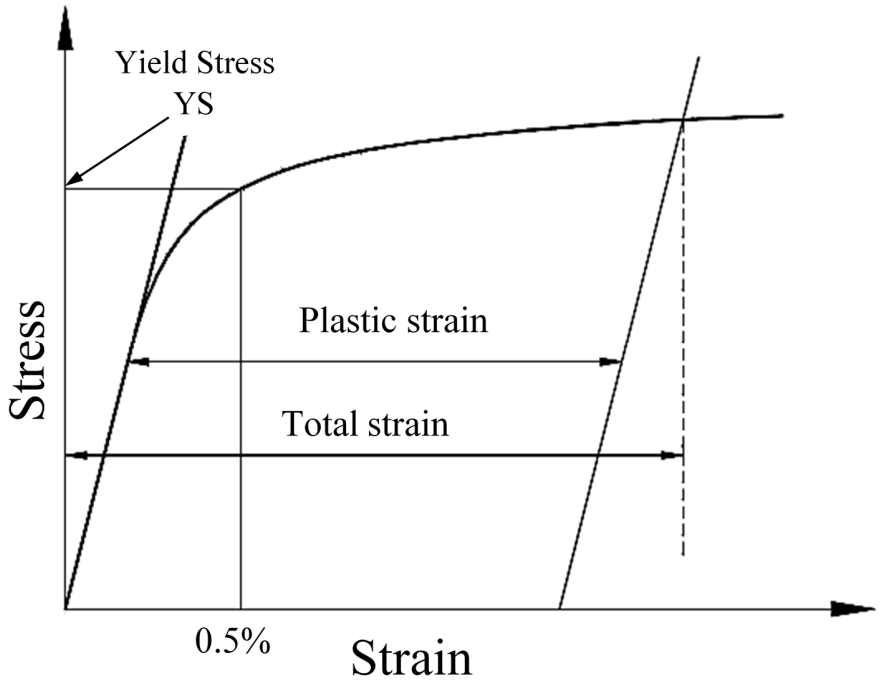

Figure 2.19 Stress-strain curve for steel (modified after DNV-OS-F101 2013).

2.5.2 Behavior of Buried Pipelines in Unsaturated Soil

Most of the previous studies published in the literature focused on the behavior of buried pipelines considering saturated soil conditions ignoring the influence of unsaturated soil zone above the GWT (Marston and Anderson 1913, Spangler 1941, Leonards and Roy 1976, Crofts et al. 1977, Chard and Symons 1982, Attewell and Woodman 1982, Suleiman 2002, Wijewickreme et al. 2009, Dilrukshi and Wijewickreme 2014, Kouretzis et al. 2014, Chaloulos et al. 2015). For example, Crofts et al. (1977) proposed a method to estimate the short and long-term strains developed in the pipelines associated with soil excavation activity considering the distance from unsupported trench, depth of trench and bracing. The proposed method was developed extending saturated soil mechanics. However, in their study, they highlighted the significant effect of soil wetting due to rain and flood toward soil stiffness and shear strength. The study indirectly referred to change in soil-pipeline system behavior upon wetting due to reduction in soil stiffness and shear strength. In other words, the soil stiffness and strength are the two key parameters that control the pipeline system behavior, which is buried in soils that are typically in a state of unsaturated condition during most of its design life period. There has been recent research interest, particularly during the last

decade, to investigate the behavior of buried pipelines in unsaturated soils (O'Rourke et al. 2008, Olson 2009, O'Rourke 2010, Jung et al. 2013, Saadeldin et al. 2015, and Robert et al. 2016). These studies highlight the need for better understanding the behavior of soil-pipeline system buried in unsaturated soils for different loading conditions.

As discussed earlier, the engineering behavior of unsaturated soils can be rationally interpreted in terms of two stress state variables; namely, the net normal stress ($\sigma - u_a$), and matric suction ($u_a - u_w$) (Fredlund and Morgenstern 1977). Soil suction is an energy potential with a tension stress on soil skeleton holding the soil particles and their packets together providing resistance to elastic and plastic deformations resulting from soil particles and their packets distortion and sliding, respectively (Han et al. 2016). Loss of soil suction due to an increase in degree of saturation, which is associated with an increase in the soil water content leads to reduction in soil stiffness and shear strength. Georgiadis et al. (2003) pointed out that the vadose zone (i.e. unsaturated zone above the GWT) is significantly affected by the variation of the GWT. They studied the effect of GWT depth towards the behavior of pile foundation that is originally installed totally or partially above GWT. They concluded that upon GWT rise, excessive settlement of pile foundation could be expected without any change in the applied load. In other words, the shear strength and stiffness of the supporting soil decreases due to loss of soil matric suction associated with an increase in the moisture content.

Recent experimental and numerical studies have highlighted significant differences in the behavior of buried pipelines in saturated and unsaturated soils due to the influence of capillary stresses (i.e. ($u_a - u_w$)) in vadose zone (O'Rourke et al. 2008, Olson 2009, O'Rourke 2010, Jung et al. 2013, Robert et al. 2014, Saadeldin et al. 2015, Robert et al. 2016). These studies suggested that there is less deformation to the soil around the pipeline system in unsaturated soils in comparison to saturated soils.

O'Rourke et al. (2008) conducted a large-scale test to simulate the performance of highly ductile pipelines during sudden ground deformation similar to landslide, surface faulting, or ground rupture induced by an earthquake. Several large-scale tests were conducted in unsaturated sand compacted with water content (w) in the range from 4.0 to 5.0% which corresponds to the residual water content. At this value of water content, there is no continuity in the water phase and change in soil suction will not result in significant change in water content (Fredlund and Rahardjo

1993, Fredlund and Xing 1994, Vanapalli et al 1998). At this stage, the residual amount of water remains primarily in the form of thin films surrounding the soil particle surface and has very limited effect towards inter-particle suction stress (Lu et al. 2009). The tests were performed on a high-density polyethylene (HDPE) pipeline of diameter of 407mm with a wall thickness of 24mm subjected to 1.22m of strike-slip displacement at a crossing angle of 65^0. The exerted stresses (i.e. shear stress and normal stress) on the pipe body and associated strains (i.e. axial and bending strains) were recorded using tactile force sensors, which are a thin, wide and flexible array of small sensors embedded in polymeric sheet or pad wrapped around the pipe, and strain gages, respectively. The results of their study conclude that there is no significant difference in the maximum horizontal force between dry condition and unsaturated condition in the residual state.

In the last few decades, the behavior of many soil-structure interaction problems (i.e. shallow and deep foundations, soil nails, pavement design, retaining wall, etc.) have been extensively investigated and interpreted utilizing the soil-water characteristic curve (SWCC), which is a relationship between the degree of saturation (S), gravimetric water content (w), or volumetric water content (θ) and soil suction (for example, Oloo et al. 1997, Costa et al. 2003, Vanapalli and Mohamed 2007, Rojas et al. 2007, Hamid and Miller 2009, Gurpersaud et al. 2011, Vanapalli and Taylan 2012, Wuttke et al. 2013, Al-Khazaali and Vanapalli 2015, Vo and Russell 2016). Similar approaches may be proposed to relate the behavior of buried pipelines in unsaturated soil to the SWCC and extend the principles of unsaturated soil mechanics in pipeline engineering practice applications.

Salaadin et al. (2015) proposed a numerical model to investigate the elastic deformation of a buried rigid and flexible pipes in unsaturated soil by extending the principles of two stress state variables (i.e. net normal stress, $(\sigma - u_a)$, and matric suction $(u_a - u_w)$). A parametric study was conducted considering the influence of different loading conditions, burial depth, end fixity, pipeline rigidity and water content. Hypothetical pipeline of 0.15 m diameter, 6.5 m length buried in Regina soil was considered in their study. Regina soil is a native expansive clay deposit of Regina city, Saskatchewan, Canada. This soil was chosen because of the continuous volume changes especially in the active zone (i.e. assumed active zone = 4 m) due to seasonal changes. The soil was assumed to have initial constant suction in the active zone equal to 2000 kPa and subject to increase in water content due to precipitation that cause a constant reduction in the initial

suction (i.e. 1000, 500, 180, and 38 kPa) and produce heave in the soil that affect the pipeline. The study concluded that significant increase in upward displacement of pipeline is associated with reduction of soil suction for different depths of burial. In addition, the vertical displacement of the pipeline is highly influenced by burial depth.

Robert et al. (2016) conducted a parametric study to determine the behavior of buried pipe subjected to strike-slip fault movement in unsaturated sand. The study considered different initial soil condition (i.e. sand type, density, and water content), pipe material, pipe burial depth, and pipeline-fault-rupture inclination. The study concluded that at low confining stress level, unsaturated condition of coarse-grained soil has more impact on buried pipelines and can cause more damages in comparison to saturated and dry conditions due to the contribution of capillarity towards shear strength and stiffness of unsaturated sand. The strains resulted from pipe loading in unsaturated sand are higher in comparison to saturated and dry conditions due to higher soil strength.

The key conclusion that can be derived based on the discussion of previous studies results published in the literature is that for reliable estimation of the external and internal forces and deformations of the soil-pipeline systems buried in unsaturated zone, the contribution of soil suction should be taken into account in the analyses. However, studies along this direction are limited in the literature.

CHAPTER THREE

A NOVEL EXPERIMENTAL TECHNIQUE TO INVESTIGATE UNSATURATED SOIL-STRUCTURE INTERACTION BEHAVIOR IN SATURATED AND UNSATURATED SANDS

3.0 Background-Information

The contents presented in this chapter are from the manuscripts of the publications summarized below:

Al-Khazaali, M., and Vanapalli, S.K. (2018). Axial force-displacement behaviour of a buried pipeline in saturated and unsaturated sand. *Géotechnique.* DOI: 10.1680/jgeot.17.p.116.
Al-Khazaali, M., and Vanapalli, S.K. (2018). A novel experimental technique to investigate unsaturated soil-pipeline interaction under axial loading in saturated and unsaturated sands. *Geotechnical Testing Journal*, *ASTM.* DOI: 10.1520/GTJ20180059.
Al-Khazaali, M., and Vanapalli, S.K. (2018). Modelling the elastic axial force-displacement behaviour of a buried pipeline subjected to permanent ground deformation. *In Proc. of the 7thInt. Conf. Unsaturated soils*, Hong Kong.

3.1 Introduction

Energy pipeline system forms key infrastructure and serves not only the many needs of human population but also contributes significantly to the global economy in general and North America in particular. USA has the largest pipeline network with 4.18 million km (2.6 million miles) that carries 14 billion barrels of crude oil and about 25 trillion cubic feet of natural gas in 2012 (Gerard 2014). With over 100,000 km, the Canadian pipeline infrastructure transports over $100 billion worth energy products annually to Canadian and international markets with less than $5 billion operation cost for the 2007 to 2012 period. The value of the exported energy contribute to

approximately one fifth of Canada's total annual merchandise export revenues (Benoit 2012). Rapid growth in petroleum industry during the last decade has supported many new pipeline projects all over the world with investments of several hundreds of billions of US dollars (Obadina 1999, Bjørnmose et al. 2009, Chow et al. 2010, Benoit 2012, Fullenbaum et al. 2013, Gerard 2014, DeMicco 2015, Mills 2016). For example, the proposed Keystone XL pipeline projects between the USA and Canada that starts from Alberta and ends at Nebraska passing through Saskatchewan in Canada and Montana, and South Dakota in USA. This project will significantly support the domestically produced energy and efficiently deliver the increasing demand of energy resources. The project once completed is expected to transport up to 830,000 barrels of oil per day from Canada and America's Bakken Shale formation to USA and is expected to create 42,000 job opportunities and provide $2 billion as wages to workers over two years (Gerard 2014).

Limit state approaches are conventionally used in the design and analyzes of underground pipeline systems to ensure safety and serviceability. These approaches are subdivided into: i) Ultimate Limit States (ULS) which can be defined as the design approach that takes into account of safety, such as soil stability problems, and ii) Serviceability Limit States (SLS) which takes into account the functional performance under various loading conditions extending theory of elasticity (Allen 1975, Meyerhof 1995, Griffis 2003). According to BS EN 1997-1:2004 (2004), design assumptions should account for the most unfavorable groundwater condition during the design lifetime of the structure for ULS or in normal circumstances for SLS. In other words, design procedures should consider the soil is in a state of fully saturated condition and groundwater table (GWT) has to be assumed to be at the natural ground level.

As the presently available oil and gas reserves that are close to traditional markets are depleting, newer and more remote sources are required (Stevens 2003). It is most likely that several of these markets would be located in semi-arid and arid regions with soils that are typically categorized as unsaturated soils. In addition, due to global warming effects, about half of the world regions are likely to experience more evaporation rather than water infiltration that contributes to develop a surficial unsaturated soil stratum that extends to more than 3m from the natural ground surface. Pipeline systems are typically buried, as recommended by BS EN 14161:2003 (BSI 2003), at depths greater than 0.8 to 1.2m from the soil surface to avoid any interference with human activities. At such shallow depths, pipeline systems are most likely buried above the natural groundwater table, where the soil is typically found in a state of unsaturated condition. The

mechanical properties of soil and interface (i.e. shear strength, volume change and stiffness), as discussed earlier, and hence the behavior soil-pipeline system, are stress level dependent. For saturated condition, overburden pressure is the sole governing stress that contributes to the soil-pipeline system behavior. However, for an unsaturated soil, both $(\sigma - u_a)$ and $(u_a - u_w)$ contribute independently to the load-displacement behavior of pipeline system. At greater depth, the overburden pressure or $(\sigma - u_a)$ level is significant comparing to $(u_a - u_w)$. At such depths, the contribution of $(u_a - u_w)$ towards mechanical properties of soil and interface is limited in comparison to $(\sigma - u_a)$. However, at shallow depths (i.e. 0.8 to 1.2 m), the contribution of $(u_a - u_w)$ is substantial since the $(\sigma - u_a)$ level is low to moderate.

The recommended analysis and design procedures by design codes such as American Society of Civil Engineers (ASCE) (1984), American Life Alliance (ALA) (2001), ALA (2005), Indian Institution of Technology Kanpur Guidelines for Seismic Design of Buried Pipelines (IITK-GSDMA) (2007), and Pipeline Research Council International (PRCI) (2009) are based on saturated soil mechanics principles. For this reason, they are not able to capture influence of the capillary stress or matric suction, $(u_a - u_w)$ on the unsaturated soil-pipeline system behavior. The mechanical properties of both, soil and interface (i.e. shear strength and stiffness) for unsaturated condition were found to be much higher than saturated condition especially in the boundary effect and transition zones of unsaturated soils (Fredlund et al. 1996, Vanapalli et al, 1996, Hamid and Miller 2009, Oh and Vanapalli 2009, Lu and Kaya 2014). Experimental and numerical evidences reported in recent studies suggested that pipeline systems buried in unsaturated soil experience much higher internal forces and deformations due to relative soil mass movement with respect to pipeline (Saadeldin et al. 2015, Robert et al. 2016, Al-Khazaali et al. 2016). Therefore, it is rational to design and analyse pipeline systems extending the principles of unsaturated soil mechanics rather than conventional saturated soil mechanics.

Experimental, numerical and analytical studies contribute to rigorous evaluation of the soil-structure interaction problems in unsaturated soils. In the present study, an experimental technique is proposed to achieve reliable soil-matric suction profile under a controlled environment in the laboratory. The proposed experimental technique was used to investigate the axial force-displacement behavior of a buried prototype pipe under different $(u_a - u_w)$ values in sand. The test results suggest that the axial force and stresses exerted on the prototype pipe due to relative

movement of the pipe with respect to soil is significantly higher for unsaturated condition in comparison to saturated condition. The experimental results were further numerically verified using commercial finite element software, SIGMA/W. The modelled behavior shows reasonable comparisons with the measured elastic axial force-displacement behavior of the pipelines in sandy soils.

3.2 Background

Longitudinal permanent ground deformation (PGD) or soil mass movement along pipeline axis is typically induced by soil subsidence, landslides, liquefaction triggered by seismic loads, faults, frost heave or thaw settlement and can result in extremely high axial forces on pipeline body and likely contribute to severe damages (Figure 3.1). Such damages in non-seismically designed pipes are estimated to be approximately 5 to 10 times higher than corresponding damages due to transverse PGD because of the higher flexibility to bending then axial tension or compression (ALA 2005).

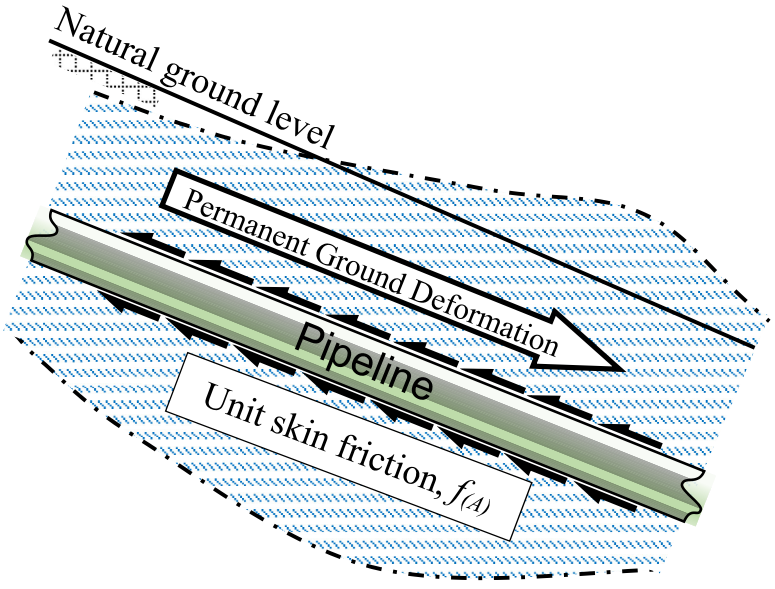

Figure 3.1 Pipeline subjected to PGD parallel to its axis.

The mechanism of mobilizing skin friction along pipeline body is similar to the skin friction in a pile foundation for both effective (ESA) and total (TSA) stress analyses. The maximum unit skin friction, $f_{(A)}$ exerted on a pipeline is a function of the mechanical properties (i.e. shear strength and stiffness) of soil and interface. Conventionally, $f_{(A)}$ is estimated considering drained loading condition (i.e., ESA) using the modified β-method by Burland (1973) and undrained loading condition (i.e., TSA) using the modified α-method by Skempton (1959) (ASCE 1984, ALA 2001, ALA 2005, IITK-GSDMA 2007, PRCI 2009, Wijewickreme et al. 2009). These models are applicable for saturated soils. However, evaluation of buried pipeline behavior requires rational determination or estimation of the mechanical properties of soil and the soil-pipeline interface. The presence of a pipeline system in the vadose zone during their service life highlights the need to consider the capillary stresses on the mechanical behavior of the soil-pipeline system.

The unsaturated shear strength, τ_{unsat} and stiffness E_{unsat} for soil and interface vary with the net normal stress, $(\sigma - u_a)$ and capillary (matric) suction, $(u_a - u_w)$. Several investigators studies support with these conclusions (for example, Bishop 1959, Fredlund et al. 1987, Sawangsuriya et al. 2009, Hamid and Miller 2009, Oh et al. 2009, Vanapalli and Oh 2010, Rahardjo et al. 2011, Lu and Kaya 2014, Hossain and Yin 2014, Adem and Vanapalli 2014, Borana et al. 2016). The soil moisture regime variation associated with environmental factors contributes to variations in soil suction. The engineering behavior of unsaturated soils can be rationally interpreted extending the principles of unsaturated soil mechanics in terms of two independent stress state variables (i.e., $(\sigma - u_a)$ and $(u_a - u_w)$). Experimental methods are time consuming and expensive; for this reason, the soil-water characteristic curve (SWCC) has been used as tool for interpreting and predicting the unsaturated soils behavior (Fredlund and Rahardjo 1993). The SWCC, which is a relationship between the soil degree of saturation and suction, has three distinctive zones of unsaturated condition (Figure 3.7). These zones are: i) Boundary effect zone in which the soil is essentially saturated up to the air entry value (AEV); ii) Transition zone where the soil starts desaturating and moisture content decreases significantly with increasing in suction; and, iii) Residual zone in which the wetted area is minimal and large changes in soil suction result in only small changes in water content (Vanapalli et al. 1996). The variation of τ_{unsat} with respect to matric suction is accounted by ϕ^b, which is defined as angle of internal friction with respect to $(u_a - u_w)$ under a constant $(\sigma - u_a)$. The τ_{unsat} increases linearly up to the AEV in the boundary effect zone with $\phi^b =$

ϕ'. In the transition and residual zones, variation of τ_{unsat} with $(u_a - u_w)$ is nonlinear with $\phi^b < \phi'$ (Vanapalli 2009).

For unsaturated interface, Hamid and Miller (2009) reported that $(u_a - u_w)$ contributes to the peak shear strength of unsaturated interface and has limited contribution beyond post-peak ultimate shear strength. Moreover, Hossain and Yin (2014) stated that both $(\sigma - u_a)$ and $(u_a - u_w)$ have significant influence on unsaturated interface dilation behavior. At lower $(\sigma - u_a)$, the unsaturated interface exhibit remarkable dilation and result in strain-hardening behavior in the pre-peak zone of the shear strength while at higher $(\sigma - u_a)$, the contribution of $(u_a - u_w)$ towards the unsaturated interface dilation is minimal. Therefore, it is essential to re-evaluate the available design procedures of pipeline systems, which are typical examples of unsaturated interface based on experimental and numerical investigations extending the state-of-the art of the mechanics of unsaturated soil.

The design of a testing equipment requires considering different factors for reliably interpret the behavior of a physical model. The stress interference that develops due to the model interaction with the soil and the adjacent physical boundaries is a significant concern that should be considered in the investigation of the performance of geostructures. Yet, considering the stress interference by itself is not sufficient for proposing reliable design procedures. It is important to mimic the soil condition considering the influence of key environmental factors. This objective has been a goal for different researchers to achieve a reliable soil-suction profile to simulate the soil condition (i.e. saturated and unsaturated condition). For example, O'Rourke et al. (2008) studied the behavior of pipeline systems during sudden ground deformation, which is similar to landslide, surface faulting, or ground rupture induced by an earthquake. They conducted a full-scale test in a specially designed large-scale tank filled with unsaturated sand. The sand was mixed with a water content of 4.0 to 5.0% which corresponds to the residual water content, as was estimated from the SWCC, before compacting it in the box. Based on their comprehensive experimental studies, they concluded that forces on the pipe under unsaturated condition are comparable to that of dry condition. In addition, they suggested that this behavior is similar to that of saturated condition. The procedure of mixing the sand with a specific water content to achieve unsaturated condition has some limitations. Firstly, this technique is time consuming to prepare large quantities of soil for testing. In addition, this technique requires a long time-period to achieve

equilibrium conditions. The equilibration time can be more than a week for some sands. In addition, this technique does not fully ensure uniform distribution of moisture content and therefore contribute to unreliable suction profile. This procedure also can result in creating air pockets contributing to spatial matric suction fluctuations for a specific water content.

More recently, Ravichandran et al. (2013) investigated the behavior of a model pile in Ottawa sand using a centrifuge system under saturated and unsaturated condition. They proposed a method, which consisted of using several water sprayers for mixing water with soil from the top surface during the test to control the soil-suction profile. However, during long period of centrifuge spinning, the proposed method showed some limitations. Ravichandran et al. (2013) suggested several recommendations to overcome the testing procedures associated problems. Due to the discussed reasons, there is a need for a more efficient, straight forward, standardized test methodology to achieve soil-suction profile that is reliable for investigating the behavior of different soil-structure interaction problems in unsaturated coarse-grained soils.

The current study, discusses a novel physical model to investigate the axial force-displacement behavior of a buried pipe under saturated and unsaturated condition. The measured axial force-displacement behavior of the buried pipe in saturated and unsaturated sand also will be further verified using a numerical analysis method proposed in this study.

3.3 Experimental Model: Design and Methodology

3.3.1 Equipment design

A test program was designed to: i) investigate the axial-force displacement behavior of an energy pipeline system subjected to relative longitudinal soil mass movement under saturated and unsaturated condition; ii) determining the effect of soil dilation on axial force on pipeline; and iii) developing simple yet reliable analytical model to estimate the axial force on pipeline body buried in coarse grained soils extending the principles of unsaturated soil mechanics and taking into account the effect of dilation.

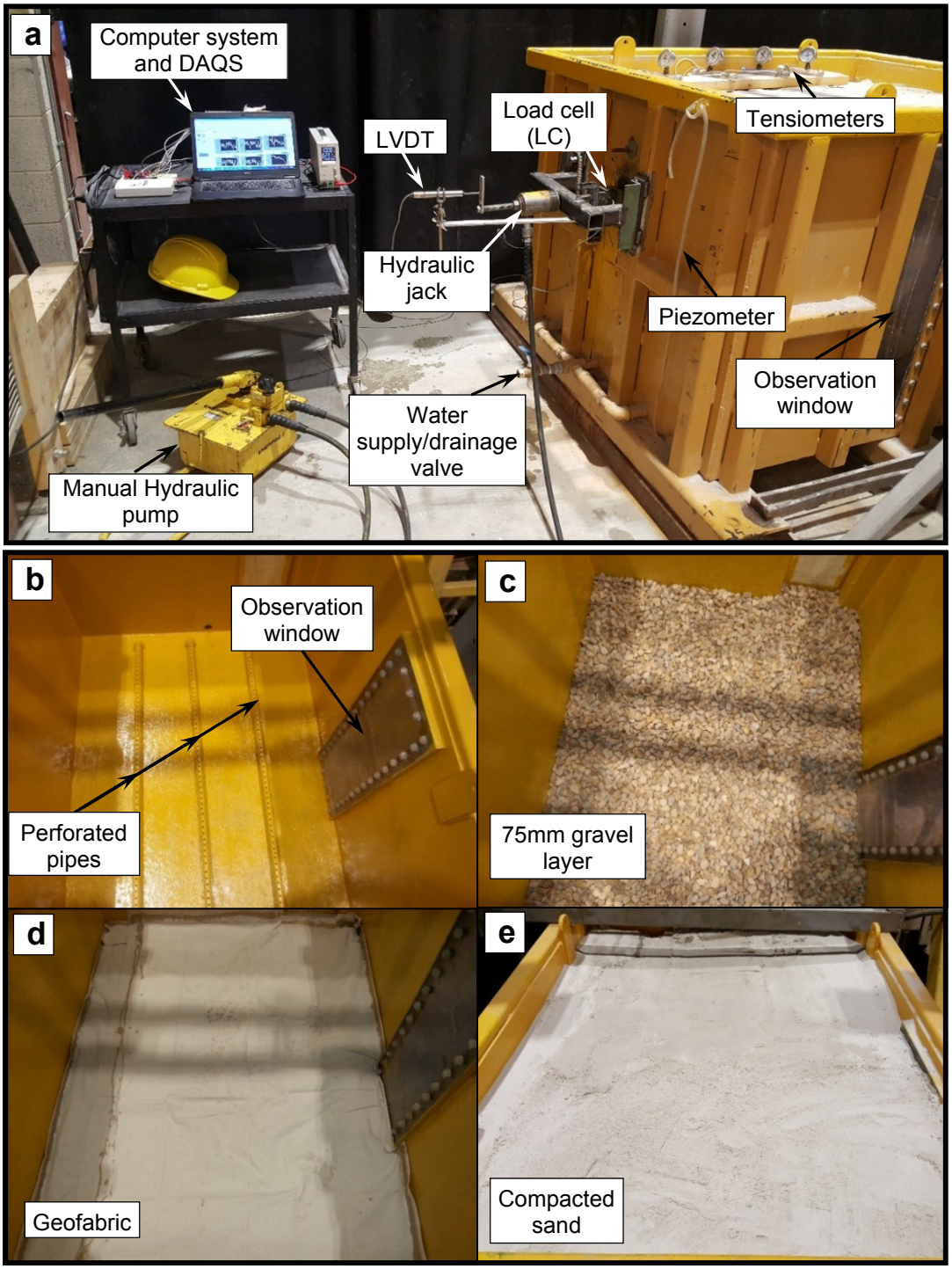

Figure 3.2 (a) The full prototype pipe test setup, (b) Empty container showing the perforated water supply/drainage pipes, (c) 75mm clean gravel layer, (d) Geofabric, and (e) Compacted sand.

The pipe pullout resistance tests were performed in a specially designed soil container of inner dimensions of 1.5m length, 1.2m width and 1.1m height (Figure 3.2). The box was fabricated out of rigid steel plate and supported by a rigid hollow steel section frame of 63.5×63.5×9.5mm. A transparent observation window of 870×330×25mm dimensions was installed on the side of the box for visual inspection and tracking water level changes during the tests along with two piezometers. Water supply/drainage system (WSDS) was installed at the bottom of the soil container. The WSDS consists of a water valve that branch into three perforated pipes of 50.8mm diameter that are aligned at 400mm centre-to-centre distance along the base of the soil container. The perforated pipes were covered with a 75mm clean gravel layer and topped by a geofabric sheet to create a filter layer preventing fine sand particles from being washed out and clogging the perforated pipes. The plumbing fixture and filter system allow uniform water movement during both saturation and desaturation stages of the soil.

The size of the pipe used in this study was chosen to provide a reasonable representation for the commonly used pipes for gathering, transporting and distributing energy. Natural resources Canada (2014) listed the sizes and lengths of the Canadian pipeline network as: i) 250,000km gathering lines of 4"-12" diameter, ii) 25,000km feeder lines, ii) 100,000km large-diameter transmission lines of 4"-48" diameter, and iv) 450,000km local distribution lines of ½"-6" diameter. A rough surface steel prototype pipeline of 114.3mm outer diameter (4" nominal diameter) and 1350mm length was used in this study. The pipe was fabricated in the University of Ottawa machine shop. The pipe surface was knurled at crossing directions at 115^0 angle at 1mm pitch and 0.25mm corrugation depth using a lathe (Figure 3.3). The knurling depth was chosen based on Yoshimi and Kishida (1981) and Kishida and Uesugi (1987) suggestions. Yoshimi and Kishida (1981) quantified the surface roughness (R_{max}) as the relative height between the highest peak and lowest valley over 2.5mm length of a surface profile. Kishida and Uesugi (1987) suggested that surface roughness can be quantified using normalized roughness (R_n) that is defined as the ratio of R_{max} to the mean particle size of the soil D_{50} (i.e. D_{50} = 0.25 mm). Garnier et al. (2007) stated that for perfectly rough interface, R_n is ranged from 0.1 to 1, and for perfectly smooth interface, R_n is less than 0.01. Therefore, to provide enough interlocking between the pipe surface and the soil, perfectly rough interface with surface roughness, R_{max} = 0.25mm (Yoshimi and Kishida 1981) and normalized roughness, R_n = 1 (Kishida and Uesugi 1987) was chosen.

A threaded hole was made at the front end of the pipe to accommodate a 19.05mm threaded loading rod, which connects the pipe to the loading setup. The loading rod passes through a hole that was drilled at the front side of the soil container and was connected to a hollow hydraulic jack from the other end.

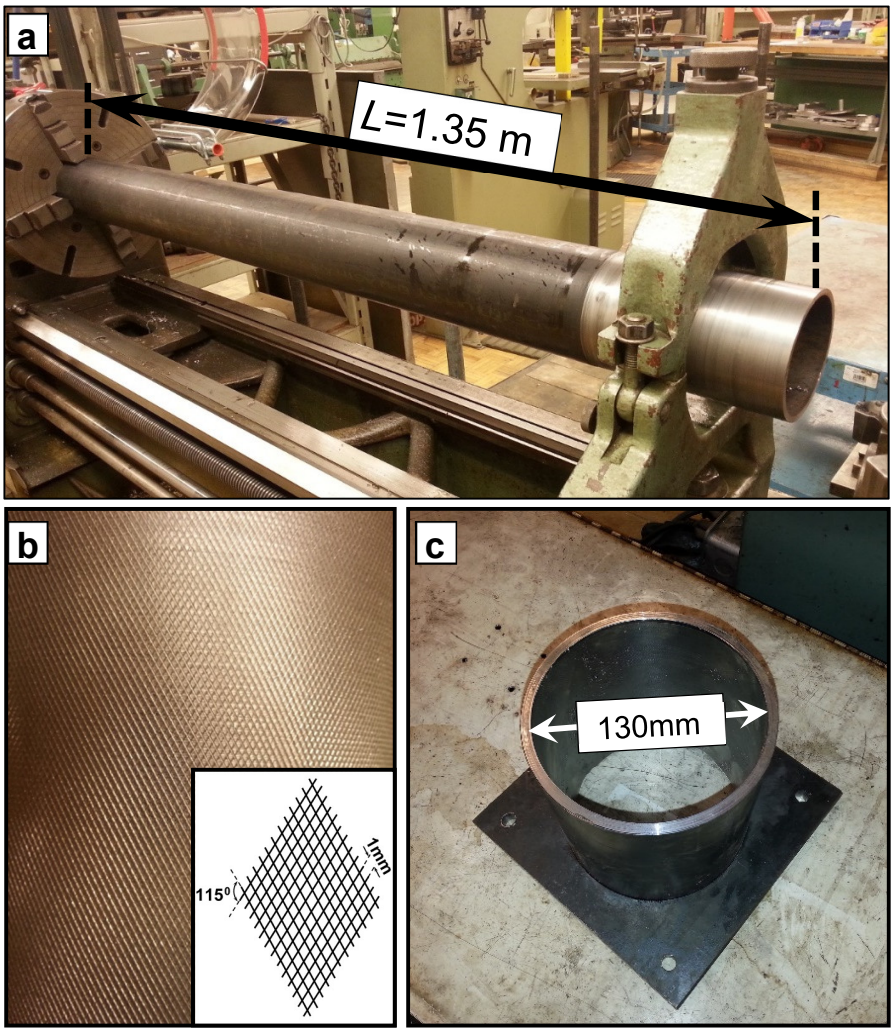

Figure 3.3 The prototype steel pipe; (a) Steel pipe, (b) Pipe smoothen and knurling, and (c) Surface roughness.

The front end of the pipe had to be free from any contact with the soil (i.e. no end bearing contributes to the pipe axial force-displacement behavior) and soil container front physical boundary since only skin friction of the pipe was the focus of study. A 130mm diameter pipe was

used to fabricate a sleeve of 200mm long that will extend along the first 75-100mm of the pipe front end. The sleeve was fixed to the inner front side of the box with four bolts. A thin plastic sheet layer of negligible strength was used to wrap the overlap point of the sleeve and the pipe to prevent the sand from filling the void between the pipe front end and the box and the gap between the sleeve and the pipe (Figure 3.4a). The clearance between the sleeve and pipe was designed based on Wijewickreme et al. (2009) findings. They performed axial load test on a large-scale pipe of 475mm diameter buried in dry sand. The study concluded that active shear zone at the soil-pipe surface zone does not exceed 2mm. In this study, the clearance between the sleeve and the pipe is 8mm from all directions, which is 4 times wider than active shear zone suggested by Wijewickreme et al. (2009).

The pullout force was applied using a hollow hydraulic jack. The hydraulic jack was supported by an external loading frame that consists of two supporting arms and a reaction beam. The frame was fabricated using a hollow steel section of 50.8×50.8×6mm (Figure 3.4b). A hole was made in the middle of the reaction beam to facilitate the connection of the loading rod to the hydraulic jack from one end and to a load cell (LC) and the pipe from the other end. The loading frame was fixed to the exterior front side of the box using two steel channel pieces that have four holes of 50mm offset clearance. The steel attachments were welded to the supported arms of the loading frame. The offset allowance was used to adjust orientation and align the pipe, LC, loading frame and hydraulic jack.

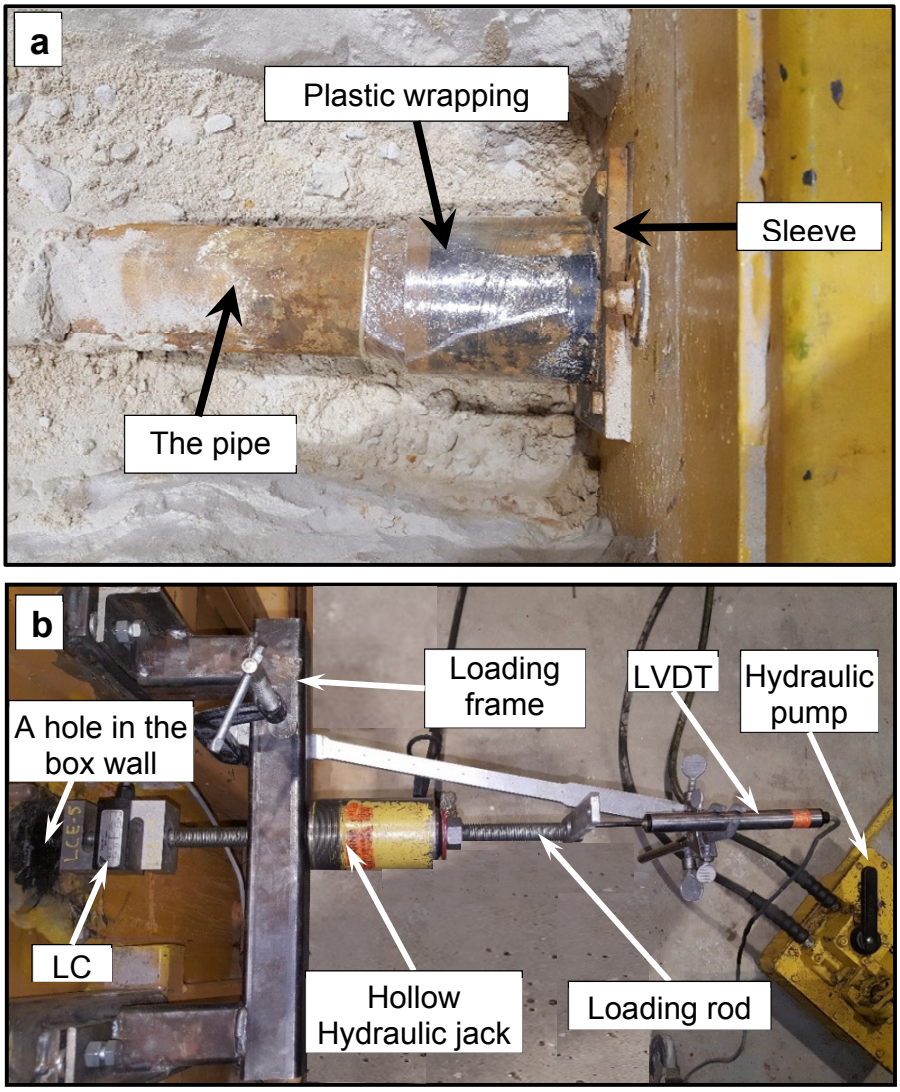

Figure 3.4 (a) Pipe-sleeve overlapping, and (b) Loading frame showing main instrumentations during the test.

3.3.2 Instrumentation

The tests were performed with aid of several instrumentations. A hollow hydraulic jack of 40mm maximum stroke and hydraulic pump were used to apply the pullout force. The pullout force was measured using an S-shaped Transducer Techniques LC of 22,241 N capacity. The LC accuracy was verified before the tests within the expected range of axial load (i.e. 1000 to 5000 N) using compression machine. Axial displacement was measured using a linear variation displacement transducer (LVDT) of 50.8mm maximum stroke. A data acquisition system (DAQS) and a

computer were used to collect the measured force and displacement data. Four soil moisture probe 2100F Tensiometers were used to measure the soil-suction profile in the box. The Tensiometer probes were buried at 100, 200 (i.e. at the top of the pipe), 310 (i.e. at the bottom of the pipe) and 450mm depths to provide full soil-suction profile.

3.3.3 Soil properties

Poorly graded silica sand, which is commercial soil and is referred to as Unimin 7030 was used in this study. The basic physical and mechanical properties of the sand and interface are listed in Table (3.1). The grain size distribution is presented in Figure (3.5).

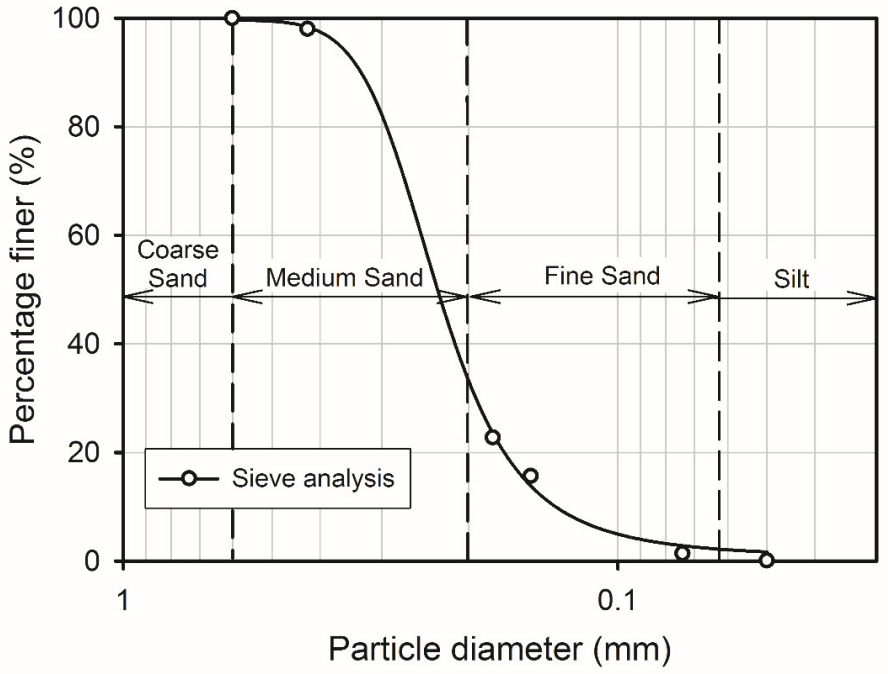

Figure 3.5 Grain size distribution curve.

The SWCC of the sand was measured using a hanging column setup (HCS) that was built in the geotechnical laboratory at University of Ottawa as per ASTM D6836-02. The full setup is shown in Figure (3.6). A Tempe cell of internal diameter of 50.1mm and height of 60.4mm with a ceramic disk was used to hold the soil sample. The Tempe cell constitutes of acrylic top and bottom caps and a solid retaining ring made of brass cylinder (Figure 3.6). A sand sample of around 65gm that was statically compacted in the brass cylinder to fill 20mm of the cylinder height assembled

within the Tempe cell following the compaction procedure that was discussed in Han and Vanapalli (2016). Triaxial machine loading frame was used to compact the sand in the cylinder. A filter paper was placed at the bottom of the brass cylinder and the sand was compacted at optimum moisture content in the brass cylinder. The brass cylinder, filter paper and the soil were moved carefully from the triaxial machine and assembled with the other parts of the Tempe cell. After installing the Tempe cell in the HCS, the sand was soaked with deaired-distilled water to achieve saturation condition. The system was left opened to air for a period of 24hrs before the test to achieve equilibrium conditions and drain the extra water.

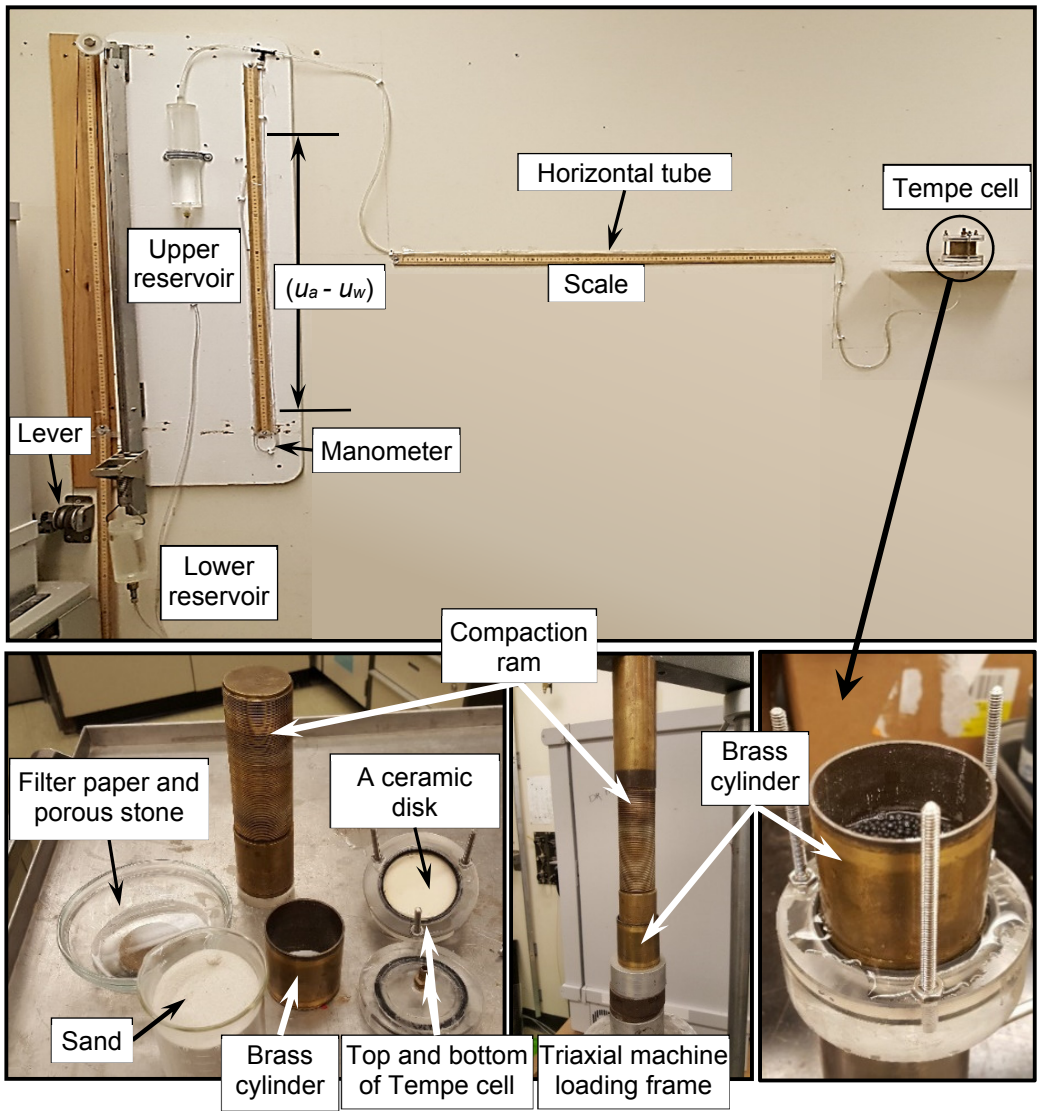

Figure 3.6 Hanging column setup that was used to measure the SWCC.

Once equilibrium is achieved, the test was initiated following the drying path, which was achieved by lowering the height of the adjustable reservoir (i.e. lower reservoir). The bottom of the lower reservoir is connected to the bottom of the upper reservoir with a plastic tube. The maximum height difference between the two reservoirs is 1m, which corresponds to 10 kPa matric suction (i.e. a height difference of 100mm equals 1 kPa of matric suction). The upper reservoir is connected from its top end to the manometer and Tempe cell with a tube. The applied ($u_a - u_w$) on the sand in the Tempe cell due to differential height of both reservoirs is measured using the manometer. The sand will lose some of its water content with each ($u_a - u_w$) increment. The volume of the extracted water is collected in the horizontal tube and measured using the adjacent scale (Figure 3.7). The volume of the extracted water and the corresponding ($u_a - u_w$) were used to generate the SWCC, which is presented in Figure (3.8). The measured data of SWCC was fitted using the Fredlund and Xing (1994) model.

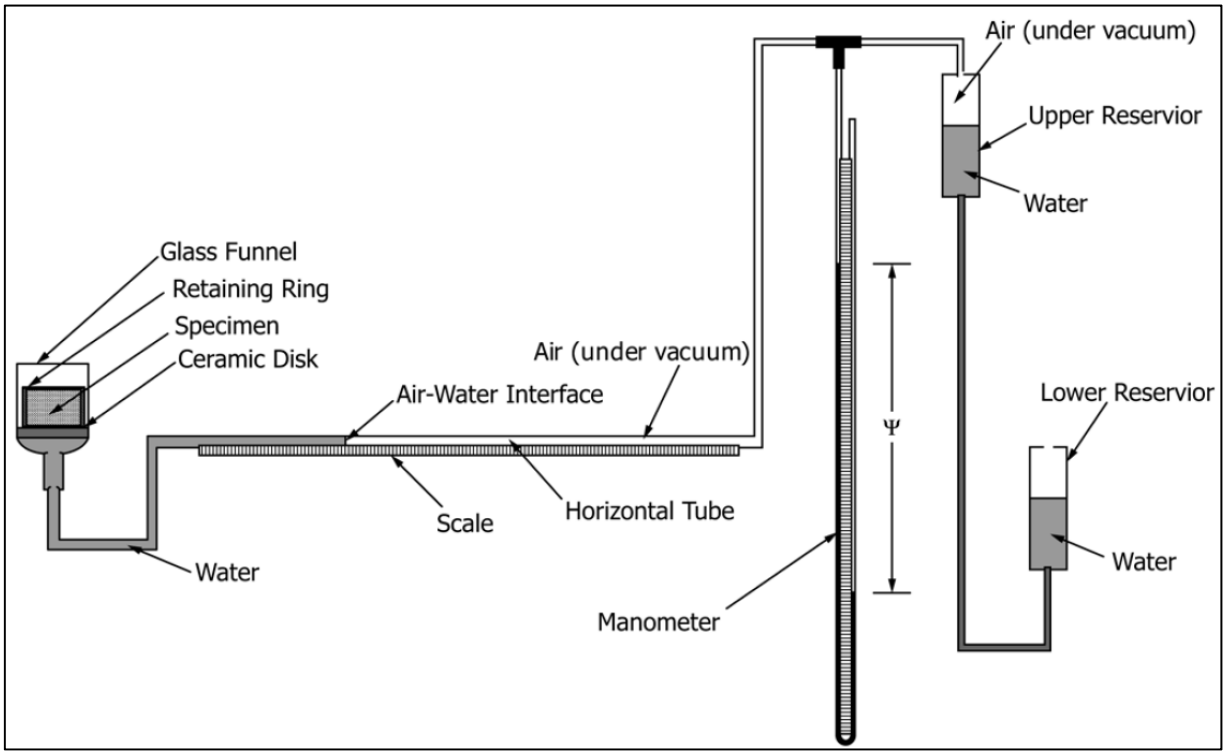

Figure 3.7 Schematic drawing of Hanging column setup (modified after ASTM D6836-02)

The mechanical properties of the sand and interface were measured using direct shear (DS) and triaxial shear apparatuses. DS test was used to measure the effective angles of internal friction

for the sand and interface (i.e. ϕ' and δ', respectively) as well as the dilation angle, ψ. Drained shear tests were performed using dry sand under four normal stresses, σ'_n (i.e. 25, 40, 75, 125 kPa) as per ASTM D3080-11. Strain controlled tests were performed at constant shearing speed rate of 0.0025mm/sec. Soil-pipe interface shear strength was measured using a specially designed and fabricated knurled steel block of 60 × 60 × 15mm dimensions. The block fully occupied the lower half of the shear box and the rough side of the block was at the level of shearing plane. The sand was compacted at the upper half using tamping method to achieve the required density. The results of DS tests are presented in Figure (3.9) and summarized in Table (3.1).

The initial modulus of elasticity of the sand under saturated and unsaturated condition was measured using the GDS-ELDYN triaxial device. Consolidated drained (CD) tests were performed on soil samples of 51.0mm average diameter and 115mm average height. Before preparing the samples, all drainage lines in the triaxial apparatus were saturated by bleeding them. The samples were prepared using moist tamping method following Mulilis et al. (1978). Saturated porous stones and filter papers were placed at the

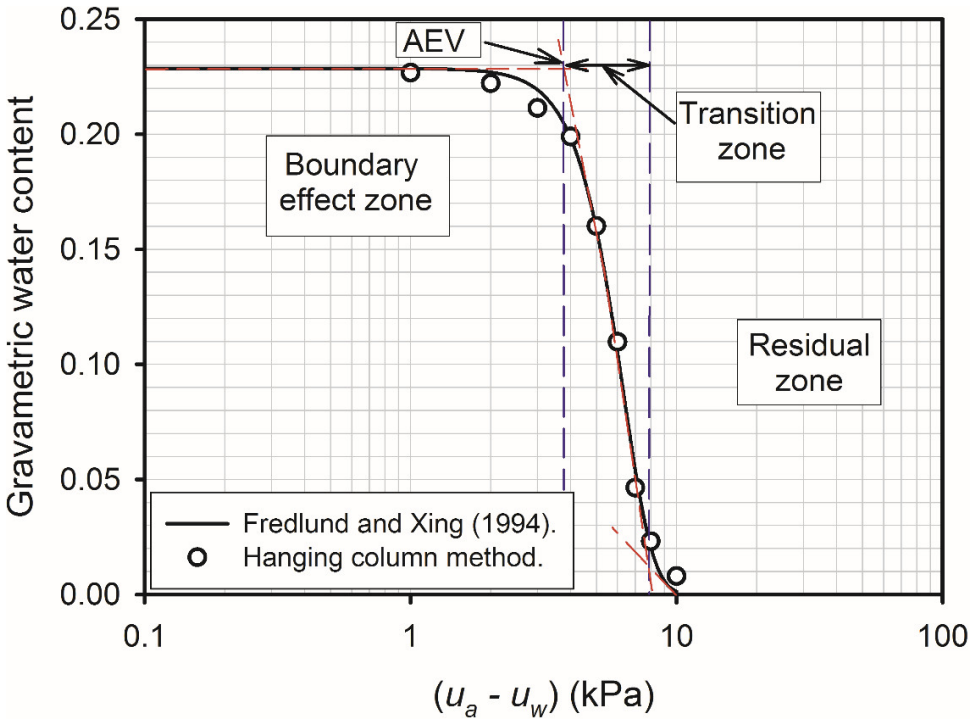

Figure 3.8 The soil-water characteristic curve (SWCC).

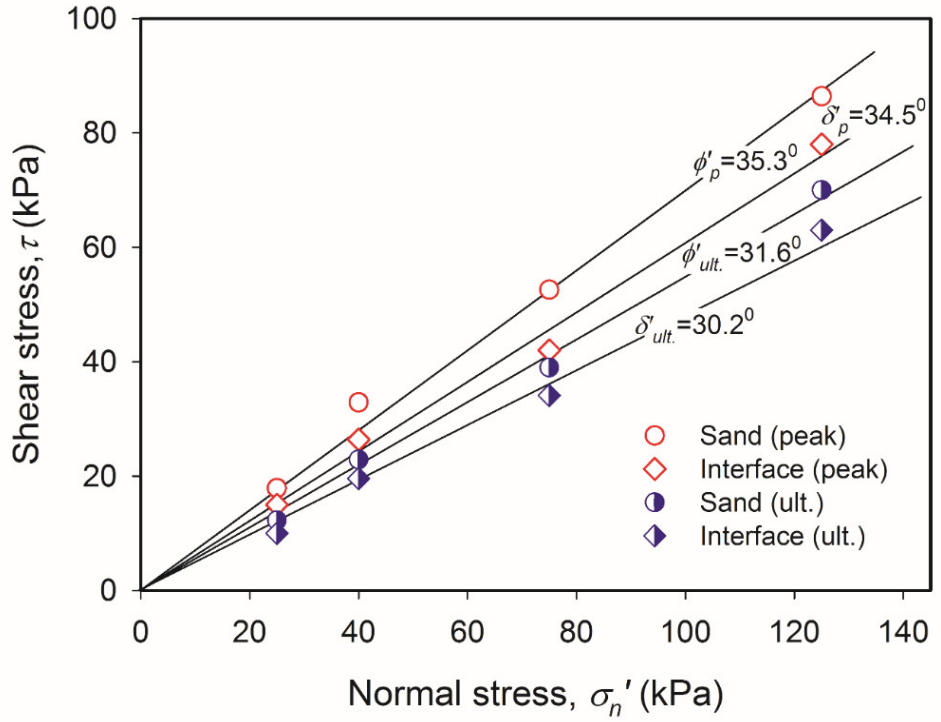

Figure 3.9 Shear strength parameters of sand and interface from DS test.

top and bottom of the samples. The matric suction was applied during the test using hanging column technique. The GDS-ELDYN Triaxial device was modified by connecting it to a HCS (Figure 3.10). The HCS consisted of one adjustable water reservoir that was used to apply suction on the soil sample. A plastic tube was connected from the bottom of the adjustable reservoir to the bottom of the soil sample through the triaxial pedestal (bottom drainage valve).

The samples were saturated from the bottom prior to shearing them. The adjustable reservoir in the HCS was raised by 100mm from a reference level to apply hydraulic pressure difference of 1 kPa between the reservoir and the sample to saturate it. The mid-height of the soil sample is taken as the reference level. The low hydraulic pressure difference forces the water gently into the sample from the bottom and will assure removing the occluded air bubbles from the upper cap (drainage) valve. After saturating the sample, the upper valve was closed and the adjustable reservoir level was brought to −1m level under the reference level, which generated suction stress that helped to hold the sample in shape and remove the split cup that was holding the sample during the preparation process. Then the triaxial cell was installed and the confining stress was applied. Once the confining stress was applied, the adjustable reservoir was brought back to the reference level (i.e. the level of the water in the reservoir to the same level of the middle of the sample) and then the upper cap valve was opened. The system were left open to atmospheric pressure for several hours to achieve equilibrium condition. After this stage, both drainage valves at the pedestal and upper cap were left open. Once equilibrium condition was achieved, matric suction was applied by lowering the adjustable reservoir beyond the reference level. As discussed earlier, 100mm height difference equals 1 kPa of ($u_a - u_w$). The samples were sheared under low effective confining stress, σ'_c of 2 kPa and different ($u_a - u_w$) (i.e. 0 (saturated), 2, 4, and 6 kPa) at constant shearing speed rate of 0.01mm/sec. The shear stress-strain results of CD triaxial test are presented in Figure (3.11).

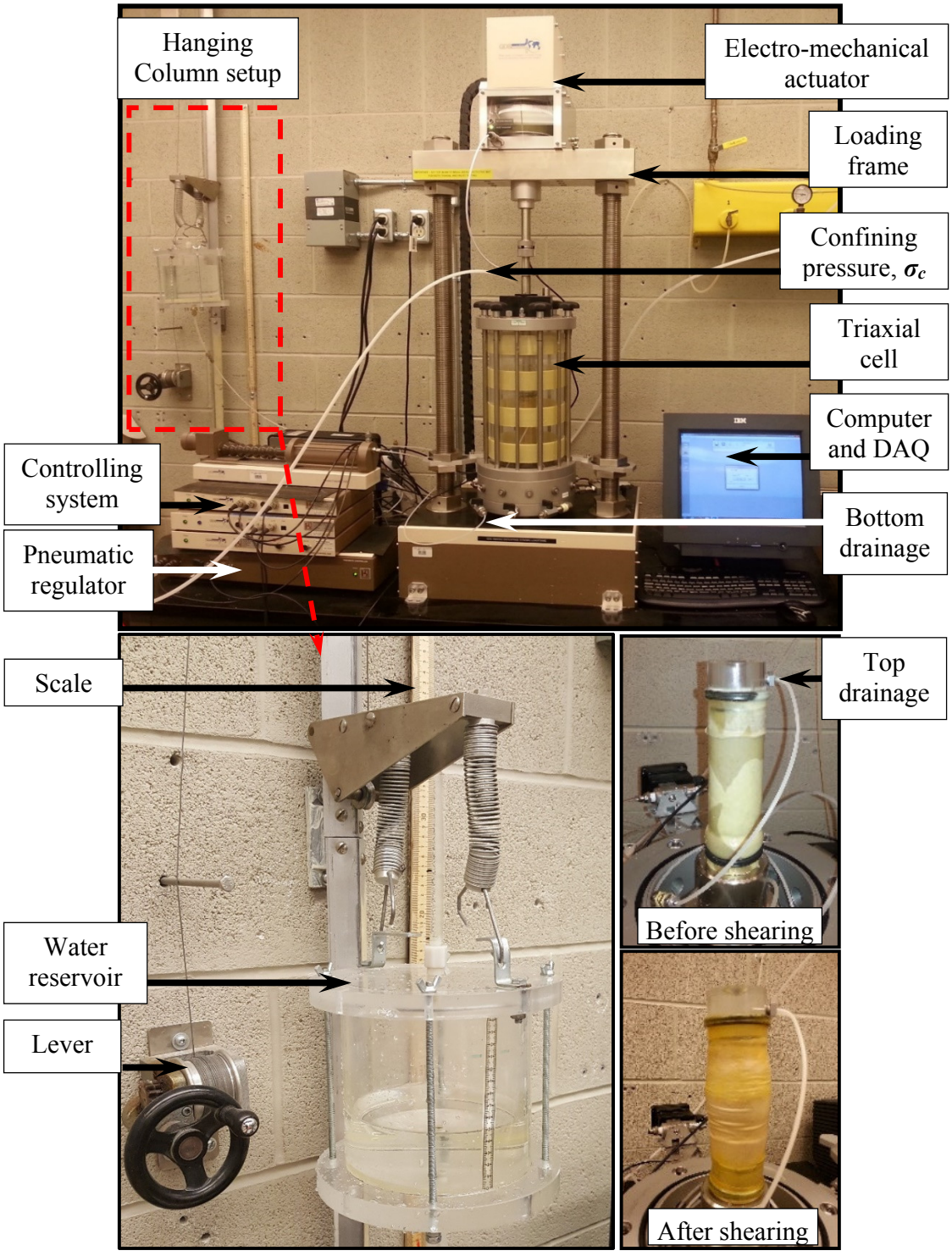

Figure 3.10 GDS-ELDYN triaxial device with HCS.

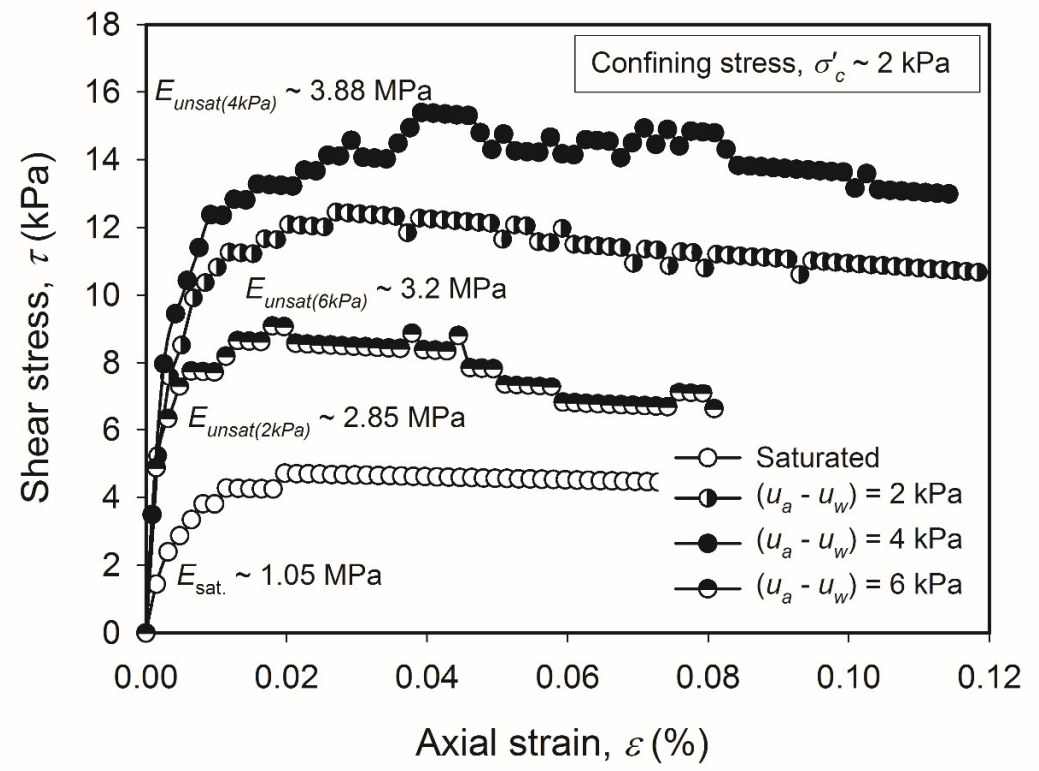

Figure 3.11 CD-triaxial shear stress-strain test results for saturated and unsaturated condition under confining stress, σ'_c = 2 kPa.

3.3.4 Test procedure and soil-matric suction profile control

The test procedure consists of several steps that contribute to reliable measurement of the pull-out resistance of the pipe under both saturated and unsaturated conditions. The tests were conducted following the stress path shown in Figure (3.12). The first step included compacting the soil and burying the pipe. The sand was compacted manually at optimum moisture content in more than four layers in the soil container using 6.5 kg manual compactor. The soil was compacted to achieve 200mm thickness layer that required 594 kg. The average relative density achieved was around 69%. The pipe was set and leveled horizontally during the sand compaction at 250mm depth from its centre to the soil surface for the first test and was aligned with the loading frame, LC, and the hydraulic jack. The effective confining stress, σ'_c at this step increased due to the compacted soil cover above the pipe.

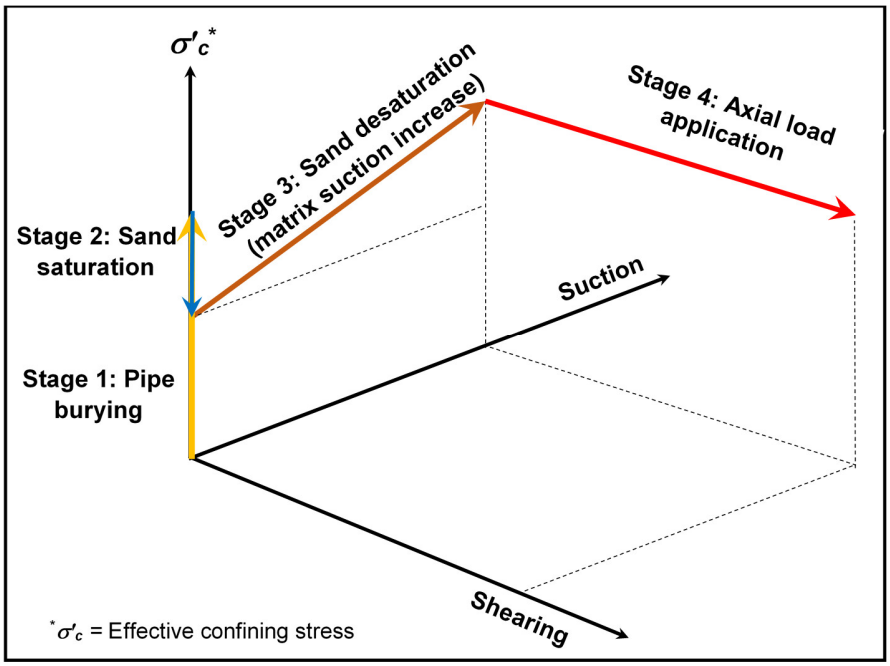

Figure 3.12 Stress path followed during the pullout tests.

The second step after compacting the sand in the box and setting the pipe comprised of saturating the sand. This step is essential for performing the pullout tests under both saturated and unsaturated conditions. This step ensures removal of the occluded air bubbles and pockets from the sand to achieve uniform saturation and generate reliable soil-matric suction profile for unsaturated condition. To achieve this objective, the WSDS was used to raise the water level from the bottom of the soil container to the soil surface (i.e., level A in Figure (3.13a)). The σ'_c at this stage decreases due to effective unit weight reduction upon saturation (Figure 3.12). Raising the water table (WT) from the bottom assures uniform water movement and remove air pockets or bubbles (Figure 3.13b).

Next step constituted of creating soil-matric suction profiles by desaturation of the saturated sand. The WT was lowered to a desired depth by draining the soil through the WSDS. The WT levels were marked based on their depths from the soil surface as: i) WT1 at soil surface (saturated), ii) WT2 at 270-320mm depth, iii) WT3 at 350-400mm, iv) WT4 at 530-550mm, v) WT5 at 700-730mm, and vi) WT6 at 870mm. The WT levels were kept constant for a minimum period of 18 to 24hrs prior to performing the tests to achieve equilibrium condition. The soil-matric suction profiles were measured using the four Tensiometer probes and the results for different WT levels

are presented in Figure (3.14). Hanging column method by Haines (1930) was utilized to develop this technique (i.e. saturating and desaturating the soil). Furthermore, six small aluminium containers were used to collect soil samples and verify the measurement of the Tensiometer probes. The samples were collected after the third test with WT3. The containers were buried at three different depths as pairs at depth levels of 100, 200 and 310mm from the top surface layer during the third test preparation. The gravimetric water contents of the collected samples were measured and related to SWCC to estimate the corresponding $(u_a - u_w)$. The estimated $(u_a - u_w)$ values for the collected samples agrees well with the measured soil-matric suction profile for the third test (Figure 3.14). The soil-matric suction profile results will be discussed in the results section. At the end of the stage, the σ'_c increased due to the increase in the effective unit weight.

Finally, the pullout test was performed by applying axial force on the buried pipe using the hollow core hydraulic jack. The pullout force was measured using the load cell (LC) and the corresponding axial displacement was measured using linear variation displacement transducer (LVDT). The analog signal results were translated to digital signal using the DAQS and collected and stored in the computer.

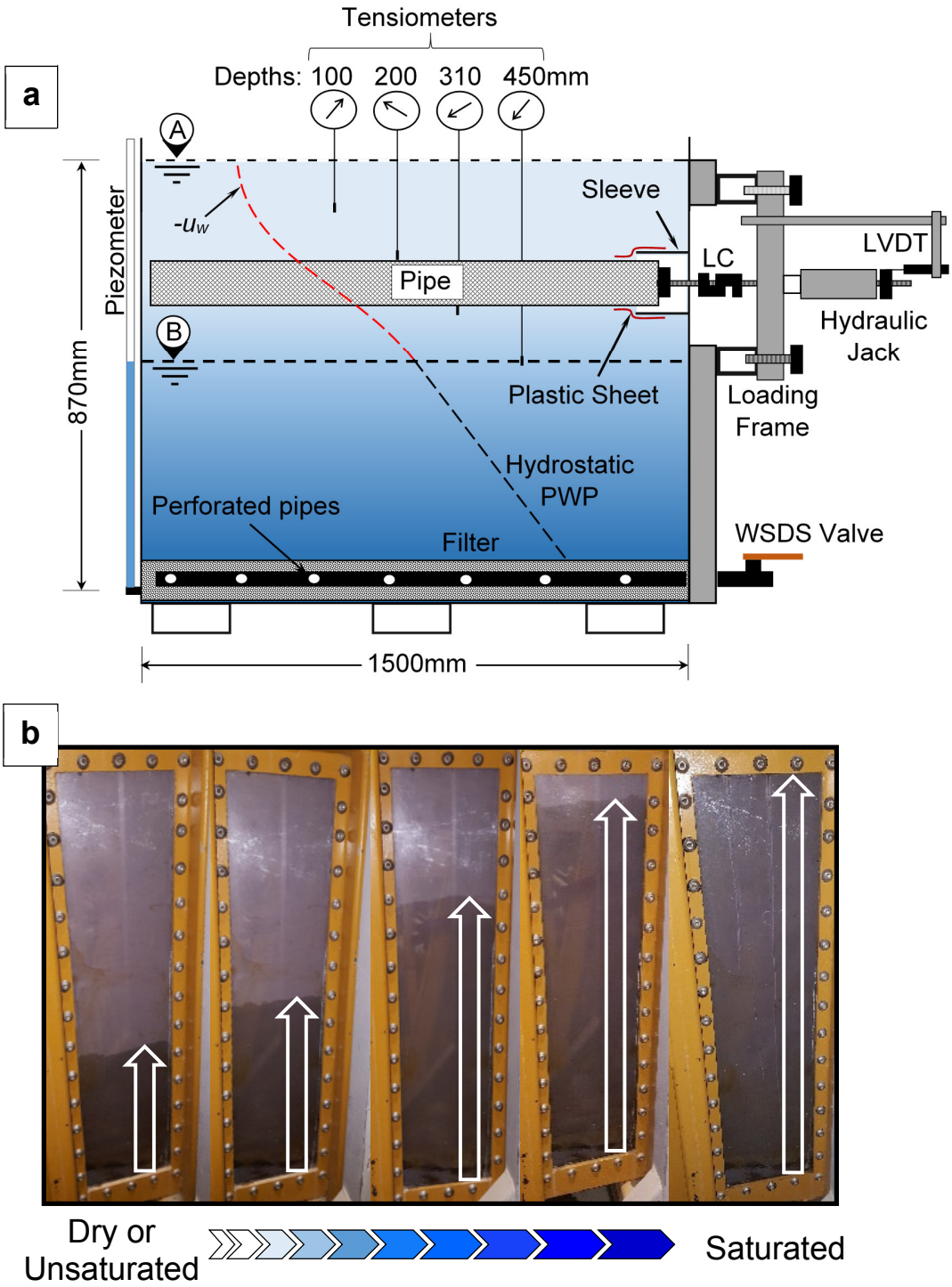

Figure 3.13 (a) Graphical illustration of the test system, and (b) Sand saturation before the test.

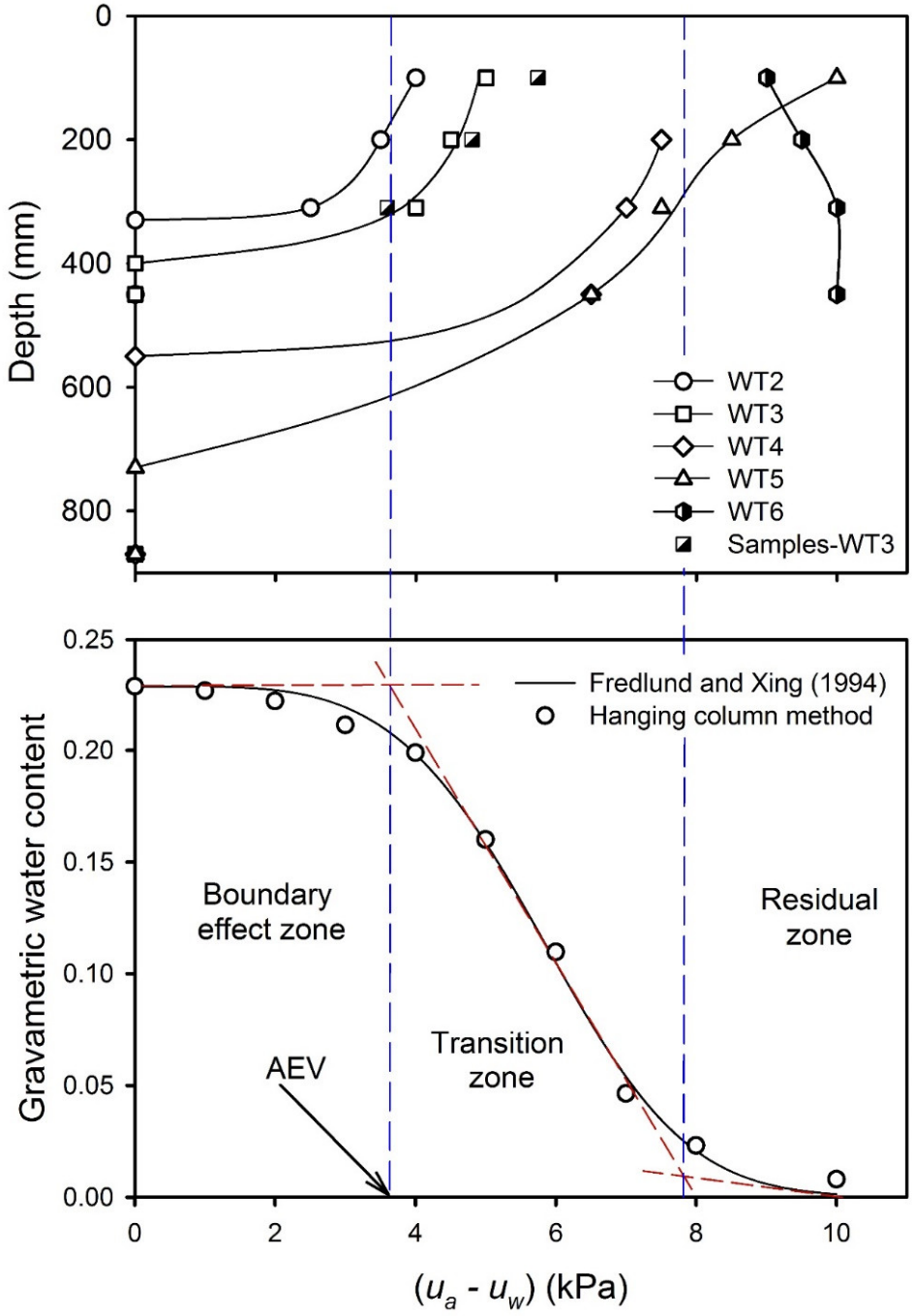

Figure 3.14 Soil-matric suction profile for different WT levels.

3.4 Numerical Modelling

3.4.1 2-Dimensional numerical model

The pipeline systems are usually analysed using 3-dimensional finite element analysis (FEA). In recent years, FEA were undertaken assuming plane-strain conditions to investigate the soil-pipeline interaction problems under different loading conditions, which include, seismic shaking, excavation, and transverse loading (Martin et al. 2013, Lanzano et al. 2014, Roy et al. 2014, Roy et al. 2015, Chaloulos et al. 2015, Roy et al. 2016, Kong et al. 2017).

In this study, plane-strain FEA were carried out to simulate the elastic pullout force-displacement behavior of the pipe using the commercial software, SIGMA/W. 2-dimensional model was built with boundary conditions extended to 870mm in depth and 1500mm in width to simulate the physical soil container (Figure 3.15). Since the container sides are rigid, the left and right boundaries were restrained only in the horizontal direction while the bottom boundary was restrained in both directions. A void of 130mm size and 200mm length was created in the wall of the container to simulate the sleeve. The sleeve boundaries were restrained in both directions.

The FEA was performed in two stages: i) In-situ condition where initial conditions of the model are set, and ii) Load-deformation condition where the soil and interface are sheared under constant rate of horizontal displacement. Since the pipe was fabricated out of a rigid steel material with extremely high stiffness in comparison to soil stiffness, the pipe was simulated during: i) In-situ stage with fixed boundary condition in both directions, and ii) Load-deformation stage, the pipe movement was simulated using boundary condition with constant horizontal displacement rate of (2mm/min) and fixed in vertical direction. The embedment length of the pipe of 1275mm was used in the FEA.

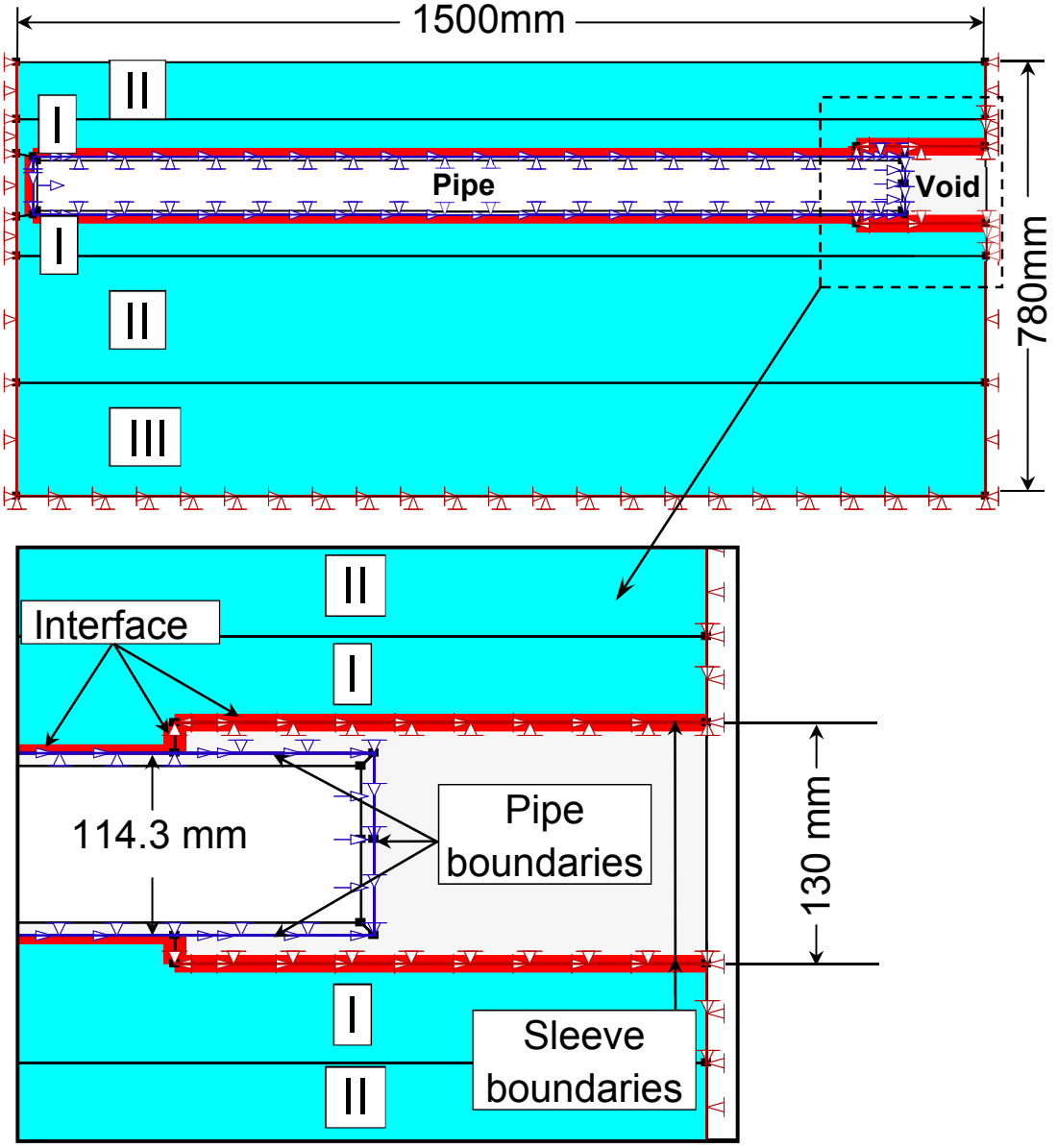

Figure 3.15 Numerical model boundary conditions and dimensions.

3.4.2 Soil modelling

The sand was modelled using Mohr-Coulomb (MC) constitutive model with effective-drained parameters considering the dilatancy effect of the sand. The ϕ_p', ψ, v and E_{sat} of the sands for saturated conditions (i.e. WT1) that were listed in Table (3.1) were incorporated into the MC model. Two elements were used to generate the meshes: i) 8-noded quadrilateral element with

integration order of nine, and ii) 6-noded triangular elements with integration order of three. The domain was divided into three zones with different element sizes. Fine mesh was assigned to the zone of the pipe and sleeve (i.e. zone I) with element length of 0.01m. Further zones from the pipe and the sleeve (i.e. zones II and III) were formed with coarser meshes of element lengths equal 0.05, and 0.075m, respectively).

Table 3.1 Key properties of the sand and interface.

Physical Properties	
Soil density key remarks	
Dry unit weight, γ_{dry} (kN/m^3)	16.2-16.7
Optimum moisture content, w (%)	14.6
Relative density, D_R (%)	69.0
Void ratio	0.606
Unified soil classification system (USCS) remarks	
D_{60} (mm)	0.25
D_{30} (mm)	0.19
D_{10} (mm)	0.13
Coefficient of uniformity, Cu	1.9
Coefficient of curvature, C_C	1.1
Specific gravity	2.65
Classification	SP
Mechanical Properties	
Shear strength from DS	
Soil peak angle of friction, ϕ'_p (^{0})	35.3
Soil ultimate angle of friction, $\phi'_{ult.}$ (^{0})	31.6
Soil dilation angle, ψ (^{0})	6.75
Interface peak angle of friction, δ'_p (^{0})	34.5
Interface ultimate angle of friction, $\delta'_{ult.}$ (^{0})	30.2
Interface dilation angle, $\psi_{int.}$ (^{0})	6.33
Stiffness parameters	
Initial soil modulus of elasticity, $E_{sat.}$ (MPa)	1.05
Initial interface modulus of elasticity, $E_{int\text{-}sat.}$ (MPa)	0.75
Poisson's ratio, v	0.344

The mechanical properties for unsaturated condition for WT2, and WT3 levels were incorporated into MC-constitutive model to simulate the unsaturated sand. The apparent cohesion, c for unsaturated condition was assumed to be constant in the domain and was derived using

Vanapalli et al. (1996) model (Eq. 3.1) using fitting parameter, $\kappa = 1$, which is valid for sand. The average value of matric suction at the top and bottom of the pipe (i.e. 3 and 4.25 kPa for WT2 and WT3, respectively) were used to determine *c*-values. The variation of the unsaturated modulus of elasticity E_{unsat} with depth were estimated using VO-model (Vanapalli and Oh 2010) (Eq. 3.2) based on soil-suction profile. Eq. (3.2) has two fitting parameters, α and β. They suggested that the value of the fitting parameter, β is a function of soil plasticity, I_p and it is equal to 1 for non-cohesive soils. The value of the fitting parameter, α is more related to soil type. α-value for the used sand was calibrated and derived from the measured E_{sat} and E_{unsat}. The measured E_{sat} and E_{unsat} were plotted vs. $(u_a - u_w)$ in Figure (3.16). The estimated variation of E_{unsat} with respect to $(u_a - u_w)$ using Eq. (3.2) was found to provide best-fit with the measured data using fitting parameter, α equals 0.8. The estimated variation of E_{unsat} with respect to depth above the WT then was derived and presented in Figure (3.17). Under the WT, the soil is saturated and *E* is assumed constant.

$$\tau = c' + (\sigma - u_a)tan\phi' + (u_a - u_w)S^{\kappa}tan\phi' \tag{3.1}$$

where c' = effective cohesion; ϕ' = effective friction angle associated with net normal stress $(\sigma - u_a)$; S = degree of saturation; κ = fitting parameter.

$$E_{unsat.} = E_{sat.}\left[1 + \alpha \frac{(u_a - u_w)}{(P_a/101.3)}\,(S)^{\beta}\right] \tag{3.2}$$

where P_a = atmospheric pressure; α and β = fitting parameters.

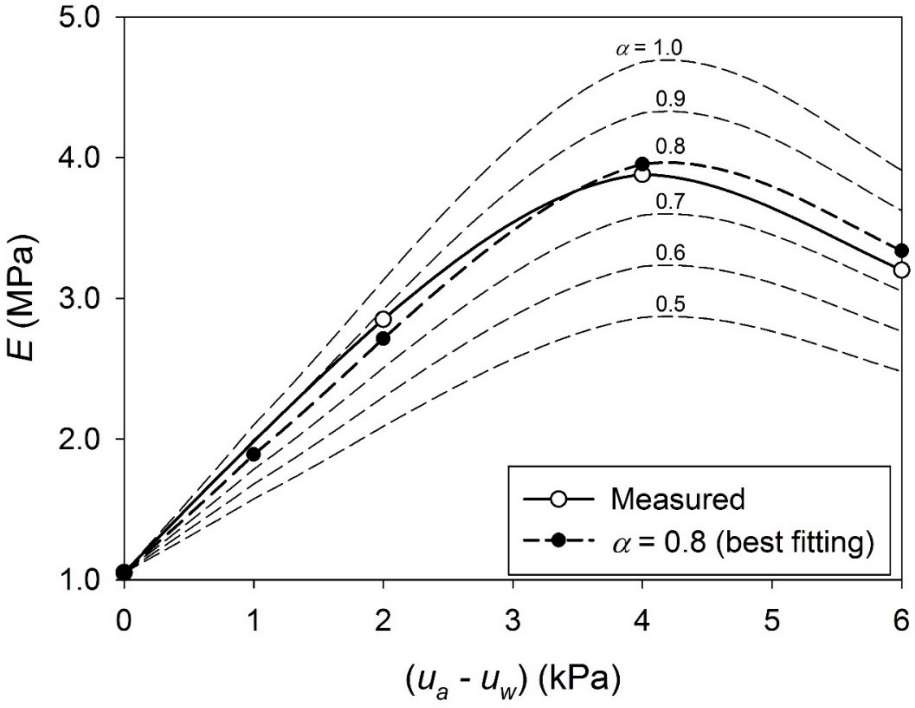

Figure 3.16 Calibration of the fitting parameter, α for Eq. (3.2).

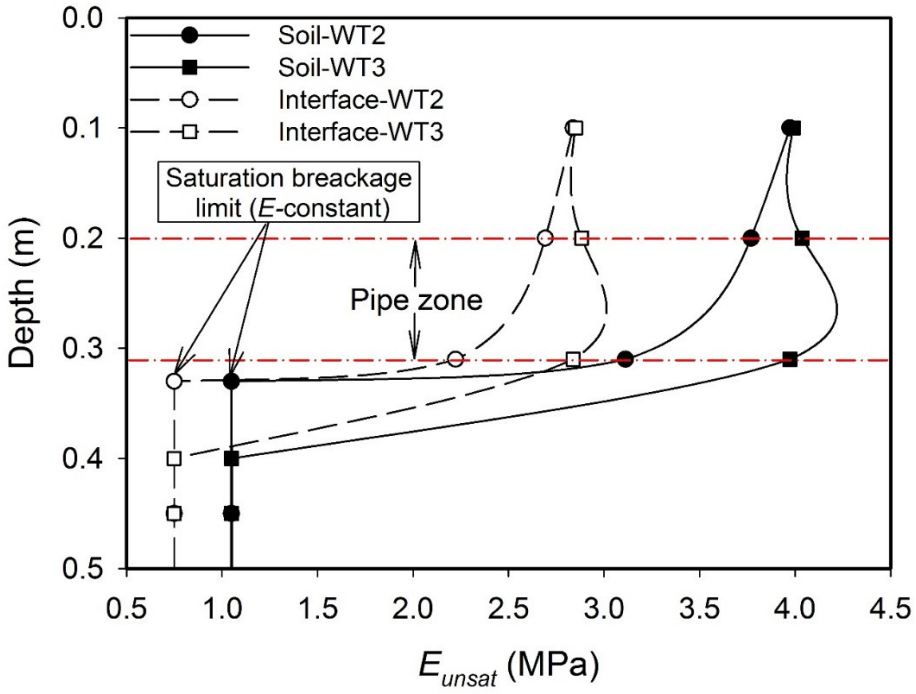

Figure 3.17 Variation of unsaturated modulus of elasticity, $E_{unsat.}$ with depth.

3.4.3 Interface modelling

The interface was generated along the pipe and the sleeve boundaries using line-area feature in the analysis. The interface thickness was designed following Wijewickreme et al. (2009) experimental findings that was discussed earlier. The interface element size was assigned to be 0.01m and its thickness is 0.0025m. MC constitutive model with effective drained parameters was used to simulate the interface behavior. Saturated interface δ'_p, $\psi_{int.}$, E_{int} and ν are listed in Table (3.1). The $E_{int\text{-}sat}$ was estimated to be around 75% of saturated modulus of elasticity for the soil. Similar approach was followed for unsaturated condition for estimating the apparent adhesion, c_a and the modulus of elasticity, $E_{int\text{-}unsat}$.

3.5 Results and Discussions

3.5.1 Matric suction profile

The soil-matric suction profile results for different WT levels are presented in Figure (3.14). Uniform soil-matric suction profiles for different WT levels were obtained from the discussed earlier testing procedure. The generated soil-matric suction profiles extended in all zones of suction (i.e. boundary effect, transition and residual zones) such that a reliable physical simulation of soil-pipe interaction can be achieved. By relating the measured soil-matric suction profiles to the SWCC, the following observations can be highlighted:

i) Lowering the WT below the springline zone results in higher average matric suction, $(u_a - u_w)_{av}$ within the soil-pipe active shear zone (i.e. at 250mm depth). However, the rate of variation of matric suction changes as the soil moves from the boundary effect to the transition and residual zones of suction.

ii) At the boundary effect zone of suction, which is primarily a small zone above the WT where the soil is still saturated with capillary stress, the rate of increases of $(u_a - u_w)$ with depth above WT is maximum.

iii) Once the soil moves into the transition zone, capillary stress will not be able to sustain free water between the soil particles in higher zone and soil starts to desaturate. Since matric suction acts along the wetted area, the reduction in the wetted area contributes to a lower rate of increase in the shear strength with depth in comparison to boundary effect zone.

iv) The last soil-matric suction profile was measured at WT6 after the soil was allowed to drain completely by keeping the drainage valve open for more than 24hrs prior to measuring the readings of the Tensiometers. At this stage, the soil was in the residual zone and was close to dry condition. Within this zone, there is no continuity in the liquid phase and the wetted area is minimal, and therefore, the measured ($u_a - u_w$) was constant with depth for the deeper Tensiometers. However, the upper Tensiometers recorded slightly lower ($u_a - u_w$) values which can be attributed to the absorbed moisture content through the soil surface from the air humidity.

3.5.2 Pullout test results

Three physical pullout force-displacement tests were performed under saturated condition (i.e. WT1) and unsaturated condition (i.e. WT2 and WT3). The measured pullout force that was exerted on the buried pipe due to relative movement between the pipe and soil mass in the parallel direction to the pipe axis are presented in Figure (3.18). The measured pull-out force for the case of WT3 (i.e. $(u_a - u_w)_{av} = 4.25$ kPa) is more than twice the pull-out force for WT1 (i.e. saturated condition where $(u_a - u_w)_{av} = 0$ kPa) (i.e. more than twice the pull-out force for WT1). For WT2 and WT3 with $(u_a - u_w)_{av}$ = 3.0 and 4.25 kPa, respectively, the pull-out force increases significantly especially in the elastic zone due to suction hardening. Similar trends in unsaturated soils behavior was highlighted by several scholars, for example; Han et al. (2016) defined soil suction as energy potential that applies tension forces on soil skeleton bringing soil particles and their packets together which contribute to resist elastic and plastic deformations. Hossain and Yin (2014) stated that at low confining stress, unsaturated interface exhibit strain hardening in the pre-peak zone of shear strength due to matric suction contribution.

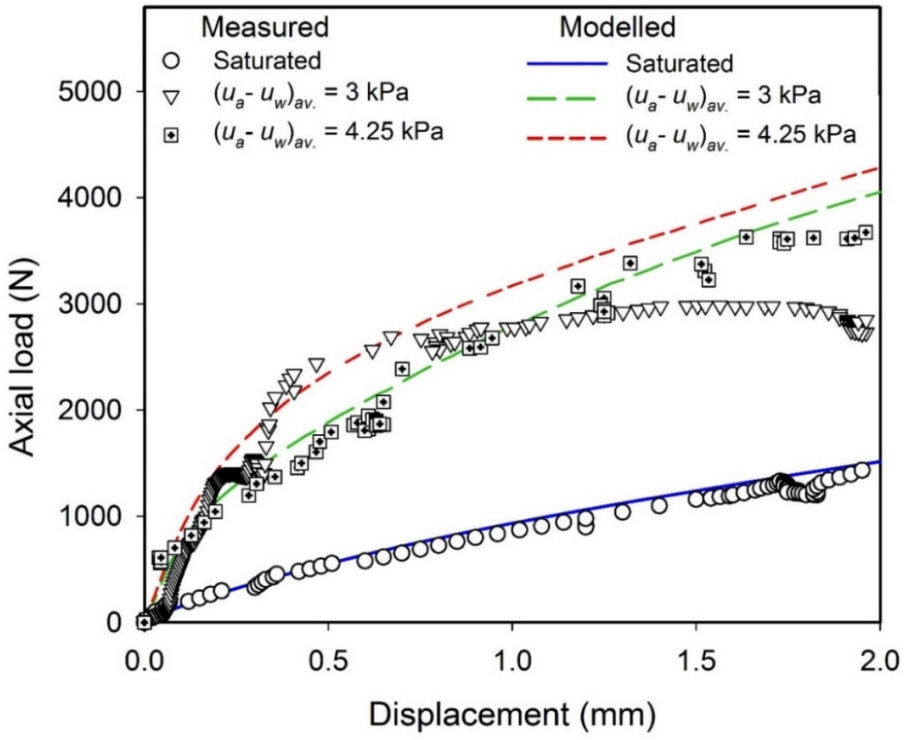

Figure 3.18 Measured and predicted pull-out force-displacement behavior of the pipe under saturated and unsaturated condition.

3.5.3 FEA results

Plane strain FEA was performed using the commercial software SIGMA/W. The predicted pullout force exerted on the pipe was estimated by considering the average boundary forces in the interface nodes along the top and bottom of the pipe (Figure 3.19). The XY-Displacement of the soil-pipe system at the end of numerical analysis for saturated and unsaturated conditions are presented in Figure (3.20). It can be seen that soil deformations extend to deeper depth as WT approaching the surface, which means that as the WT depth (i.e. matric suction) increases, soil stiffness increases resulting in less deformation.

Figure (3.21) shows contour plots highlighting variation of the maximum shear stress in the model and along the pipe at the end of the analysis for different WT levels. Shear stress concentration was observed at the edges which was reflected on the shear stress variation along the top and bottom interface of the pipe at the end of shearing process as presented in Figure (3.22). The process of shearing the interface along the pipe is consistent with the direct shear test results.

Rahardjo et al. (2011) performed numerical analysis to simulate the process of shearing compacted residual soil in direct shear test. They stated that concentrated shear stresses at the interface near the edges of the soil specimen is common in direct shear and they exclude the concentrated shear stresses at the edges in estimating the shear stress, τ. Similarly, the concentrated shear stresses at the top and bottom interface along the pipe near the edges can be excluded.

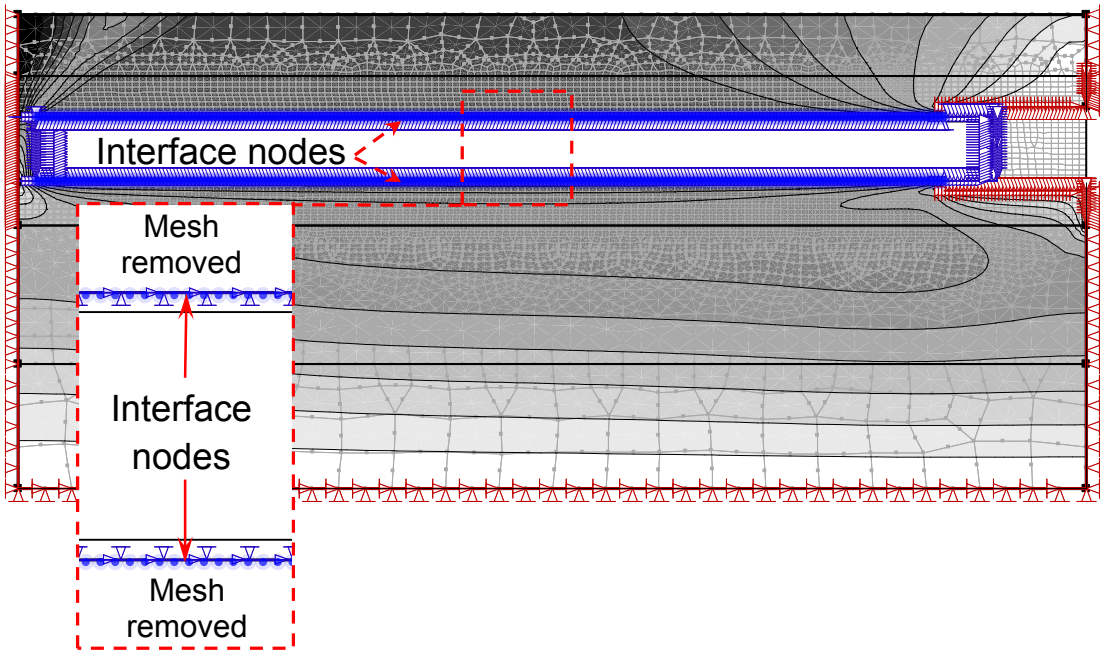

Figure 3.19 Illustration of FE boundary force from interface nodes at the top and bottom of the pipe.

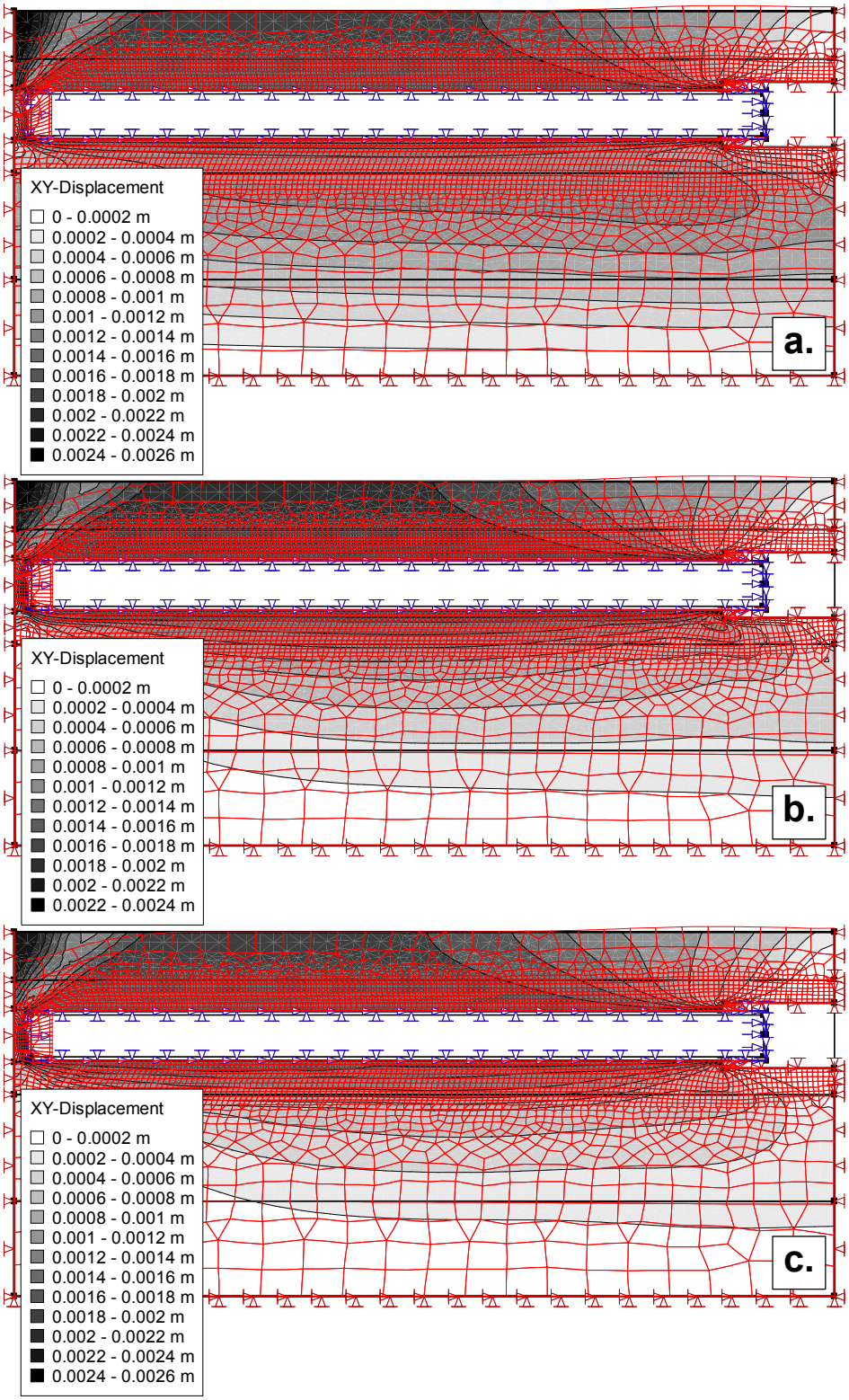

Figure 3.20 XY-Displacement at the end of numerical analysis for; (a) WT1, (b) WT2, and (c) WT3.

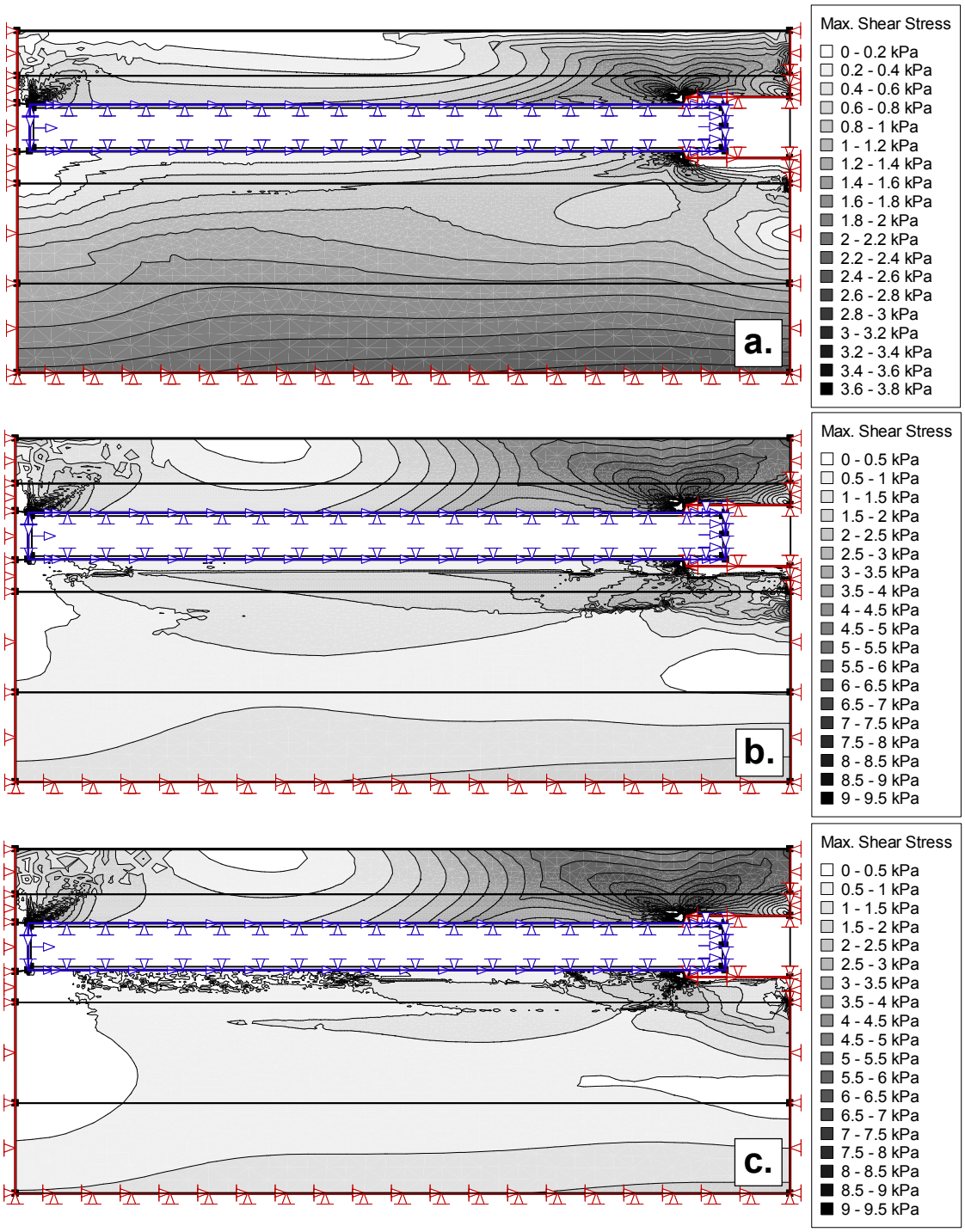

Figure 3.21 Maximum shear stress contours at the end of numerical analysis for: a) WT1, b) WT2, and c) WT3.

A close examination of Figure (3.22) reveals that the maximum shear stress on the interface along the pipe increases as WT depth (i.e. matric suction) increases. The increment is also reflected on the predicted axial force mobilized along the pipe resulting in higher axial force for unsaturated condition in comparison to saturated condition. In addition, the variation of the maximum shear stress along the top and bottom of the pipe is not uniform. At the front end of the pipe, higher shear stress was predicted in comparison to the other end. These results suggest that the soil deformation around the pipe is a result of the relative movement of the pipe with respect to soil. The cumulative horizontal load is transferred through shear stresses from the pipe to the soil. Due to this reason, the soil movement takes place in the direction the load is applied and contributes to the development of a compression zone at the front end as can be seen in the deformed mesh in Fig. 16. Such deformations result in non-uniform volumetric changes along the pipe leading to development of non-uniform dilation along the pipe. The maximum dilation is typically expected at the front end and less dilation is expected at the far end. Moreover, higher shear stresses can be observed at the top of the pipe comparing to the bottom of the pipe. This observation can be related to the level confining stress and the degree of freedom for the soil above and below the pipe. The soil above the pipe has more room to expand and hence dilate resulting in higher shear stresses. Furthermore, matric suction contribute to increase the dilation behavior (Hamid and Miller 2008 and 2009, Hossain and Yin 2014, and Borana et al. 2016) resulting in higher shear strength for unsaturated condition comparing to saturated condition.

The FEA results show good agreement with the measured values for saturated condition (Figure 3.18). For unsaturated condition (i.e. WT2, and WT3), the predicted pullout force-displacement behavior agrees reasonably well with the measured behavior in the elastic zone. In the plastic or strain-hardening zone, the predicted behavior slightly overestimate the pullout force. Such a behavior can be explained by considering the change in void ratio, *e* and moisture regime during physical pullout tests. Research studies have shown that shearing unsaturated soil with constant water content results in a reduction in the initial matric suction (Cunningham et al. 2003, and Rahardjo et al. 2004). The change in void ratio and moisture content, *w* and therefore, the initial matric suction of the soil and interface lead to a reduction in the apparent cohesion and soil stiffness. Simulating such behavior require more demanding unsaturated models that are not always available in commercial FE software and require additional parameters. In addition, it is also important to note that the soil-pipeline interaction problems are usually designed and analysed

using 3-dimensional models. However, using constant apparent cohesion and E_{unsat} during the FEA with the most widely used MC-model will reduce the number of variables that are required to conduct such analysis and provide reasonable results for pipelines behavior.

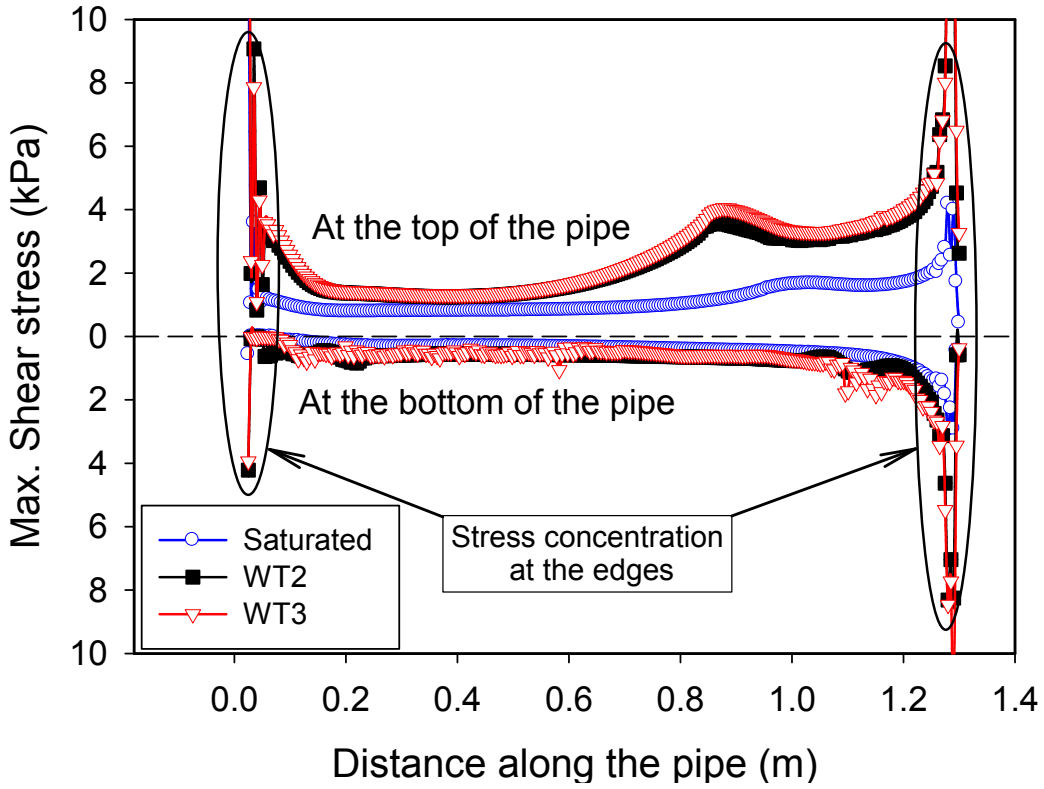

Figure 3.22 Variation of the maximum shear stress along the top and bottom of the pipe at the end of numerical analysis.

3.6 Conclusions

In this chapter, the pullout force-displacement behavior of prototype pipe under saturated and unsaturated condition was investigated. A comprehensive physical setup was designed and fabricated in the University of Ottawa for this reason. The study extended a systematic procedure for achieving reliable soil-matric suction profiles for coarse-grained soils that was developed based on the hanging column technique. The resulting soil-matric suction profiles showed consistent profiles for different WT levels with good repeatability in creating uniform profiles, which indicate that the proposed physical model and procedure are reliable and applicable for coarse-grained soils.

The pullout test results for different WTs indicate that as the WT depth increases (i.e. matric suction increases) the pullout force significantly increases. In other words, axial stresses exerted on the pipe in unsaturated sand is more than doubled in comparison to saturated condition, which implies that pipeline systems in unsaturated soil may experience higher external and internal forces and strains. Such observations highlight the need for revising the available design procedures, codes and guidelines, which were developed based on saturated soil mechanics, of pipeline systems and other soil-structure interaction problems that are in direct contact with unsaturated soils.

The FEA results suggest that designing pipeline systems using conventional approaches can underestimate the external and internal forces as well as damages and result in unsafe design procedures. Despite some limitations of assumptions used in the numerical analysis approach followed in this chapter, it is a simple methodology based on the principles of unsaturated soil mechanics that has provided reasonable estimation of the measured external axial force associated with the permanent ground deformation within the elastic range and conservative ultimate design loads in the strain-hardening zone. The FEA results are reasonable and promising to encourage practicing engineers to apply unsaturated soil mechanics in the design of pipelines in the field.

CHAPTER FOUR

AXIAL FORCE-DISPLACEMENT BEHAVIOR OF BURIED PIPELINES IN SATURTATED AND UNSATURATED SAND SUBJECTED TO RELATIVE SOIL MOVEMENT IN THE AXIAL DIRECTION

4.0 Background-Information

The contents presented in this chapter are summarized from the article below.

Al-Khazaali, M., and Vanapalli, S.K. (2018). Axial force-displacement behavior of a buried pipeline in saturated and unsaturated sand. *Géotechnique*. DOI: 10.1680/jgeot.17.p.116.

4.1 Introduction

Permanent ground deformation (PGD) associated with soil subsidence, differential settlement, landslide, frost heave or thaw settlement, and soil liquefaction, lateral spread movement or fault displacement induced by seismic activities contribute to large bending and tensile forces along with significant settlements of buried pipelines that may severely damage the pipelines. In such scenarios, pipeline body will be subjected to axial stresses due to soil mass movement parallel to its axis.

Pipelines are often buried above groundwater table where the soil is typically in a state of unsaturated condition and is covered with unsaturated backfill soil. For this reason, conventional design procedures are not reasonable for evaluating the mechanical behavior of pipeline systems buried in unsaturated soils as they can lead to erroneous estimation of loads exerted on pipeline body from the surrounding soil. Rational interpretation of the behavior of pipelines buried in

unsaturated soils leading to reliable estimation of the mechanical behavior can be achieved by extending the principles of unsaturated soils mechanics.

In this Chapter, axial stress that generates on a prototype steel pipeline of 114.3 mm in outer diameter due to soil movement under both saturated and unsaturated conditions (i.e. ($u_a - u_w$) = 0 (saturated), 2.75, 4.5, 7.25, 8, and 9.75 kPa) is determined in sand from laboratory investigations using a specially designed testing system. The axial force exerted due to relative movement on 1.35 m pipeline length was measured in a steel tank of 1.5 m length, 1.2 m width and 1.06 m height. Influence of dilation on the axial load-displacement was interpreted at different values of average matric suction above and below the crown and invert of the pipe, respectively. The results of the experimental tests were used to propose two analytical models to estimate the peak and ultimate axial stresses exerted on pipelines utilizing the principles of unsaturated soil mechanics. The framework developed in this article is promising for developing tools for the rational design of pipeline infrastructure buried in typical sands to ensure their stability, safety and at the same time provide economical solutions.

4.2 Background

4.2.1 Stress on pipeline due to axial soil movement

Figure 4.1 shows a pipeline buried in a slope that is subjected to an earthquake. Landslide, liquefaction or PGD may take place along the pipe axis (i.e. longitudinal PGD) that induce axial forces at the interface between liquefied (i.e. soil) and non-liquefied (i.e. pipeline) materials. The pipeline will experience large deformations at the boundaries (i.e. tension strains at the head and compression strains at the toe). Damages in steel pipelines induced by longitudinal PGD are typically 5 to10 times higher than those expected by transverse PGD due to higher flexural flexibility of steel pipes in comparison to axial tension or compression deformations (ALA 2005).

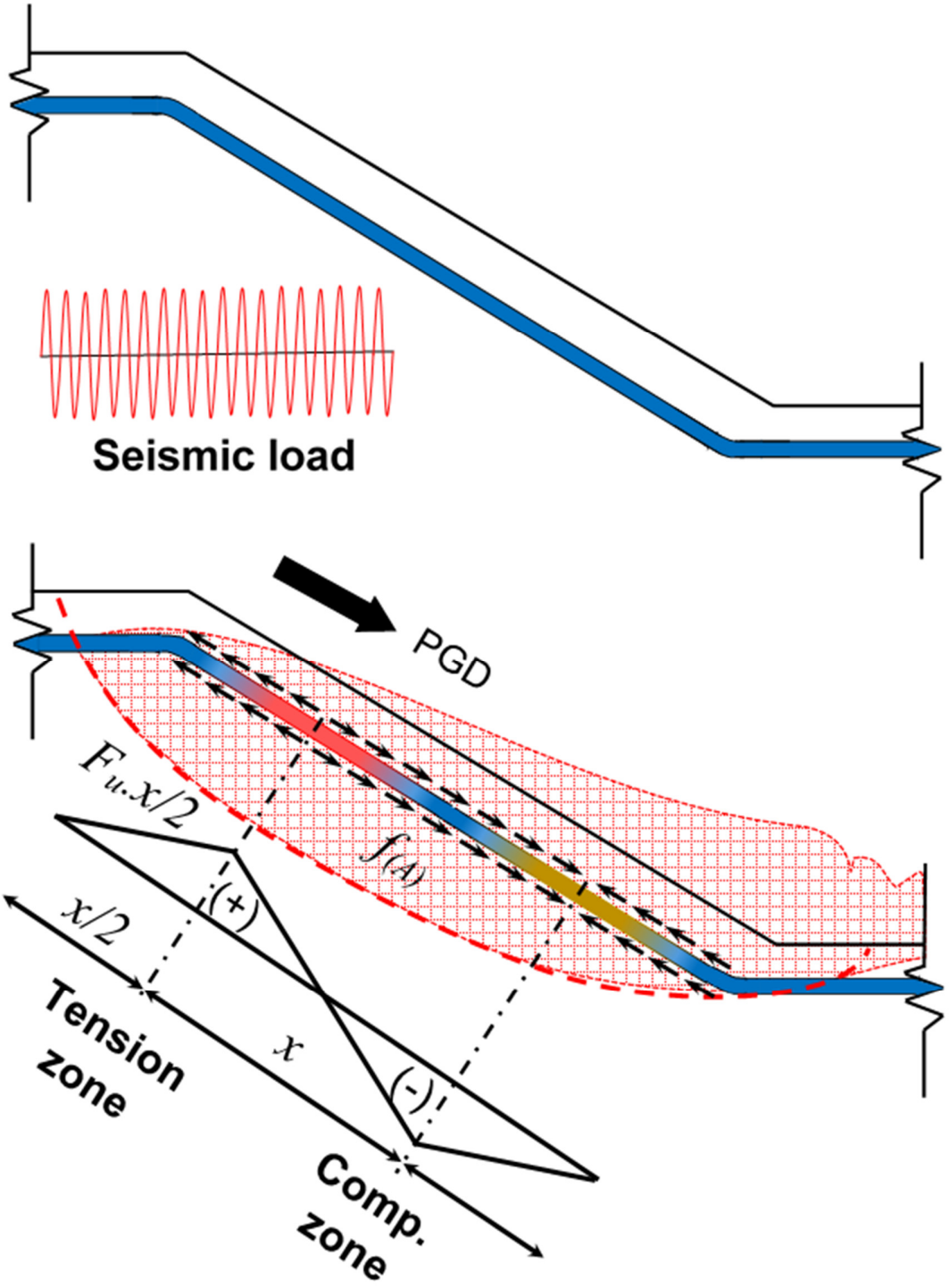

Figure 4.1 A pipeline subjected to soil body movement in the axial direction due to seismic activity and the axial forces diagram exerted on the pipe.

Different analytical methods are used to determine the axial force that is exerted on the pipeline due to longitudinal PGD. ALA (2005) suggests that the maximum axial force due to transient ground strains on a continuous pipeline associated with ground shaking or seismic activities can be estimated as the minimum value of Eq. (4.1) or Eq. (4.2). Eq. (4.1) takes account for soil-pipe interface unit skin friction while Eq. (4.2) is developed based on the mechanical properties pipe material assuming the pipe is fully compliant with the soil (i.e. ground strain, ε_g is transferred to the pipe without any slip).

$$F_A = \frac{F_u . \lambda}{4} \tag{4.1}$$

$$F_A = E_P . A . \varepsilon_P \tag{4.2}$$

$$\varepsilon_P = \varepsilon_g = \frac{PGV}{C} \tag{4.3}$$

where F_A is maximum axial force, F_u is the maximum skin friction force per unit pipe length, λ is the seismic wavelength in soil at pipe location, E_P is Young's modulus of pipe, A is pipe cross sectional area, ε_P is pipe strain, PGV is peak ground velocity (unit length/unit time), and C is seismic wave propagation speed in the soil at the pipe location (unit length/unit time).

The axial force on a continuous pipeline due to longitudinal PGD can also be estimated as the lower value of Eq. (4.4) which assume the pipe is elastic and fully compliant with soil or Eq. (4.5) that takes into account the ultimate force that transfers from soil to pipe (ALA 2005).

$$F_A = \sqrt{E_P . A . F_u . \Delta} \tag{4.4}$$

$$F_A = \frac{F_u . L}{2} \tag{4.5}$$

where Δ is the maximum PGD, L is the length of pipe in soil mass undergoing longitudinal movement.

The nonlinear behavior of the pipe material is simulated using regression analysis extending the beam model. Axial soil resistance is typically idealized using elastic-perfectly plastic discrete springs, which provide specified resistance per unit length (ALA 2001) (Figure 4.2). Soil

subgrade reaction, k (i.e. spring reaction) can be estimated using Eq. (4.6) which relates the force F_u to the mobilized horizontal displacement, Δ.

$$k = \frac{F_u}{\Delta} \tag{4.6}$$

The mobilized skin friction, $f_{(A)}$ is a key parameter that is required to estimate F_u on buried pipeline due to PGD. The longitudinal mechanical behavior of buried pipeline is similar to skin friction resistance of pile foundation. A modified version of β-method by Burland (1973) extending effective stress analysis approach (ESA) and α-method by Skempton (1959) (i.e. total stress analysis approach (TSA)) are used to estimate the axial resistance of pipeline.

- For cohesionless soils:

$$F_u = \pi . D .\ f_{(A)} \ = \pi . D . \left[\gamma' H \left(\frac{1 + K_o}{2}\right) \tan \delta\right] \tag{4.7}$$

- For cohesive soils:

$$F_u = \pi . D .\ f_{(A)} = \ \pi . D . \alpha . c_u \tag{4.8}$$

where D is the pipe outside diameter in meter, γ' is the effective unit weight in (kN/m^3), H is the soil cover thickness to the springline in meter, K_0 is the coefficient of lateral earth pressure at rest, δ is the angle of internal friction for the interface, α is the adhesion factor, and c_u is the soil undrained cohesion in (kPa). The value of δ depends on the pipeline external surface coating or roughness and can be estimated as a ratio of soil effective angle of internal friction, ϕ' using a reduction factor (ALA 2001). The term [{(1+K_0)/2}*tan δ] in Eq. (4.7) is a modified form of the original Burland-Bjerrum coefficient, β (i.e. β = K_0*tan δ). The modification is based on the assumption that the average normal stress on the perimeter of the pipe is equal to the arithmetic mean of the effective vertical overburden stress and lateral effective stress (Wijewickreme et al. 2009). In this study, focus will be directed towards better understanding the axial behavior of buried pipeline in a cohesionless soil (i.e. sand).

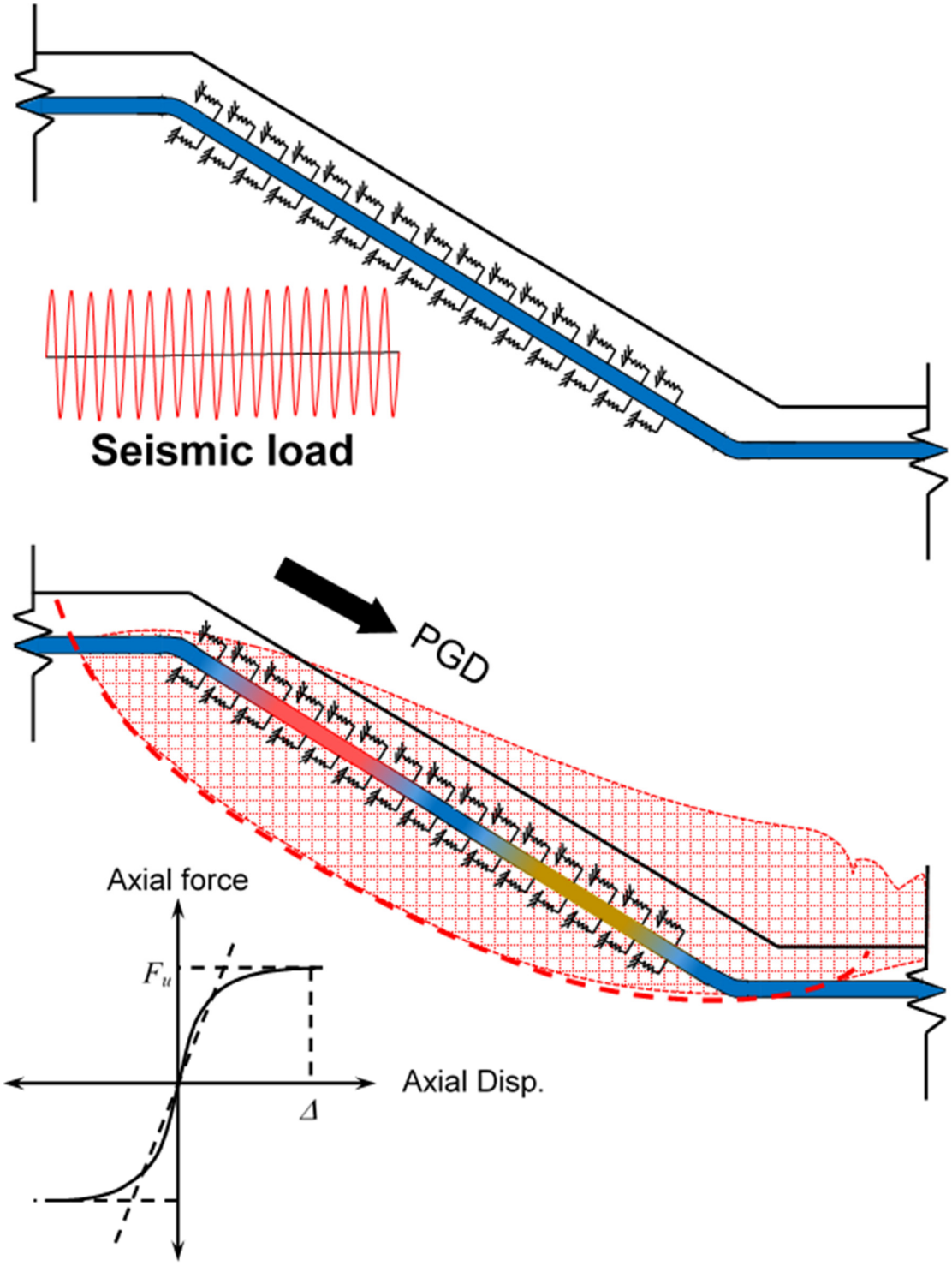

Figure 4.2 Idealization of soil with axial discrete springs.

Excess pore water pressure under different loading conditions is not likely to develop in cohesionless soils due to its relatively high coefficient permeability. Thus, ESA approach is used to estimate the axial force applied on a pipeline buried in sandy soils associated with relative soil movement in the parallel direction to the pipe axis (Scarpelli et al. 2003, ALA 2005, Wijewickreme et al. 2009, and Revie 2015). Usually the unit skin friction along a pipeline, $f_{(A)}$ in cohesionless soil is determined considering fully saturated condition extending conventional soil mechanics parameters according to Ng (1994), ALA (2001), and Wijewickreme et al. (2009) (Eq. 4.7).

In conventional geotechnical engineering practice, unsaturated soils or soil layers above the groundwater table are classified or assumed non-liquefiable under the impact of earthquake (Tsukamoto et al. 2014, and Zhang et al. 2016). In other words, 100% degree of saturation condition is a key prerequisite condition for liquefaction to occur. The possibility of liquefaction triggering in unsaturated cohesionless soils such as sands during earthquakes is well established from many experimental studies and field observations (i.e Sherif et al. 1977, Chaney 1978, Yoshimi et al. 1989, Hsu et al. 1995, Chillarige et al. 1997, Grozic et al. 2000, and Uzuoka et al. 2005). Furthermore, mechanical behavior (i.e. stress and volume change) of unsaturated soil and unsaturated soil-structure interface have been extensively examined during the past few decades (Toll 1990, Alonso et al. 1990, Gallipoli et al. 2003, Lins and Schanz 2005, Schanz and Alabdullah 2007, Hamid and Miller 2009, Sivakumar et al. 2010, Hossain and Yin 2014, Lu and Kaya 2014, Borana et al. 2016, and Han and Vanapalli, 2016). These studies along with our present state-of-the-art understanding of the mechanics of unsaturated soils can be extended for reliable interpretation and estimation of the axial forces exerted on pipeline systems for engineering practice applications.

4.2.2 Mechanical behavior of unsaturated soil and interface

Evaluation of buried pipeline behavior requires rational estimation of the mechanical properties of soil and the soil-pipeline interface. In conventional soil mechanics, Mohr-Coulomb (MC) failure criteria is employed extending Terzaghi's effective stress principle for interpretation of the shear strength of saturated soils. Soil effective shear strength parameters (i.e. effective cohesion, c', and, ϕ') are conventionally measured using the triaxial shear equipment while interface shear strength parameters (i.e. adhesion, c_a', and, δ) are measured using the direct shear test apparatus. The mechanical behavior of unsaturated soils can be described by extending MC constitutive model

using two stress state variables; namely, the net normal stress, ($\sigma - u_a$) and matric suction, ($u_a - u_w$) extending the ESA approach (Bishop 1959, Fredlund et al. 1978). The ($u_a - u_w$) is a stress state variable that acts on the wetted contact area of the soil-water-air interphase. The ($\sigma - u_a$) and ($u_a - u_w$) contribute independently to shear strength and volume change behavior of unsaturated soil. A modified MC model proposed by Fredlund et al. (1978) for unsaturated soil is given in Eq. (4.9). The modified MC model by Fredlund et al. (1978) requires an additional shear strength parameter that is directly related to the stress state variable, ($u_a - u_w$). This parameter which is designated as ϕ^b, is the angle of internal friction with respect to ($u_a - u_w$) variation under a constant $(\sigma - u_a)$.

$$\tau_{unsat} = c' + (\sigma - u_a) \tan \phi' + (u_a - u_w) \tan \phi^b \quad (4.9)$$

where σ is normal stress, u_w is pore water pressure, and u_a is pore air pressure.

Modified triaxial or direct shear equipment is required for measuring the shear strength parameters for unsaturated soil and interface (i.e. c', ϕ', ϕ^b, c_a' and δ). The modified equipment employs axis translation technique (Hilf 1956) and can be used for both fine- and coarse-grained soils, or hanging column technique (Haines 1930) for coarse-grained soils (Schanz and Alabdullah 2007, Sun and Xu 2007, Vanapalli et al. 2008, Hamid and Miller 2009, Lu et al. 2009, Hossain and Yin 2014, Borana et al. 2016).

Determination of the shear strength of unsaturated soils from experimental studies needs elaborate test equipment and highly trained personnel. Hence, it is expensive and time consuming. For these reasons, several researchers proposed semi-empirical models for respectively predicting the long and short-term shear strength of unsaturated soils extending the ESA and TSA approaches. These models utilize the soil-water characteristic curve (SWCC) and the saturated soil property information to estimate or predict the variation of the mechanical or hydraulic properties with respect to suction (for example, Bishop 1959, van Genuchten 1980, Vanapalli et al. 1996a, Fredlund et al. 1996, Khalili and Khabbaz 1998, Agus et al. 2003, Sawangsuriya et al. 2009, Hamid and Miller 2009, Hossain and Yin 2014, Lu and Kaya 2014, Han and Vanapalli 2016). The modified approaches for interpreting the unsaturated soils behavior are referred to as the modified total stress analysis (MTSA) and modified effective stress analysis (MESA) approaches (Vanapalli and Oh 2010). These approaches have been used to estimate the behavior of different soil-structure interaction problems. For example, the bearing capacity of shallow and deep foundations, retaining

walls, soil nails in unsaturated soils were interpreted extending MESA approach by several investigators (e.g. Oloo et al. 1997, Vanapalli and Mohammed 2007, Gurpersaud et al. 2013) and MTSA has been used for the bearing capacity of shallow and deep foundations (e.g. Oh and Vanapalli 2009, Vanapalli and Taylan 2012). These models provide smooth transition of the mechanical behavior from unsaturated to saturated soil condition.

Extending MESA approach, Vanapalli et al. (1996a) proposed semi-empirical model to predict the effective shear strength of unsaturated soil (Eq. 4.10).

$$\tau_{unsat} = c' + (\sigma - u_a)tan\phi' + (u_a - u_w)S^{\kappa}tan\,\phi' \quad (4.10)$$

where S = degree of saturation, and κ = fitting parameter.

The angle of internal friction, ϕ' is not significantly influenced by the soil suction (Vanapalli et al. 1996b). The contribution of $(u_a - u_w)$ towards the shear strength can be expressed as apparent cohesion, c using the relationship in Eq. (4.11).

$$c = c' + (u_a - u_w)S^{\kappa}tan\,\phi' \quad (4.11)$$

This model can be extended to predict the unsaturated interface apparent adhesion, c_a along a pipeline body with some minor modifications to Eq. (4.7). More information of these modifications are detailed in later paragraphs. Such a model would be useful to predict the maximum unit skin friction, $f_{(A)}$ and maximum axial force per unit length, F_u along pipeline surface considering the influence of $(u_a - u_w)$ for unsaturated soils.

4.3 Test Program and Methodology

Test program was discussed earlier in Chapter 3. In this chapter, measuring the shear strength of sand and the interface parameter will be discussed and presented in this chapter.

4.3.1 Direct shear and plane strain shear strength parameters

Direct shear tests (DST) can be conveniently used to measure the shear strength parameters for soil and soil-structure interface (ϕ'_{ds}, δ_{ds} and dilation angle, ψ). Two angles of internal friction can

be deduced from the DST; peak angle of internal friction, $\phi'_{ds\text{-}p}$ or $\delta_{ds\text{-}p}$ and ultimate or critical angle of internal friction, $\phi'_{ds\text{-}r}$ or $\delta_{ds\text{-}r}$. Due to similarity of cohesionless soil and rough interface behavior, discussions will be limited to cohesionless soil behavior from the DST in the following paragraphs.

In DST, linear strain increments take place in two directions (i.e. parallel, $d\varepsilon_{xx}$ and perpendicular, $d\varepsilon_{yy}$ to the applied shear force direction) and constrained in the third direction (i.e. $d\varepsilon_{zz} = 0$). Consequently, the volumetric strain increments, $d\varepsilon_v$ will be equal to:

$$d\varepsilon_v = d\varepsilon_1 + d\varepsilon_3 = d\varepsilon_{xx} + d\varepsilon_{yy} \tag{4.12}$$

where $d\varepsilon_1$ and $d\varepsilon_3$ are the principle linear strain increments that are corresponding to zero shear strain, $\gamma/2$.

Typical behavior of medium to dense sand and sand-structure interface from DST is summarized in Figure (4.3). The soil sample experiences contract during the early stage of shearing in the DST as soil particles start filling the voids. The shear stress linearly increases in this stage. Once the voids are filled and when there is no more room for particles to move, soil particles start overriding at points of contacts leading to a remarkable volumetric expansion during shearing stage. (A-B). The shear stress-strain behavior of the soil is nonlinear in this stage. At point (B), the dilation rate is maximum and hence the shear stress reaches the peak state. At the peak state, the applied stresses are not varying, so there is only plastic strain increments (Jewell and Wroth 1987). The $\phi'_{ds\text{-}p}$ can be obtained from the ratio of the measured shear stress, τ_{yx} in DST to the applied normal stress, σ'_{yy} (for simplicity, τ_{yx} and σ'_{yy} are denoted as τ and σ', respectively).

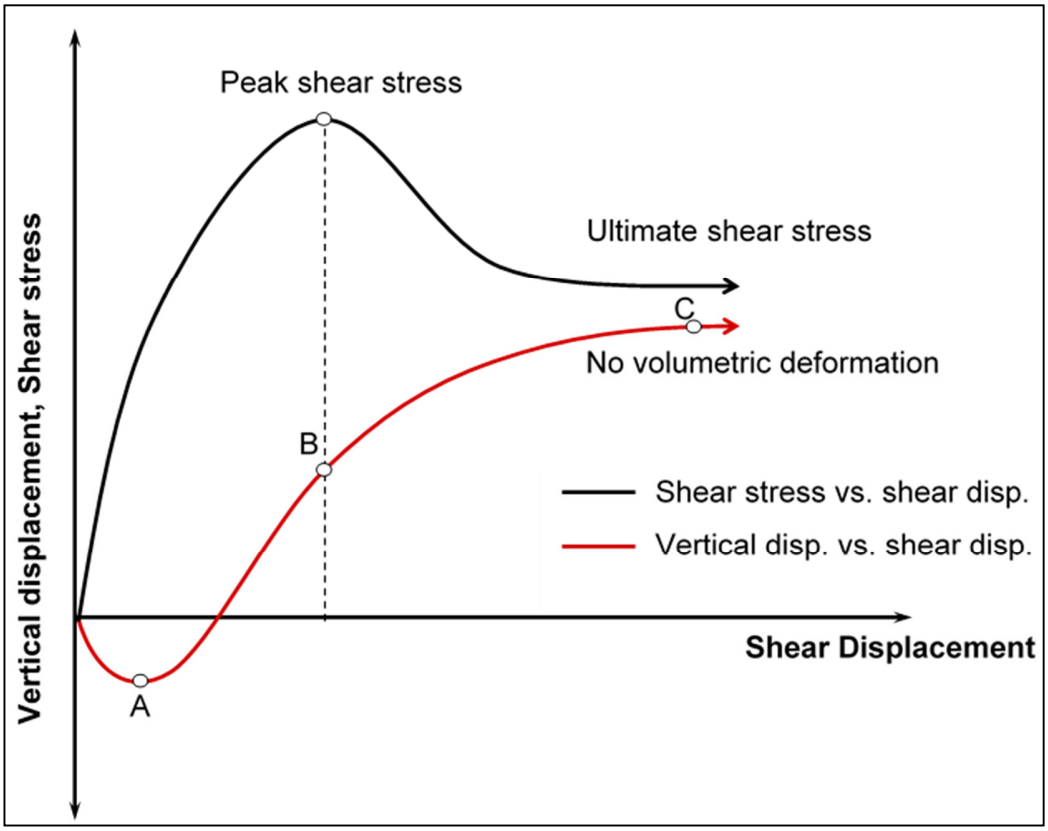

Figure 4.3 Typical shear stress-shear displacement and vertical displacement-shear displacement behaviors during direct shear test.

$$tan\,\phi'_{ds-p} = \frac{\tau_{yx}}{\sigma'_{yy}} = \frac{\tau}{\sigma'} \tag{4.13}$$

At the peak state, Jewell and Wroth (1987) and Lings and Dietz (2004) stated that the stress and incremental linear strain axes coincide. In addition, the ϕ'_{ds-p} is mobilized on a plane along which there is no linear incremental strain (i.e. zero extension). If the direction of zero incremental strain is the horizontal direction (i.e. $d\varepsilon_{xx} = 0$) (Figure 4.4b), then the dilation angle of sand at the peak state, ψ_p can be defined as the ratio of the vertical displacement increment, d_v to horizontal displacement increment, d_h (Jewell 1989).

$$tan\,\psi_p = \frac{d_v}{d_h} = -\frac{d\varepsilon_{yy}}{d\gamma_{xy}} \tag{4.14}$$

From point B to C in Figure (4.3), there is gradual reduction in the stress ratio (i.e. τ/σ') until there is no further volumetric strain (i.e. $d\varepsilon_v = 0$). The stress ratio reaches to a constant value which is defined as the critical or ultimate angle of internal friction, $\phi'_{ds\text{-}r}$.

$$tan\,\phi'_{ds-r} = \frac{\tau_r}{\sigma'} \tag{4.15}$$

Nevertheless, the boundary condition restriction in the DST prevents peak stress ratio from being mobilized along the horizontal plane (Jewell and Wroth 1987). In fact, the peak stress ratio is mobilized on a plane inclined at an angle ω to the horizontal plane (Figure 4.4a). The maximum stress ratio (i.e. τ/σ') plane rotation from the direct shear plane can be determined from the geometry of Mohr's circle.

$$\omega = \frac{\phi'_{ps-p} - \psi}{2} \tag{4.16}$$

where $\phi'_{ps\text{-}p}$ is the peak plane strain angle of internal friction.

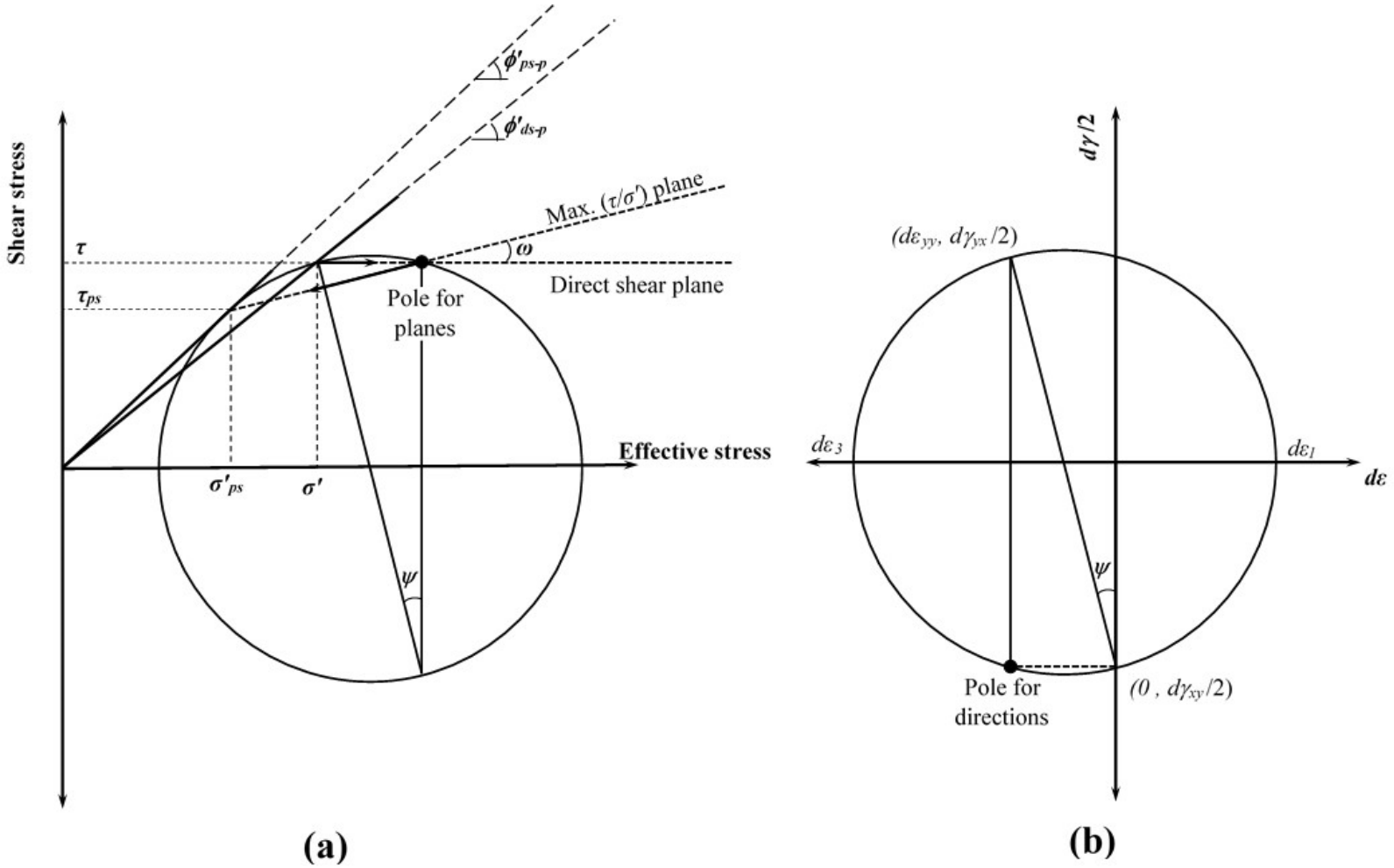

Figure 4.4 Mohr's circles for dense sand in DST; (a) stress, and (b) incremental strain (modified after Jewell and Wroth 1987).

Davis (1986) related the stress ratio or the mobilized angle of friction in DST to the plane strain angle of internal friction, ϕ'_{ps} and ψ using the following expression:

$$tan\,\phi'_{ds} = \frac{sin\phi'_{ps}\,cos\psi}{1 - sin\phi'_{ps}sin\psi} \tag{4.17}$$

At critical state when there is no dilation or volumetric change, Eq. (4.17) reduces to:

$$tan\,\phi'_{ds-r} = sin\phi'_{ps-r} \tag{4.18}$$

Bolton (1986) developed a simple empirical approach for the flow rule that relate $\phi'_{ps\text{-}p}$, $\phi'_{ps\text{-}r}$ and ψ_p:

$$\psi = \frac{\phi'_{ps-p} - \phi'_{ps-r}}{0.8} \tag{4.19}$$

The $\phi'_{ps\text{-}p}$ can be estimated from the $\phi'_{ds\text{-}p}$. A relationship between the $\phi'_{ps\text{-}p}$, $\phi'_{ds\text{-}p}$, and $\phi'_{ps\text{-}r}$ from Rowe (1969) is summarized in Figure (6). This relationship was developed from direct shear and plane strain test results at comparable stress levels on feldspar sand, quartz sand and glass ballotini. Rowe's results suggested a difference of 9^0 between the peak shearing angle from direct shear and plane strain tests. Lings and Dietz (2004) suggested a simple expression (Eq. 4.20) to predict the $\phi'_{ps\text{-}p}$ from the $\phi'_{ds\text{-}p}$ based on the results of Rowe (1962), Davis (1968) and Rowe (1969). They conclude that Eq. (4.20) provides conservative estimation for $\phi'_{ps\text{-}p}$. In this study, Eq. (4.18) and Figure (6) in Rowe (1969) were utilized to obtain $\phi'_{ps\text{-}r}$, and $\phi'_{ps\text{-}p}$, respectively using the results of DST (i.e. $\phi'_{ds\text{-}r}$, and $\phi'_{ds\text{-}p}$). ψ_p was determined using Bolton's (1986) flow rule given by Eq. (4.19).

$$\phi'_{ps-p} = \phi'_{ds-p} + 5 \tag{4.20}$$

The effective shearing and dilation angles of the soil and interface (i.e. ϕ' and δ, respectively) were measured using the DST results. Strain controlled tests were conducted at low constant shearing speed rate (i.e. 0.0025 mm/s.) to achieve drained loading condition. A specially designed rough surface steel block of (60 x 60 x 15 mm) was used to simulate the pipe surface

roughness and measure δ (Figure 4.5). The block was designed to occupy the lower part of the shear box fully such that the rough surface of the block will be at the same level of the horizontal failure plane. The sand was compacted in the upper part of the shear box by tamping method at a relative density around 69%.

The DST results for the sand and soil-pipe interface is presented in Figure (4.6). Four normal stresses (i.e. 25, 40, 75 and 125 kPa) were applied for shearing the samples. With D_r around 69% and the normal stress range, the sand exhibited dilatancy under all normal stresses that were applied. Such behavior is compatible with Bolton (1986) findings. He suggested that soil dilation and the peak angle of shearing are directly related to the relative density, D_r, and inversely to mean effective stress of soil. Moreover, angle of friction at critical state (i.e. ultimate state), in which soil is sheared under constant volume, is also dependent on soil mineralogy. Substantial portion of quartz and feldspar formation consist of mica, calcite or other materials that have significant effect on both angle of friction at critical state and particles crushing at high stresses (Bolton 1986). Sadrekarimi and Olson (2013) stated that loose sand at critical state are continuously

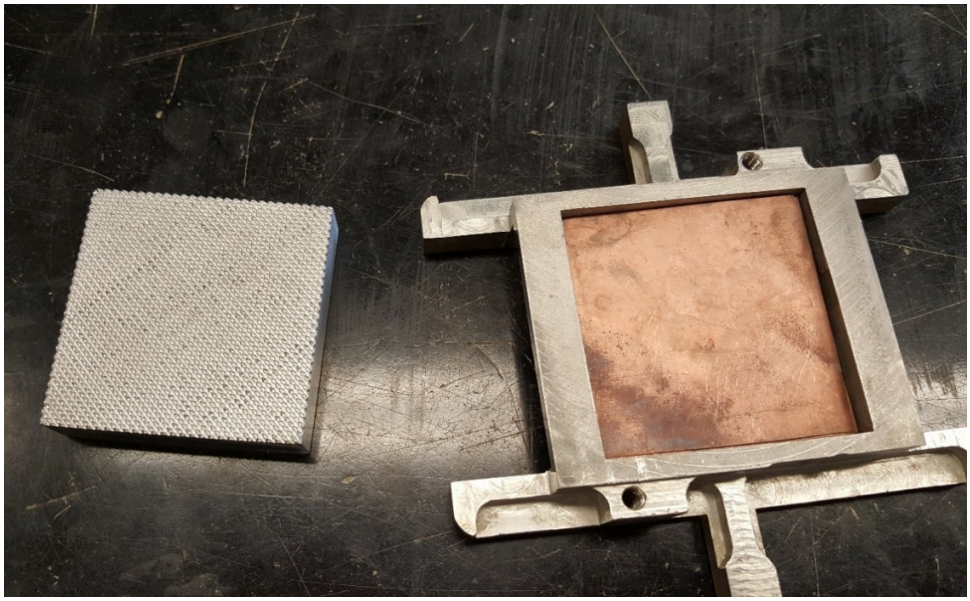

Figure 4.5 Knurled interface block and lower half of shear box.

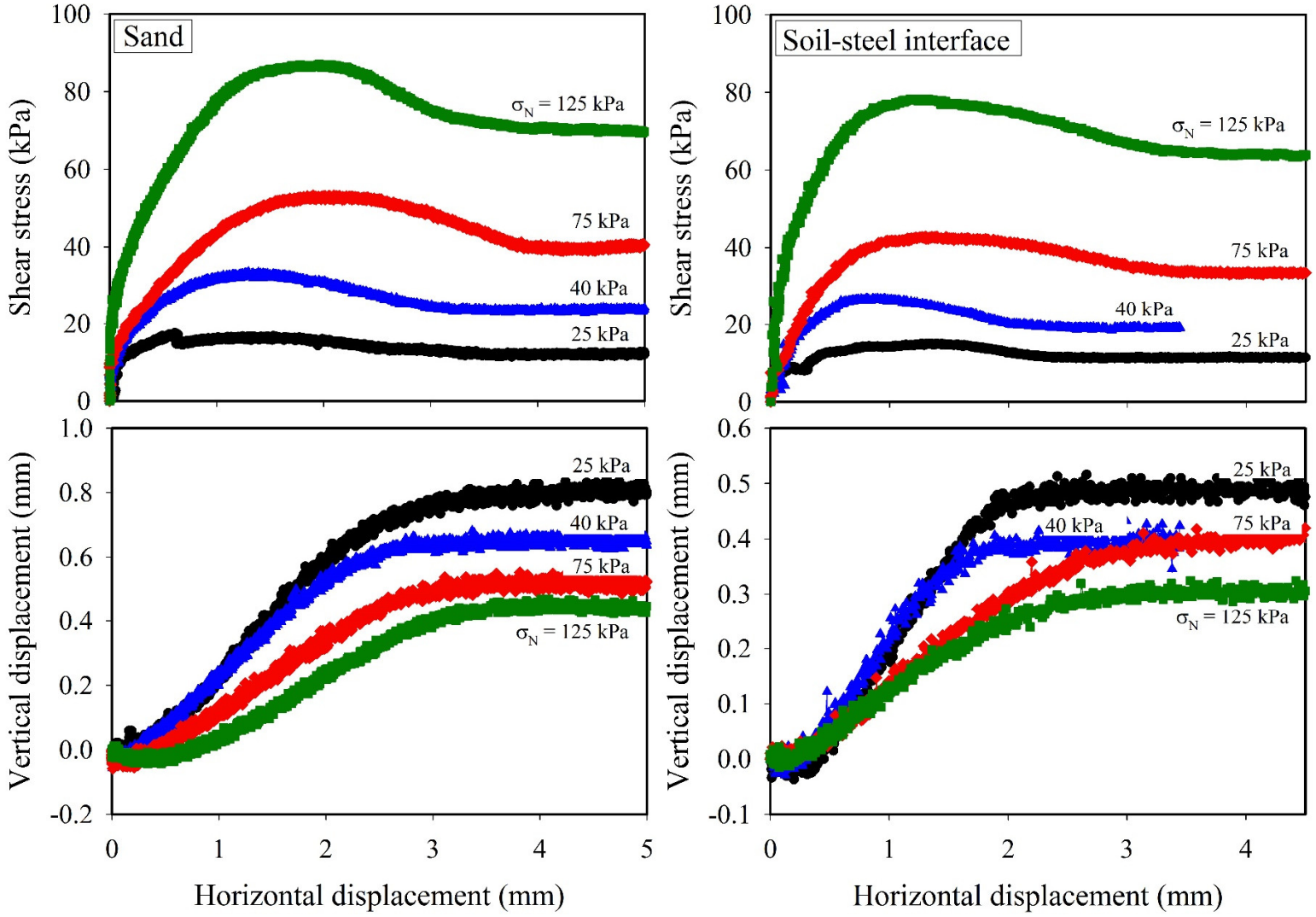

Figure 4.6 Direct shear test results for sand and interface.

remolded and the particles are continuously rolling, rearranging, and reorienting with insignificant particles crushing, while shearing dense sands results in particles crushing and significant contractive behavior in ultimate state.

The results show that the peak shear stress for the rough steel was mobilized at relatively low shear displacements compared to sand. The peak and ultimate shear stresses plotted as a variation of the applied normal stresses for both soil and soil-rough steel interface in Figure (3.9). Peak stress ratio from the DST for sand and interface were close to each other as well as for the ultimate stresses. The measured or calculated ϕ'_{ds}, δ_{ds}, ϕ'_{ps}, δ_{ps}, and ψ_p values are summarized in Table (4.1).

Table 4.1 Summary of shearing and dilation angles of the soil and interface.

Properties	DST	Plane strain	ψ_p
Peak angle of friction (^{0})	35.3	43.4*	6.75 ‡
Ultimate angle of friction (^{0})	31.6	38 †	
Peak rough steel–soil interface friction angle (^{0})	34.5	41.5*	7.33‡
Ultimate rough steel–soil interface friction angle (^{0})	30.2	35.64 †	

* Figure 6 (Rowe 1969), † Eq. (4.18), and ‡ Eq. (4.19)

4.4 Test Results

The results of six pipe pullout tests at different soil capillary (i.e. matric) suction values are presented in Figure (4.7). The pullout test results are presented as a relationship between the axial force and $f_{(A)}$ vs. axial displacement. The axial load that was transferred from unsaturated sand on to the pipe increased by almost 2.5 folds in comparison to saturated condition. In addition, the required displacement to mobilize the peak axial resistance is much less than for saturated condition. Moreover, the load-displacement in the pre-peak zone exhibits strain-hardening behavior and strain-softening behavior in the post-peak zone. Figure (4.8) shows variation of both peak and ultimate $f_{(A)}$ with respect to the average matric suction in the vicinity of pipe body. The results demonstrate that the peak and ultimate $f_{(A)}$ significantly increased due to matric suction contribution.

4.5 Discussion of Test Results

4.5.1 Influence of matric suction

Figure (4.7) and (4.8) show that axial load transferred from the sand to the pipe body increased with matric suction. This behavior can be explained by relating the test results to the SWCC. The SWCC has typically three distinctive zones; namely, the boundary effect zone, transition zone and residual zone of unsaturation as discussed in Vanapalli et al. 1999) (Figure 4.8). In this figure, linear increase trend with a constant increase rate can be observed for $f_{(A)}$ in the boundary effect zone due to matric suction increase up to the air entry value (AEV). In this zone, the soil is fully saturated by capillary effect as $(u_a - u_w)$ increases. This can be explained by considering that the $(u_a - u_w)$ is an energy potential that applies tension stress on soil particles and their packets which provide resistance to sliding deformation (i.e. elastic strains) and distortion deformation (i.e. plastic strain) (Han et al. 2016). Once the $(u_a - u_w)$ exceeds the AEV and moves to transition zone (i.e. soil starts to desaturate and the wetted area of contact between the soil particles decreases), the variation of $f_{(A)}$ becomes nonlinear with respect to $(u_a - u_w)$ with a descending increase rate. The water phase substantially reduces when the sand reaches the residual state of unsaturation; at which the contribution of matric suction decreases significantly. Consequently, the axial force or $f_{(A)}$ also decreases. The axial force or $f_{(A)}$ approaches a constant value when the soil is further subjected to desaturation (i.e. approaching the dry condition) as the contribution of $(u_a - u_w)$ becomes negligible.

Figure (4.9) shows the variation of axial subgrade reaction, k_a, which is the ratio of peak axial load to the corresponding axial displacement, with respect to matric suction. The k_a values for unsaturated condition increased by several folds in the boundary effect and transition zones in comparison to the saturated axial subgrade reaction, $k_{a\text{-}sat}$. However, the k_a decreased significantly in the residual zone of unsaturation and became almost equal to $k_{a\text{-}sat}$. Using the $k_{a\text{-}sat}$ in numerical analysis will lead to erroneous prediction of axial soil-pipeline behavior, which may lead to unsafe design. For this reason, it is important to consider the contribution of $(u_a - u_w)$ towards the behavior of soil-pipeline system in unsaturated soils.

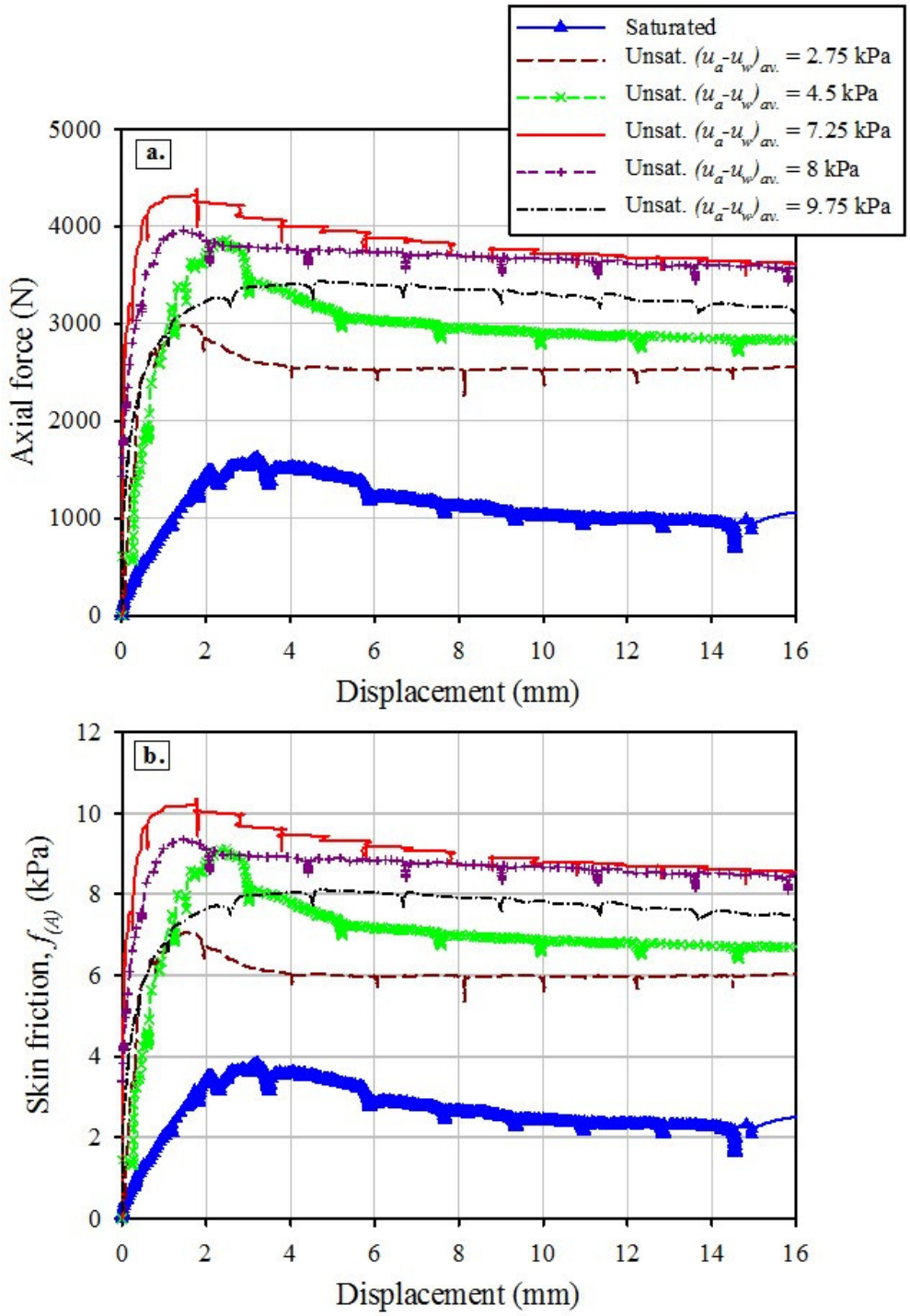

Figure 4.7 Variation of mobilized; (a) Axial force with respect to axial displacement, and (b) Unit skin friction, $f_{(A)}$ with respect to axial displacement during pullout tests under different matric suction values.

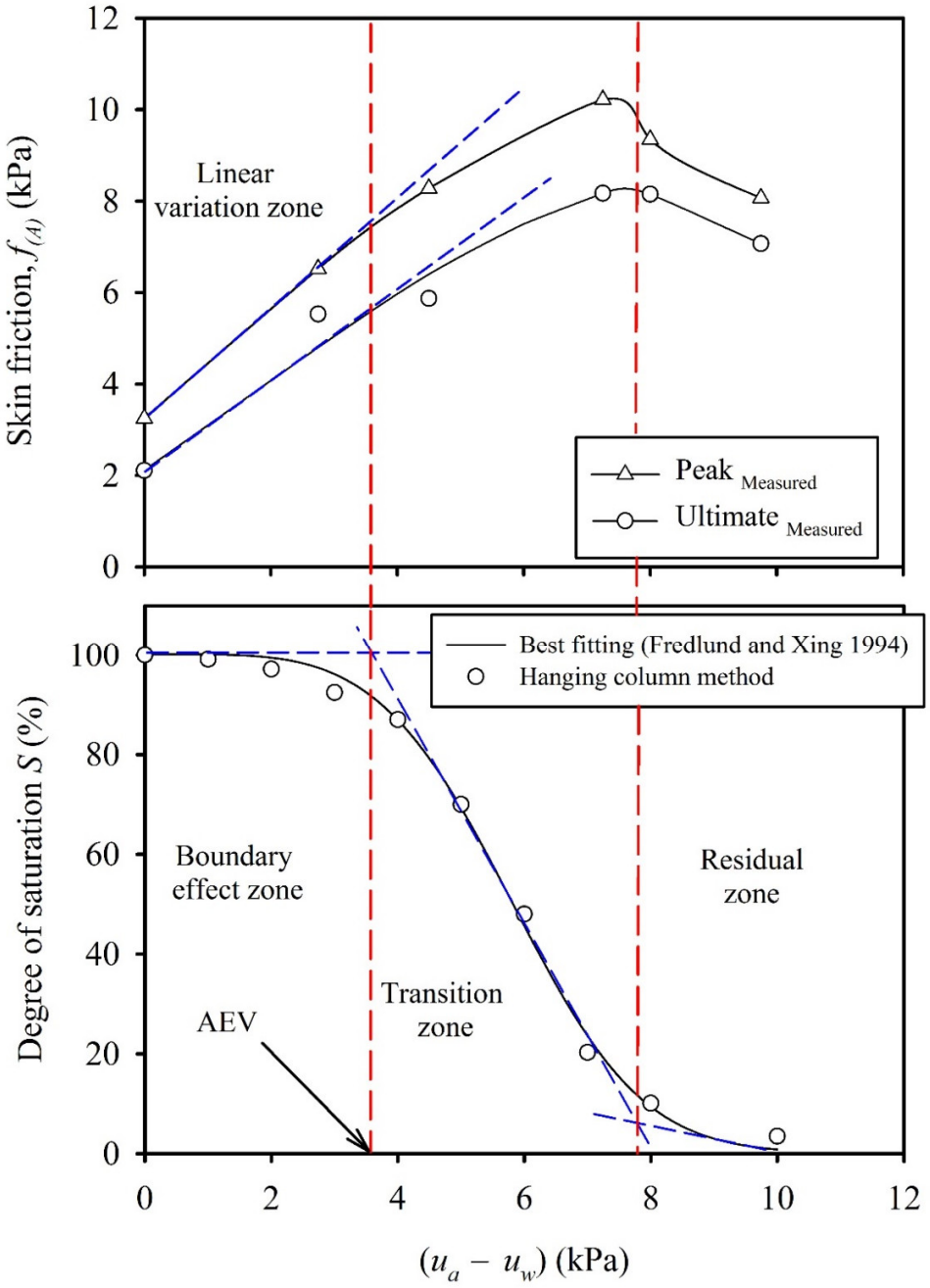

Figure 4.8 Variation of the measured peak and ultimate unit skin friction, $f_{(A)}$ in various zones of unsaturation.

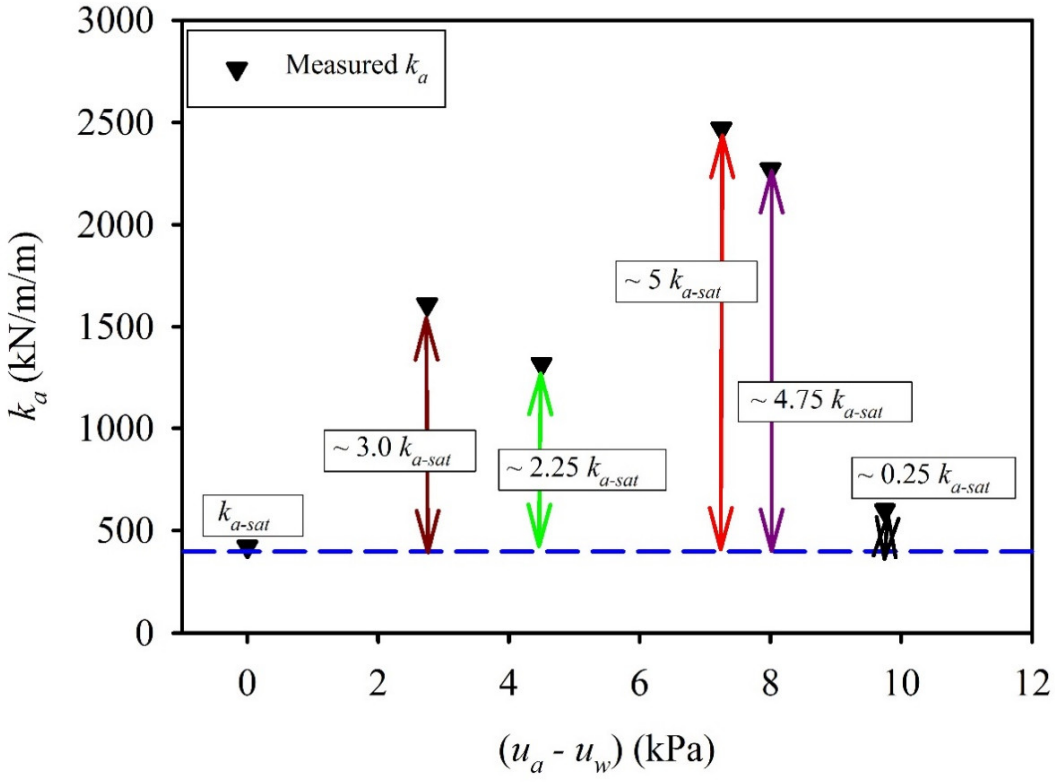

Figure 4.9 Variation of measured axial subgrade reaction, k_a with respect to matric suction.

4.5.2 Dilation effect

Figure (4.7) shows typical load-displacement and stress-displacement behavior with three distinctive zones; elastic zone, strain-hardening or pre-peak zone and strain-softening or post-peak zone. Roy et al. (2015 and 2016) stated that linear and nonlinear elastic strains are mainly controlled by soil modulus of elasticity, E and Poisson's ratio, μ. Strain-hardening or pre-peak plastic zone is defined by yield and peak points. The initial yield surface in MC constitutive model is defined by the mobilized angle of internal friction, ϕ'. In this zone, plastic strains occur when the stress state passes the initial yield surface. Both ϕ' and dilation angle, ψ are increased from initial values to peak values with the accumulated engineering plastic shear strains. In the post-peak softening zone, both ϕ' and ψ decrease with engineering plastic shear strain.

Hamid and Miller (2009) investigated the behavior of Minco silt-steel interface using two different surfaces (i.e. smooth and rough steel surfaces). The tests were performed under saturated and unsaturated condition using a modified DST. They conclude that the $(u_a - u_w)$ contribute to

the peak shear strength of interface and has limited contribution to post-peak shear strength. Hossain and Yin (2014) investigated the dilatancy of unsaturated completely decomposed granite (CDG) soil-cement grout interface using a specially designed DST. Their results showed that the shear strength of interface behavior exhibit strain-hardening behavior in the pre-peak zone for the entire suction range at lower $(\sigma - u_a)$ range. They conclude that the dilation angle of CDG-cement grout interface increases with matric suction at lower $(\sigma - u_a)$ and decreases significantly at higher $(\sigma - u_a)$.

Design codes such as, ALA (2001) and (2005), IITK-GSDMA (2007), and PRCI (2009) assume uniform unit skin friction per unit length, $f_{(A)}$ distribution along the pipe length (Figure 4.1). The $f_{(A)}$, however, is affected by soil dilatancy. Figure (4.10) suggests that volumetric and shear deformations occur along the soil-pipe interface during the test. At the load application point, high plastic (volumetric and shear) deformations occur at the interface zone (i.e. compression zone at the vicinity of the box boundary). The dilatancy is predominant in this zone and contributes to the mobilized axial stresses in the interface. On the other end, less plastic volumetric and shear strains can be expected which mimics the zone of pipe extension in Figure (4.1). The variation of dilatancy can significantly affect the distribution of $f_{(A)}$ along the pipe body. Furthermore, as discussed earlier, dilatancy of interface increases significantly with matric suction (Hossain and Yin 2014). The same argument can be extended for postulated deformation presented in Figure (4.10) which may be attributed to nonlinear $f_{(A)}$ distribution along the pipe length due to the dilation effects. Therefore, the peak mobilized $f_{(A)}$ that develops along the pipe body should be taken into account. The methodology of taking account of dilation effect for predicting the peak mobilized $f_{(A)}$ will be discussed in a later section providing more details.

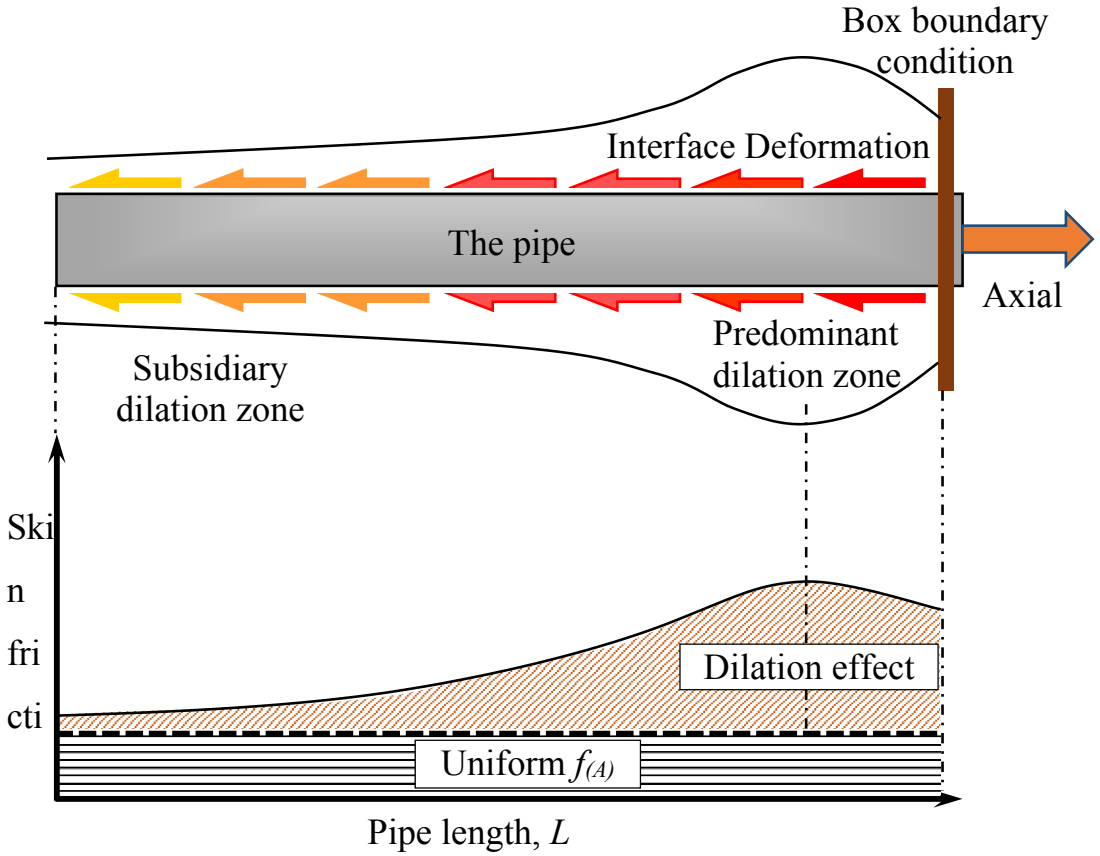

Figure 4.10 Soil-pipe interface deformation and unit skin friction, $f_{(A)}$ variation along the pipe shaft taking into account dilative behavior.

4.6 A Modified Analytical Model to Estimate $f_{(A)}$

Design codes, for example ALA (2001) and (2005) and IITK-GSDMA (2007) suggest using Eq. (4.7) to estimate $f_{(A)}$ on a buried pipeline in non-cohesive soils. However, using Eq. (4.7) to predict the measured behavior of the buried pipe in this study neither provided good agreement nor follow the trend of $f_{(A)}$ variation with respect to $(u_a - u_w)$ (Figure 4.11). Therefore, a modified form of Eq. (4.7) that can satisfy the measured trends in behavior for different conditions (i.e. saturated and unsaturated conditions) is required.

The modification should provide a smooth transition from unsaturated to saturated condition. Such modification requires measuring the unsaturated soil-interface shear strength parameter (i.e. interface friction angle due to the contribution of $(u_a - u_w)$ when

($\sigma - u_a$) is held constant, δ^b). Measurement of this parameter requires extensive equipment facilities and are time consuming as discussed earlier. As a result, the shear strength of the unsaturated interface will be derived from saturated shear strength parameters with aid of the SWCC, which will be utilized to derive the nonlinearity in the soil-pipe axial behavior. Such a procedure was highlighted by Han and Vanapalli (2016) by proposing a unified model to predict the unsaturated soil shear strength and other stiffness properties. According to their model, Eq. (4.21) utilizes the saturated soil properties and the SWCC to provide a smooth transition from saturated to unsaturated condition.

$$\Omega_{Unsat} = \Omega_{Sat} + f(s)S^{\xi} \tag{4.21}$$

where Ω_{Unsat} is stiffness or shear strength properties under consideration of unsaturated soil, Ω_{Sat} is the corresponding saturated properties, s is soil suction, S is degree of saturation, and ξ is a fitting parameter that depends on soil type and plasticity index.

Eq. (4.7) can be modified by considering the contribution of matric suction towards the interface shear strength. This can be achieved by substituting the second part of Vanapalli et al. (1996a) model (i.e. Eq. (4.11)) into Eq. (4.7). The modified model is given by Eq. (4.22).

$$\begin{aligned} f_{(A)Unsat} &= f_{(A)\,sat} + (u_a - u_w)_{av.} S^{\eta} \tan \delta_{ps-r} \\ f_{(A)Unsat} &= \left[\gamma' H \left(\frac{1 + K_o}{2}\right) + (u_a - u_w)_{av.} S^{\eta}\right] \tan \delta_{ps-r} \end{aligned} \tag{4.22}$$

where $(u_a - u_w)_{av.}$ is the average matric suction around the pipe, η is a fitting parameter, $\delta_{ps\text{-}r}$ is the interface plane strain friction angle.

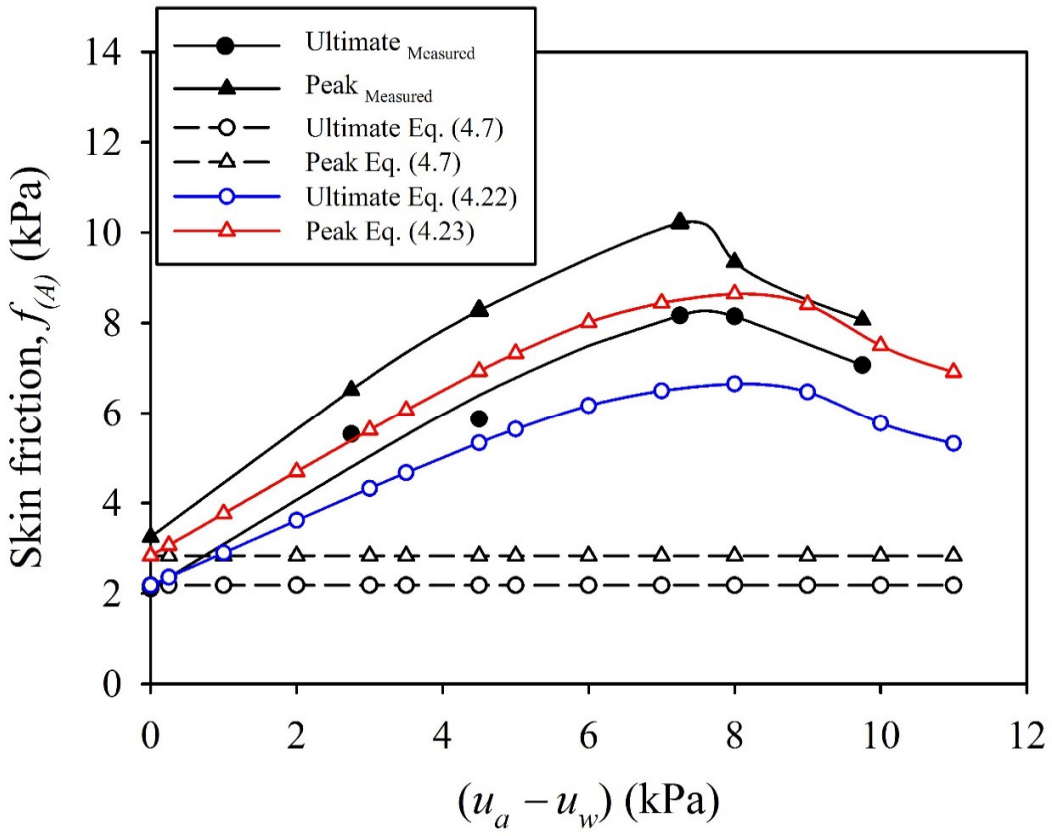

Figure 4.11 Comparison between the measured peak and ultimate skin friction, $f_{(A)}$ for unsaturated condition and predicted ones using the proposed models and conventional model.

Eq. (4.22) was able to capture the trend of the ultimate unit skin friction with respect to matric suction with small deviations from the measured behavior resulting in good predictions. The peak unit skin friction, however, requires considering the dilatancy of the interface. The interface peak angle of internal friction as discussed earlier is mobilized due to contribution arising from dilation. Consequently, the ψ_p is incorporated in Eq. (4.22) by adding it to the $\delta_{ps\text{-}r}$ to capture the peak skin friction for saturated and unsaturated conditions and rewritten as Eq. (4.23). The same procedure that was extended with Eq. (4.7) (i.e. incorporating ψ_p) was able to capture the peak skin friction for saturated condition only.

The deviation of the predicted unit skin friction from the measured values is presented in Figure (4.12). There is a good agreement between the measured and predicted $f_{(A)}$. Both equations

provide linear increase in the estimated $f_{(A)}$ up to the AEV (i.e. boundary effect zone) and change to nonlinear increase with a descendent rate of increase after the AEV (i.e. transition zone). Once the soil reaches the residual zone of unsaturation, the predicted $f_{(A)}$ starts decreasing to an ultimate value.

$$f_{(A)Unsat} = \left[\gamma' H\left(\frac{1+K_o}{2}\right) + (u_a - u_w)_{av}.S^{\eta}\right] tan(\delta_{ps-r} + \psi_p) \tag{4.23}$$

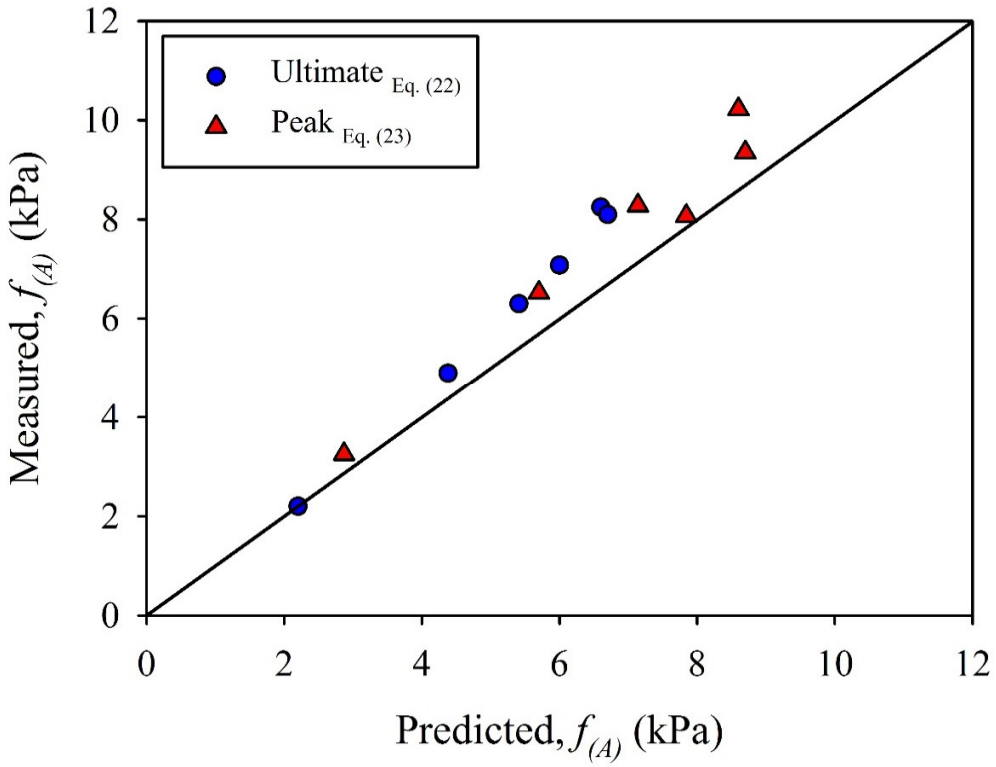

Figure 4.12 Deviation of measured-predicted peak and ultimate unit skin friction, $f_{(A)}$ from 45^0 line.

4.6.1 Sensitivity of η parameter

Several investigators have achieved reasonable comparisons between the measured non-linear behavior of unsaturated soil properties and predicted behavior using the SWCC as a tool with the aid of fitting parameters (Gallipoli et al. 2003, Sawangsuriya et al. 2009, Wuttke et al. 2013, and

Lu and Kaya 2014). For example, Vanapalli et al. (1996a) pointed out that the normalized area of water, which is directly related to the volume of water in the soil, controls the rate at which the ($u_a - u_w$) contributes towards shear strength of soil. They defined the normalized area of water as a dimensionless number, which varies from a unity at saturation to a small value at residual state to zero at dry condition. In addition, they concluded that it varies in a similar fashion to the variation of the degree of saturation over the suction range and provided a mathematical relationship between the normalized area of water and the degree of saturation that is governed by a fitting parameter. Consequently, the nonlinearity trend of unsaturated soil as well as the unsaturated interface shear strength are controlled by the SWCC and the fitting parameter.

The pullout resistance on a pipeline is a function of soil-interface shear strength. For unsaturated sandy soils, the significant variation of shear strength with matric suction is typically within 0 to 10 kPa matric suction range. As discussed earlier, the variation of $f_{(A)}$ with ($u_a - u_w$) shows similar trends to shear strength variation with ($u_a - u_w$). The following remarks should be considered to choose a proper fitting parameter, η:

i) Linear increase in $f_{(A)}$ (i.e. $\eta = 0$) will provide conservative estimation up to the residual suction. After the residual suction, η value equal to zero will result in unreasonable overestimation of pullout resistance.

ii) The nonlinearity is more pronounced after the residual suction. However, However, $f_{(A)}$ variation with matric suction can be simplified to bimodal variation as follow: i) In the boundary effect and transition zones of suction, linear increase can be assumed. ii) After the residual suction, there are three possible scenarios for $f_{(A)}$ variation: linear increase (i.e. $\eta = 0$), constant and linear decrease. Since there is no feasibility of using linear increase, it is more suitable to consider either constant or linear decrease.

iii) The maximum measured $f_{(A)}$ is typically in the transition zone. As discussed earlier, η equal to 0 will provide conservative prediction within this zone. However, using a low value for η will provide reasonable prediction for the nonlinear $f_{(A)}$ variation with matric suction for all zones. This can be achieved by considering the residual degree of saturation, S_r for sandy soils that is typically within 10% range. S_r can be used to estimate the fitting parameter, η.

Furthermore, Figure (4.13) shows the sensitivity of fitting parameter, η for predicting the variation of the peak and ultimate $f_{(A)}$ over the entire suction range. The figure also shows that η has no effect on the predicted peak and ultimate $f_{(A)}$ up to the AEV. This can be attributed to the fact that the rate of change of S with respect to $(u_a - u_w)$ is zero up to the AEV (i.e. boundary effect zone) and the soil is in a state of full saturation. The negative pore-water pressure (i.e. $(u_a - u_w)$) in the boundary effect zone acts directly to increase the effective stress in contributing to the interface shear strength (Vanapalli et al. 1996b). Once the $(u_a - u_w)$ exceeds the AEV, predicted $f_{(A)}$ for different η values starts deviating nonlinearly with $(u_a - u_w)$. In this study, a fitting parameter, η equal 0.1 was found to provide a good fit between the measured and predicted $f_{(A)}$ and was also capable to capture the nonlinearity trend of the $f_{(A)}$. Higher values of η (i.e. 1.0, and 0.9) dampen the predicted $f_{(A)}$ and prevent the maximum values from being achieved. Using η values higher or lower than the suggested range for this study (i.e. within the S_r range) results in either under estimated $f_{(A)}$ or linear increase in prediction of $f_{(A)}$ that will overestimate the $f_{(A)}$ beyond the residual suction.

4.7 Summary and Conclusions

In this study, the force-displacement behavior of soil-pipeline system subjected to relative soil movement in the axial direction under saturated and unsaturated conditions was investigated. The axial force-displacement behavior of a prototype pipe was evaluated with respect to matric suction as well as interface dilatancy. Several pullout tests were performed on a rough surface steel prototype pipe of 114.3 mm diameter buried in compacted sand in a specially designed box that allows achieving different degrees of saturation that span over various zones of the SWCC (i.e. boundary effect zone, transition zone and residual zone of unsaturation). Moreover, two analytical models are introducedto estimate the peak and ultimate unit skin friction that is transferred from the soil on the pipe body. The proposed analytical models take into account of the matric suction contribution towards the transferred axial load on the pipe. The models only require the information of saturated interface shear strength, angle of dilation and SWCC and use only one fitting parameter. One of the models takes account of the dilation effect by incorporating the dilation angle into it. Key conclusions of this study are summarized below:

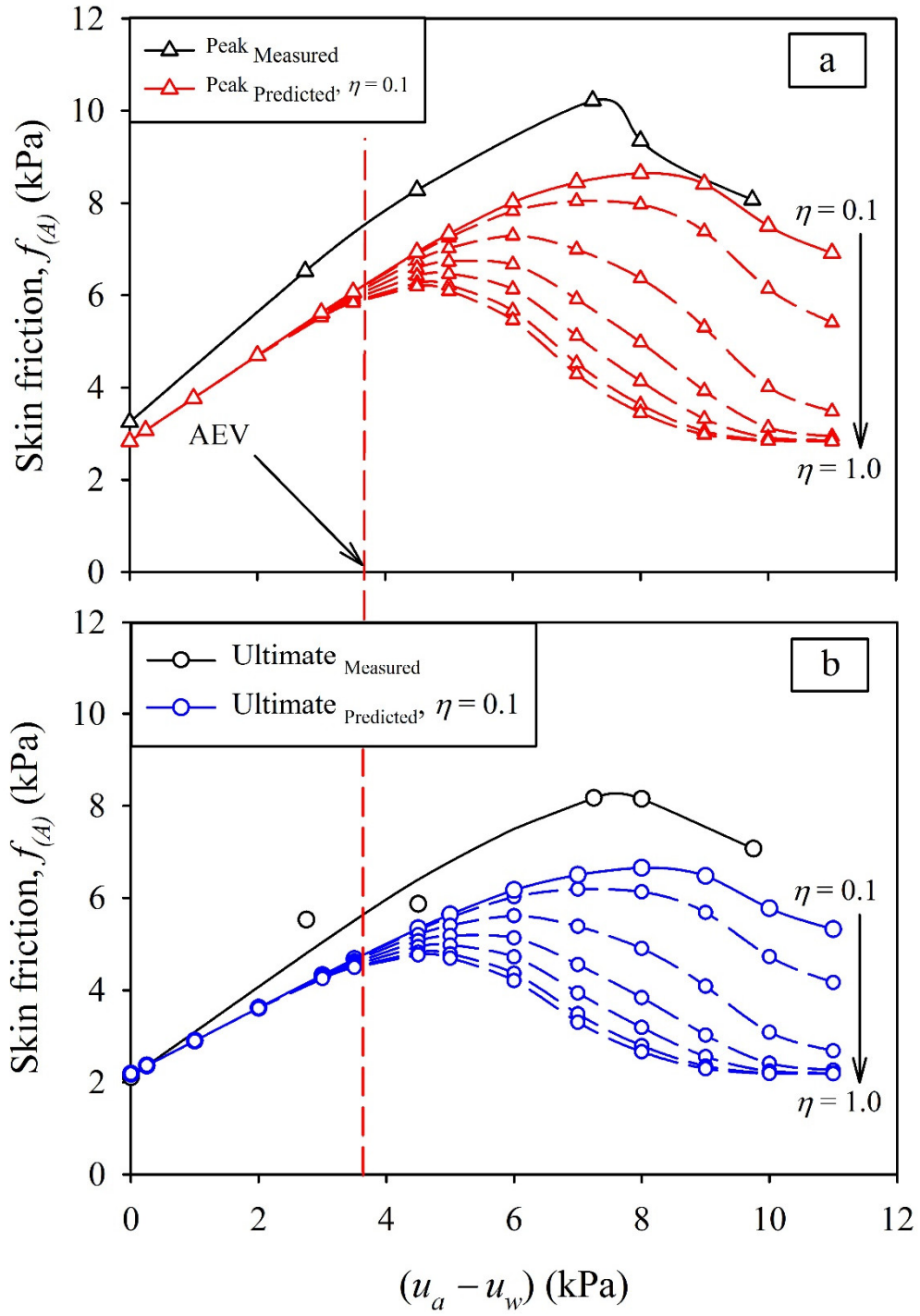

Figure 4.13 Sensitivity of the fitting parameter, η of the proposed models; (a) Peak $f_{(A)}$, and (b) Ultimate $f_{(A)}$.

1. The matric suction and dilatancy have significant influence on the axial load-displacement behavior of buried pipe. The transferred axial load from soil on the pipe under unsaturated condition is approximately 2.5 times greater than the saturated condition. Similarly, the axial subgrade reaction also has increased several folds for unsaturated condition in comparison to saturated soil.
2. Strain-hardening followed by strain-softening behavior was observed for all the tests conducted in the present study. The dilatancy contributed to an increase in mobilized axial force both in saturated and unsaturated soil conditions. However, the dilation effect was more pronounced under unsaturated condition up to the residual zone of unsaturation. Beyond this zone, the matric suction has no effect on the dilatancy and both the peak and ultimate unit skin friction have similar variation rate with matric suction.
3. The analytical models were proposed using the saturated soil parameters, SWCC and only a single fitting parameter to capture reliably the trends of the measured behavior with limited deviations. The proposed models are of interest in engineering practice to predict the maximum axial stresses on the soil-pipeline systems that can be used in their rational design for different loading scenarios.
4. The influence of η in predicting $f_{(A)}$ is more predominant in the transition zone and the residual zone of unsaturation in comparison to the boundary effect zone. In the boundary effect zone, up to the AEV, the η has negligible or no effect on the predicted peak nor ultimate $f_{(A)}$. Such a behavior can be attributed to the fact that the soil is saturated (i.e. $S \sim 1$) up to the AEV. Once the $(u_a - u_w)$ exceeds the AEV, the predicted $f_{(A)}$ starts varying nonlinearly with $(u_a - u_w)$. The nonlinear variation of $f_{(A)}$ is derived from the SWCC along with the fitting parameter η. In the current study, $\eta = 0.1$ was found to be suitable to provide reasonable predictions of the measured values of ultimate and peak $f_{(A)}$.

The present study provides evidence that the principles of saturated soil mechanics underestimate the axial force exerted on pipeline buried in unsaturated soil leading to unsafe design procedures. For this reason, the axial force should be estimated based on careful consideration of the soil condition taking into account the matric suction as well as the dilatancy of the compacted sands. The proposed models are promising for use in engineering practice to predict the axial force with a reasonable accuracy that will lead to more reliable design procedures for pipelines systems infrastructure.

CHAPTER FIVE

NUMERICAL INVESTIGATION OF SOIL-PIPELINE SYSTEM BEHAVIOR NEARBY UNSUPPORTED EXCAVATION IN SATURATED AND UNSATURATED GLACIAL TILL

5.0 Background-Information

The contents presented in this chapter are from the manuscript of the publication:

Al-Khazaali, M., Vanapalli, S.K., and Oh, W.T. (2018). Numerical investigation of soil-pipeline system behavior nearby unsupported excavation in saturated and unsaturated glacial till. *Canadian Geotechnical Journal.* DOI: 10.1139/cgj-2017-0411.

5.1 Introduction

Energy pipeline systems have significantly contributed to the Canadian economy. Canadian Energy Pipeline Association (CEPA) (2005) performed studies on the economic benefits that results from pipeline investment and potential costs to Canadian residential, commercial and industrial consumers that would result from delaying new pipeline projects in North America. The studies suggested that a hypothetical $1.52 billion worth project of 1000 km natural gas pipeline that is equally distributed in Alberta and British Columbia provinces would increase the Canadian gross domestic product by $1.2 billion. In addition, this investment would create thousands of jobs (i.e. 17,384 jobs) in both Alberta and British Columbia, including 2907 jobs in other regions of Canada, which mainly include Ontario, Quebec, Saskatchewan, and Manitoba provinces. The studies also suggest that the costs to Canadian natural gas consumers due to delays in the construction of new pipeline infrastructure could be as much as $57.7 billion over a period from

2006 to 2025 based on a constant 2005 dollar value. These details highlight the importance of the present and future impacts of pipelines systems for Canada.

Several scholars have studied the behavior of buried pipelines that are subjected to external loads due to ground movement induced by nearby trenches, foundation excavation of new structures, and activities associated with tunnelling (Crofts et al. 1977, Chard and Symons 1982, Attewell and Woodman 1982, O'Reilly and New 1982, Rogers and O'Reilly 1991, Lee et al. 1992, Bickel et al. 2004). Wijewickreme et al. (2009) stated that soil deformation around pipeline systems associated with excavation activities, slope failures, ground subsidence or earthquake lead to serious damages in pipeline systems. Chard and Symons (1982) conducted a full-scale field study in London clay to assess the reasons for fractures in a shallow buried pipeline. They concluded that the main reason for fractures that arise in pipelines is due to ground movement associated with deep trenching in urban areas that in turn induces large lateral loads on the pipelines.

Oil resources are wide spread in many regions of Western Canada, where glacial tills are extensively distributed. The natural GWT in the Western and Central-Canada is typically greater than 10m. Perez-Valdivia (2009) studied the variation of GWT taking account of climate factors in Canadian provinces of Alberta, Saskatchewan, and Manitoba using a large database. The database include information from 136 wells for a period extended over 51 years from 1957 to 2007 in Alberta, 61 wells for the period from 1964 to 2007 in Saskatchewan, and 33 wells for the period from 1963 to 2007 in Manitoba. The study revealed that the GWT is greater than 15, 10, and 6m in provinces of Alberta, Saskatchewan, and Manitoba, respectively. For such regions, ignoring the influence of soil suction within the vadose zone to estimate soil deformations and stresses and design suitable supporting system is not reasonable. In other words, it is important to investigate the behavior of buried pipelines for such regions considering the influence of soil suction taking account of different scenarios that are commonly encountered in practice (O'Rourke et al. 2008, Olson 2009, O'Rourke 2010, Jung et al. 2013, Saadeldin et al 2015, Robert et al 2016).

In this chapter, numerical analyses were undertaken to investigate the pipeline displacement and subsequent strain, rotation, and radial forces in the pipeline due to the unsupported vertical excavation in an unsaturated soil. The focus of the analyses are mainly directed to address: i) the contribution of matric suction, $(u_a - u_w)$ toward the soil-pipeline system

behavior, ii) the effect of the pipeline rigidity (i.e. rigid and flexible pipes), and iii) providing a framework to estimate the adequate excavation depth without supporting system to alleviate damages to nearby parallel pipelines in the event of nearby excavation. Finite element analysis (FEA) was carried out using the commercial finite element software SIGMA/W (GeoStudio 2012) extending the Modified Effective Stress Approach (MESA). A 1m in diameter rigid and flexible pipelines were assumed to be buried at 2m depth from the natural ground level in Indian Head till (IHT) soil, which is a sandy clay from Indian Head, Saskatchewan, Canada. Two different type of pipelines were considered in the analyses (i.e. rigid and flexible pipelines) to investigate the influence of rigidity of pipeline on the safe excavation depth based on the strain, rotation, and radial forces in the pipeline. The ground disturbance associated with mechanical equipment should be avoided within three metres (10 feet) of the pipe as per the National Energy Board Pipeline Damage Prevention (NEBPDP) (2016). For this reason, in the present study, it was assumed that the excavation took place 6m (i.e. twice the minimum distance) from the centerline of the pipeline.

5.2 Modeling of Soil-Pipeline Interaction

Numerical analyses were conducted to investigate the pipeline-soil interaction behaviors nearby excavation under both saturated and unsaturated condition. The soil-pipeline interaction problems analyzed using three-dimensional models can be more realistic. However, pipeline system behavior analyses using plane-strain models has been receiving more attention due to its simplicity and validity based on reasonable estimation of soil-pipeline system problems. For example, different loading conditions which include seismic shaking, excavation, and transverse loading were investigated using plane-strain models successfully in recent years (Martin et al. 2013, Lanzano et al. 2014, Roy et al. 2014, Roy et al. 2015, Chaloulos et al. 2015, Roy et al. 2016, Kong et al. 2017).

Commercial software SIGMA/W (GeoStudio 2012) (2-Dimensional analysis) was used in the present study extending the elastic-perfectly plastic Mohr-Coulomb (MC) constitutive model. The MC model has been successfully used to interpret the pipeline-soil interaction by many researchers (Yimsiri et al. 2004, Kouretzisw et al. 2014, Roy et al. 2015). A uniform soil profile is assumed to extend up to 14m depth under the natural ground level (NGL) that extends 35m horizontally (Figure 5.1). Typically, the pore-water pressure (PWP) variation above the GWT is

negative and non-linear. However, analyses were carried out assuming negative pore-water distribution above the GWT is hydrostatic, which leads to conservative, simple and straightforward design. The negative pore-water ($-u_w$) above the GWT is equal to the matric suction, ($u_a - u_w$) since the pore air pressure (u_a) is usually assumed to be atmospheric pressure (i.e. zero). The model is assumed restrained in horizontal direction at the vertical ends and restrained in both directions at the bottom. Flow boundary conditions were set at the left end using constant total head (i.e. H= 14, 12, 10, 8, and 6m) while at the excavation face no flux was allowed with potential seepage face during each excavation step. The 'In-situ' feature was used as 'Analysis Type' to setup initial conditions. The excavation was simulated by removing soil up to 8m from the natural ground level at 2m increments (i.e. 2m, 4m, 6m and 8m depths). The time-period of 24-hour interval was allowed after each excavation to achieve equilibrium condition with respect to soil suction. The meshes were generated automatically using quadrilateral and triangle elements. Fine meshes of 0.25m size were used in excavation face and pipeline zones.

In conventional geotechnical engineering practice applications, the mechanical behavior (i.e. shear strength and volume change) of soil is interpreted considering undrained analysis using the total stress approach (i.e. TSA) or drained analysis using the effective stress approach (i.e. ESA). Volume change behavior associated with different loading condition arises mainly from water and air movement while both soil particles deformation and water compressibility are small and therefore negligible. Water and air movement depends on pores size, and it is a time dependent process (i.e. water drainage is rapid in coarse-grained soil and slow in fine-grained soil). TSA is not a time dependent process and there will be no changes in soil volume for saturated soils. Unsaturated soils, however, experience volume change under external loads; hence, it is more appropriate to use ESA in the numerical analysis. The ESA can be conducted using effective stress parameters only or effective stress parameters along with the information of pore-water pressure changes. The first approach is called uncoupled ESA in which the change in effective stress due to external loads equals the change in total stress. The second approach referred to as Coupled ESA/PWP that takes into account the variation of pore-water pressure and its influence on the soil properties. The mechanical behavior of soil and flow behavior of water phase of unsaturated soil element are governed by two fundamental equations; namely, the partial differential force equilibrium and water continuity equations (Qi and Vanapalli 2015). These equations are

incorporated into SIGMA/W which facilitate performing two-dimensional saturated and unsaturated hydro-mechanical analysis (i.e. coupled analysis) (Wong et al. 1998).

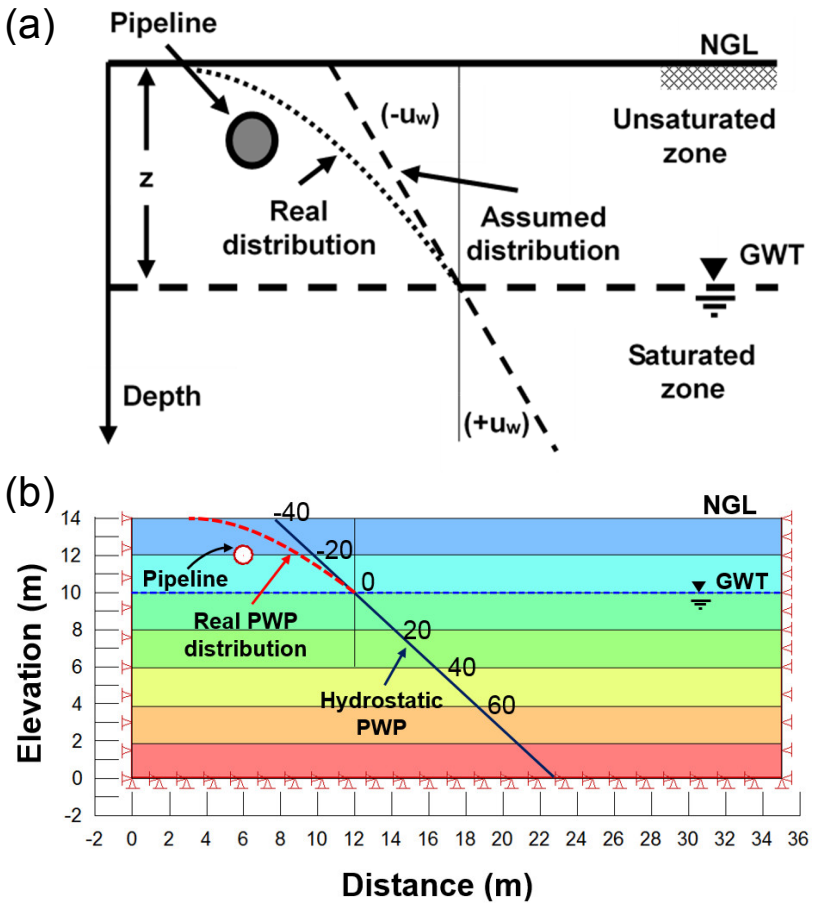

Figure 5.1 (a) Pore-Water Pressure (PWP) distribution with respect to GWT, and (b) Finite element model.

Rapid excavation process can contribute to significant soil deformations and result in higher stresses exerted on pipe body. The stresses exerted on pipelines due to the soil movements in unsaturated soils can be several folds higher in comparison to saturated soils for comparable soil mass movement. In other words, saturated soil can deform more around the pipe due to its low stiffness in comparison to unsaturated soil. On the other hand, for unsaturated soil condition, higher energy is required to displace the pipeline from its original or initial position to the new position. This energy is transformed to shear force, axial force, and bending moment in the pipe. Consequently, allowing enough time for the excess pore-water and pore-air to dissipate would

reduce the excessive deformations in soils, which leads to less influence on the pipelines nearby excavations.

5.2.1 Shear strength and modulus of elasticity of unsaturated soils

Figure (5.2) shows typical soil stress-strain behavior from a triaxial test in which three distinctive zones are described; elastic, strain-hardening, and strain-softening zones. In the elastic zone (i.e. O to A), linear and nonlinear elastic strains are mainly controlled by the soil modulus of elasticity, E and Poisson's ratio, ν, while plastic strains in strain-hardening (i.e. A to B) and strain-softening (i.e. B to C) zones are controlled by the mobilized angle of internal friction, ϕ' and dilation angle, ψ respectively (Roy et al. 2015 and 2016). In strain-hardening, plastic strains occur when the stress state passed the initial yield point which is defined by the mobilized angle of internal friction, ϕ'. Both ϕ' and, ψ are increased from initial values to peak values with the accumulated plastic shear strains, γ^P. In post-peak softening zone, both ϕ' and ψ decrease with γ^P. Since the dilation is more pronounced in coarse-grained soils, ignoring the dilation effect for fine-grained soils will not contribute to serious errors in the behavior especial at elastic zone. Hence, constant internal friction angle and zero dilation angle were used in the analyses.

Effective shear strength parameters for saturated soil (i.e. cohesion, c', and angle of internal friction, ϕ') and effective modulus of elasticity E' are conventionally measured using triaxial shear test results. Matric suction, $(u_a - u_w)$, as an independent stress state variable contributes to shear strength and volume change behavior of unsaturated soils. A modified triaxial shear test device that facilitate axis translation technique for fine-grained soils or hanging column technique for coarse-grained soils is required to measure the contribution of $(u_a - u_w)$, which is referred to as the angle of internal friction, ϕ^b. The shear strength of unsaturated soil can be described by extending MC constitutive model using two stress state variables $(\sigma - u_a)$ and $(u_a - u_w)$ (Fredlund et al. 1978) (Eq. (2.3)).

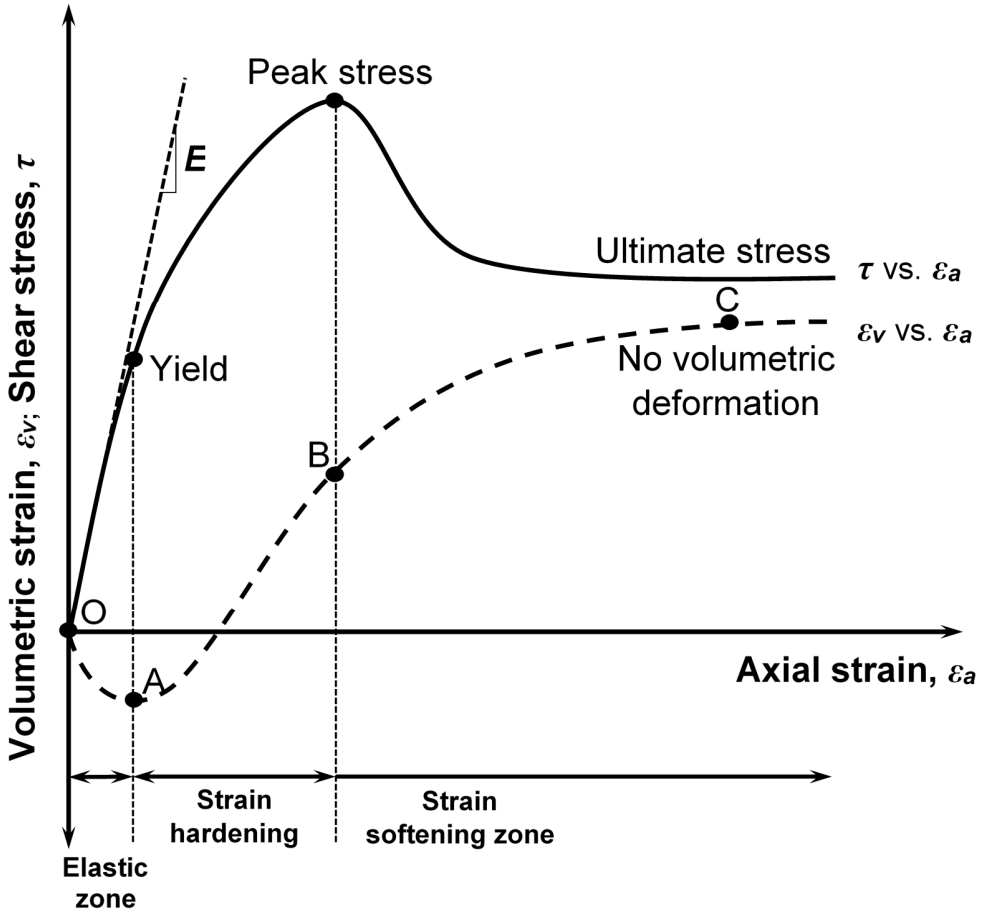

Figure 5.2 Typical shear stress-axial strain and volumetric strain-axial strain behaviors in triaxial shear test.

Measuring the unsaturated shear strength and stiffness parameters is time consuming, expensive and requires elaborate testing equipment and highly trained staff. To overcome these problems, several researchers have proposed semi-empirical methods to estimate the unsaturated soil properties using the saturated soil property and the soil-water characteristic curve (SWCC) relationship (Vanapalli et al. 1996, Fredlund et al. 1996, Oh and Vanapalli 2009, Oh et al. 2009, Lu and Kaya 2014, Han and Vanapalli 2016). Such approaches provide smooth transition from unsaturated to saturated condition. These methods have also been found to be applicable to different soil-structure interaction problems (Hamid and Miller 2009, Gurpersaud et al. 2013, Vanapalli and Taylan 2012, and Hossain and Yin, 2014). In this study, semi-empirical model proposed by Vanapalli et al. (1996) is used to predict the effective shear strength of unsaturated soil (Eq. (5.1)) extending the MESA.

$$\tau_{unsat} = c' + (\sigma - u_a)\tan\phi' + (u_a - u_w)\left(\frac{\theta - \theta_r}{\theta_s - \theta_r}\right)\tan\phi' \quad (5.1)$$

where $(\sigma - u_a)$ = net normal stress, θ = volumetric water content, θ_s = volumetric water content at saturated condition, and θ_r = volumetric water content at residual condition.

The contribution of $(u_a - u_w)$ towards the shear strength can also be expressed as apparent cohesion, c using the relationship in Eq. (5.2). This model is utilized in SIGMA/W to estimate the variation of shear strength with respect to matric suction.

$$c = c' + (u_a - u_w)\left(\frac{\theta - \theta_r}{\theta_s - \theta_r}\right)\tan\phi' \quad (5.2)$$

Data reported in the literature suggests that the modulus of elasticity of unsaturated soils increase significantly with capillary stress (i.e. $(u_a - u_w)$) for various types of soils (Miao et al. 2002, Liangtong 2003, Oh et al. 2009, Vanapalli and Oh 2010, Rahardjo et al. 2011, Lu and Kaya 2014, Adem and Vanapalli 2014, Al-Khazaali and Vanapalli 2015, Han et al. 2016). Oh et al. (2009) and Vanapalli and Oh (2010) proposed a semi-empirical to predict the variation of modulus of elasticity with respect to matric suction utilizing the saturated modulus of elasticity, E_{sat} and SWCC for coarse and fine-grained soils, respectively (Eq. (2.6)).

$$E_{unsat} = E_{sat}\left[1 + \alpha\frac{(u_a - u_w)}{(P_a/101.3)}(S^{\beta})\right] \quad (5.3)$$

where E_{unsat} = modulus of elasticity under unsaturated condition, S = degree of saturation, and α, β = fitting parameters.

For non-cohesive soils (plasticity index, $I_P = 0$), $\beta = 1$ was found to provide good agreement with back calculated modulus of elasticity. Vanapalli and Oh (2010) suggested that the inverse of fitting parameter, α (i.e. $1/\alpha$) is related to the soil plasticity based on in-situ plate load test results for various type of soils. This model does not take into account the influence of confining stress on the modulus of elasticity. In addition, the change in void ratio upon shearing is not considered, which can affect degree of saturation and modulus of elasticity.

The effect of confining pressure and matric suction on apparent cohesion, c can be incorporated into SIGMA/W automatically during coupled-ESA analysis by defining in-situ stress and hydrology conditions. Unlike apparent cohesion, c, the variation of modulus of elasticity coupled with $(u_a - u_w)$ cannot be simulated automatically within SIGMA/W. For this reason, the variation of modulus of elasticity with respect to $(u_a - u_w)$ was estimated using Eq. (5.3) and was manually assigned to meshes depending on the matric suction distribution profiles (Figure 5.3). This model, as was stated earlier, does not consider the influence of confining pressure in the analysis. However, pipelines are commonly buried at a shallow depth; therefore, it can be postulated that the effect of confining pressure on the mechanical properties of soils can be minimal and a conservative design can be achieved.

Deformations in the soil can lead to a change in the matric suction (or degree of saturation). If pore-air pressure is assumed atmospheric with no change in water content, constant water content, (CW) test can most reliable represent this drainage condition. Matric suction value in an unsaturated soil can increase, decrease, or remain constant while soil is experiencing deformation. Rahardjo et al. (2004) studies from CW test results on low plasticity clay (I_p = 15%) suggest matric suction decreases during the shearing stage. In addition, the unconfined compression tests (alternative to CW test for shallow depths, Cunningham et al. 2003) on a soil (I_p = 18%) also showed decrease in matric suction during shearing. These research studies indicate that using the initial suction value in estimating soils properties (i.e. cohesion and elastic modulus) can lead to conservative analyses.

Eq. (5.2) and Eq. (5.3) used in the analyses to estimate the variation of apparent cohesion and modulus of elasticity, respectively have not been validated for wetting path of the SWCC. In other words, hysteresis of SWCC is not taken into account in the analyses. Hence, the proposed methodology can only be applicable only for the discussed field condition.

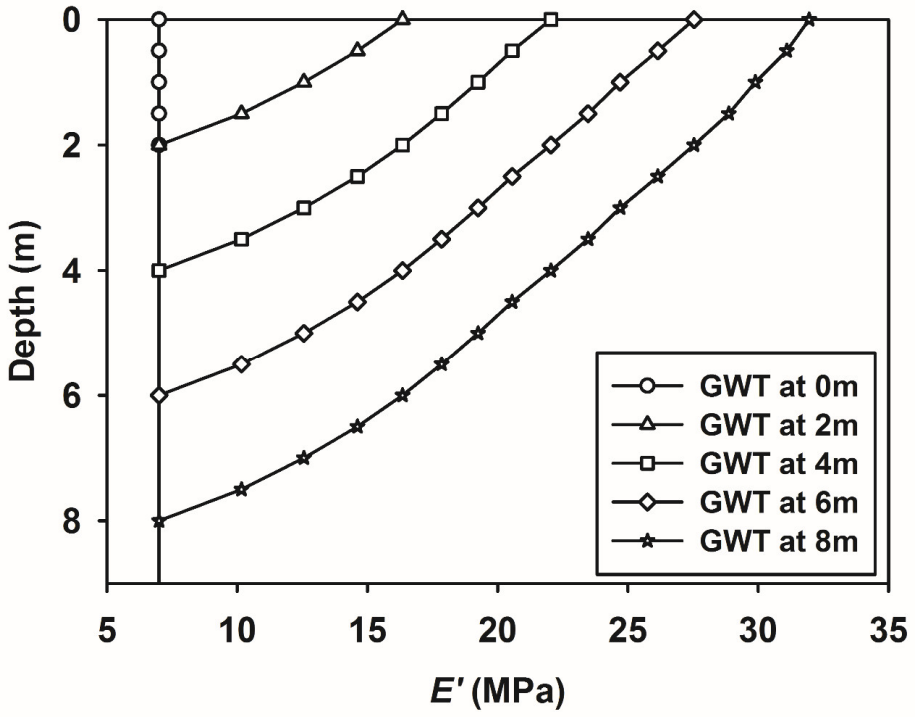

Figure 5.3 Variation of modulus elasticity, E' of the soil for different GWT.

The shear strength parameters, c', and ϕ' were obtained from direct shear test while the E_{sat} was back calculated from simulating the stress-strain curves of direct shear test using the FE software, PLAXIS 2D (Han et al. 2016). Below the GWT (i.e. saturated zone), both, c' and E_{sat} were assumed to be constant. Table (5.1) summarizes the physical and mechanical soil properties for the IHT.

5.2.2 SWCC and hydraulic conductivity function

The SWCC was measured using pressure plate apparatus and the data was fitted using the Fredlund and Xing (1994) model (Eq. (5.3); Figure 5.4).

$$S = \left(\frac{1}{ln\left[2.718 + \left(\frac{u_a - u_w}{a}\right)^n\right]} \right)^m \tag{5.4}$$

where S = degree of saturation, and a, n, and m are fitting parameters.

The analyses involve the movement of pore-water due to the excavation in an unsaturated soil. Hence, hydraulic conductivity function was established using Fredlund and Xing (1994) method and incorporated in SIGMA/W (Figure 5.5). This method requires the information of saturated hydraulic conductivity k_{sat} (Vanapalli et al. 1997) and the SWCC in terms of volumetric water content function.

5.2.3 Pipelines

A 25.4mm thickness steel pipeline of 1m diameter is assumed buried at a depth of 2m from the NGL. The steel pipeline was simulated using beam element assuming linearly elastic material. The pipe rigidity depends on the material stiffness, which is a function of its modulus of elasticity and section dimensions. The modulus of elasticity for steel is significantly higher in comparison to that of soil. Several researchers used different modulus of elasticity values for steel (i.e. 200 GPa (30×10^6 psi) (Watkins and Anderson 2000), 20 GPa (Potts and Zdravković 2001), and 2 GPa (Han et al. 2016)). In this study, two different values of modulus of elasticity of 20 GPa and 2 GPa, for steel were used to simulate rigid and flexible pipes, respectively. Choosing the right section for moment of inertia determination is crucial for the FEA. For plane-strain analysis, Figure (5.6) shows 1m length of the proposed pipe with dimensions. Section A-A′ was used to determine the moment of inertia that is required for the analysis.

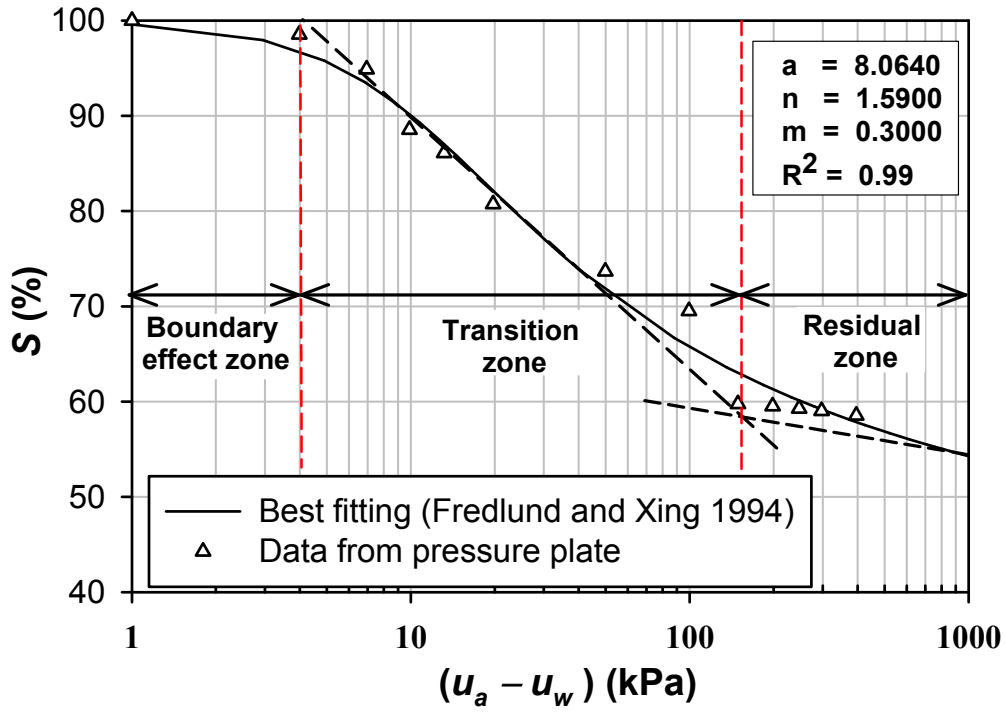

Figure 5.4 IHT soil-water characteristic curve (SWCC).

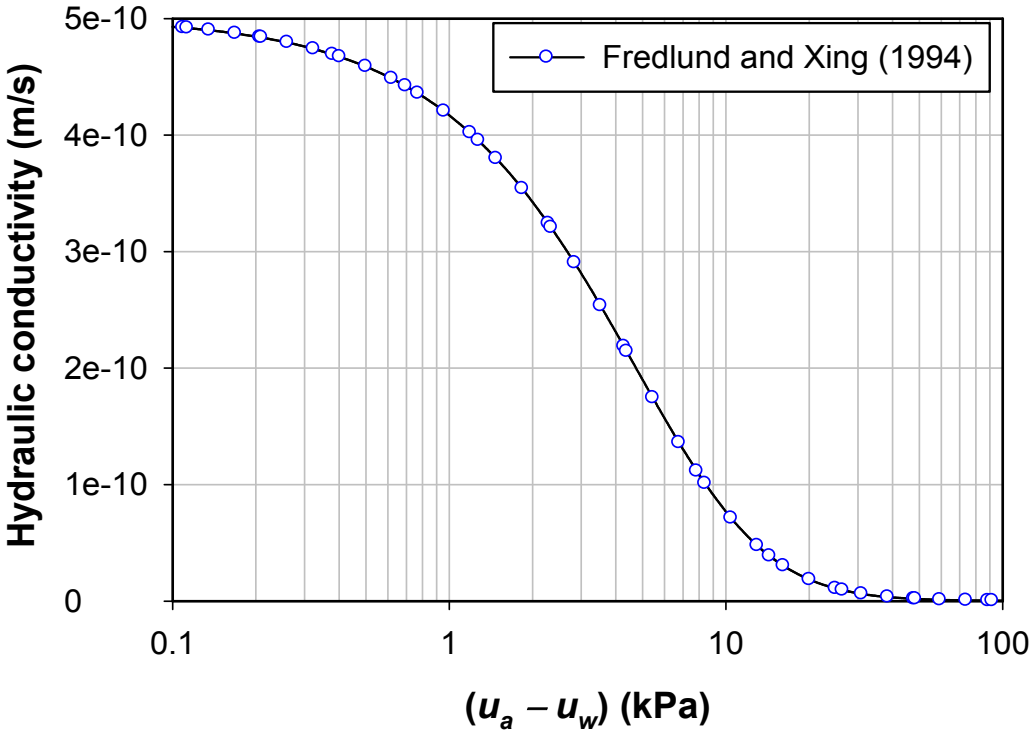

Figure 5.5 Hydraulic conductivity function.

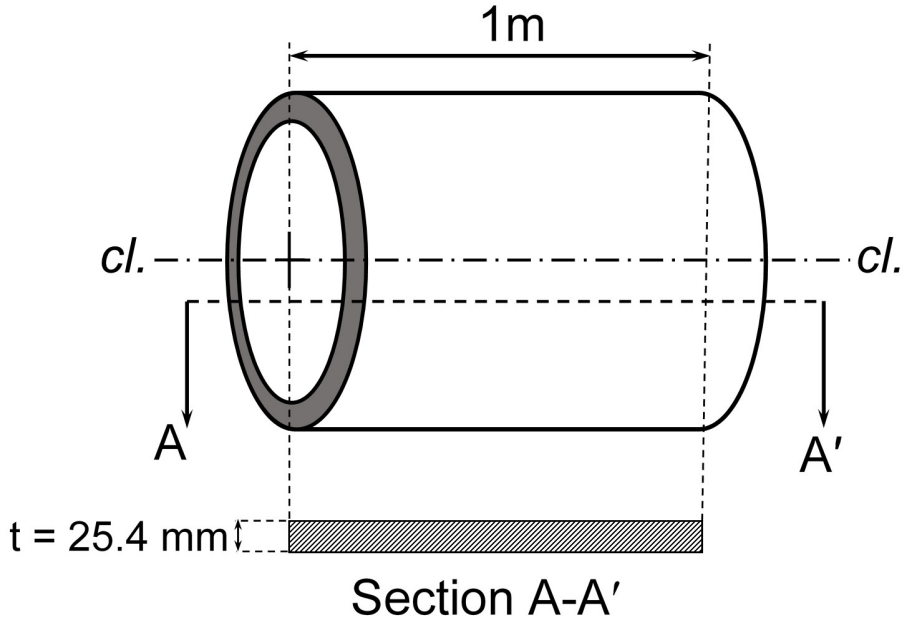

Figure 5.6 Pipe dimensions used for plane strain FEA.

5.2.4 Interface between the soil and pipeline

Soil-pipeline interface was generated around the external surface of the pipe using line area. The interface element size was 0.2m, which is smaller than the soil element size. Smooth surface are most often chosen for pipeline system to minimize frictional or axial forces on pipe body. The interface information that was used in the analysis was chosen to satisfy smooth IHT soil-pipe interface. The interface properties were obtained from Han et al. (2016). They performed direct shear test for smooth IHT soil-steel interface under saturated and unsaturated condition. The results presented in Figure (5.7) are for saturated condition. The same information was used in the numerical analysis. The IHT soil-steel interface mechanical properties (i.e. saturated angle of internal friction for interface, δ', effective saturated adhesion, c'_a and saturated effective modulus of elasticity for interface, $E'_{int\text{-}sat}$) for drained loading for saturated condition is close to the IHT (Han et al. 2016) (Table 5.1). The interface mechanical and hydraulic properties for unsaturated condition were derived similarly to the unsaturated IHT.

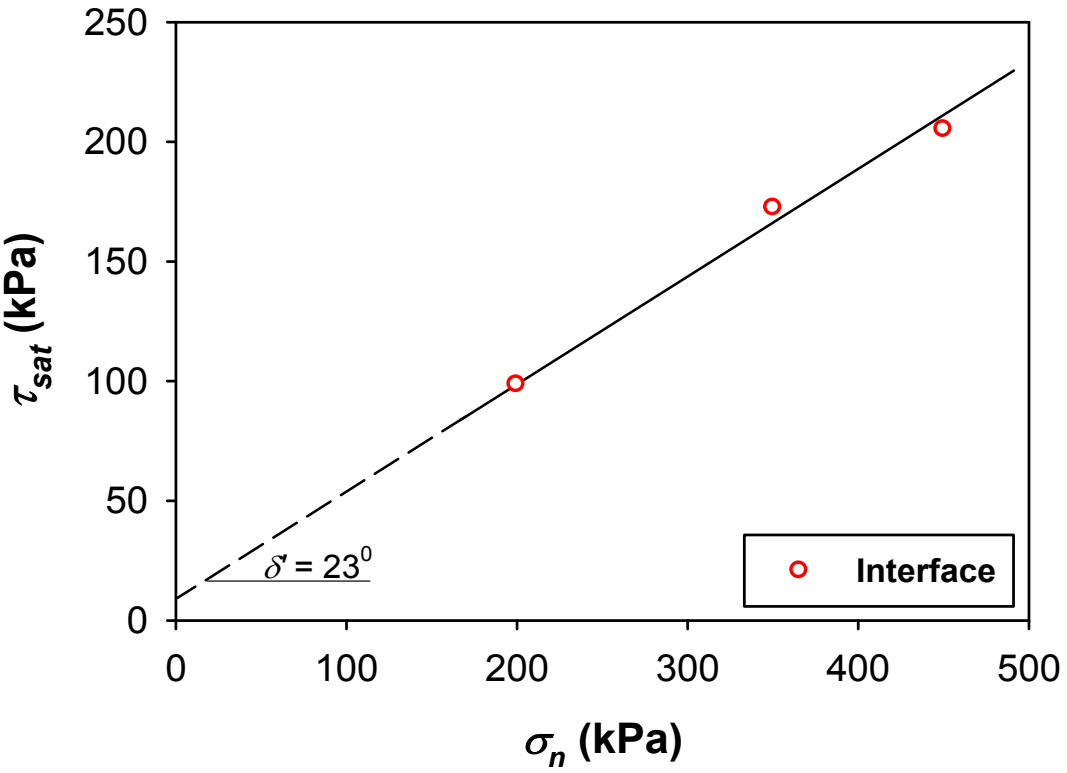

Figure 5.7 Shear strength of saturated interface (modified after Han et al. 2016)

5.3 Results and Discussions

5.3.1 General behavior

Unsupported vertical excavation can be extended to a certain depth in the soil without reaching failure conditions. Failure occurs when the lateral earth pressure, σ'_h or active earth pressure, σ'_a reaches failure values (i.e. $\sigma'_{h\text{-}f}$, or $\sigma'_{a\text{-}f}$) due to excavation. For saturated soils, σ'_a that develops at the face of vertical cut can be calculated using Eq. (5.5). Figure (5.8) shows the staged excavation and subsequent successive Mohr's circles for each excavation depth. As the excavation proceeds the lateral effective stress or the active earth pressure decreases while the effective overburden pressure, σ'_v remains constant. Once Mohr's circle touches the failure envelope, the soil fails and the corresponding active earth pressure becomes $\sigma'_{a\text{-}f}$.

$$\sigma'_a = \sigma'_v \tan^2\left(45 + \frac{\phi'}{2}\right) - 2c' \tan\left(45 + \frac{\phi'}{2}\right) \quad (5.5)$$

In case of unsaturated soils, excavations can be extended to a greater depth when compared to saturated soils due to the contribution of soil suction towards the shear strength. Figure (5.9) illustrates that, for unsaturated condition, Mohr-Coulomb failure envelope is higher in comparison to saturated condition. The same active earth pressure at failure state for saturated condition will not cause failure under unsaturated soil condition. The figure shows that failure may occur under lower lateral earth pressure, which can be derived from the fifth Mohr's circle for unsaturated condition. This characteristic behavior of unsaturated soils was utilized in the FEA to predict the soil-pipeline system behavior under both saturated and unsaturated conditions. Once failure occurs upon a decrease in the lateral stress, excessive soil deformation occurs and soil mass collapse under its own weight causing permanent ground deformation in the pipe zone.

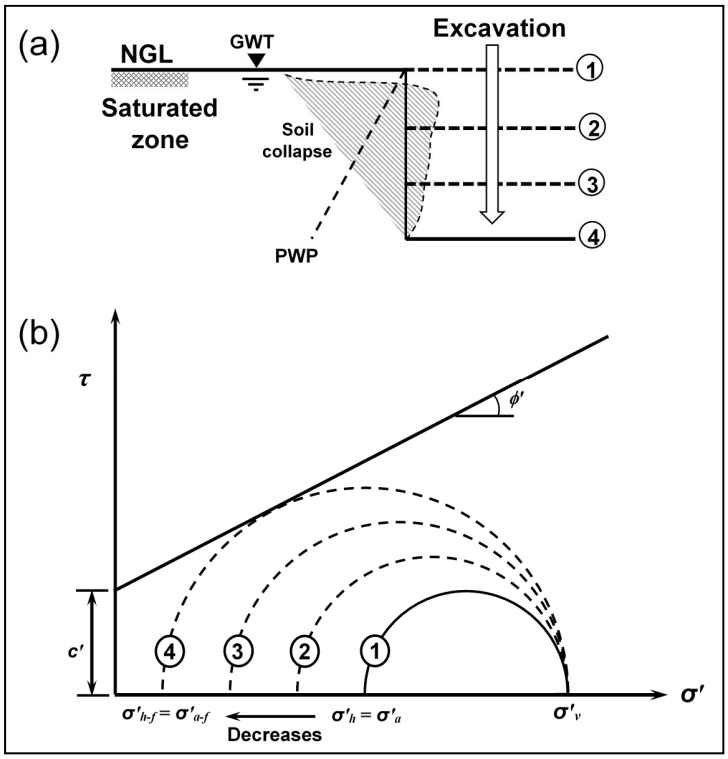

Figure 5.8 (a) Slope failure due to excavation; (b) Mohr's circles extending the principles of saturated soil mechanics during unsupported excavation.

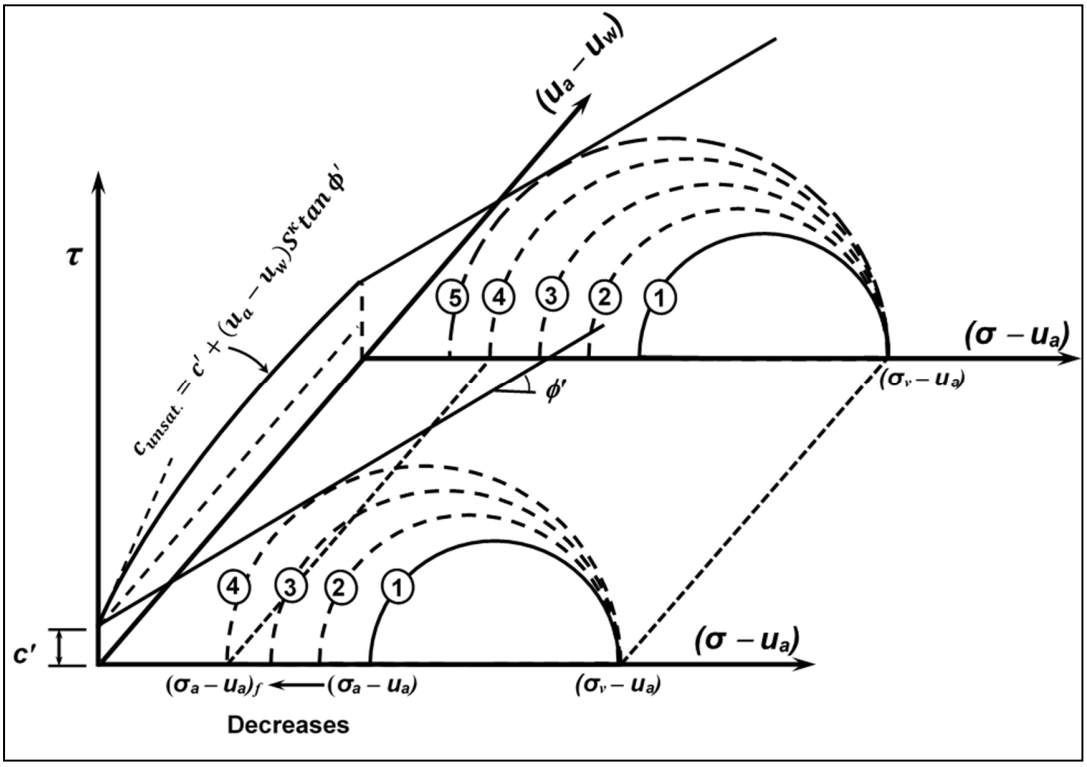

Figure 5.9 Mohr's circles extending the principles of unsaturated soil mechanics during unsupported excavation.

Figure (5.10) and Figure (5.11) show the deformations in the soil when excavation depth reached to 8m for rigid and flexible pipes, respectively for different levels of GWT. The red arrows indicate the direction and magnitude of soil deformation. It is obvious that the deformations in soils decrease as the depth of GWT increases because of the contribution of soil suction towards the shear strength and the stiffness of soils. Note that Figure (5.10a, b, and c), and Figure (5.11 a, b, and c) are presented to provide a comparison for the same depth of excavation (i.e. 8m).

Figure (5.12) shows the normalized horizontal (X) and vertical (Y) pipeline displacement in terms of pipe diameter (D) at the end of each excavation stage. The normalized displacements were obtained by comparing the initial and final position of a reference node on the pipe hoop. When the soil is in a state of fully saturated condition, the pipeline displaced significantly due to soil body movement. For the case of GWT at 0 and 2m depth, the soil deformed significantly after 4m of excavation. The simulation for the case of GWT at 4m depth shows that the depth of excavation could be extended up to 6m before soil collapses. The soil deformation decreased

significantly and no collapse was observed for the situation of GWT at 6 and 8m. Such a behavior can be attributed to significant increase in soil shear strength and modulus of elasticity.

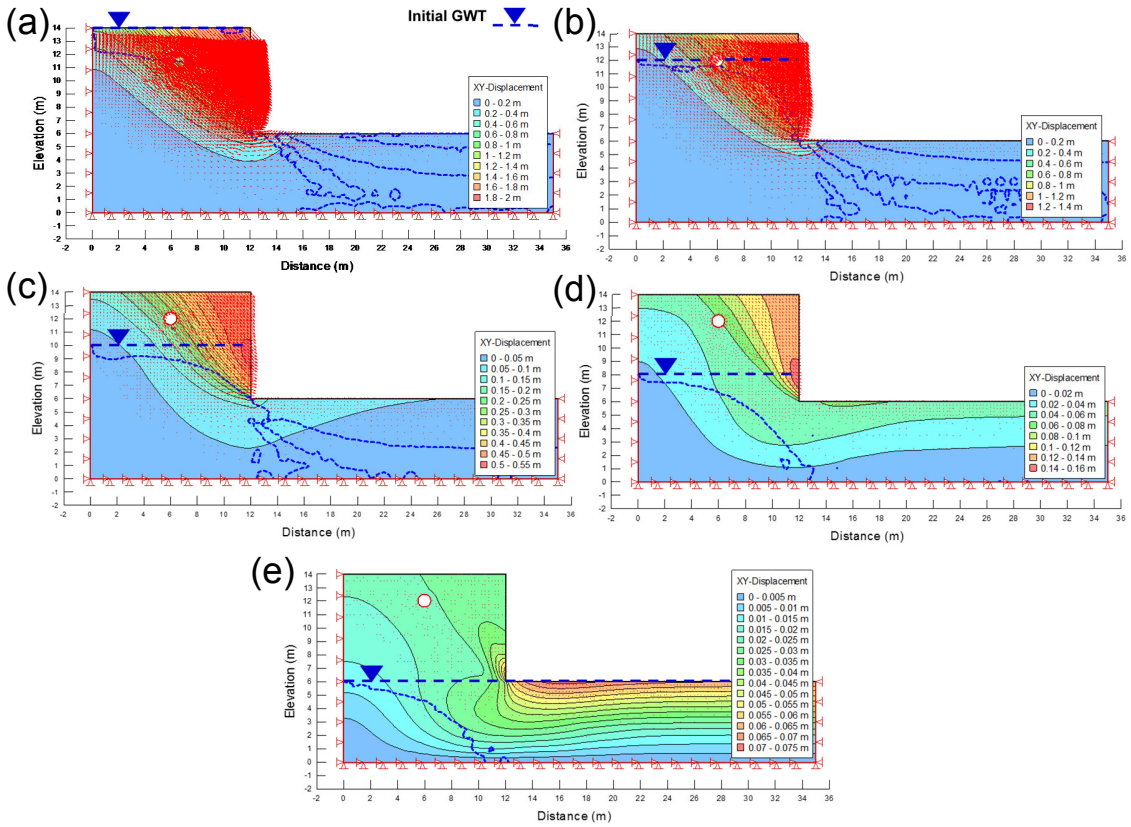

Figure 5.10 General soil-rigid pipe deformation due to 8m of excavation considering deferent GWT depth; (a) GWT at the surface, (b) GWT at 2m depth, (c) GWT at 4m depth, (d) GWT at 6m depth,and (e) GWT at 8m depth.

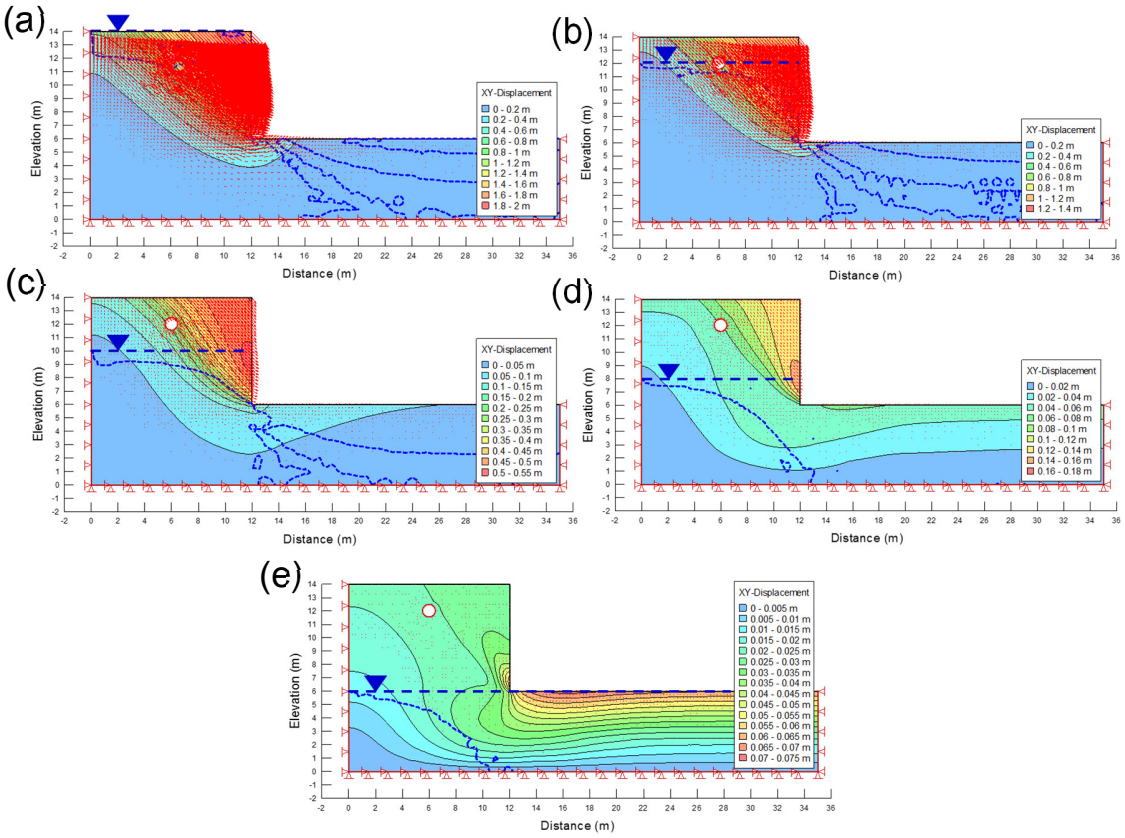

Figure 5.11 General soil-flexible pipe deformation due to 8m of excavation considering deferent GWT depth; (a) GWT at the surface, (b) GWT at 2m depth, (c) GWT at 4m depth, (d) GWT at 6m depth, and (e) GWT at 8m depth.

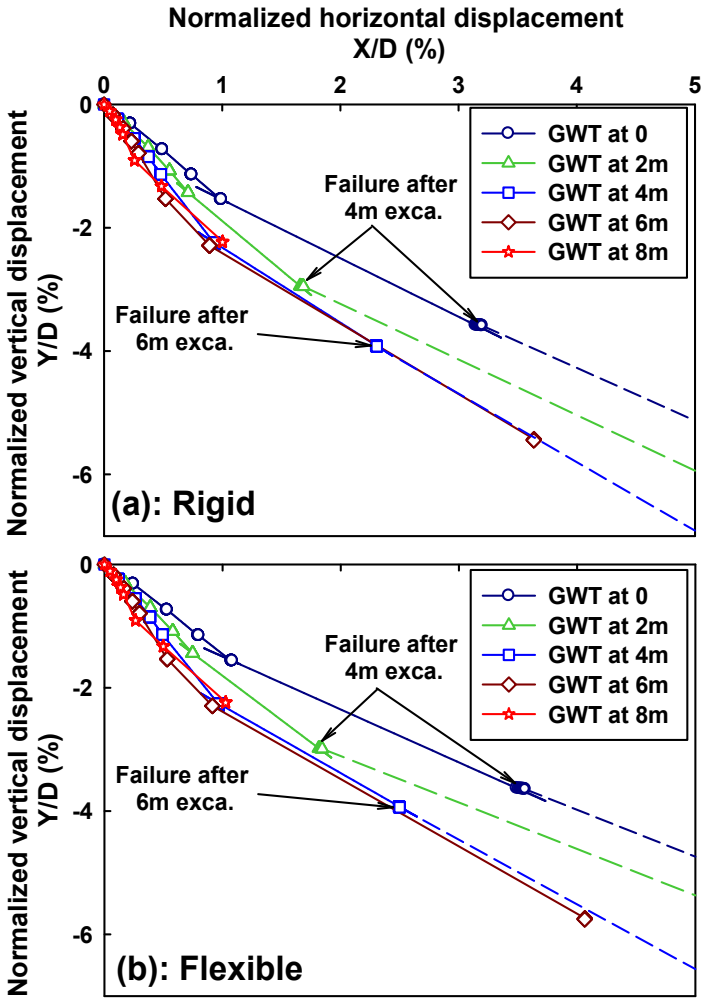

Figure 5.12 Final normalized displacement of the pipeline with respect to its initial position considering different GWT depth; (a) Rigid; (b) Flexible.

Since soil deformation around the rigid and flexible pipes due to excavation for the same GWT is comparable, the rotation of both rigid and flexible pipelines with respect to their original position was similar as well (Figure 5.13) for the same levels of GWT. However, recognizable difference between X and Y displacements of rigid and flexible pipelines was observed (Figure 5.14). In addition, results from Figure (5.14) suggest that for each excavated layer, the difference of X and Y displacements for rigid and flexible pipes increases. As has been stated earlier, rigid pipes can resist the applied loads due to its relatively high elasticity modulus while flexible pipes partially depends on the support of the surrounding soil (Zhao et al. 1998).

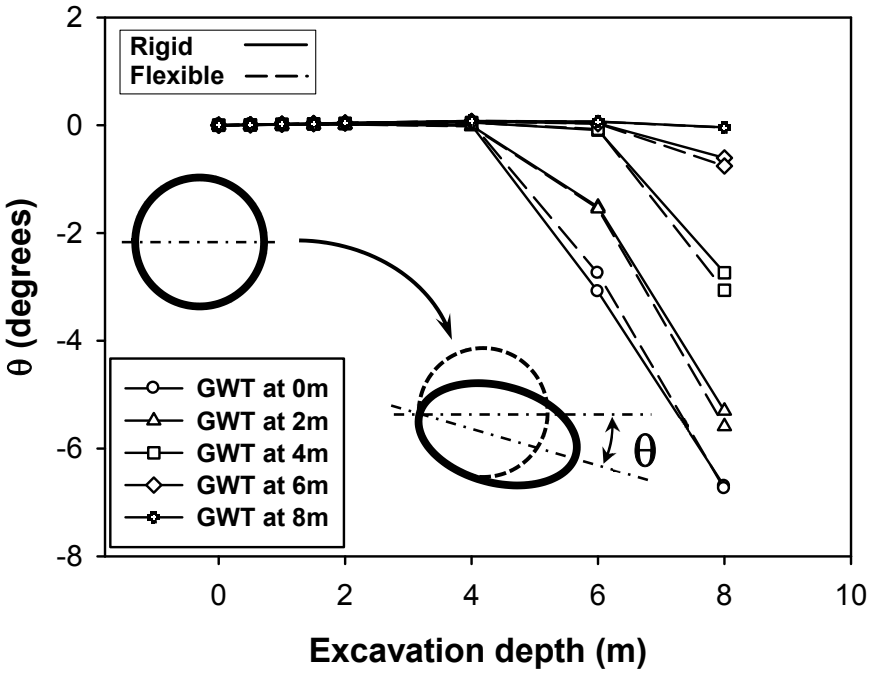

Figure 5.13 Rotation of rigid and flexible pipe due to soil mass movement.

5.3.2 Strains and rotation of the hoop

Strains in rigid and flexible pipeline hoops are presented in Figure (5.15) with respect to matric suction and excavation depth. The hoop strains were estimated using four reference nodes, two at the opposite sides of the springline and two at the top and bottom of the hoop. The final displacement and rotation of each node was taken into account to estimate the elongation and shortening deformations in the hoop. Rigid pipeline shows much less strains in comparison to flexible pipeline for the same corresponding excavation depth. For both pipes, the deformations increase with excavation depth and decrease with average matric suction, $(u_a - u_w)_{av.}$ at the top and bottom of the pipe (i.e. ring deflection decreases as the GWT depth increases). Several codes summarized the maximum strains that can be anticipated in pipeline hoops for different scenarios (Table 2.6). DNV-RP-F116 (2009), DNV-OS-F101 (2013), OPSS 401 (2013), and OPSS 421 (2013) suggest that 2% deflection is the maximum strain that rigid pipelines can sustain without cracks while flexible pipes can deflect up to 5%. In addition, DNV-OS-F101, 2013 define the yield strain for rigid pipes as strain corresponding to 0.5% deflection.

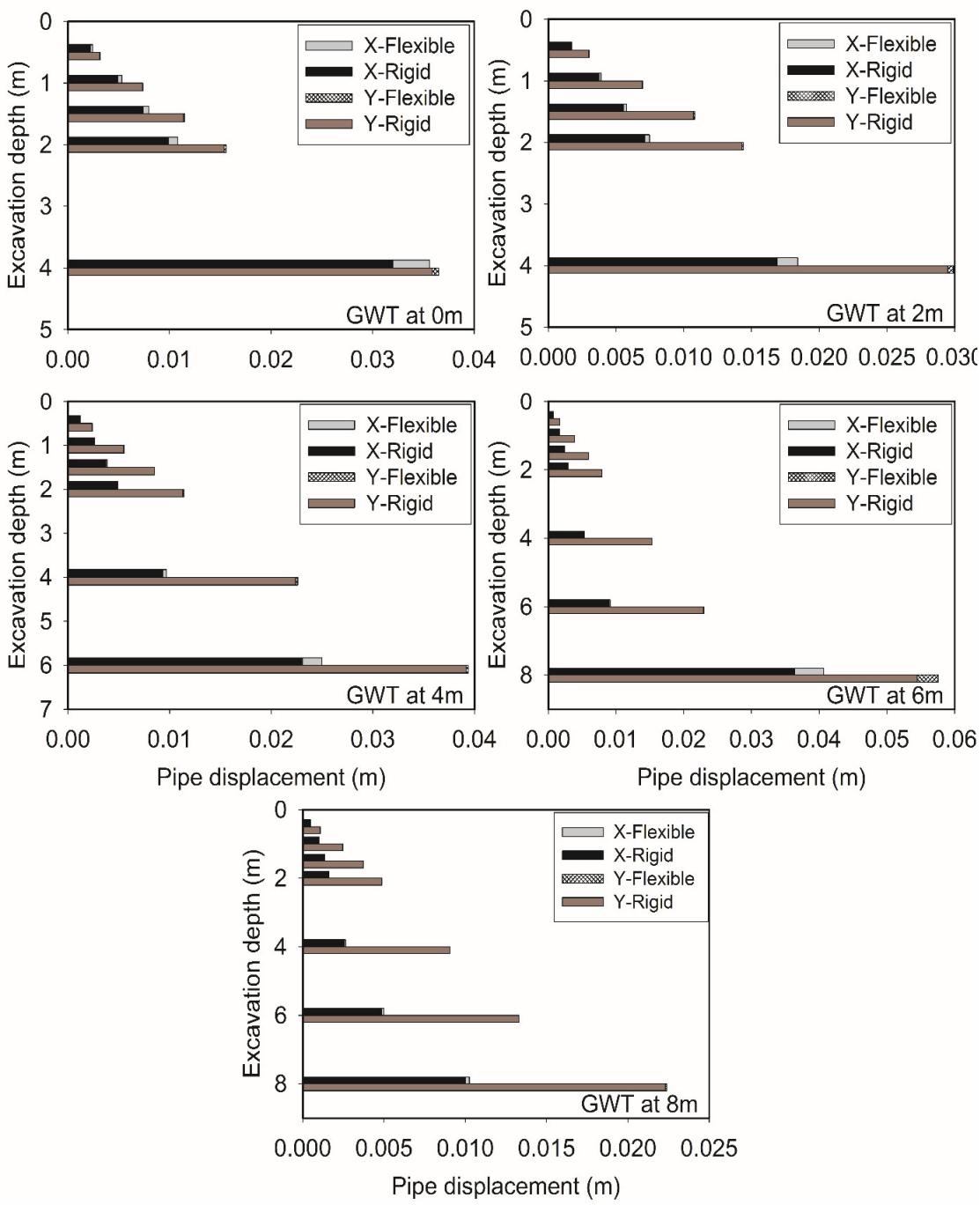

Figure 5.14 Difference in the final horizontal, X and vertical, Y displacements between rigid and flexible pipe.

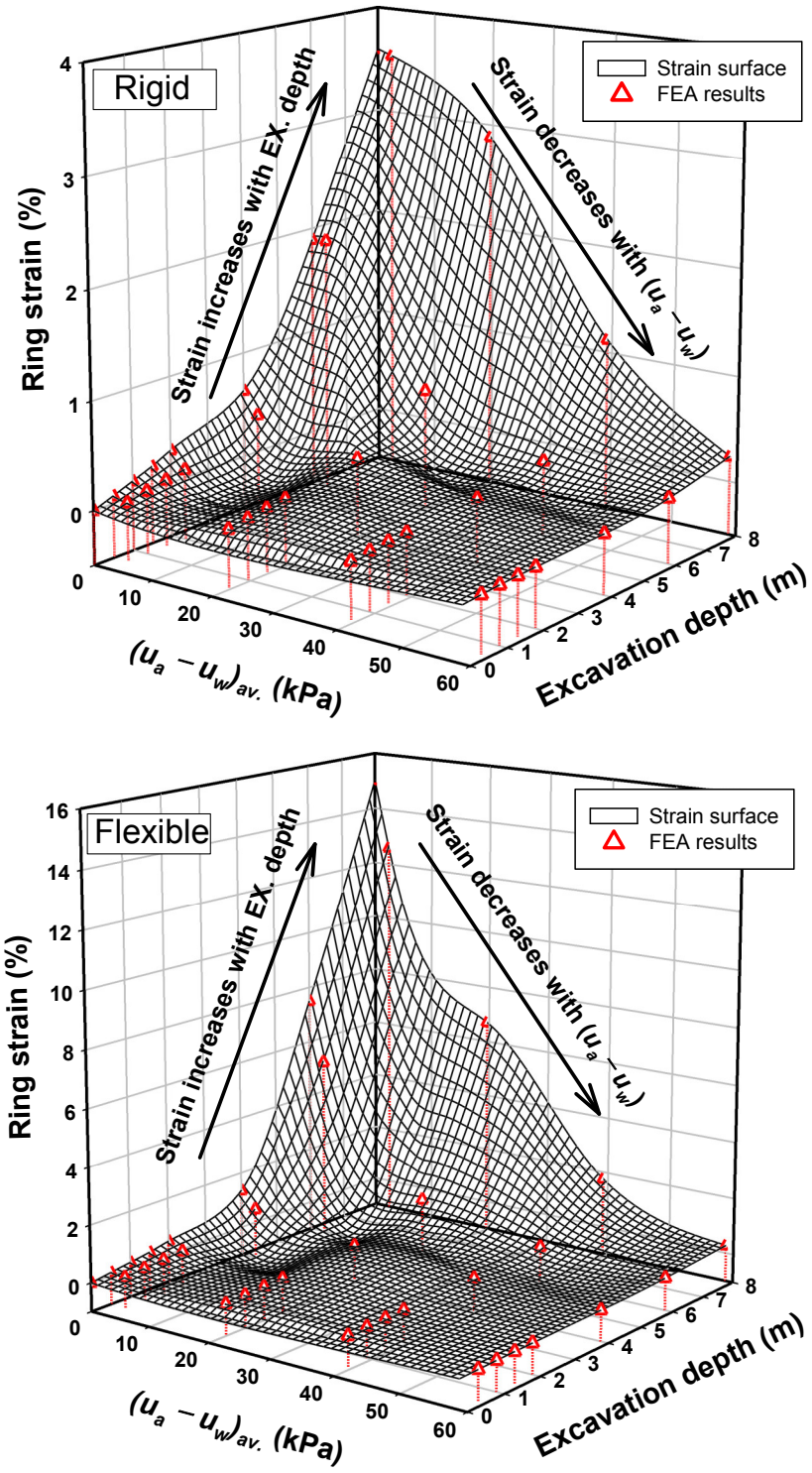

Figure 5.15 Strains of rigid and flexible pipe at the springline with respect to average matric suction and excavation depth.

Figure (5.16a and b) show strains in the hoop of rigid pipeline with respect to excavation depth and average matric suction, $(u_a - u_w)_{av.}$. Positive and negative signs indicate elongation and shortening in the ring diameter, respectively. Average matric suction, $(u_a - u_w)_{ave}$ was defined as the matric suction value at the springline level. All the strains are recoverable as the pipe behaves elastically up to the yield strain value. Plastic strains will be predominant once the strains increase a value beyond 0.5%. Figure 20a and b shows the strains for flexible pipe as well. The red dotted line represents the maximum allowable strain after which the flexible pipe fails. Figures (5.16 and 5.17) suggest that deformation in pipeline ring decreases with an increase in the GWT depth and $(u_a - u_w)_{av.}$ values. The results from Figures (5.16 an5.17) are consistent with Figure (5.12) which provide details soil failure depth for different GWT level and excavation depths. Relationships such as Figures (5.16 and 5.17) can be developed for the local soil conditions and may be used as design charts to estimate the adequate excavation depth without supporting system based on $(u_a - u_w)_{av.}$ value or GWT depth. For example, using Figures (5.16a and 5.17a) with GWT at 2m depth information, the maximum unsupported excavation depth that does not cause plastic strains in the rigid pipe is 4m while for flexible pipe the excavation depth may extend to 5m. Similarly, Figures (5.16b and 5.17b) can be used with $(u_a - u_w)_{av.}$ information to estimate the adequate excavation depth.

5.3.3 Radial internal forces

Radial axial force distribution around the pipeline ring for both rigid and flexible pipes for the four excavated layers is shown in Figure (5.18). At the crown and invert of the pipeline ring, tension (negative) axial force is developed for all GWT depths, while compression (positive) axial force is developed in the springline. For the cases where GWT = 0m and 2m, up to 4m of excavation, the compression axial force is higher than other cases where the GWT is at greater depth. The axial compression force after 4m of excavation increased due to the significant deformation in the soil. The axial tension force for different excavation depth, however, (i.e., for the cases where the GWT at 0 and 2m) is lower in comparison to GWTs with greater depths. Such a behavior can be attributed to contribution of soil suction towards shear strength and stiffness of soil. Increasing the soil shear strength and stiffness at the springline will provide a strong support or confining pressure to the pipeline which will decrease both axial force as well as deformation.

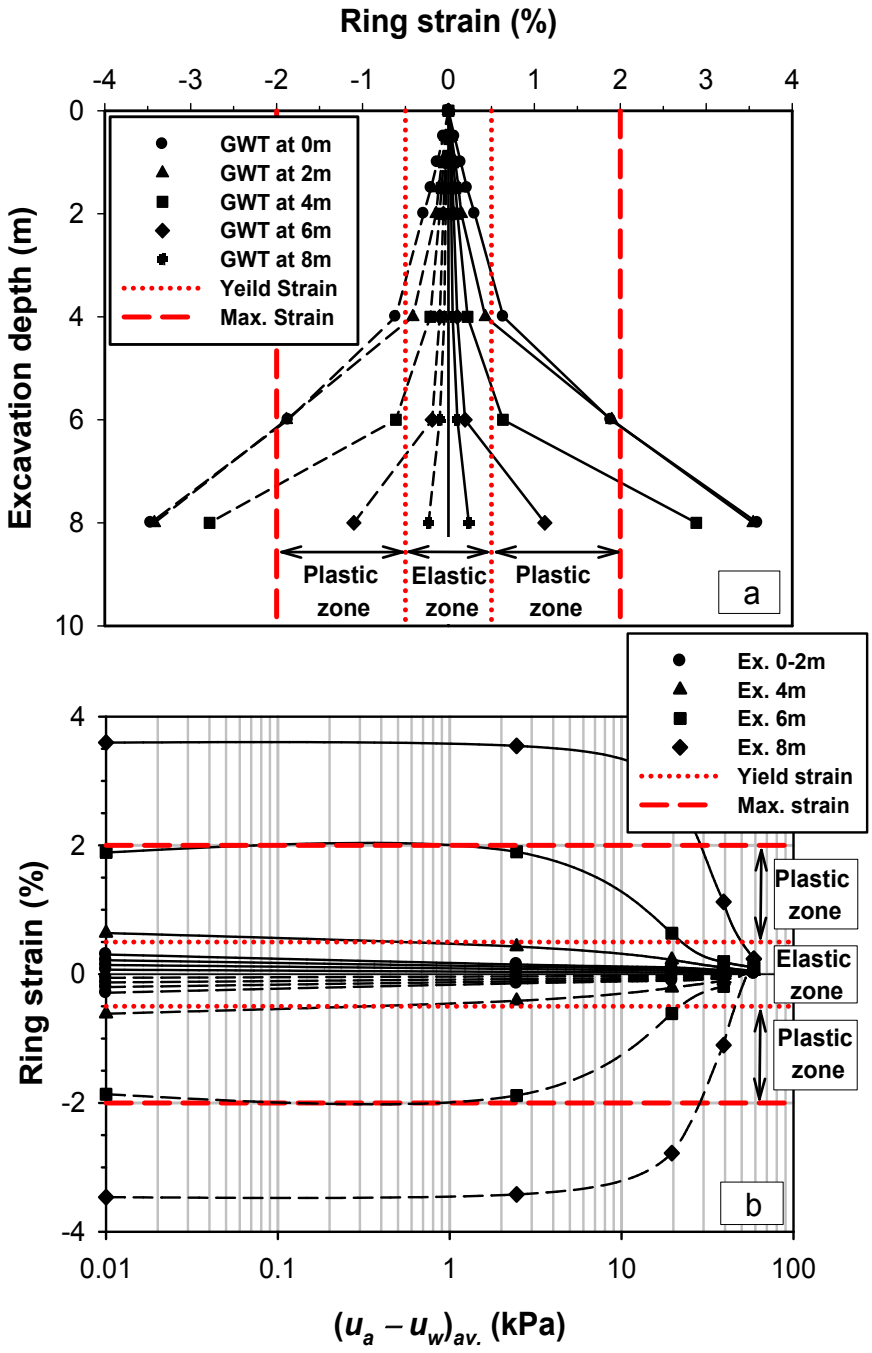

Figure 5.16 Strain envelops for rigid pipe with respect to; (a) Excavation depth, and (b) $(u_a - u_w)_{av.}$.

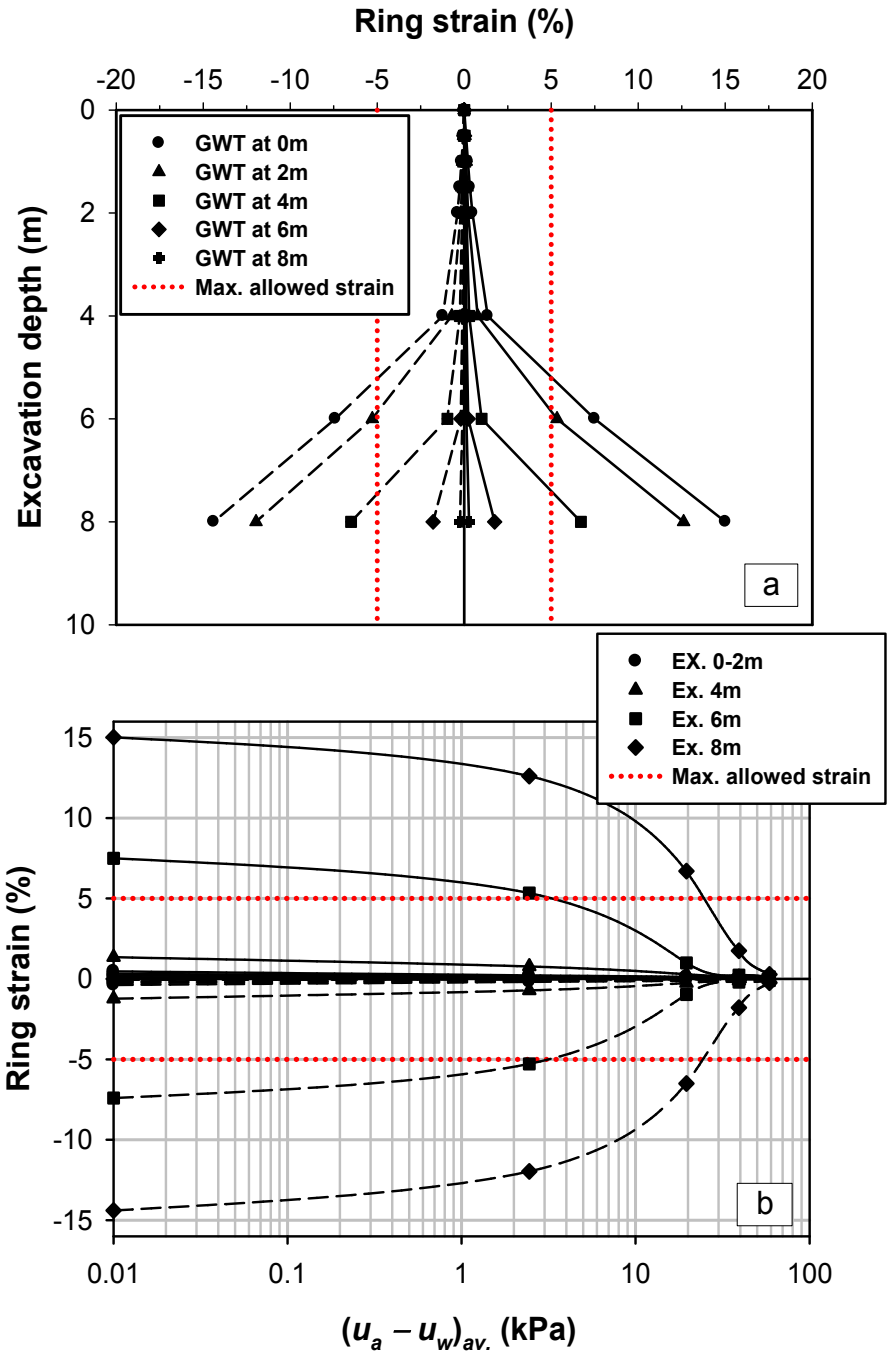

Figure 5.17 Strain envelops for flexible pipe with respect to; (a) Excavation depth, and (b) $(u_a - u_w)_{av.}$.

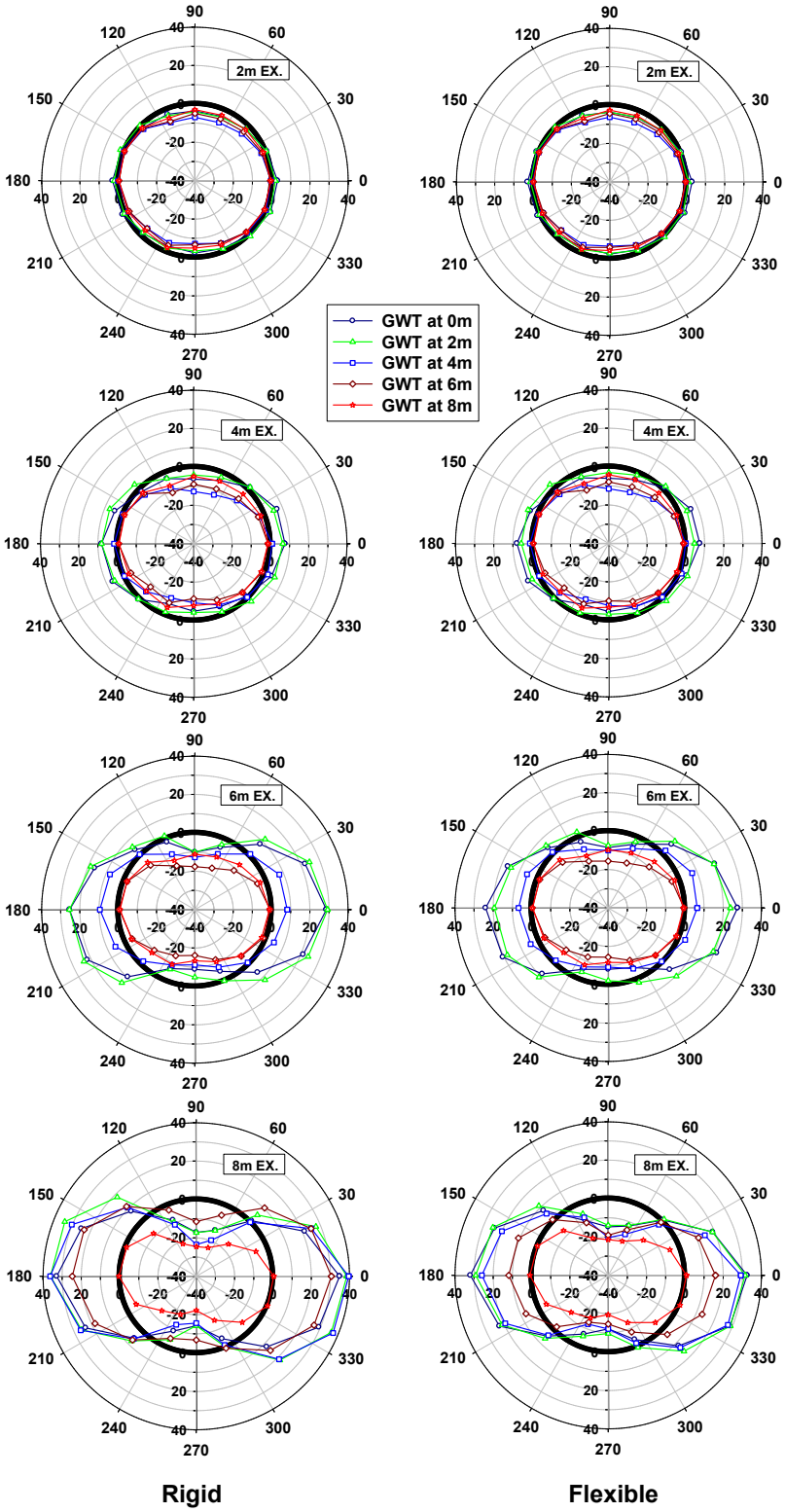

Figure 5.18 Axial force distribution along the pipeline ring (kN) for rigid and flexible pipe.

On the contrary, increasing the soil shear strength and stiffness will cause higher pressures at the top and invert of the ring due to soil mass movement toward the soil cut. In addition, compression and tension axial force exhibited different behavior with respect to GWT depth.

Figure (5.19) shows the variation of the radial shear force along the rigid and flexible pipe perimeters. The shear force in flexible pipe is much less in comparison to that of rigid pipe. The maximum positive shear force was observed at angles 135^0 and 315^0 while the maximum negative shear force was observed at angles 45^0 and 215^0, respectively. Shear force becomes almost double for each excavation regardless of the levels of GWT. However, for greater GWT level (i.e. higher $(u_a - u_w)$), the shear force and deformations due to trenching, as discussed earlier in Figures (5.16 and 5.17), significantly decreased.

The variation of bending moment in the pipeline ring also shows similar behavior of shear forces (Figure 5.20). The maximum bending moment is located at points of zero shear stress. The maximum positive bending moment was observed at angles 0^0, 90^0, and 270^0 while the maximum negative bending moment observed at 60^0, 180^0, and 290^0, respectively. Both bending moment and shear force for GWT = 8m were not significant, which implies that the contribution of matric suction toward shear strength and stiffness provided strong support to the pipeline and reduced the strains and improve its performance behavior. The results indicate generally that internal forces in the rigid pipe is higher than that for flexible one.

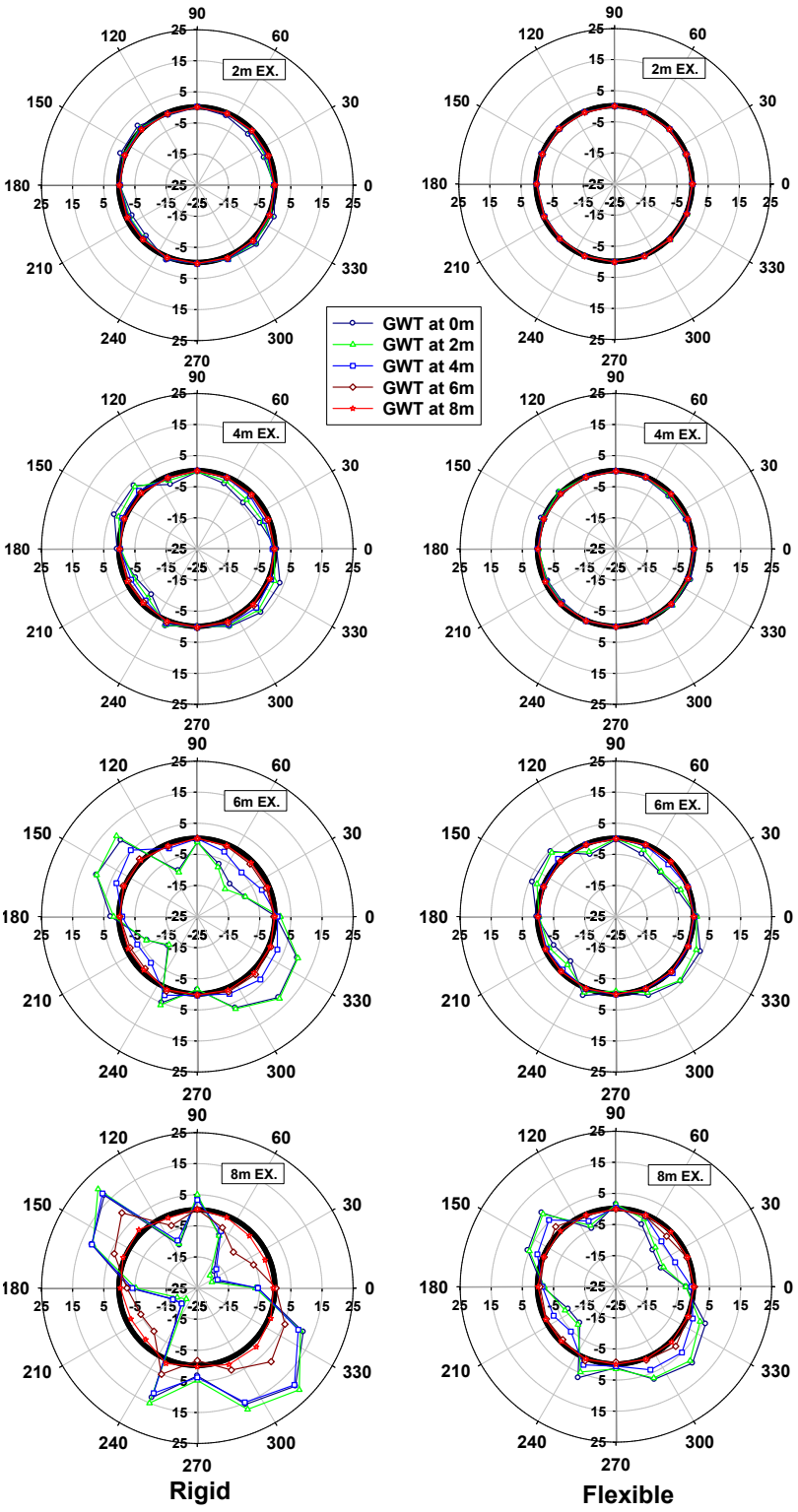

Figure 5.19 Shear force distribution along the pipeline ring (kN) for rigid and flexible pipe.

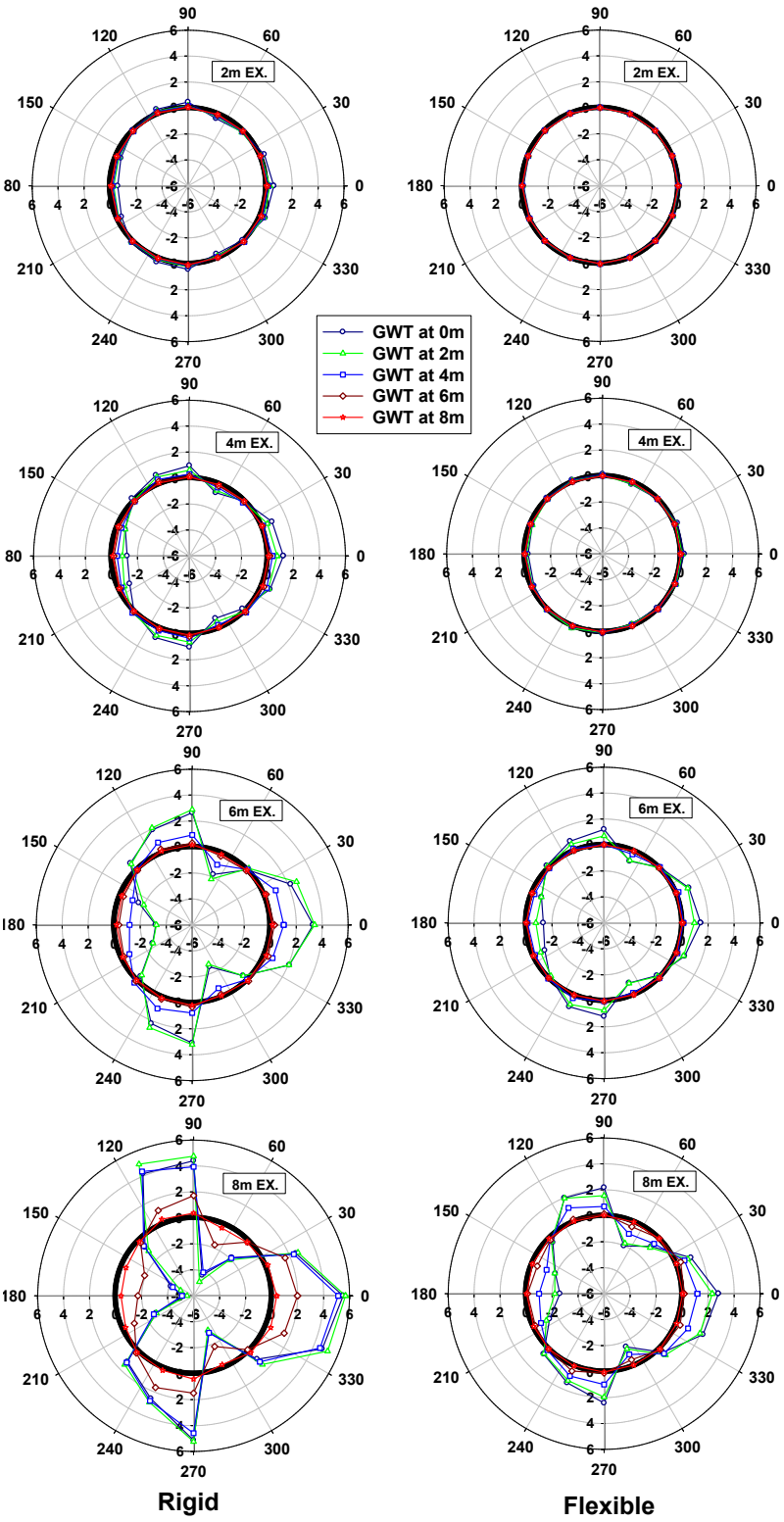

Figure 5.20 Bending moment distribution along the pipeline ring (kN.m) for rigid and flexible pipe.

5.4 Summary and Conclusions

In the present study, numerical analyses were carried out to investigate the soil-pipeline system behavior associated with nearby unsupported vertical excavation extending the principles of saturated and unsaturated soil mechanics. The study employed the conventional Mohr-Coulomb constitutive model in the commercially available two-dimensional numerical software. It was assumed that pipelines (rigid and flexible pipelines) are buried at the depth of 2m from the soil (Indian Head till) surface and levels of ground water table were 0, 2, 4, 6, and 8m. A hydrostatic pore-water pressure distribution was assumed above and below the GWTs (i.e.) to simplify the analysis. The modified effective stress analysis (MESA) was used in the analyses to simulate slow excavation that allows the dissipation of both pore-water and pore-air. The results suggest that soil deformations are relatively less when the GWT is at a greater depth, which is attributed to the effect of matric suction on the shear strength and stiffness of the soils. The proposed modeling technique is suitable for estimation of the adequate excavation depth without supporting system to avoid unexpected pipe hoop strains and internal forces considering the levels of GWT and distance between the location of pipeline and excavation.

Present study also suggests that internal shear and axial forces and bending moment in pipelines buried in unsaturated soils can be overestimated by extending conventional saturated soil mechanics. This practice may lead to erroneous force-displacement estimation and over conservative design procedure. For these reasons, geotechnical engineers should consider the influence of $(u_a - u_w)$ and excavation duration for both stability of unsupported excavation and internal forces in the pipeline when considering trench excavation in engineering practice for rational analysis. More large-scale laboratory studies and field investigations are required in the future for better understanding the soil-pipeline system behavior taking account of both saturated and unsaturated soil conditions.

CHAPTER SIX

EXPERIMENTAL INVESTIGATION OF SINGLE MODEL PILE AND PILE GROUP BEHAVIOR IN SATURATED AND UNSATURATED SAND

6.0 Background-Information

The contents presented in this chapter are summarized from the manuscript below:

Al-Khazaali, M., and Vanapalli, S.K. (2018). Experimental investigation of single model pile and pile group behavior in saturated and unsaturated sand. *Manuscript under review with an International Journal*.

6.1 Introduction

Piles or pile groups as foundations assure satisfactory performance in different types of soils by safely transmitting loads from the superstructures and alleviate problems associated with settlement. Several billions of dollars are invested annually towards design and construction of pile foundations, which contributes to several thousands of job opportunities, all over the world. A comprehensive understanding of the mechanical behavior of soil and pile interface is required for the rational design of pile foundations. The mechanical properties of the soil and pile-interface such as the stiffness and shear strength influence the load-settlement (P-δ) behavior of pile foundations. Poulos (1989) studies suggest that the pile settlement is governed by modulus of elasticity of the pile, E_P, modulus of elasticity of the soil, E_S, and pile length to diameter ratio (L/D). However, E_P is significantly higher in comparison to E_S; therefore, in a homogeneous soil deposit, E_S is the key parameter that controls the elastic settlement of the pile foundations. Schanz et al. (1999) concluded P-δ behavior of a pile foundation in the elastic zone is governed by E_S; however, shear strength parameters (i.e. effective cohesion, c', effective angle of internal friction,

ϕ', and dilation angle, ψ) contribute significantly to the maximum or ultimate load (P_{ult}) of pile foundation (Figure 1.2) (Potts and Zdravković 2001). All the above studies were based on the principles of saturated soil mechanics.

During the last two decades, several experimental and numerical research studies were also undertaken to investigate the *P*-δ behavior of shallow and deep foundations in unsaturated soils (for example, Oloo et al. 1997, Georgiadis et al. 2003, Mohamed and Vanapalli 2006, Rojas et al 2007, Vanapalli and Mohamed 2007, Vanapalli et al. 2007, Vanapalli et al. 2010, Vanapalli and Taylan 2012, Oh and Vanapalli 2013, Wuttke et al. 2013, Sheikhtaheri 2014, Han et al.2016, and Tang et al. 2018). All these studies suggest that the load carrying capacity significantly increases due to the contribution of ($u_a - u_w$) and the corresponding settlement decreases. However, to the best of the author's knowledge, there are no studies reported in the literature that have addressed the influence of ($u_a - u_w$) towards pile group behavior in unsaturated soils.

In the current study, experimental investigations related to the behavior of a single model pile and (2×2) pile group in saturated and unsaturated sand are undertaken. Two sets of model piles with smooth and rough shafts were used, with three different pile centre-to-centre spacing, *s* (i.e. 3*D*, 4*D*, and 5*D*) for the pile group. In total, 40 tests were performed by varying the water table (WT) level (i.e. at depths = 0 (at the surface), 300, 400, 550, and 850mm). The focus of investigation was directed to study the influence of matric suction, roughness of soil-shaft interface, dilation and group action. The test results suggest that the mechanical behavior (i.e. carrying capacity and settlement) of single pile and pile group significantly improved with an increase in the WT depth (i.e. ($u_a - u_w$) increases). It is important to extend the mechanics of unsaturated soils to alleviate erroneous estimation of the pile group capacity and group efficiency factor in unsaturated sandy soils. In other words, rigorous interpretation of pile load tests is required for soils in semi-arid and arid regions with a deep ground water table by the practicing engineers.

6.2 Background

As per AASHTO (2002), piles are classified into two different categories based on their load carrying mechanism; i) friction piles, which derive their load carrying capacity predominantly from soil resistance that mobilizes along the shaft of the embedded pile, and ii) end bearing piles,

derive their load capacity from the resistance of the material on which the pile end rests. The P_{ult} of a single pile is typically a combination of resistances arising from shaft and end bearing and are determined using full-scale pile load tests (PLT) following ASTM D1143. The most reliable information about the *P-δ* behavior, pile capacity and load transfer mechanism can be derived from full-scale in-situ load tests on instrumented piles. The data from these tests can be used to validate or modify the assumptions for rational design of pile foundations. However, there is no specific test procedure or recommendation to determine the ultimate carrying capacity of pile group ($P_{ult.G}$) from pile group tests (Lee and Chang 2005). For engineering practice applications, $P_{ult.G}$ is conventionally estimated based on in-situ full-scale load test results of single piles.

Several methods are available in the literature for estimating the ultimate load carrying capacity of a pile foundation. For example, Davisson (1973) developed the offset limit criterion (OLC) to estimate the ultimate capacity of end bearing driven piles and suggested that it can be also extended to friction piles (Figure 6.1). This method is conservative and widely used in North America. The method utilizes the elastic load-displacement line of a fixed-base, free standing pile (line OA) which is defined by Eq. (6.1) to identify the ultimate load capacity of single pile (P_{ult}). The suggested criterion defines the P_{ult} as the intersection point (C) on the *P-δ* curve with a line BD which is parallel to OA and defined by an offset (Δ) determined by Eq. (6.2).

$$\delta_{\varepsilon} = \frac{PL}{AE_p} \tag{6.1}$$

$$\Delta = 0.15'' + (D/120) \tag{6.2}$$

where *P* = load, *L* = pile length, *A* = area of the pile tip, and *D* = pile diameter in (inch).

Double tangent method was suggested by Butler and Hoy (1977) to estimate the P_{ult} from PLT. The method can be summarized with the aid of Figure (6.1): i) draw a line tangent to the initial portion of the *P-δ* curve (line OA′); ii) draw a second line with a slope of (1.4mm/9.81 kN) for driven pile test and (0.3mm/9.81 kN) for drilled shaft test tangent to the final portion of the *P-δ* curve (line B′D′); and iii) the intersection point (C′) defines the P_{ult} of the pile.

Canadian Foundation Engineering Manual (CFEM) (2006) and International Building Code (IBC) (2006) recommended using the OLC method by Davisson (1973) in addition to other

methods such as 80% and 90% failure criteria by Brinch-Hansen (1961 and 1963), Chin's (1970), and Butler and Hoy's (1977) criteria. Further information on strengths and limitations of these methods and that of others are available in Fellenius (1975 and 1980).

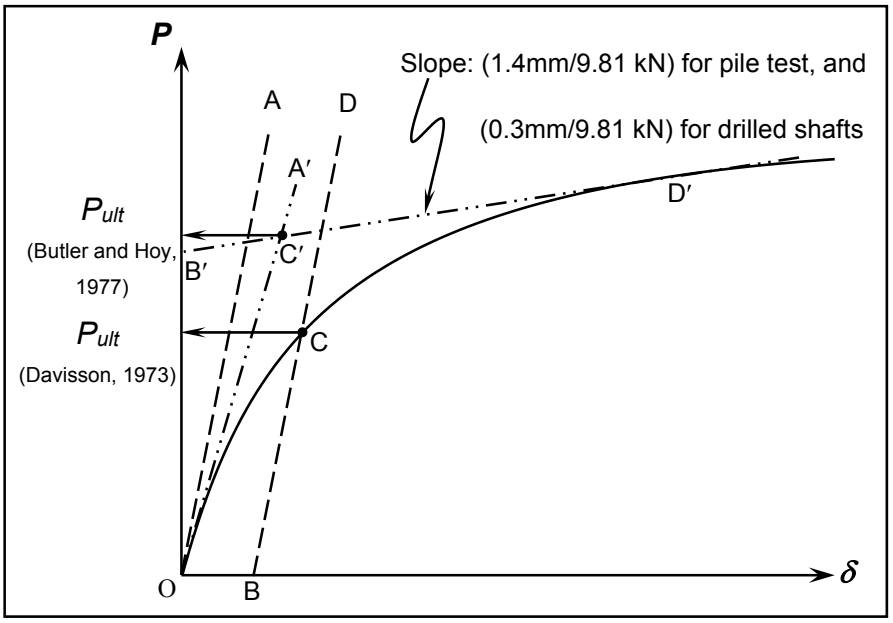

Figure 6.1 Ultimate failure load of a single pile after Davison (1973) and Butler and Hoy (1977).

In spite of the many advantages associated with the reliable data that can be derived from the full-scale PLTs for the rational design of pile foundations; they are elaborate, need trained personnel, time consuming and hence are expensive. In order to alleviate the drawback associated with the full-scale PLTs, small-scale physical and numerical models have been extensively used to simulate different loading scenarios of pile foundations (i.e. static, and dynamic loads) (Beredugo 1966, Boominathan and Lakshmi 2000, Al-Mhaidib 2006, Lee and Chung 2005, Vanapalli et al. 2010, Vanapalli and Taylan 2011 and 2012, Gaaver 2013, Khari et al. 2013, Taylan 2013, Sheikhtaheri 2014). Several limitations may be associated with the results derived from small-scale models due to scaling and test boundary conditions issues. Some of the key problems with small-scale models are discussed in the next section.

6.3 Test Equipment Design

Several criteria should be satisfied to perform successful model PLTs. These criteria include stress bulb interference with the physical boundaries of soil container, number of the piles and pile group geometry, and relative spacing between piles, *s/D* both in design of a model single pile or pile group tests.

6.3.1 Soil containers

A relatively large rigid steel box of 1500mm (length) × 1200mm (width) × 1060mm (depth) with 3 tons of soil maximum capacity was used to perform the model pile and pile group load tests. The soil container was designed to accommodate special features that facilitate the variation of water table and achieve reliable soil-matric suction profile to investigate different soil-structure interaction problems. More details the soil container design are summarized in Chapter 5.

6.3.2 Model pile and pile group: Design and fabrication

The focus of model pile and pile group tests program was directed towards investigating; i) variation of load carrying capacity for a single pile and pile group in saturated and unsaturated sand; ii) variation of shaft capacity for smooth and rough surface piles with respect to matric suction; and iii) spacing effect on the maximum carrying capacity of pile group constructed in unsaturated sand. Two approaches were followed to evaluate and choose the size of the model pile for the current study. The first approach is based on the recommendations and guidelines available in literature. The second approach utilizes numerical analysis along with experimental results for estimating model piles dimensions for the proposed testing program in saturated and unsaturated sand.

(a) First approach: Based on the recommendations and guidelines from the literature

Any stress interference with the physical boundaries of the testing box will increase the confining stress, which in turn contributes to load carrying capacity of the pile. Such interference should be eliminated for achieving reliable model PLT results. Based on the elastic theory, Boussinesq (1885) relationship suggests that the influence of the applied pressure of a foundation extends approximately twice the foundation width beneath the foundation. In other words, both deep and shallow foundations transfer their loads to the underneath bearing stratum in the form of a pressure

bulb of (1.5–2*D*) (Prakash and Sharma 1990, Vanapalli and Mohamed 2007, Rajapakse 2008). Therefore, enough depth should be provided under the model piles to prevent any stress interference with the bottom boundary of the box.

Gui et al. (1998) and Bolton et al. (1999) who studied the influence of soil container/cone diameter ratio, *B/d* considering different cone sizes have highlighted several other aspects. It is suggested from these studies that a *B/d* ratio greater than 22% would have no influence on the cone tip resistance. Moreover, ratio of the distance from the test location to the nearest container side, *l* to the box width, *B* will have no effect on tip resistance, when *l*/*B* exceeds 8% for dense and 14% for loose sand. However, there are no guidelines available in the literature to perform model pile group load tests. Several researchers used different container to pile group size ratios (for example, Beredugo 1966, Vesić 1969, Boominathan and Lakshmi 2000, Al-Mhaidib 2006, Lee and Chung 2005, Gaaver 2013, Khari et al. 2013). Size and geometry of model piles and pile groups from these studies are summarized in Table (2.2)

(b) Second approach: Numerical modelling

Finite element analysis (FEA) was performed to investigate the stress interference with the boundaries of the soil container, and pile diameter to mean particle size of soil ratio (D/D_{50}) to choose a suitable model pile size. The load test results of three stainless steel model piles with different diameters of 38.1, 31.75, and 19.25mm and a unique length of 200mm in two different sandy soils namely, Unimin 7030 and Industrial sand that were reported by Sheikhtaheri (2014) were used for performing FEA. In this study, Sheikhtaheri (2014) performed model PLTs under saturated and unsaturated soil conditions in a specially designed cylindrical container of 700mm height and 300mm diameter. Three average matric suction values: 0 (saturated), 2, and 4 kPa under the pile tip were considered. Soil properties, SWCC and test methodology are presented in detail in Sheikhtaheri (2014). This approach, however, was applied only for single model pile since there was no data available for pile group tests under unsaturated condition.

An axisymmetric FEA was performed using the commercial software PLAXIS 2D to simulate the P-δ behavior of the three model piles. The dimension and main features of the numerical model are shown in Figure (6.2). The soil and pile cluster were modeled using 15-node triangle element. The soil and interface along the model pile were modelled using Mohr-Coulomb (MC) constitutive model extending effective stress analysis (ESA) (i.e. drained condition). Sand

dilation was taken into account by including its influence as an angle of dilation, ψ into MC model. The angle of dilation was estimated as 10% of ϕ' of the sands as per the Danish Code of Practice recommendations (D.S. 415-1984). The model pile was modelled as a nonporous isotropic linearly elastic material with E_P = 20GPa and Poisson's ratio equals to 0.15.

The unsaturated mechanical properties (i.e. the apparent cohesion, c and initial unsaturated modulus of elasticity, E_{unsat}) of the sands and interface were derived from the saturated soil properties and the soil-water characteristic curve (SWCC) using published procedures from the literature. The E_S for both sands were estimated based on the confining stress level and recommended values from previous studies for the same sands (Oh et al. 2009, Sun 2010, Mohamed 2014). The c values for different $(u_a - u_w)$ for the sand and interface were derived using Vanapalli et al. (1996a) model that uses a fitting parameter (κ = 1 for sand). The E_{unsat} values were derived using VO-Model (Vanapalli and Oh 2010). The mechanical properties for saturated and unsaturated condition were assigned directly to the mesh in the FEA. The model parameters for the soil and interface are listed in Table (6.1).

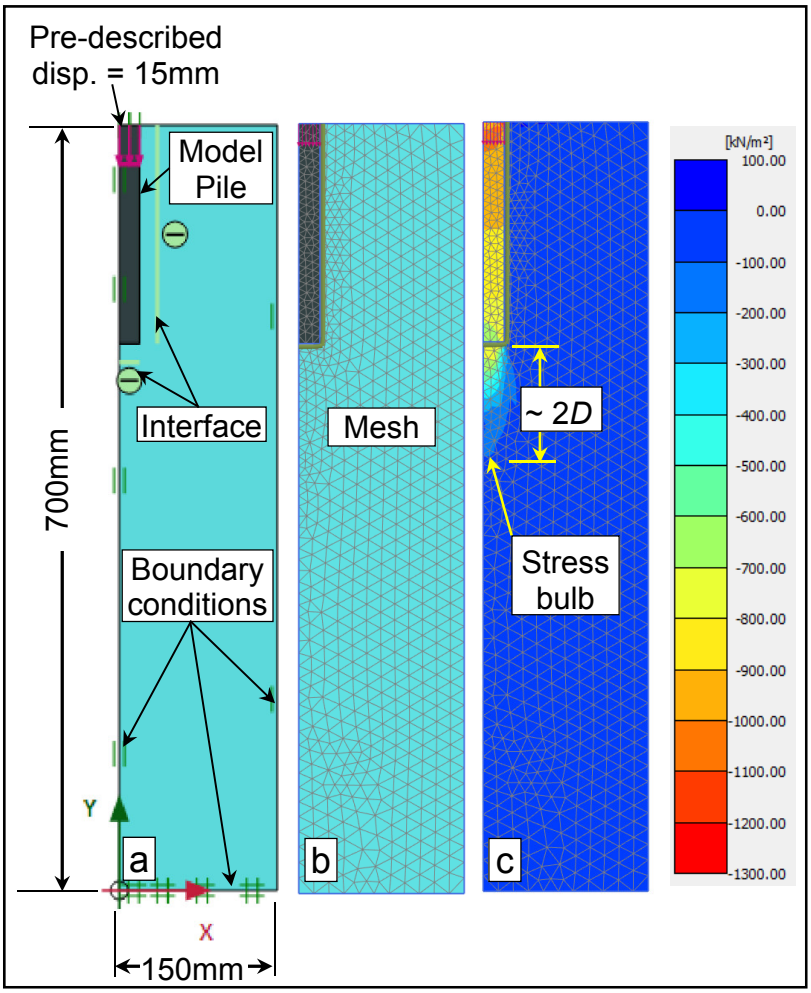

Figure 6.2 (a) The numerical model, (b) The mesh, and (c) vertical stress distribution.

Table 6.1 Sands and interfaces model parameters for FEA.

$(u_a - u_w)$ (kPa)		0	2	4
Unimin 7030	ϕ'		35.3	
	δ'		24.2	
	c (kPa)	0	1.35*	2.27*
	E_0 and E_{unsat} (kPa)	2000	3900‡	5200‡
Industrial sand	ϕ'		40.3	
	δ'		33.1	
	c (kPa)	0	1.67*	2.55*
	E_0 and E_{unsat} (kPa)	4000	7920‡	10000‡

*Vanapalli et al. (1996) model; ‡ VO-Model (Vanapalli and Oh 2010).

The results of the numerical analysis along with the experimental results are presented in Figure (6.3). The FEA provide good agreement with measured behavior with high coefficient of determinations (Figure 6.4a). The FEA can be assumed reasonably representative of the measured behavior. These results suggest that there is no interaction between the stress bulb under the pile tips and the boundary conditions of the soil container. However, by relating the normalized (predicted/measured) load to D/D_{50} (Figure 6.4b), the largest model pile size (i.e. D = 38.1mm) was found to provide the best agreement between the modelled and measured load while other sizes showed scattered results. For this reason, model pile of diameter 38.1mm was chosen for the current study based on the FEA results.

Two sets of 4-model piles, with smooth and rough surfaces were designed and fabricated using stainless steel pipe of 38.1mm diameter and total length, L of 360mm with an embedment depth in the sand of 300mm. Smooth and rough (i.e., threaded) pile surfaces were chosen to investigate the influence of pile shaft roughness on the total carrying capacity (Figure 6.5a). Four model piles were fabricated with smooth and rough shaft surfaces. The rough model pile has 24 threads per inch and a pitch or thread depth equal to 0.25 mm. The thread depth was chosen to match D_{50} for the sand to provide enough interlocking (Figure 6.5b).

The piles in a group are usually connected by a pile cap. The main duty of a pile cap is to transfer and distribute the load from the superstructure to the piles. Use of a flexible pile cap will result in load concentration on the central piles rather than the edge piles resulting in large settlement under the central piles. To prevent differential settlement, loads on piles need to be redistributed such that the central piles will have the same settlement as the edge piles. Rigid pile cap is widely used to assure uniform settlement for all the piles. However, such a measure will result in higher loads carried by the outer piles. In the current study, a small axisymmetric 2 × 2 pile group is under investigation. A rigid steel plate pile cap of 305×305mm and thickness of 12.5mm was fabricated to distribute the static load equally on four piles (Figure 6.5c). A pattern of several threaded holes was drilled in the pile cap to satisfy the required pile group center-to-center spacing, s (i.e., $s = 3D$, $4D$, and $5D$) (Figure 6.5d). The pile cap was assumed rigid following Chow and Poulos (2015) findings. They concluded that for small pile group, such as the one under consideration, using flexible or rigid pile cap results in uniform load distribution on piles.

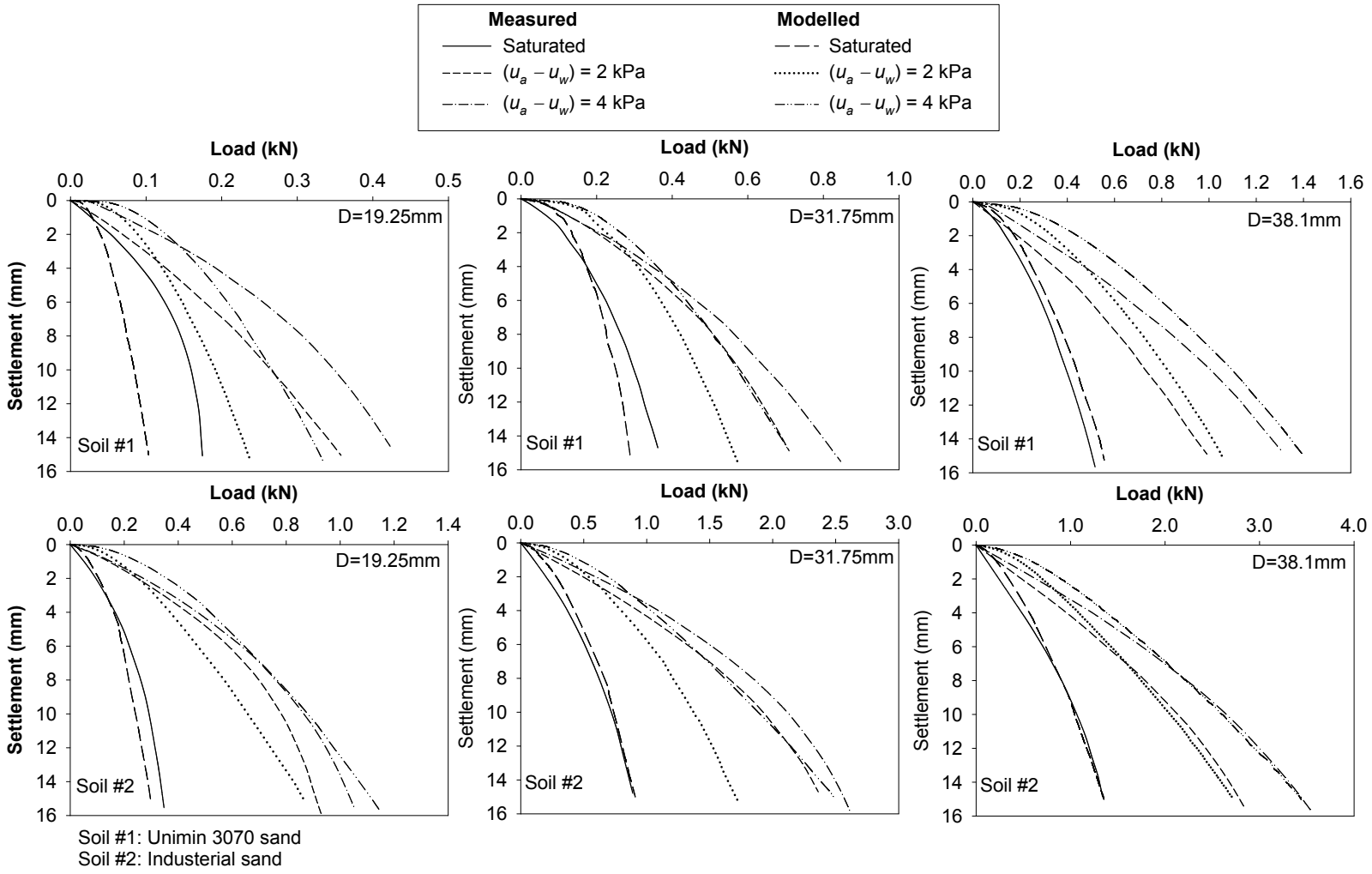

Figure 6.3 Measured and modelled *P-δ* behavior of the three model piles.

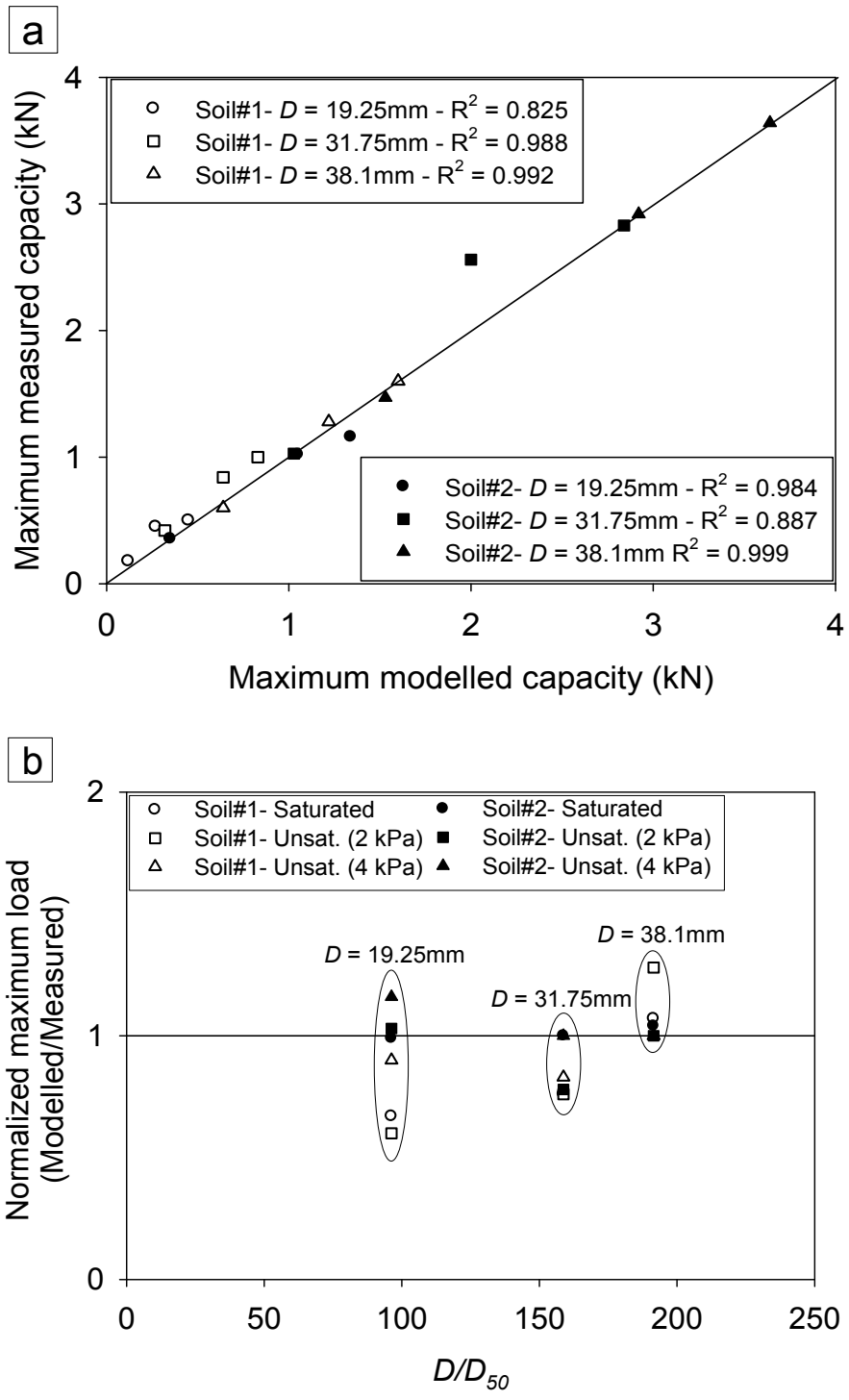

Figure 6.4 (a) Maximum carrying capacity: Measured vs. modelled 45^0 line, and (b) Normalized maximum load with respect to D/D_{50} ratio.

The designed model and soil container satisfied the discussed earlier guidelines; i) the recommendations of Gui et al. (1998) and Bolton et al. (1999) for single model pile and ii) for model pile group were similar to or even greater than the dimension ratios that were reported in literature (Beredugo 1966, Vesić 1969, Boominathan and Lakshmi 2000, Al-Mhaidib 2006, Lee and Chung 2005, Gaaver 2013, and Khari et al. 2013).

One of the objectives of this study was to evaluate the shaft resistance contribution and the effect of $(u_a - u_w)$ towards the shaft resistance. To satisfy this objective, three load cells were used: i) the actuator load cell (LACT) to measure the total applied load on the model pile or pile group, and ii) two load cells (LC1 and LC2) are attached at the tips of two opposite piles in the group (Figure 6.5g) and buried under the soil. LC1 and LC2 have the same diameter as the model piles to prevent any contribution to the bearing resistance. The piles tips were modified to have a void of 11mm diameter and 1mm depth at the center of the tips to accommodate the 2mm height load cell button (Figure 6.5e and f). To prevent the load cell damage, the data cable of the load cell was passed through a sleeve that is made of a plastic tube and buried into the sand. The sleeve facilitates the cable movement during the test and prevent tension stresses on the cable due to load cell displacement. The difference between the measured bearing resistances using these load cells and the actuator load cell were helpful to calculate the shaft resistance contribution.

6.3.3 Instrumentations

Several instruments were used in the testing program for collecting, sorting and saving the data. MTS hydraulic actuator of 25 kN capacity that had 240mm stroke length was used to apply vertical load. The actuator was mounted on a loading frame that consists of two rigid supporting arms and two rigid reaction beams that were made of hollow steel section of 150 × 63.5 × 9.5mm. The main load cell was the MTS load cell, denoted as LACT, which is a part of the actuator. The LACT has 25 kN (5600 lbs) capacity and was used to measure the total carrying capacity of the single pile or the pile group.

The original testing program plan was to have four interface load cells model LBM-5K-38, denoted as LC1, LC2, LC3 and LC4 (Figure 6.5h and i) with maximum capacity of 22,241 N (5000 lbs) and 38.1mm diameter to measure the force under each model pile. The interface load cells were specially designed environmentally sealed, load cells with 3m data cable. However, LC3 and LC4 were found faulty while conducting the first series of the proposed test program.

Due to this reason, remainder of the tests were performed with only two interface load cells (i.e. LC1 and LC2) in addition to LACT.

The settlement was measured using two linear variation displacement transducer (LVDT) of 50.8mm and 25.6mm maximum stroke. The analog test results data was translated to digital signal using data acquisition system (DAQ) and stored on a computer for later use. The soil-matric suction profile in the soil container during the tests were measured using four soil moisture probe 2100F Tensiometers that were installed at different depths as follow: 150mm (i.e. middle of the shaft), 300mm (i.e. at the pile tip), 450mm and 600mm. The full setup is shown in Figure (6.6a).

Figure 6.5 Model pile and pile cap; (a) Smooth and rough surface model piles, (b) threading of the rough pile, (c) the full pile group, (d) offset hole pattern on the pile cap, (e) pile tips modification to accommodate the LC1 and LC2, (f) close look at the pile tip modification, (g) LC1 and LC2 at the piles tips, (h) LBM-5K-38 Interface load cell, and (i) schematic diagram illustrate the load cell (all dimensions are in (mm)) (Interface Inc.).

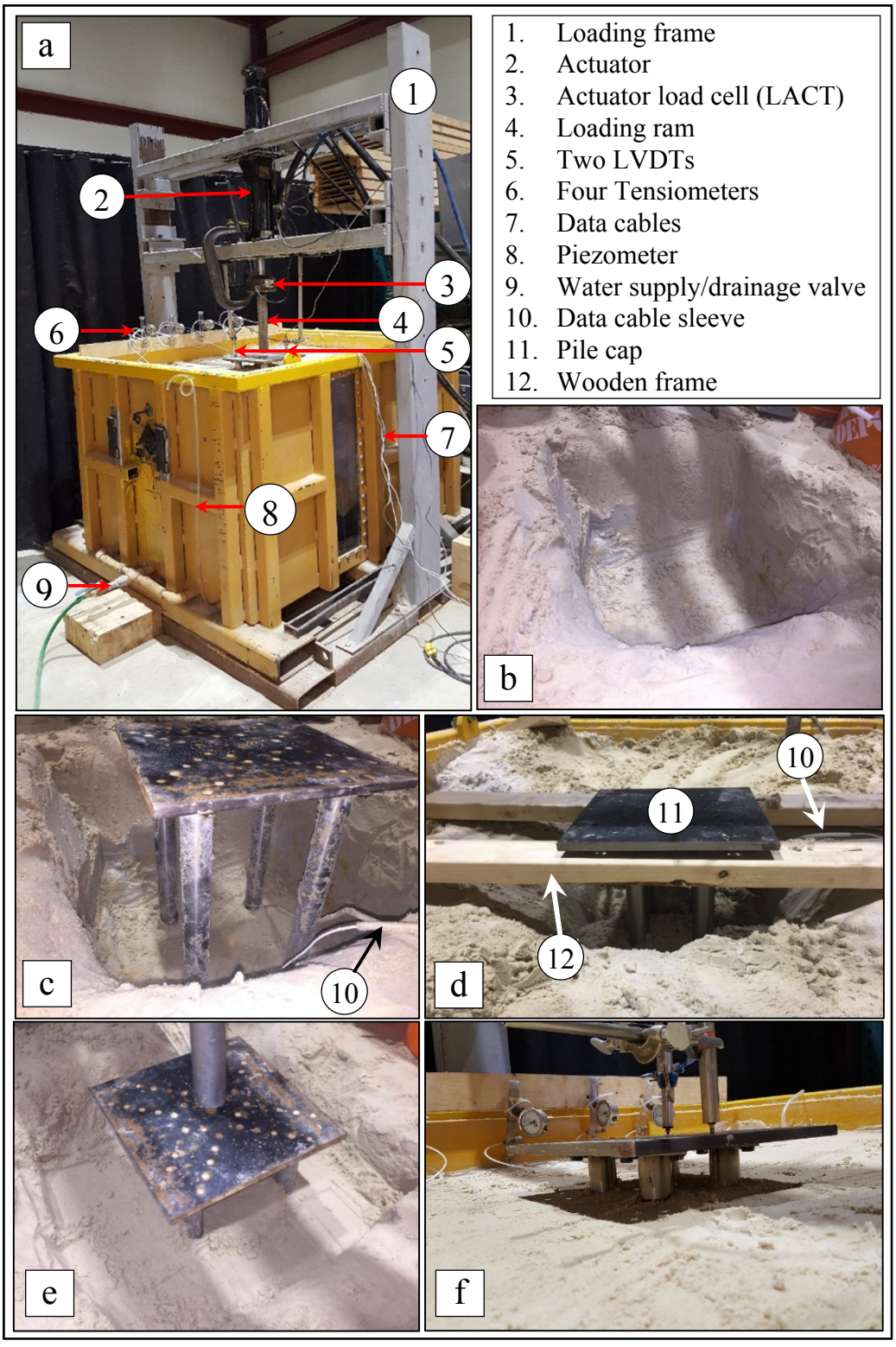

Figure 6.6 The main characteristics of the test setup showing model pile group setup preparation for the test.

6.4 Soil and Interface Properties

The physical properties of the quartz silica sand used in this study are presented in Table (6.2). The sand is classified according to the Unified Soil Classification System (USCS) as poorly graded sand (SP). The sieve analysis results are presented in Figure 6.7a. Hanging column technique was used following ASTM D6836-02 to measure the SWCC (Figure 6.7a). More details on the setup and test procedure of hanging column test are available in Chapter 3.

Table 6.2 Sand and interface properties.

Physical Properties	
Specific gravity, G_s	2.65
D_{60} (mm)	0.27
D_{30} (mm)	0.19
D_{10} (mm)	0.11
Coefficient of uniformity, C_u	2.45
Coefficient of curvature, C_c	1.2
Max. void ratio, $e_{max.}$	0.826
Min. void ratio, $e_{min.}$	0.507
Dry unit weight, γ_d (kN/m^3)	16.30 - 16.70
Average void ratio, e	0.606
Range of relative density, D_r (%)	60 - 70
Optimum gravimetric water content, w (%)	14.60
Mechanical properties	
Peak shearing angle of sand, ϕ'_p (^{0})	~ 35^0
Ultimate shearing angle of sand, $\phi'_{ult.}$ (^{0})	~ 34^0
Peak shearing angle of threaded interf., δ'_p (^{0})	~ 31^0
Ultimate shearing angle of threaded interf., $\delta'_{ult.}$ (^{0})	~ 29^0
Shearing angle of smooth interf., δ' (^{0})	~ 24^0
SWCC Results	
AEV (kPa)	3.6
Residual suction (kPa)	7.8
Residual degree of saturation, S_r (%)	6.0

Direct shear device was used to measure ϕ' and effective interface angle of friction, δ'. Four drained direct shear tests with different normal stresses namely 25, 40, 75 and 125 kPa were conducted. The δ's were measured using two steel interface blocks, smooth and threaded surfaces

(Figure 6.8). The blocks were fitted in the lower half of the shearing box such that the interface surface will be located at the shearing plane. The upper half of the box filled with compacted sand. The results of sand and interface shear are presented in Figure (6.9). The sand and the threaded surface showed strain hardening behavior due to the contribution of dilation followed by strain softening behavior that contributed to the peak and ultimate shear strength, respectively. The smooth interface did not exhibit distinct peak stress. However, for all normal stresses, continuous dilation behavior was observed that contributed to the ultimate shear strength of the smooth interface.

6.5 Test Methodology

The soil container was equipped with three perforated pipes that were connected to an external water supply/drainage valve. The perforated pipes were covered with a clean gravel layer of 75mm thickness, which was covered using a geofabric. The designed system of perforated pipes, gravel and geofabric served as a filter layer facilitating saturation and desaturation of the sand in the soil container by varying WT to achieve different soil-matric suction profiles. The sand was compacted manually at optimum moisture content in several layers using 6.5 kg manual compactor. Each layer was compacted at 200 mm thickness using a soil mass of 594 kg to achieve average relative density around 65%.

Forty PLTs were performed under saturated and unsaturated conditions following the same stress path that was discussed in Chapter 3. This can be summarized as below: i) setting the model piles and compacting the soil, ii) saturating the soil by raising WT from the perforated pipes that are at the bottom of the soil container to the soil surface, this technique assures removal of occluded air bubbles, iii) lowering the WT to different desired levels to achieve variation in soil-matric suction profiles, and vi) the model piles were loaded after achieving equilibrium condition with respect to matric suction profile. The load was applied at a relatively low but constant loading rate equal to

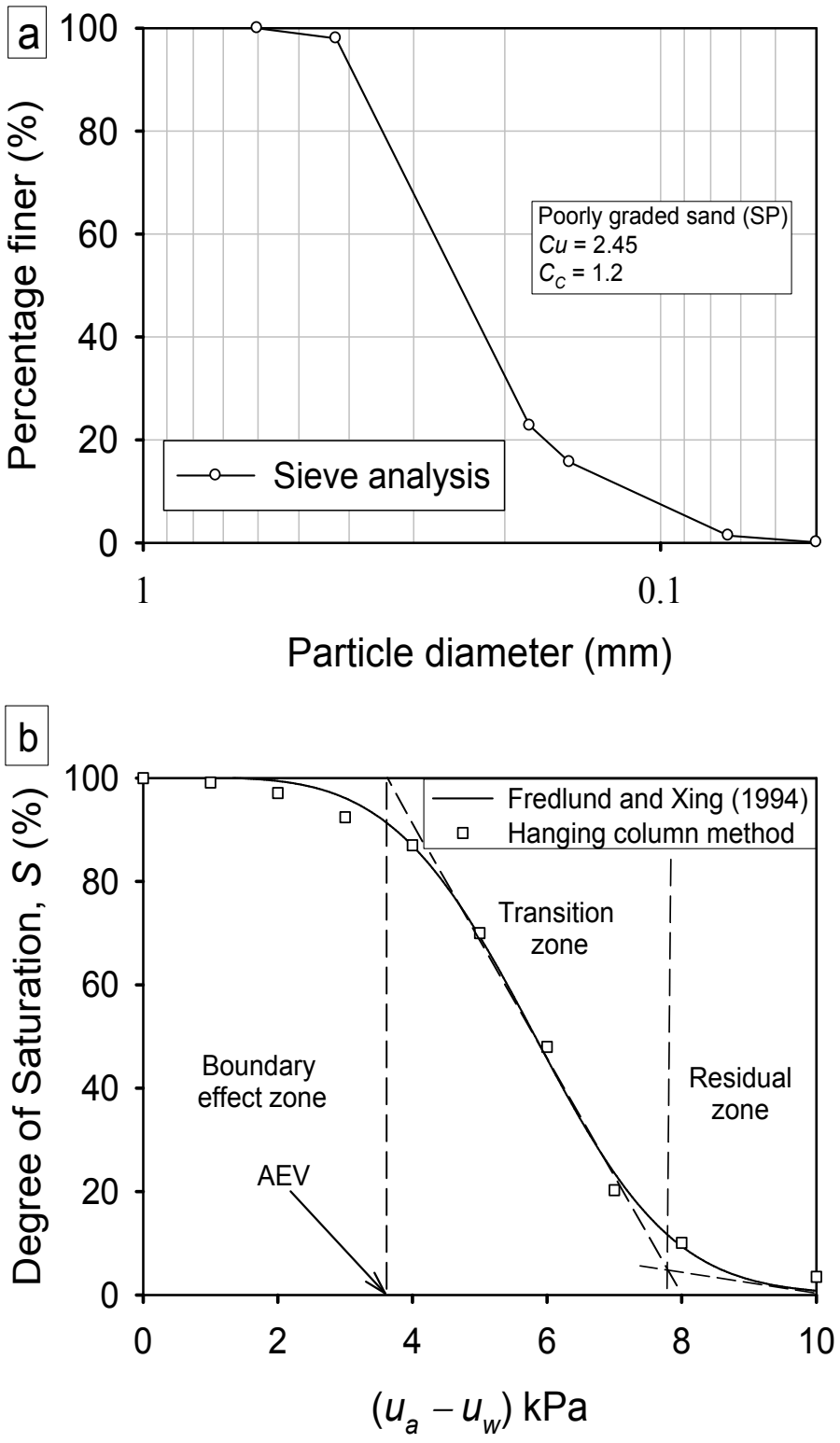

Figure 6.7 Soil properties: (a) Unimin sand 7030 grain size distribution curve, and (b) SWCC.

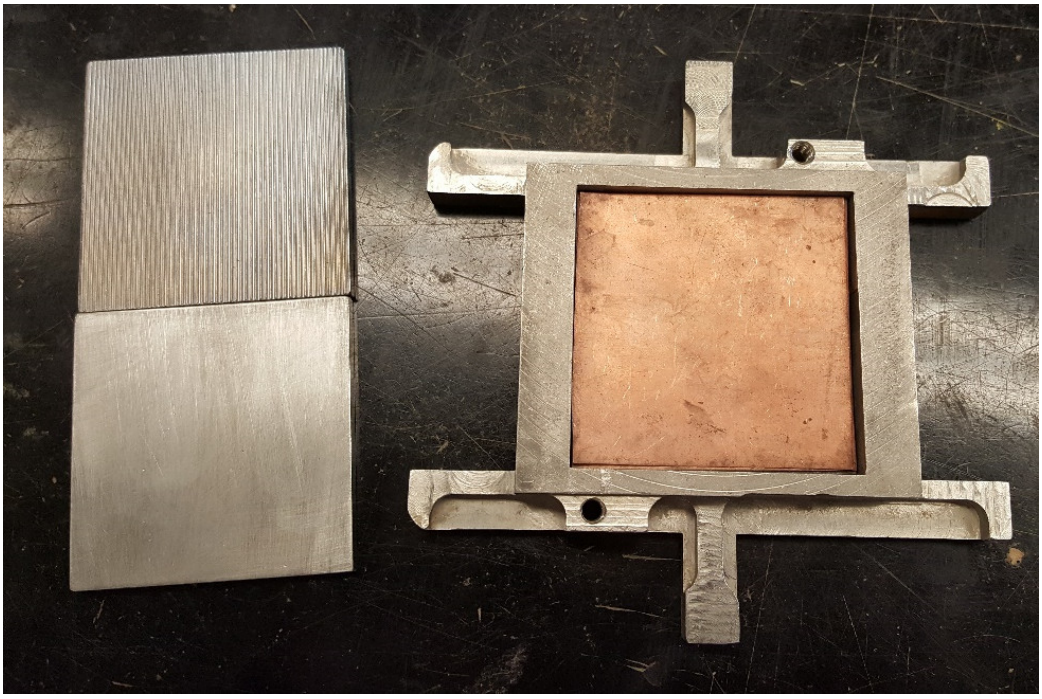

Figure 6.8 Smooth and rough steel interface blocks and lower half of shear box.

0.5mm/sec to assure drained loading condition in sand. The testing program constituted of; i) five tests on single smooth surface model pile, ii) five tests on single rough surface model pile, iii) five tests for each spacing (i.e. 3*D*, 4*D*, and 5*D*), in total fifteen, on 2×2 smooth surface pile group, and v) five tests for each spacing (i.e. 3*D*, 4*D*, and 5*D*), in total fifteen, on 2×2 threaded surface pile group. The model pile and pile group were placed in the middle of the soil container and was buried to a depth of 300mm (Figure 6.6). First, a pit was made in the middle of the soil container (Figure 6.6b), and then the model pile or pile group was placed and leveled (Figure 6.6c). To level the pile group and compact the sand, two wooden pieces of 25.4×50.8×1100mm were used to support the model pile group (Figure 6.6d). The soil then was manually compacted at the optimum moisture content around the piles in several layers (Figure 6.6e).

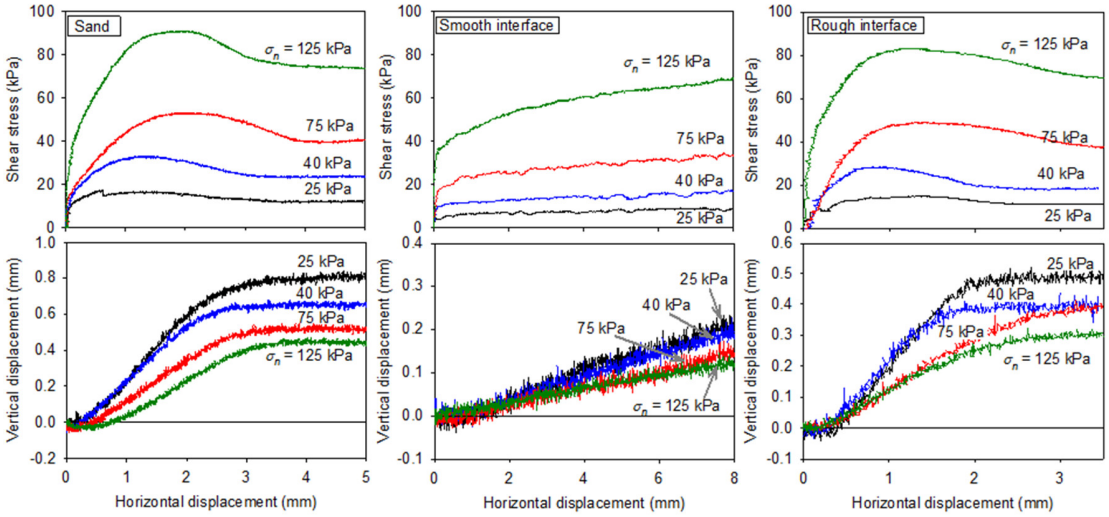

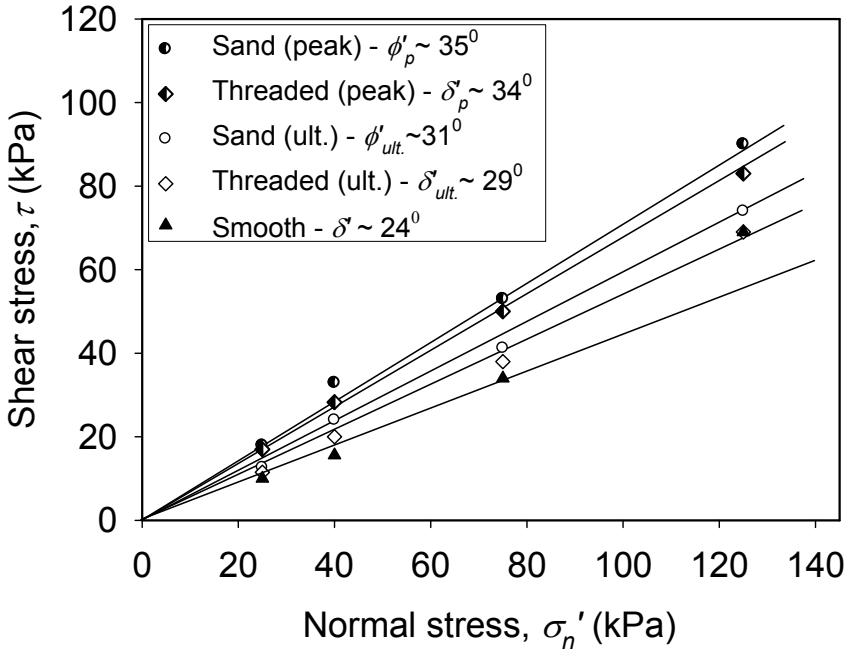

Figure 6.9 Direct shear test results.

The tests were performed with different WT levels. The WT levels where chosen to simulate saturated (i.e. WT at soil surface) and unsaturated conditions by varying the WT levels as follows: 300mm which is at the pile tip level, 400mm which is expected to be below the stress bulb of a single pile and within the stress bulb of pile groups, 550mm which is expected to be below the stress bulb of pile groups, and 850mm where the soil was fully drained. The soil-matric suction profiles for different WTs are presented in Figure (6.14b).

The contribution of pile cap towards the carrying capacity of pile foundation is usually neglected. The pile-cap-soil contact likely shrinks in clayey soil or undergoes settlement in sand, which will result in a complete loss of contact (Prakash and Sharma 1990). The New York City (NYC) building code (2014) section 1808.2.4-2014 recommends that the soil immediately below the pile cap should not be considered carrying any vertical load. In the current study, free pile-cap-soil contact was assured and only 4-pile group was considered such that both piles settlement and load transfer is uniform (Figure 6.6f).

6.6 Test Results and Analysis

6.6.1 General behavior

The P-δ results of 10 single model pile tests and 30-model pile group tests with different WT levels (i.e. 0, 300, 400, 550, and 850mm) are presented in Figures (6.10, 6.11, 6.12 and 6.13). The test results summarized in these figures demonstrate that the total carrying capacity of the single model piles and pile groups increases with an increase in the WT depth. The carrying capacity increased by 2 to 2.5 times for the case of WT level at 850mm in comparison to saturated condition (i.e. WT at the surface). In addition, using LC1 and LC2 at the tips of two opposite piles on the same diagonal allows instantaneous evaluation of the load application process. In addition, this information is also helpful in understanding loading eccentricity, if any. Figures (6.11, 6.12 and 6.13) show close to identical P-δ curves from LC1 and LC2 for all the tests.

The P_{ult} for the single model pile tests were determined using two methods. The first one is the OLC method by Davisson (1973), which is widely used in North America and is recommended by CFEM (2006). In addition, since scaled model was used in the present study, the P_{ult} was also determined following Oh and Vanapalli (2018) suggestions to determine the ultimate load capacity of a model footing. This method suggests that the P_{ult} corresponds to the intersection of two tangential lines to the initial and final segments of the P-δ curve. This approach is similar to Butler and Hoy (1977) method but it is more suitable for model pile foundations. Both criteria resulted in similar results and the variation of P_{ult} of single model pile vs. ($u_a - u_w$) are presented in Figure (6.14c and d).

Different approaches are available in the literature to define $P_{ult.G}$ from pile group P-δ results. Vesić (1963, and 1969) defined the ultimate load of pile and pile group in sand as the load corresponding to maximum displacement rate (i.e. the point after which the load varies with the settlement at a constant rate). Lee and Chang (2005) used two reference settlement values (0.5mm and 3mm) instead of using $P_{ult.G}$ to compare the single pile and pile group capacities. Sales et al. (2017) defined the ultimate load of single pile and pile group as the load corresponding to a settlement equals 10% of pile diameter. Taylor et al. (2013) conducted centrifuge model pile group test with different pile combination and arrangement in clayey soil. They derived the $P_{ult.G}$, by dividing the P-δ behavior of pile group by the number of piles in the group. In addition, they determined the P_{ult} and $P_{ult.G}$ based on settlement that equals 20% of model pile diameter.

In the current study, the P-δ test results of the pile groups were divided by the number of piles in the group (i.e. 4) following Taylor et al. (2013) approach. The P-δ curves determined using this procedure along with the corresponding P-δ curves for single pile for the same WT are summarized in Figure (6.15). However, using a settlement corresponding to 20% of D to define $P_{ult.G}$ was found to be too high and was not followed in the present study. Instead, the $P_{ult.G}$ was defined using the Davisson (1973) method. The Davisson (1973) method facilitated in evaluating the ultimate capacity for single pile and pile group within a settlement of 10% of D beyond which the load increases with the settlement at a constant rate for most of the tests.

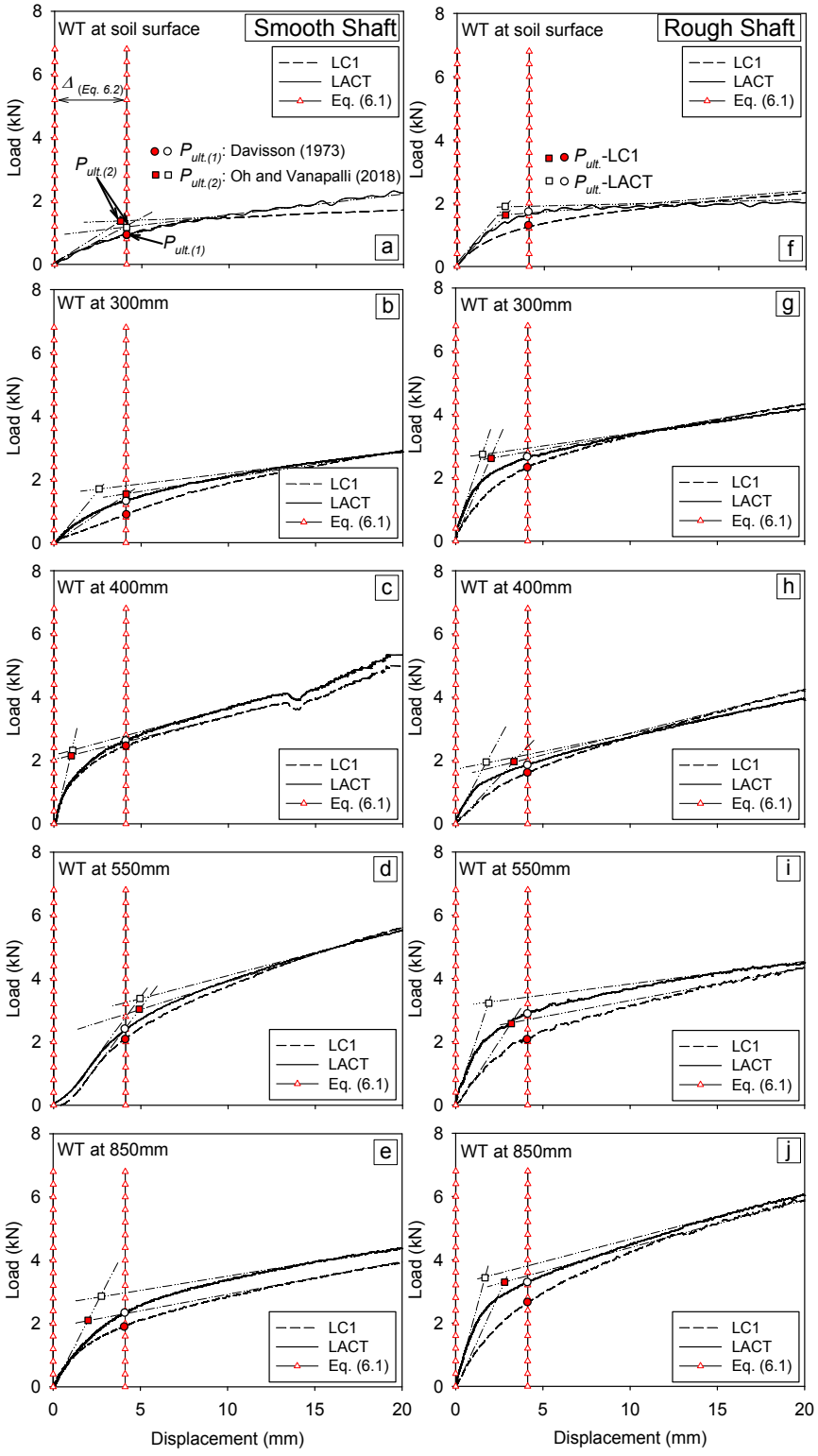

Figure 6.10 The $P-\delta$ relationship of smooth and rough surface single model pile tests with different water table levels.

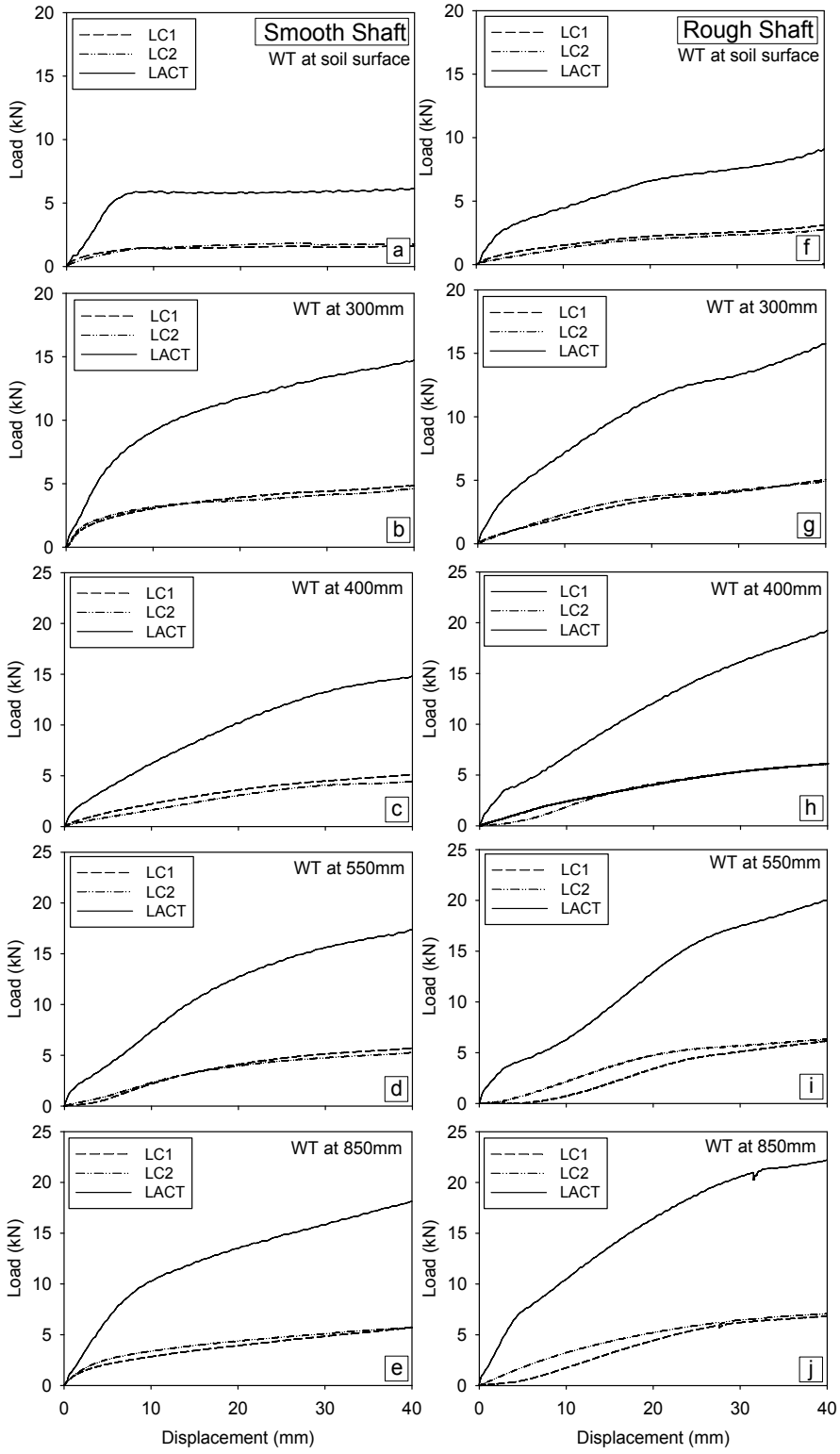

Figure 6.11 The $P-\delta$ relationship of smooth and rough surface model pile group with 3*D* spacing centre-to-centre tests with different water table levels.

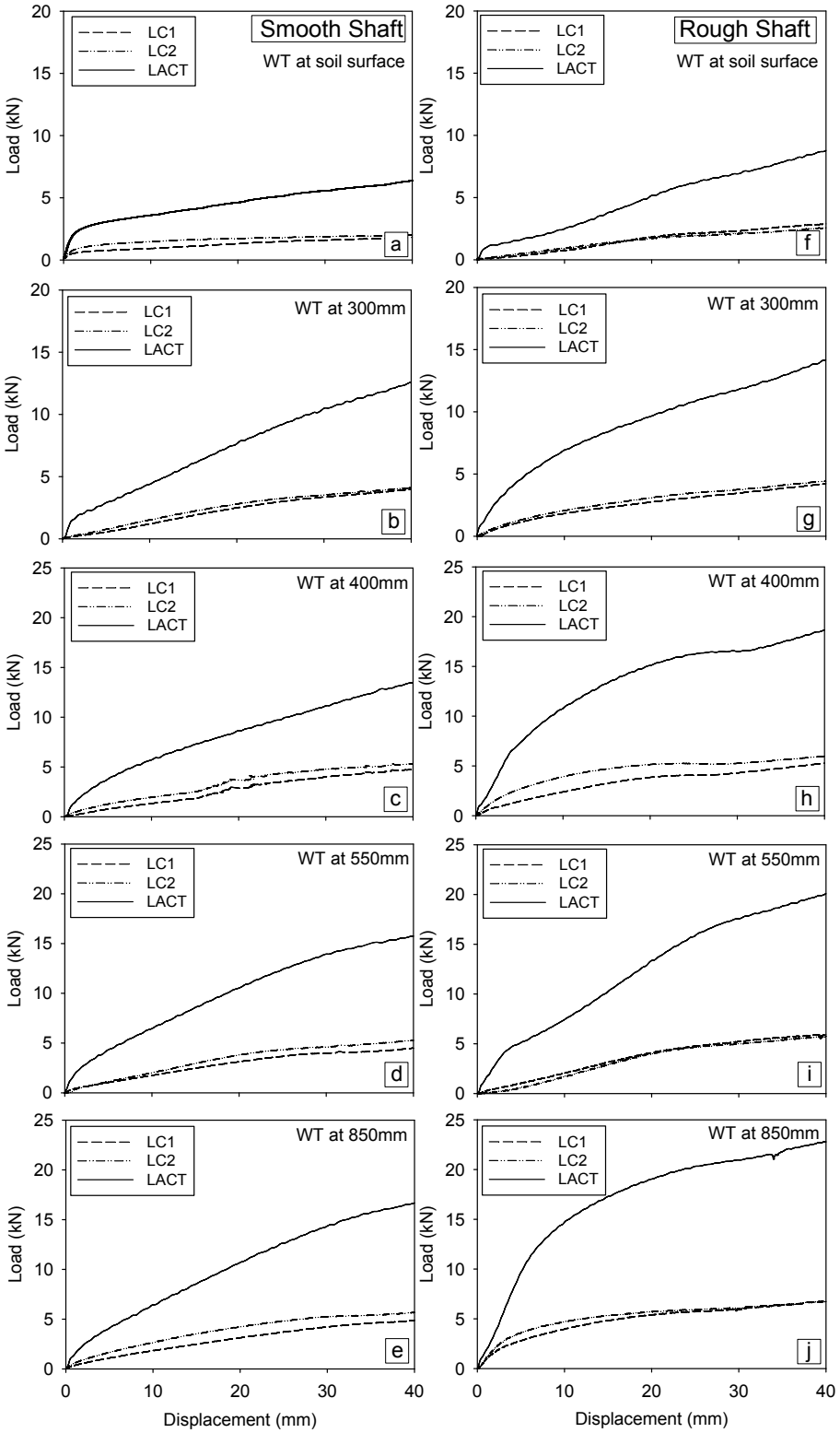

Figure 6.12 The $P-\delta$ relationship of smooth and rough surface model pile group with 4*D* spacing centre-to-centre tests with different water table levels.

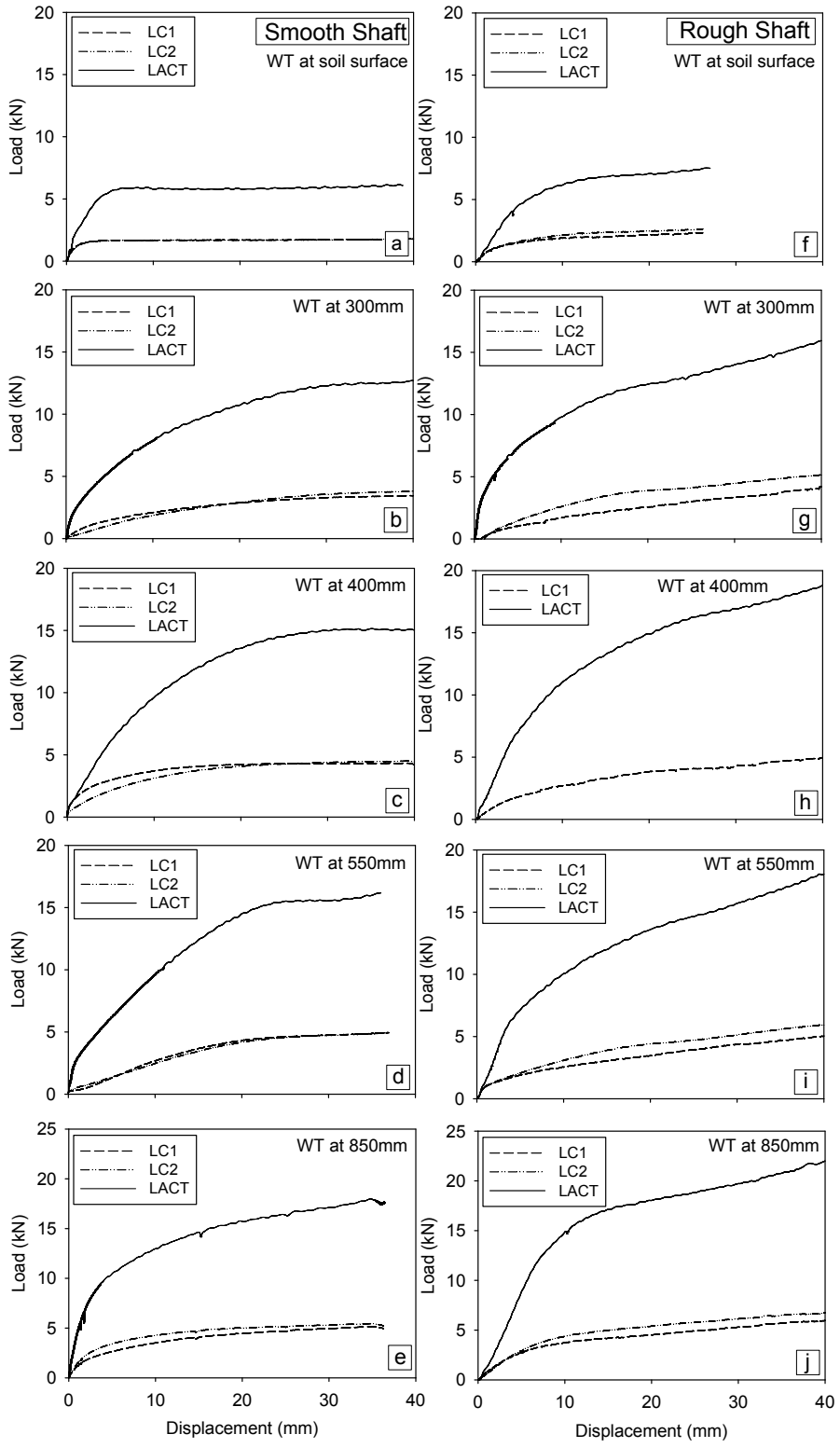

Figure 6.13 The $P-\delta$ relationship of smooth and rough surface model pile group with 5*D* spacing centre-to-centre tests with different water table levels.

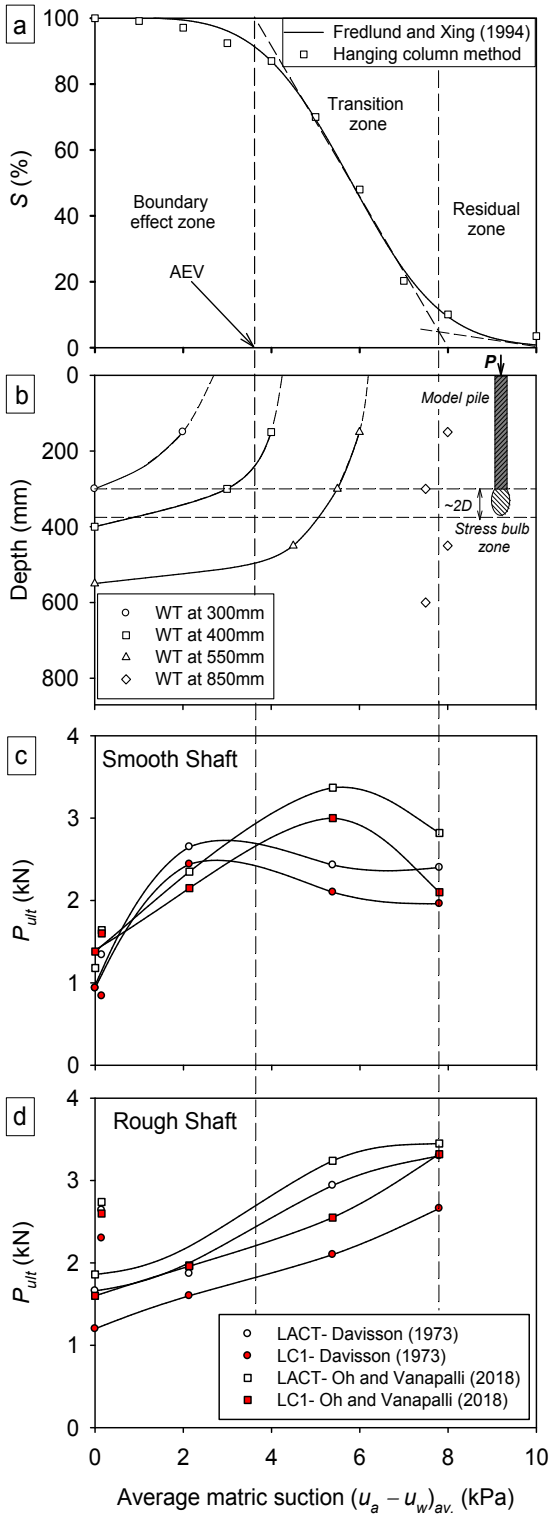

Figure 6.14 (a) SWCC, (b) soil-matric suction profiles for different water table levels, (c) P_{ult} of smooth surface single model pile vs. $(u_a - u_w)_{av.}$, and (d) P_{ult} of rough surface single model pile vs. $(u_a - u_w)_{av.}$.

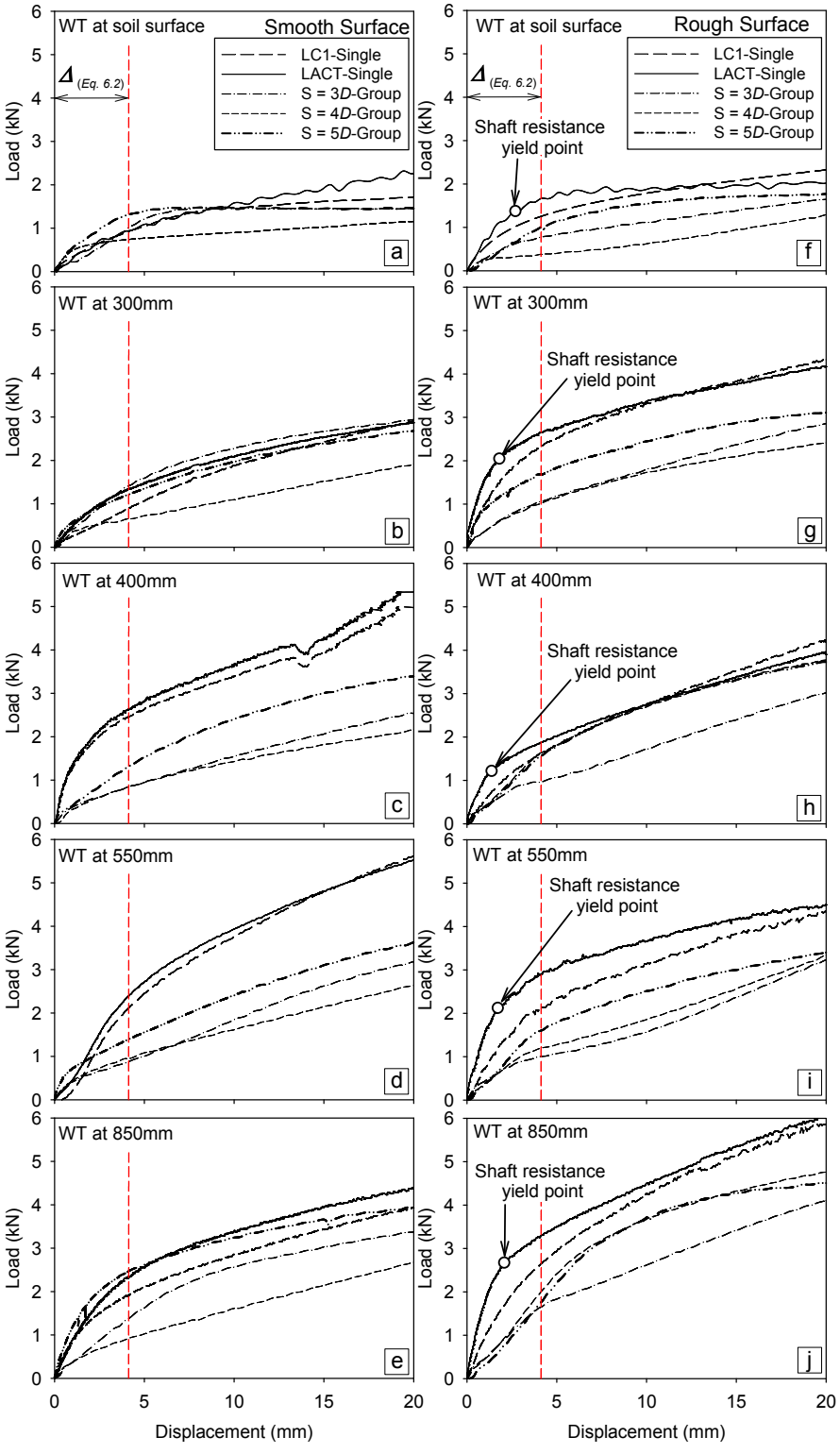

Figure 6.15 Group effect on pile group $P-\delta$ behavior for smooth and rough surface model piles with different centre-to-centre spacing at different water table levels.

6.6.2 Matric suction effect

Figure (6.14a and b) summarizes soil-matric suction profile for different WT levels and the relationship between the soil-matric suction profile and the SWCC. Lowering the WT level results in the development of capillary stresses or matric suction ($u_a - u_w$) in the vadose zone (i.e. above the WT). The ($u_a - u_w$) is a stress state variable that is transferred in the liquid phase and acts on the soil-water-air interphase. The rate of change in ($u_a - u_w$) with respect to different suction zones (i.e. boundary effect, transition and residual zones) is not constant. The soil immediately above the WT is in a saturated state by capillary action (i.e. boundary effect zone). The ($u_a - u_w$) in this zone is representative of hydrostatic condition with relatively higher ($u_a - u_w$) values. As the distance above the water table increases, the soil moves from the boundary effect zone of suction to transition and residual zones and become in unsaturated condition. The rate of change in ($u_a - u_w$) increases as it moves towards soil surface. For WT at 850mm, soil was approaching close to dry condition and ($u_a - u_w$) corresponds to the residual suction.

Matric suction, as discussed earlier, has a significant influence on the mechanical properties (i.e. stiffness and shear strength) of unsaturated soil and interface. The elastic settlement of a foundation constructed in cohesionless soil, in many situations, is governing parameter in the design of the foundation. Lowering the WT depth under the pile and pile group level will develop ($u_a - u_w$) along the shafts and under the piles. The ($u_a - u_w$) applies tension stresses on soil particles and their packets providing resistance to elastic and plastic deformations. The contribution arising from ($u_a - u_w$) is reflected on the P-δ behavior of single model pile that is presented in Figure (6.10). As the WT depth is lowered, the developed ($u_a - u_w$) contributed to increase the E_0 resulting in a steeper slope in the elastic zone of the P-δ behavior. For pile group, however, the stress interaction from adjacent piles is complex that requires considering the influence of group action. More discussions will be provided later in *Group Action* section.

Figure (6.14c and d) present the P_{ult} of single model piles with respect to average matric suction, $(u_a - u_w)_{av}$ in the stress bulb zone using both Davisson (1973) and Oh and Vanapalli (2018) failure criteria. Different trends can be identified for the P_{ult} variation for different zones of matric suction. The P_{ult} increases with $(u_a - u_w)_{av}$ linearly in the boundary effect zone up to the air entry value (AEV) for smooth surface pile, using Oh and Vanapalli's method. Such a behavior is consistent with associated increases in the mechanical properties due to contribution of the (u_a –

u_w) in the boundary effect zone. Vanapalli et al. (1996b) stated that an increase in the ($u_a - u_w$), up to the *AEV*, contributes towards the shear strength same as the net normal stress, ($\sigma - u_a$). Once ($u_a - u_w)_{av}$ exceeds the AEV, the soil starts to desaturate resulting in a reduction in the soil-water-air interphase. As a result, the contribution of ($u_a - u_w$) towards the soil shear strength and stiffness starts decreasing. This behavior is reflected on the variation of P_{ult} with respect to $(u_a - u_w)_{av}$ resulting in positive nonlinear variation followed by negative nonlinear variation as the soil approaches the residual zone of suction. Similar trends were also observed using Davisson's method; however, the maximum P_{ult} determined following this method was found to be less than the Oh and Vanapalli's method for smooth shaft model pile with WT at 550mm. Close examination of Figure (6.10d) can explain the relatively low value estimated for P_{ult} using Davisson's method. The initial segment of P-δ curves exhibit a flatter slope, which may be attributed to seating errors. As a result, Davisson's method could not provide better estimation of the P_{ult} for WT at 550mm. For threaded surface piles, ($u_a - u_w$) and dilation of sand and interface contributed simultaneously to the ultimate carrying capacity. Therefore, the P_{ult} increases almost linearly in the boundary effect zone and nonlinearly in the transition zone.

Figures (6.11, 612, and 6.13) show that pile group capacity also increases as the WT depth increases. However, a consistent increasing trend in the $P_{ult.G}$ with respect to ($u_a - u_w$) could not be developed for several reasons. The average matric suction within the stress bulb for different pile group spacing is not comparable. For pile group with s = 3D, the stress interaction from adjacent piles will results in developing large stress bulb for the pile group. As pile spacing increases (i.e. for s = 4D and 5D), the stress interaction effect reduces and group action due to this reason is less pronounced. Therefore, individual stress bulbs under piles of the group can be expected to fully develop which means $(u_a - u_w)_{av}$ will vary with the spacing. More discussion with respect to group action is summarized in a later section.

6.6.3 End bearing vs. Shaft resistance

The P-δ behavior of the model pile and pile group was measured using multiple load cells. The major load cell, which is a part of the actuator (LACT), was used to measure the total applied load on the pile or the pile group. The extra load cells, LC1 for single model pile and LC1 and LC2 for pile group, at the pile tips were used to measure the transferred load from the pile tip to the bearing soil. For single model pile (Figure 6.10), the contribution of shaft resistance for smooth shaft was

less pronounced in comparison to threaded surface. The P-δ curves for smooth surface has almost the same initial trend. However, as loading process proceeds, there is a diversion between the two curves, which merge later. This behavior can be explained using the direct shear test results for smooth interface surface. The shear resistance of the smooth shaft developed during shearing of the pile surface is similar to the direct shear tests results of smooth interface due to continuous dilation.

For the threaded shaft, the shaft resistance emerged immediately after load application due to sand interlocking with shaft threading. The shaft roughness contributed to dilation along the shaft interface that contributed to strain hardening behavior. The sand in the interface zone around the shaft experiences volumetric expansion in the radial direction upon shearing resulting in higher shaft resistance. The shaft resistance keeps increasing as long as volumetric strains are taking place. Such behavior was elaborately explained by Jewell and Wroth (1987), Jewell (1989), and Lings and Dietz (2004). At early stage of shearing, the soil particles start filling the voids and shear stress increases linearly. When all the voids are filled and when room for particles movement is reduced, strain-hardening take places and soil particles override each other at contact points resulting in volumetric expansion with unrecoverable strains. At this stage, the dilation rate is maximum and contributes to maximum shear stress along shaft-soil interface. The shaft resistance reaches its maximum resistance that is shown on Figure (6.15) as yield shaft resistance and the P-δ curve changes its trend beyond this point. For pile group, it was difficult to separate the contribution of shaft resistance from end bearing due to group action.

Several researchers investigated dilation behavior of unsaturated interface (Hamid and Miller 2008, Hamid and Miller 2009, Hossain and Yin 2014, and Borana et al. 2016). Hamid and Miller (2008 and 2009) investigated the behavior of smooth and rough unsaturated soil-steel interface. They stated that maximum or peak shear stress of rough interface increases with suction under constant ($\sigma - u_a$). In addition, tendency for the dilation increases with an increase in ($u_a - u_w$); however, it decreases with an increase in ($\sigma - u_a$). In the post-peak zone, ($u_a - u_w$) has limited contribution to ultimate shear stress. Smooth interface exhibits similar behavior as the rough interface; however, dilation tendency is less pronounced. Similar conclusions were reported by Hossain and Yin (2014), who investigated the dilation effects on a completely decomposed unsaturated granite soil-cement grout interface using a specially designed direct shear device. They

concluded that unsaturated interface exhibits strain-hardening behavior in the pre-peak zone due to the contribution arising from dilation effect. The dilation of unsaturated interface increases with $(u_a - u_w)$ at lower $(\sigma - u_a)$ and decreases significantly at higher $(\sigma - u_a)$.

In the current study, shaft resistance contributed to the P-δ behavior of the pile and pile group as discussed earlier. Figures (6.10 and 6.15) show that the shaft resistance for single model pile increases with matric suction. Such behavior can also be observed in Figure (6.14) which relates the P_{ult} from LACT and LC1 to $(u_a - u_w)_{av.}$. As $(u_a - u_w)_{av}$ increases, the corresponding P_{ult} from both load cells increases. However, slight deviation arises as $(u_a - u_w)_{av}$ develops. The deviation increases as the soil moves from boundary effect zone to transition and residual zones of suction. This behavior is consistent with previous studies findings where $(u_a - u_w)$ contributes to increase apparent adhesion and dilatancy behavior of the unsaturated interface along the pile shaft.

Nevertheless, in cohesionless soils, end bearing capacity forms the major component of P_{ult}. Potts and Zdravković (2001) stated that ultimate shaft capacity is typically mobilized at settlement corresponding to 10% of pile diameter, while ultimate end bearing is reached at much higher settlement. Moreover, Vanapalli et al. (2018) stated that skin friction of a pile foundation in coarse-grained soils constitutes only 5% of the total carrying capacity. In the current study, the maximum contribution of shaft resistance to total pile capacity reached at small settlement (2-3mm). As shearing process continued, shaft contribution diminishes and the P-δ curves from LACT and LC1 are approximately the same at higher settlements. Further loading of the model piles showed that the end bearing keeps increasing with settlement and exceeds P_{ult} (LC1 in Figure 6.10). In addition, the end bearing resistance increases with $(u_a - u_w)$ following the same trends that were discussed earlier which attributes $(u_a - u_w)$ in the bearing layer contribution towards both the stiffness and shear strength of the soil.

6.6.4 Group action

Closely spaced pile group develops bulb-shaped heavily stressed zone that extends several times deeper in the bearing stratum than the stress bulb associated with a single pile. This behavior is called group action and is attributed to the non-uniform stress interaction from adjacent piles resulting in developing lower pile group capacity in comparison to the sum of individual pile

capacities in the group. Driving or jacking piles in cohesionless soils will disturb the surrounding soil compaction and increase density in the surrounding soil (Prakash and Sharma 1990). Vesić (1969) concluded that there is no group effect on ultimate end bearing capacity of jacked pile group in dry and submerged sandy soil. However, ultimate shaft capacity for jacked piles increases significantly when placed in a group. These observations were made by extending the principles of saturated soil mechanics where pile group capacity was evaluated based on a single pile capacity under saturated or fully dry condition. On the contrary, drilled or bored piles construction causes some loosening of the surrounding soil. As noted before, for driven pile groups, group efficiency, E_g can be greater than unity (Kézdi 1957, Bowles 1996, Dia et al. 2012) while for drilled or bored pile group it can be as low as 0.67 (Meyerhof 1976).

For model pile group, such guidelines with respect to E_g likely have some limitations associated with size effects. For instance, model pile group installation is not similar to the other procedures that were discussed (i.e. Jacked, driven, or bored piles). The sand was manually compacted between the model piles in the groups. However, uniform compaction between the model piles was challenging due to limited space and attached instrumentations (LC1 and LC2). Due to this reason, there may be some loose pockets of sand between the piles. In addition, the overburden stress level along the shafts and at the tips of the model piles is low in comparison to a typical in-situ full-scale test. Due to these reasons, there may be less confining stress within the stress bulb zone, which may contribute to different values for E_g other than the suggested ones.

Figure (6.15) presents the P-δ tests results of model pile groups for different WT levels against the corresponding P-δ test results of individual piles. The figure highlights that group action results in lower carrying capacity of pile group in comparison to the summation of individual piles capacities in the group. Figure (6.16) is used for evaluation of the group action of pile group under saturated and unsaturated conditions. Figure (6.16a) presents an illustrative drawing of pile and pile group that are embedded in cohesionless soil showing the stress bulbs for both cases. A single pile develops a stress bulb that typically extends between 1.5-2D. For pile group, however, the stress bulb extends several times deeper than of an individual pile. For the case when the WT is at the soil surface, the soil is considered saturated and $(u_a - u_w)$ is zero. As the WT depth increases, the $(u_a - u_w)$ starts to contribute to the shaft resistance yet has no effect on the end bearing. Up to this stage, there is no significant difference in the stress state variables

in the bearing layer between the single pile and pile group. Once the WT depth exceeds the pile and pile group depths, there will be some changes in the stress state variables in the bearing layer due to ($u_a - u_w$) contribution. The ($u_a - u_w$) will contribute to increase both shear strength and stiffness of the bearing layer and thus will increase the bearing resistance.

However, this contribution is not consistent for both foundations since it is subjected to group action effect. For the case shown in Figure (6.16a), the WT is at a depth greater than the stress bulb of a single pile, yet it interacts with the stress bulb of the pile group. Three zones with different moisture regime conditions are likely within the pile group stress bulb: i) soil in Zone A is fully saturated and ($u_a - u_w$) is zero; ii) soil in Zone B is saturated by capillary action, and ($u_a - u_w$) has a value; and iii) soil in Zone C is unsaturated and the degree of saturation decreases as it moved towards soil surface. The moisture regime is sensitive to changes in the stress state, which will result in developing excess *PWP*, and/or void ratio (i.e. pore size). For cohesionless soil, it is unlikely to develop excess *PWP* upon changing the stress level. However, extending the capillary theory, the size of pore is inversely related to capillary stress (for example, Fredlund and Rahardjo 1993, Jaafar and Likos 2013). Therefore, only a change in void ratio will result in significant change in the moisture regime.

Figure (6.16b) illustrates moisture regime in the stress bulb. In Zone A, the *PWP* will not change within this zone and there will be no change in the stress state. In Zone B, the soil is in the boundary effect zone where it is saturated with capillary water and has ($u_a - u_w$) that equals or less than *AEV*. The reduction in void ratio will contribute to an increase in capillary stresses that will change boundary line between Zone B and C pushing the capillary zone to higher level. Zone C, which is in unsaturated state with decreasing moisture content with distance from WT (i.e. moving from transition to residual zone of suction), will suffer from similar changes in void ratio as in Zone B. However, moisture regime change variation is nonlinear with depth following the dashed line in Figure (16.6b). Such changes will affect both the shear strength and stiffness of the soil and the bearing capacity of the pile group. The nonlinear variation in -*PWP* within this zone can be derived utilizing the SWCC. This objective is beyond the scope of the present research program. After this zone, the -*PWP* will return to its original path.

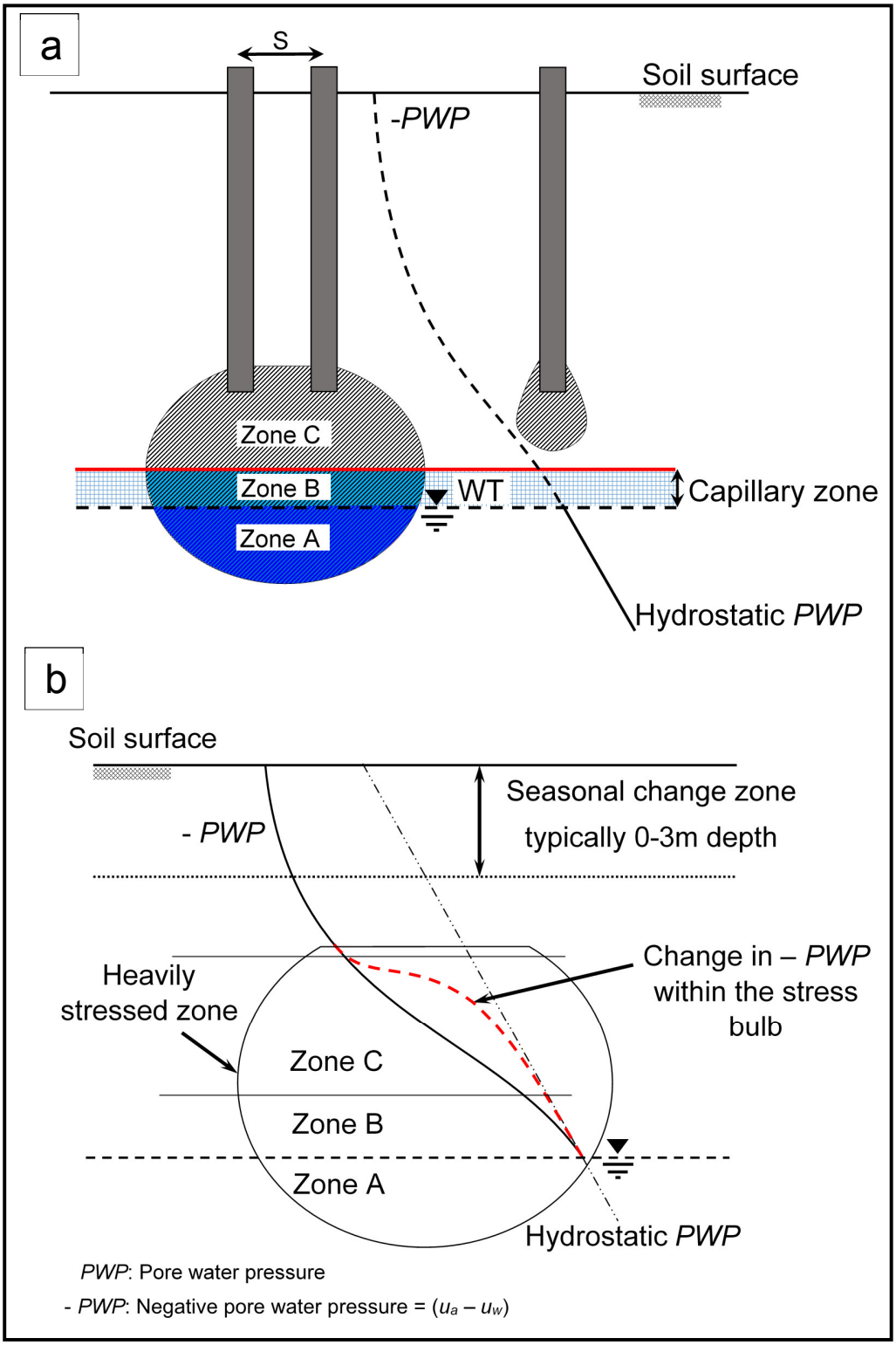

Figure 6.16 Postulated pile group action for unsaturated cohesionless soil and soil moisture regime change within the pile group stress zone.

In the present study, to evaluate the E_g, the $P_{ult.G}$ for different centre-to-centre spacing and different surfaces were normalized and plotted against respective WT levels (Figure 6.17). The $P_{ult.G}$ was divided by the P_{ult} to normalize the results. Four lines are shown in Figure (6.17) that represent the variation of normalized $P_{ult.G}$ with respect to: i) the continuous lines, Line A and C represent the normalized $P_{ult.G}$ with respect to corresponding P_{ult} for the same WT level for smooth and threaded shafts, respectively; and ii) the dashed lines, Line B and D represent the normalized $P_{ult.G}$ with respect to P_{ult} for the WT at the surface (i.e. saturated) for smooth and threaded shafts, respectively. Line A and C show scattered, inconsistent, low E_g for different spacing. The reason for such a behavior can be attributed to the contribution of matric suction towards single pile capacity, which is much more pronounced in comparison to pile group. Group action changes the moisture regime in the stress bulb under the pile group resulting in lower pile group capacity than what it should be. In other words, estimating pile group capacity with $E_g = 1$ for jacked or driven piles or $E_g = 0.67$ for drilled or bored piles using load test results of a single pile in unsaturated sand is not necessarily adequate. On the other hand, Line B and D were more consistent where E_g increases as the pile spacing increases. Moreover, as the WT depth increases, E_g also increases.

The above evidence highlights the need for careful evaluation or estimation of pile group capacity in cohesionless soil based on a load test of a single pile. The presence of GWT at a depth lower than the pile tip level may result in misleading estimation of pile group capacity. The change in the stress states associated with the variation moisture regime within the stress bulb should be taken into account while designing or evaluating the performance of pile group in unsaturated cohesionless soil.

6.7 Conclusions

The axial P-δ behavior of a model single pile and pile group was investigated extending the principles of saturated and unsaturated soil mechanics. Forty model pile and 2×2 pile group with three different centre-to-centre spacing (i.e., 3D, 4D, and 5D) tests were conducted in saturated and unsaturated sand. The tests were performed by varying WT levels. The WT table was placed at the soil surface to achieve saturated condition. The WT was varied i.e. WT at 300, 400, 550, and 850mm) to achieve unsaturated conditions. Different WT levels contributed to different soil-matric suction profile that allowed to evaluate the influence of $(u_a - u_w)$ on the model pile and pile

group behavior. Two sets of model piles that were fabricated with smooth and rough surfaces with two extra load cells (LC1 and LC2) were used to evaluate the combined influence of the shaft roughness and $(u_a - u_w)$ on the behavior of pile and pile group. Group action for unsaturated condition was also evaluated considering the mutual effect of group action and $(u_a - u_w)$ towards the pile group behavior in unsaturated soil. Following are the key conclusions of this study:

1. The total carrying capacity of the model pile and pile group under unsaturated condition increased by 2 to 2.5 times in comparison to saturated condition (i.e. WT at soil surface) due to the contribution of $(u_a - u_w)$ towards shear strength and stiffness of unsaturated soil and interface. The P_{ult} increases linearly with $(u_a - u_w)_{av}$ in boundary effect zone of suction up to the *AEV*. In the transition zone, a positive nonlinear variation was observed followed by reduction in P_{ult} in the residual suction zone.
2. The shaft resistance in single piles develops at relatively small values of settlement and influences the P-δ behavior. The shaft roughness has significant effect on shaft resistance. Smooth shaft has less pronounced influence on the behavior of a single pile in comparison to threaded shaft. The shaft roughness is responsible for remarkable dilation that contributes to develop strain-hardening behavior within 2-3mm settlement before strain softening for all the tests. As WT level lowered, sand dilatancy increases with $(u_a - u_w)$ resulting in steeper P-δ trends and contributes to a higher P_{ult}.
3. The stress state in the unsaturated stress bulb zone changes due to pile group action and contributes to variation in pore structure, which influences the moisture regime within this zone. This is equivalent to saying that there will be void ratio reduction due to increase in the stress within this zone that will tend the unsaturated soil towards a saturation condition and extend the capillary zone to a higher level above the WT. This will affect both the shear strength and stiffness of the bearing layer; due to this reason, the bearing capacity of the pile group also will be significantly influenced.
4. Pile group foundations develop a heavily stressed zone under the group that extends several times deeper in comparison to single piles. When the GWT is below a single pile, it develops well-defined failure pattern and the impact of $(u_a - u_w)$ towards the pile mechanical behavior is well established. However, for a group of piles, a GWT with the same depth may interfere with

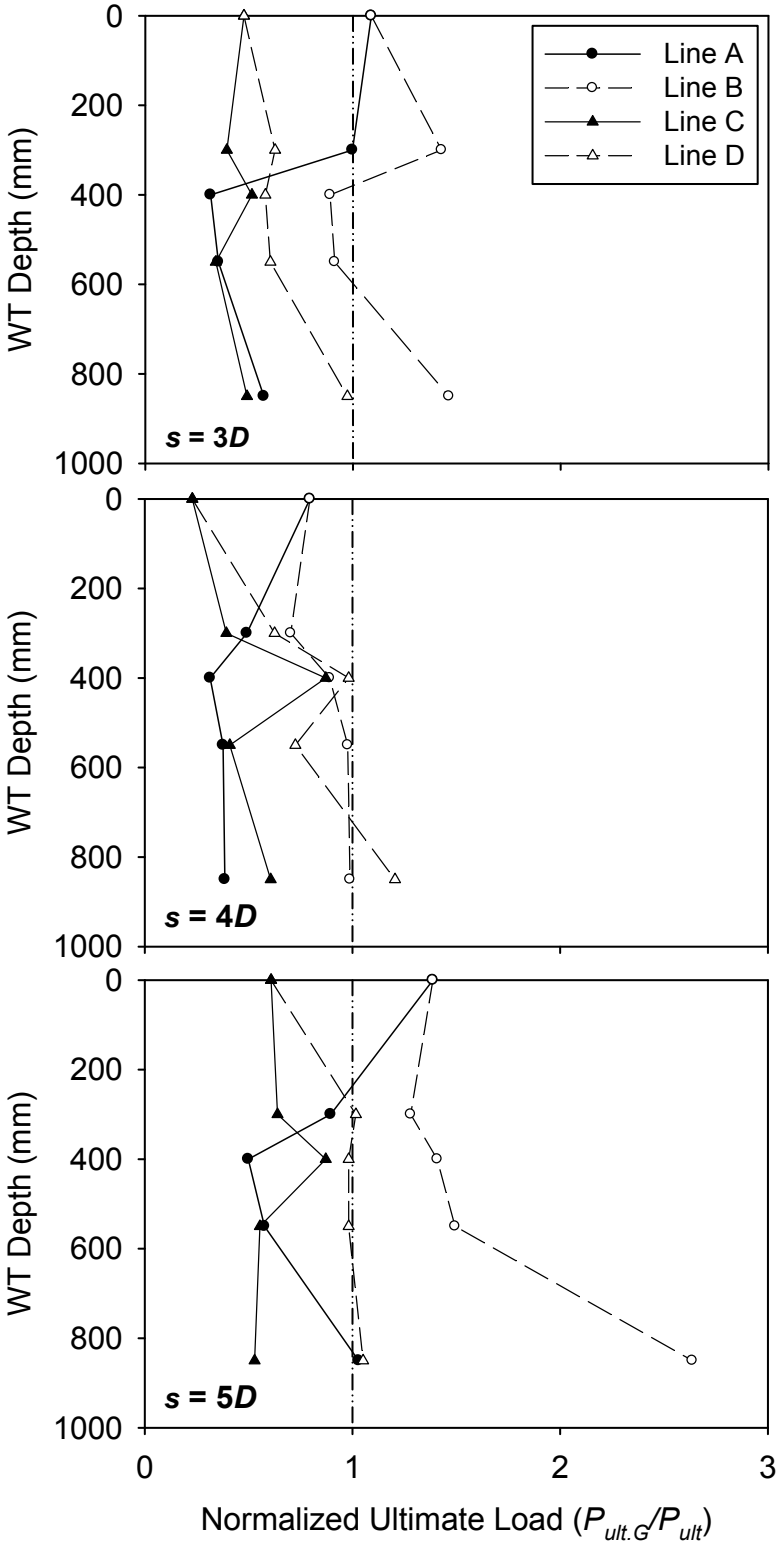

Figure 6.17 Variation of normalized ultimate load of pile group based on a single pile capacity with respect to water table level.

the stress bulb. Stress overlap will produce volume changes and influence the moisture regime within the stress bulb under the pile group resulting in lower pile group capacity than what it should be. Therefore, for a GWT below the pile and pile group, interpretation of load test results of a single pile constructed in unsaturated cohesionless soil to estimate the $P_{ult.G}$ under the same conditions can be misleading. The resultant E_g for such a procedure is scattered, inconsistent, and relatively low, and does not agree with available recommendations.

The present study demonstrated that the behavior of both single pile and pile group foundations constructed in unsaturated cohesionless soil significantly improved due to matric suction contribution towards shear strength and stiffness of the soil and interface. However, the study highlights the need for more rigorous evaluation of pile group capacity under unsaturated condition using the results derived from single PLTs under the same condition. Group action plays major role in changing the moisture regime under the pile group leading to incompatible stress state condition in comparison to single pile behavior and contributes to erroneous results in the estimation of the pile group capacity.

CHAPTER SEVEN

SUMMARY AND CONCLUSIONS

7.1 Summary

This research study aims at developing simple yet reliable experimental, analytical and numerical design procedures for pile and pile group foundations and pipeline systems that utilize the principles of saturated and unsaturated soil mechanics. With this objective, a comprehensive experimental program that includes performing forty model pile and pile group load tests with three different centre-to-centre spacing (i.e., 3D, 4D, and 5D) and six prototype pipe axial load tests along with building a test setup capable of simulating different saturated and unsaturated soil conditions was designed. The study extended a systematic procedure for achieving reliable soil-matric suction profiles for coarse-grained soils that was developed based on the hanging column technique. The resulting soil-matric suction profiles showed consistent profiles with good repeatability. The load test results of the forty model single pile and pile group and the six prototype pipe tests suggest that the ultimate carrying capacity of the model pile and pile group and the peak and ultimate pull-out force increase significantly following nonlinear trend with matric suction under unsaturated condition.

In addition, the study proposed two analytical models to predict the nonlinear variation of pull-out force on pipeline systems with respect to matric suction taking into account overburden pressure and dilation behavior of coarse-grained soil. The proposed models were verified using the result of the prototype pipe tests and found to provide a good agreement with the nonlinear measured behavior and smoothly transit from unsaturated to saturated condition for both peak and ultimate conditions.

Moreover, a numerical methodology that utilizes the most popular Mohr-Coulomb (MC) constitutive model, which is available in different commercial software, for example, PLAXIS 2D and GeoStudio, to simulate the behavior of the two structures in saturated and unsaturated soils.

The methodology requires limited number of saturated soil shear strength and stiffness parameters and SWCC as a tool to predict the most demanding unsaturated soil parameters. The results of elastic axial load test of the prototype pipe from this study and the load settlement behavior of single model piles in coarse-grained soil that are available in literature were used to validate the proposed numerical methodology. The numerical modelling methodology was further extended to investigate the behavior of rigid and flexible pipeline systems buried in Indian Head till (IHT) soil in the proximity of unsupported excavation under saturated and unsaturated condition. The results of the analysis showed that excavation can be extended to several meters under unsaturated condition without the need for supporting system.

The proposed experimental program, analytical design procedure and numerical methodology are applicable in real practice and are promising to implement in design codes, guidelines and foundation design manuals.

7.2 Major Conclusions

Most of the available design codes and guidelines are developed based on conventional saturated soil mechanics focused for proposing conservative design procedures. However, it is well known that many of the geotechnical infrastructure never fully saturated conditions. For this reason, it is important to take into account of the influence of suction in the rational design of geotechnical infrastructure. This is particularly true for arid and semi-arid regions where the soils are in a state of unsaturated condition as there is evaporation in comparison to precipitation in these regions. For this reason, our present understanding of unsaturated soil mechanics can be used as a tool for interpreting the hydro-mechanical behavior of different geotechnical infrastructure. This understanding can be used in conventional practice and in the design codes, guidelines, and manuals.

Some of the experimental methodologies used in the literature for testing geotechnical infrastructure in unsaturated soils have some limitations. For example, spraying water from the top of the soil or compacting the soil at a moisture content corresponding to the required suction may not yield suction profiles that are representative of in-situ conditions. In the current study proposed a standardized, systematic experimental procedure is suggested to achieve soil-suction profile for

different zones of unsaturation (i.e. boundary, transition and residual zones) in coarse-grained soil, which can be used to investigate variety of soil-structure interaction problems.

The pile foundation and pipeline system behavior have several similarities based on their soil-structure interactions. However, their mechanical behaviors with respect to serviceability requirements are not similar. Higher shear strength soil stiffness contributes to an increase in the ultimate pile foundation carrying capacity and reduces the settlement, which is a favorable scenario in engineering practice applications. However, on the other hand, pipeline systems can be subjected to severe damages due to relative movement of unsaturated soil mass that can contribute to a stress that is several folds higher in saturated soil mass movement on pipelines. Neglecting the influence of moisture content or capillary stresses may result in unreasonable or unsafe design for pile and pipeline systems, respectively.

7.2.1 Pile Foundation

The behavior of both single pile and pile group foundations constructed in unsaturated cohesionless soils significantly improved due to matric suction contribution towards shear strength and stiffness of the soil and interface. The total carrying capacity of the model pile and pile group under unsaturated condition increased by 2 to 2.5 times in comparison to saturated condition due to the contribution of matric suction towards the shear strength and stiffness of the unsaturated soil and interface. The ultimate carrying capacity of single piles (P_{ult}) increases linearly with average matric suction ($(u_a - u_w)_{av.}$) in the boundary effect zone of suction up to the *AEV*. In the transition zone, a positive nonlinear variation was observed followed by reduction in P_{ult} in the residual suction zone.

The soil and interface dilation along with shaft roughness contribute significantly to the $P - \delta$ behavior of single piles. The rough shaft pile exhibits remarkable dilation behavior that contributes to strain-hardening behavior within 2-3mm settlement followed by strain-softening. Increasing the matric suction along the pile shaft contributes to increase the dilation behavior of the interface resulting in steeper $P - \delta$ trends and contributes to a higher P_{ult}. The smooth shaft, however, has less pronounced influence on the behavior of a single pile in comparison to rough shaft.

However, estimating the ultimate pile group capacity ($P_{ult.G}$) needs rigorous evaluation of pile group capacity under unsaturated condition using the results derived from single pile load tests under the same condition. Group action plays a major role in changing the moisture regime under the pile group leading to incompatible stress state condition in comparison to single pile. When the GWT is below a single pile, it develops well-defined failure pattern and the impact of ($u_a - u_w$) towards the pile mechanical behavior is well established. However, for a group of piles, a GWT with the same depth may interfere with the stress bulb. The stress overlap will produce volume changes or reduction in void ratio and influence the moisture regime within the stress bulb under the pile group. The stress state in the unsaturated stress bulb zone changes due to void ratio reduction within this zone. Due to this reason, it is likely in some scenarios; the unsaturated soil may tend towards a saturation condition and extend the capillary zone to a higher level above the GWT resulting in lower pile group capacity. Therefore, for a GWT below the pile and pile group, interpretation of load test results of a single pile constructed in unsaturated cohesionless soil to estimate the $P_{ult.G}$ under the same conditions can be misleading. The resultant E_g for such a procedure is scattered, inconsistent, and relatively low, and does not agree with available recommendations.

7.2.2 Pipeline System

Buried pipelines in unsaturated soils may experience much higher external and internal forces due to the contribution of matric suction towards soil and interface shear strength and stiffness which may jeopardize the integrity of pipeline system. The results of the prototype pipe pull-out tests showed that peak and ultimate axial force exerted on the prototype under unsaturated condition varies nonlinearly with matric suction and is approximately 2.5 times higher to saturated condition.

Similar to pile foundation, matric suction and dilation of interface have significant influence on the axial load-displacement behavior of buried pipes. The dilatancy contributed to an increase in mobilized axial force both in saturated and unsaturated soil conditions contributes to strain-hardening followed by strain-softening behavior. However, the dilation effect was more pronounced under unsaturated condition up to the residual zone of unsaturation. Beyond this zone, the matric suction has no effect on the dilatancy and both the peak and ultimate unit skin friction have similar variation rate with matric suction.

Two analytical models to estimate the peak and ultimate unit skin friction of pipeline systems were proposed. The proposed analytical models take into account the matric suction contribution towards the transferred axial load on the pipe. The models only require the information of saturated interface shear strength, angle of dilation and SWCC and use only one fitting parameter, η. The predicted skin friction nonlinearity is controlled by η-value. This value has no effect in the boundary zone of unsaturated where the skin friction variation is almost linear. However, the nonlinearity is derived from η in the transition zone and the residual zone of unsaturation in comparison. This can be explained as in the boundary the soil is saturated (i.e. $S \sim 1$) up to the AEV. Once the $(u_a - u_w)$ exceeds the AEV, the predicted skin friction starts varying nonlinearly with $(u_a - u_w)$. The nonlinear variation of skin friction is derived from the SWCC along with the fitting parameter η. In the current study, $\eta = 0.1$ was found to be suitable to provide reasonable predictions of the measured values of ultimate and peak skin friction. The proposed models can be used to predict the maximum axial stresses on the soil-pipeline systems in geotechnical engineering practices since it only required limited input parameters.

7.2.3 Numerical Modelling

Numerical modelling methodology to design and investigate soil-structure interaction problems in saturated and unsaturated sand and IHT was suggested. The methodology suggests a procedure to predict the most demanding nonlinear unsaturated soil properties, E_{unsat} and c variation with respect to matric suction from the saturated soil shear strength and stiffness properties deriving the nonlinearity from SWCC. The proposed methodology can be used with various constitutive models that are available in different commercial FE packages. However, for its simplicity purposes, modelling in the present study is based on parameters (i.e. c', ϕ', μ, ψ and E_{sat}), using the most widely used MC-constitutive model. Such a simple technique would to encourage practitioner engineers to implement the unsaturated soil mechanics into real practice. Despite the limitations of the proposed FEA methodology that are related to soil dilation and volume change behavior associated with soil and interface shearing, reasonable agreement was achieved with measured behavior. The methodology extended three approaches for estimating the soil-suction profile; i) considering constant matric suction value through the soil profile, ii) real measured soil-suction profile using several Tensiometers, and iii) assuming linear variation of matric suction with depth following hydrostatic condition.

The first approach was employed in modeling the $P - \delta$ behavior of single pile foundation in saturated and unsaturated sand and was verified with measured load test results of three model piles that were obtained from literature. Good agreement between the measured and modelled $P - \delta$ behavior has been achieved with coefficient of determination greater than 0.9 using the proposed methodology. The second approach was used to model the elastic axial load-displacement behavior of a buried pipeline and was verified with three pipe pull-out tests from the current study. The numerical analyses showed good agreement with measured behavior. The third approach was utilized to investigate the behavior of rigid and flexible pipeline in the proximity of unsupported excavation. The results of the analysis was employed to generate design charts to estimate the safe unsupported excavation depth considering groundwater table (GWT) level or matric suction and allowable strains as per several design codes.

The present study provides evidence that using the principles of saturated soil mechanics can result in misleading understanding of soil-structure interaction problems when extend to interpret the behavior of structures constructed in unsaturated soils. Sincere efforts are required to revise and re-evaluate the presently used design methods, codes of practice and guidelines to consider different aspects that contribute to soil-structure interaction and the soil-atmosphere interaction. For such an ambitious goal, unified design methods should be proposed taking account both saturated and unsaturated soil mechanics and provide design guidelines for engineering practice applications.

7.3 Recommendations for Future Research

Research studies presented in this thesis were focussed to investigate the axial load-displacement behavior of single pile, pile group foundations and pipeline systems and pipeline system behavior in the proximity of unsupported excavation under saturated and unsaturated condition from experimental and numerical studies. Based on these studies the following recommendations are suggested for future research work:

7.3.1 Pipeline Systems

- Investigate the behavior of instrumented buried pipeline system in unsaturated soil subjected to: i) relative transverse soil movement, and ii) cyclic loading.

- Perform 3D FE analysis for pipeline system extending the same methodology that was discussed in Chapter 5 and compare the results with 2D FE analysis.

7.3.2 Pile Foundations

- Propose a general design model extending the saturated and unsaturated soil mechanics.
- Investigate the pile shaft capacity in unsaturated sandy soil using longer instrumented model pile and perform pile group pull-out tests.
- Perform 3D FE analysis using advanced constitutive model that can capture volume change behavior under shearing.
- Investigate the behavior of short, medium and long pile and pile group under static and cyclic lateral loads in unsaturated sandy soil.
- Perform full-scale instrumented pile and pile group tests under unsaturated soil condition.

REFERENCES

AASHTO. 2002. Standard Specification for Highway Bridges. 17th ed. American Association of State Highway and Transportation Officials, Washington DC.

Achten, W.M.J., Trabucco, A., Maes, W.H., Verchot, L.V., Aerts, R., Mathijs, E., Vantomme, P. Singh, V.P., and Muys, B. 2013. Global greenhouse gas implications of land conversion to biofuel crop cultivation in arid and semi - arid lands – lessons learned from Jatropha. J. of Arid Environ. 89: 135-145. https://doi.org/10.1016/j.jaridenv.2012.06.015.

Adem, H., and Vanapalli, S.K. 2014. Elasticity moduli of expansive soils from dimensional analysis. *Geotechnical Research* 1(2): 60-72. doi: 10.1680/gr.14.00006.

African Development Bank and African Union. 2009. *Oil and Gas in Africa*. Joint study by the African Development Bank and African Union. Oxford University Press Inc., New York, USA.

Agus, S.S., Leong, E.C., and Schanz, T. 2003. Assessment of statistical models for indirect determination of permeability functions from soil-water characteristic curves. *Géotechnique* 53(2): 279-282, http://dx.doi.org/10.1680/geot.2003.53.2.279.

ALA. 2001. Guidelines for the design of buried steel pipe. American Lifelines Alliance (ALA) in partnership with the Federal Emergency Management Agency (FEMA) and American Society for Civil Engineers (ASCE).

ALA. 2005. Seismic guidelines for water pipelines. American Lifelines Alliance (ALA) in partnership with the Federal Emergency Management Agency (FEMA).

Allen, D.E. 1975. Limit states design - a probabilistic study. *Can. J. Civil Eng.* 2(1): 36-49. https://doi.org/10.1139/l75-004.

Al-Khazaali, M., Han, Z. and Vanapalli, S.K. 2016. Modelling the load-settlement behavior of model piles in unsaturated sand and glacial till. *Proc*. Geotech. and Struct. Eng. Cong., ASCE Special Publication: 2075-2087, Phoenix, AZ, 14-17 February 2016. https://doi.org/10.1061/9780784479742.178.

Al-Khazaali, M., and Vanapalli, S.K. 2015. Numerical modelling technique to predict the load versus settlement behavior of single piles in unsaturated coarse-grained soils. *Proc*. 68th Can. Geotech. Conf., Québec, QC, 20-23 September 2015. doi: 10.13140/RG.2.1.3500.0081.

Al-Khazaali, M., Oh, W.T., and Vanapalli, S.K. 2016. Estimation of deformations in soil-pipeline systems nearby unsupported trenches excavated in unsaturated soils. *Proc*. 69th Can. Geotech. Conf., Vancouver, BC, 1-5 October 2016.

Al-Khazaali, M., and Vanapalli, S.K. 2017. Experimental model to investigate the axial force-displacement behavior of a pipeline in unsaturated sandy soil. *Proc*. 70th Can. Geotech. Conf., Ottawa, ON, 1-4 October 2017.

Alonso, E.E., Gens A. and Josa A. 1990. A constitutive model for partially saturated soils. *Géotechnique* 40(3): 405-430. http://dx.doi.org/10.1680/geot.1990.40.3.405.

API 17B. 2002. Recommended practice for flexible pipe. Technical report 3rd ed. American

Petroleum Institute (API).
API 17J. 2008. Specification for unbonded flexible pipe. Technical report 3rd ed. American Petroleum Institute (API).
API 17K. 2002. Specification for bonded flexible pipe. Technical report 1st ed. American Petroleum Institute (API).
ASCE. 1984. Guidelines for the seismic design of oil and gas pipeline systems. Committee on Gas and Liquid Fuel Lifelines, American Society for Civil Engineering (ASCE), New York.
ASME B31.4. 2003. Pipeline transportation systems for liquid hydrocarbons and other liquids. American Society of Mechanical Engineers (ASME).
ASME B31.8, 2003. Gas Transmission and distribution piping system. American Society of Mechanical Engineers (ASME).
ASTM D1143-81. 1994. Standard test method for piles under static axial compressive load. American Society for Testing and Materials (ASTM) International, West Conshohocken, PA, USA.
ASTM D3966-90. 1995. Standard test method for piles under lateral loads. American Society for Testing and Materials (ASTM) International, West Conshohocken, PA, USA.
ASTM D4945-00. 2000. Standard test method for high-strain dynamic testing of piles. American Society for Testing and Materials (ASTM) International, West Conshohocken, PA, USA.
ASTM D6836-02. 2008. Standard test methods for determination of the soil water characteristic curve for desorption using hanging column, pressure extractor, chilled mirror hygrometer, or centrifuge. American Society for Testing and Materials (ASTM) International, West Conshohocken, PA, USA.
ASTM F1668-08. 2008. Standard guide for construction procedures for buried plastic pipe. American Society for Testing and Materials (ASTM) International, West Conshohocken, PA, USA.
Attewell, P.B., and Woodman, J.P. 1982. Predicting the dynamic of ground settlement and its derivatives caused by tunnelling in soil. *Ground Engineering* 15(8): 13-36.
Barkan, D.D. 1962. *Dynamics of bases and foundations*. McGraw-Hill Book Company, Inc. New York.
Benoit, L. 2012. Current and future state of oil and gas pipeline and refining capacity in Canada. Repot of the Standing Committee on the Natural Resources, Parliament of Canada, Ottawa, Ontario, Canada. http://publications.gc.ca/collections/collection_2012/parl/XC49-1-411-02-eng.pdf.
Beredugo, Y.O. 1966. An experimental study of the load distribution in pile groups in sand. *Can. Geotech. J.*, 3(3): 145-166. https://doi.org/10.1139/t66-017.
Bjørnmose, J., Roca, F., Turgot, T., and Hansen, D.S. 2009. An assessment of the gas and oil pipelines in Europe. European Parliament, Brussels.
Bishop, A.W. 1959. The principle of effective stress. Technisk Ukeblad 106(39): 859–863.
Bickel, J.O., Kuesel, T.R., and King, E.H. 2004. *Tunnel Engineering Handbook*. 2nd ed. Kluwer Academic Publishers, Norwell, Massachusetts.

Bond, A.J., Schuppener,B., Scarpelli, G., Orr, T.L.L., Dimova, S., Nikolova, B.,and Pinto, A.V. 2013. *Eurocode 7: Geotechnical Design Worked Examples*. Report: EUR 26227 EN, 2013.

Bolton, M.D. 1986. The Strength and dilatancy of sands. *Géotechnique* 36(1): 65-78.

Bolton, M.D., Gui, M.W., Garnier, J., Corte, J.F., Bagge, G., Laue, J., and Renzi, R. 1999. Centrifuge cone penetration tests in sand. *Géotechnique* 49(4): 543–552.

Boominathan, A. and Ayothiraman, R. 2007. An experimental study on static and dynamic bending behaviour of piles in soft clay. *Geotech. and Geological Eng.*, 25: 177-189.

Boominathan, A. and Lakshmi, T. 2000. Dynamic characteristics of pile groups under vertical viprations. 12th World Conf. on Earthquake Eng., Auckland, New Zealand.

Borana, L., Yin, J-H., Singh, D.N., and Shukla, S.K. 2016. Interface behavior from suction controlled direct shear test on completely decomposed granitic soil and steel surfaces. *Int. J. Geomech.* ASCE, doi: 10.1061/(ASCE)GM.1943-5622.0000658.

Bowles, J. E. 1997. *Foundation analysis and design*. 5th ed., The McGraw-Hill Companies, Inc.

Boussinesq, V.J. 1885. *Application des potentiels à l'étude de l'equilibre et du mouvement des solides élastiques, avec des notes étendues sur divers points de physique mathématique et d'analyse*. GauthierVillars, Paris.

BSI (1997). BS EN 1295-1:1997. Structural design of buried pipelines under various conditions of loading - Part 1: General requirements. BSI, London, UK.

BSI (2003). BS EN 14161:2003. Petroleum and natural gas industries-Pipeline transportation systems. BSI, London, UK.

BSI (2004). BS EN 1997-1:2004. Geotechnical design – part 1: General rules. BSI, London, UK.

Brinch-Hansen, J. 1961. The ultimate resistance of rigid piles against transversal forces. Geoteknisk Institution Bull (12), Copenhagen.

Brinch-Hansen, J. 1963. Discussion: Hyperbolic stress-strain response. Cohesive soils, *Journal of Soil Mechanics and Foundations Division*, ASCE, 89(SM4): 241-242.

Brinkgreve, R.B.J. and Vermeer, P.A. 1997. Plaxis finite element code for soil and rock analysis-Version 7. Balkema, Rotterdam.

Burland, J.B. 1964. Effective stresses in partly saturated soils. Discussion of: Some aspects of effective stress in saturated and partly saturated soils, by Bishop, A.W. and Blight, G.E., *Géotechnique* 14(1): 64-68. https://doi.org/10.1680/geot.1964.14.1.64.

Burland, J.B. 1965. Some aspects of the mechanical behavior of partly saturated soils. Moisture Equilibrium and Moisture Changes in Soils Beneath Covered Areas, Butterworths, Sydney, Australia, pp. 259-269.

Burland, J.B. 1973. Shaft friction of piles in clay-a simple fundamental approach. *Ground Engineering* (6-3): 30-42.

Butler, H.D., and Hoy, H.E. 1976. *User manual for Taxes quick-load method for foundation load testing*. FHWA-IP-77-8, Federal Highway Administration, Office of Development, Washington DC.

Byun, Y.H., Lee, J.S., Cho, S.H. and Yoon, H.K. 2013. Evaluation of Void Ratio and Elastic Modulus of Unsaturated Soil Using Elastic Waves. *Proc*. 18th Int. Conf. on Soil Mech. and

Geotech. Eng., Paris, France: 1089-1092.
Canadian Energy Pipeline Association (CEPA), 2005. The importance of timely construction of new pipeline infrastructure to Canada and Canadians. Available from http://www.cepa.com/wp-content/uploads/2011/06/CEPA-The-Importance-of-New-Pipeline-Infrastructure-to-Canada.pdf. [accessed 09 September 2016].
Canadian Geotechnical Society. 2006. *Canadian Foundation Engineering manual*. Canadian Foundation Engineering Manual.
Chaney, R.C. 1978. Saturation effects on the cyclic strength of sands. *Proc*. ASCE Geotechnical Engineering Division Specialty Conference. Pasadena, California.
Chard, B.M., and Symons, I.F. 1982. Trial trench construction in London clay: A ground movement study at Bracknell. Department of the Environment, Department of Transport, Transport and Road Research Laboratory, report No. LR1O51, Crowthorne, Berkshire.
Chaloulos, Y.K., Bouckovalas, G.D., Zervos, S.D., and Zampas, A.L. 2015. Lateral soil-pipeline interaction in sand backfill: Effect of trench dimensions. *Comp. and Geotech.* 69: 442 – 451. doi: 10.1016/j.compgeo.2015.05.014.
Chillarige, A.V., Morgenstern, N.R., Robertson, P.K., and Christian, H.A. 1997. Seabed instability due to flow liquefaction in the Fraser River delta. *Can. Geotech. J.* 34(4): 520–533, doi: 10.1139/T97-019.
Chin, F.K. 1970. Estimation of ultimate load of piles not carried to failure. *Proc*. 2nd Southeast Asia Conf. on Soil Eng.: 81-90.
Choo, Y.W., Abdoun, T.H., O`Rourke, M.J., and Ha, D. 2007. Remediation for buried pipeline systems under permanent ground deformation. *Soil Dynamics and Earthquake Eng*., 27(12): 1043-1055, http://doi.org/10.1016/j.soildyn.2007.04.002.
Chow, E., Hendrix, L.E., and Herberg, M.E. 2010. Pipeline politics in Asia: the intersection of demand, energy markets, and supply routes. The National Bureau of Asian Research (NBR), Report 23.
Chow, H.S.W. and Poulos, H.G. 2015. The significance of raft flexibility in pile group and piled raft design. *Australian Geomech. J*., 50(4): 113-119.
Chung, S.H., and Yang, S.R. 2014. Loading behaviour of small scale single pile in unsaturated clayey soil. *Materials Research Innovations* 18(S2): 177-181.
Coop, M.R., Sorensen, K.K., Bodas Freitas, T. and Georgoutsos, G. 2004. Particle breakage during shearing of Carbonate Sand. *Géotechnique* 54(3): 157-163.
Costa, Y.D., Cintra, J.C., and Zornberg, J.G. 2003. Influence of matric suction on the results of plate load test performed on a lateritic soil deposit. *Geotech. Test. J.*, ASTM 26(2): 219 – 226.
Coyle, H.M., and Reese, L.C. 1966. Load transfer for axially loaded piles in clay. *J. Soil Mech. and Foundations Div.*, ASCE, 92(2): 1-26.
Coyle, H.M. and Sulaiman, I.H. 1967. Skin friction for steel piles in sand. *J. Soil Mech. and Foundations Div.*, ASCE, 92(SM6): 261-278.
Coyle, H.M. and Sulaiman, I.H. 1970. Bearing capacity of foundation piles: State of the art. *Proc*.

of the 49th Annual Meeting of the Highway Research Board, Washington DC, US.
Crofts, J.E., Menzies, B.K., and Tarzi, A.I. 1977. Lateral displacement of shallow buried pipelines due to adjacent deep trench excavations. *Géotechnique* 27(2): 161-179. doi: 10.1680/geot.1977.27.2.161.
Dia G., Salgado, R., Gong, W., and Zhang, Y. 2012. Load test on full-scale bored pile groups. *Can. Geotech. J*., 49(11):1293-1308. https://doi.org/10.1139/t2012-087.
Davis, E.H. 1968. Theories of plasticity and the failure of soil masses. In Soil mechanics: Selected topics. *Edited by I. K. Lee*, Elsevier, New York, USA: 341–380.
Davisson, M.T. 1973. High capacity piles. *Proc.*, Lecture series, Innovations in Foundation Construction, ASCE, Illinois section.
DeMicco, P. 2015. Changing pipelines, shifting strategies: Gas in south-eastern Europe, and the implications for Ukraine. European Parliament, Brussels.
Desai, C.S., Drumm, E.C., and Zaman, M.M. 1985. Cyclic testing and modeling of interfaces. *J. Geotech. Eng.* 111(6): 793-815.
Dilrukshi, S., and Wijewickreme, D. 2014. Use of discrete element modeling to capture the effect of backfill particle size on the soil restraints of buried pipelines subjected to lateral ground movement. *In* Proceedings of the 10th International Pipelines Conference IPC2014, Calgary, AB, September 29 - October 3, 2014. IPC 2014-33318.
DNV-OS-F101. 2013. Offshore standard: Submarine pipeline systems. Det Norske Veritas (DNV).
DNV-RP-F116, 2009. Recommended practice: Integrity management of submarine pipeline systems. Det Norske Veritas (DNV).
D.S. 415. 1984. Danish Code of Practice for Foundation Engineering, Danish Society of Civil Engineering.
Edil, T.B. 1973. Influence of fabric and soil-water potential on stress-strain response of clay. Ph.D. thesis, Northwestern University, Evanston, IL, USA.
Edil, T.B., Motan, S.E. and Toha, F.X. 1981. Mechanical behaviour and testing methods of unsaturated soils. In R.N. Yong & F.C. Townsend (eds), *Laboratory strength of soil*, ASTM STP 740: 114-129. Philadelphia.
Energy Information Administration (EIA). 2007. Annual energy outlook 2007 with projections to 2030. Energy Information Administration, Office of Integrated Analysis and Forecasting, U.S. Department of Energy Washington, DC.
Fellenius, B.H. 1975. Test loading of piles. Methods, interpretation and new proof testing procedure. *Proc*. ASCE, 101 (GT9): 855-869.
Fellenius, B.H. 1980.The analysis of results from routine pile test loading. *Ground Engineering*, Foundation publications Ltd., London, 13(6): 19-31.
Fredlund, G.D., Bergan, A.T., and Sauer, E.K. 1975. The deformation characteristics of subgrade soils for highways and runways in northern environments. *Can. Geotech. J.* 12(2), 213–223.
Fredlund, D.G., and Morgenstern, N.R. 1977. Stress state variables for unsaturated soils. *J. Geotech. and Geoenviron. Eng.*, ASCE, 103(GT5): 447-466.

Fredlund, D.G., Morgenstern, N.R., and Widger, R.A. 1978. The shear strength of unsaturated soils. *Can. Geotech. J.* 15(3): 313-321, doi: 10.1139/t78-029.

Fredlund, D.G., Rahardjo, H., and Gan, J.K.M. 1987. Non-linearity of strength envelope for unsaturated soils. Proc. 6th Int. Conf. on Expansive Soils, New Delhi, India: 49-54.

Fredlund, D.G., and Xing, A. 1994. Equations for the soil-water characteristic curve. *Can. Geotech. J.* 31(4): 521–532. doi: 10.1139/t94-061.

Fredlund, D.G., Xing, A., Fredlund, M.D. and Barbour, S.L. 1996. The Relationship of the Unsaturated Soil Shear Strength to the Soil-Water Characteristic Curve. *Can. Geotech. J.* 33(3): 440-448. doi: 10.1139/t96-065.

Fullenbaum, R., Fallon, J., and Flanagan, B. 2013. Oil & natural gas transportation & storage infrastructure: Status, trends & economic benefits. IHS Global Inc. and American Petroleum Institute (API), http://www.api.org/~/media/Files/Policy/SOAE-2014/API-Infrastructure-Investment-Study.pdf.

Gaaver, K.E. 2013. Uplift capacity of single piles and pile groups embedded in cohesionless soil. *Alexandria Eng. J.* 52(3): 365-372. https://doi.org/10.1016/j.aej.2013.01.003.

Gallipoli, D., Gens, A., Sharma, R., and Vaunat, J. 2003. An elasto-plastic model for unsaturated soil incorporating the effects of suction and degree of saturation on mechanical behaviour. *Géotechnique* 53(1): 123–135. http://dx.doi.org/10.1680/geot.2003.53.1.123.

Gan, J.K.M. 1986. Direct Shear Strength Testing of Unsaturated Soils. M.Sc. thesis, University of Saskatchewan, Saskatoon, Canada.

Garven, E., and Vanapalli, S.K. 2006. Evaluation of empirical procedures for predicting the shear strength of unsaturated soils. Proc. 4th Int. Conf. on Unsaturated Soils. ASCE Geotechnical Special Publication: 2570–2581. doi: 10.1061/40802(189)219.

Georgiadis, K., Potts, D.M., and Zdravković, L. 2003. The influence of partial soil saturation on pile behaviour. *Géotechnique* 53(1): 11-25. doi: 10.1680/geot.2003.53.1.11.

Gerard, J.N. 2014. The state of American energy: America's energy, America's Choice. American Petroleum Institute (API). Available from http://energytomorrow.org/~/media/Files/Policy/SOAE-2014/API-2014-State-of-American-Energy-Report.pdf. [accessed 12 June 2017].

Griffis, L.G. 1993. Serviceability limit states under wind load. *Engineering Journal*, 30(1), 1–16.

Grigoryev, Y. 2006. Pipelines to remain dominant force despite threat for LNG. *Int.Energy Journal* 7(2): 161–177.

Grozic, J.L., Robertson, P.K., and Morgenstern, N.R. 2000. Cyclic liquefaction of loose gassy sand. *Can. Geotech. J.* 37(4): 843–856. doi: 10.1139/t00-008.

Gui, M.W., and Bolton, M.D. 1998. Geometry and scale effects in CPT and pile design. Geotechnical Site Characterization, Robertson and Mayne (eds): 1063-1068.

Gurpersaud, N., Vanapalli, S.K., and Sivathayalan, S. 2013. Semiempirical method for estimation of pullout capacity of grouted soil nails in saturated and unsaturated soil environments. *J. Geotech. and Geoenviron. Eng.*, ASCE 139(11): 1934 – 1943. doi: 10.1061/(ASCE)GT.1943-5606.0000883.

Haines WB 1930. The hysteresis effect in capillary properties and the modes of moisture distribution associated therewith. *J. Agricultural Science* 20: 96-105.

Hamid, T. B., and Miller, G. A. 2008. A constitutive model for unsaturated soil interfaces. *Int. J. Num. and Anal. Methods in Geomech.* 32(13):1693–1714. doi: 10.1002/nag.692.

Hamid, T.B., and Miller, G.A. 2009. Shear strength of unsaturated soil interfaces. *Can. Geotech. J.* 46(5): 595-606. doi: 10.1139/T09-002.

Han, Z., and Vanapalli, S.K. 2016. Stiffness and shear strength of unsaturated soils in relation to soil-water characteristic curve. *Géotechnique*. doi: 10.1680/jgeot.15.P.104.

Han, Z., Vanapalli, S.K., and Kutlu, Z.N. 2016. Modelling the behavior of a friction pile in compacted glacial till. *Int. J. Geomech.* ASCE. doi: 10.1061/(ASCE)GM.1943-5622.0000659.

Hilf, J.W. 1956. An Investigation of pore-water pressure in compacted cohesive soils. Ph.D. Thesis, Technical memorandum, United States Bureau of Reclamation, Denver, USA.

Holmgren, P. 2006. Global land use area change matrix: input to the fourth environmental outlook (GEO-4). Rome, Food and Agriculture Organization of the United Nations, FAO. http://www.fao.org/docrep/010/ag049e/AG049e00.htm#TopOfPage.

Hopkins, P. 2007. Pipelines: Past, present and future. Proc. 5th Asian Pacific IIW Int. Cong., Sydney, Australia, 7-9 March 2007.

Hossain, M., and Yin, J. 2012. Influence of grouting pressure on the behavior of an unsaturated soil-cement interface. *J. Geotech. and Geoenviron. Eng.* 138(2): 193-202.

Hossain, M., and Yin, J. 2014. Dilatancy and strength of an unsaturated soil-cement interface in direct shear tests. *Int. J. Geomech.* ASCE. doi: 10.1061/(ASCE)GM.1943-5622.0000428, 04014081.

Hsu, J.R.C., Jeng, D.S. and Lee, C.P. 1995. Oscillatory soil response and liquefaction in an unsaturated layered seabed. *Int. J. Num. and Anal. Methods in Geomech.* 19(12): 825–849, doi: 10.1002/nag.1610191202.

IBC. 2006. *International building code*. International Code Council, Inc., USA.

IITK-GSDMA. 2007. Guidelines for seismic design of buried pipelines. Indian Institution of Technology Kanpur- Gujarat State Disaster Management Authority (IITK-GSDMA), National Information Center of Earthquake Engineering, Kanpur, India.

International Energy Agency (IEA). 2008. World energy outlook. International Energy Agency and Organisation for Economic Co-operation and Development (OECD).

Infante Sedano, J.A. 2006. A Modified Ring Shear Test Device for Testing Hydro-Mechanical Behavior of Saturated Soils. Ph.D. thesis, University of Ottawa, Ottawa, Canada.

ISO 13628-2. 2006. Petroleum and natural gas industries - design and operation of subsea production systems -part 2: Unbonded flexible pipe systems for subsea and marine applications. ISO.

ISO 13628-11. 2007. Petroleum and natural gas industries - Design and operation of subsea production systems - Part 11: Flexible pipe systems for subsea and marine applications. ISO.

Janbu, N. 1963. Soil compressibility as determined by oedometer and triaxial tests. Proc. Europ.

Conf. on Soil Mech. and Found. Eng., Wiesbaden, Germany, 1: 19-25.
Jewell, R.A. 1989. Direct shear tests on sand. *Géotechnique* 39(2): 309–322. http://dx.doi.org/10.1680/geot.1989.39.2.309.
Jewell, R.A., and Wroth, C.P. 1987. Direct shear tests on reinforced sand. *Géotechnique* 37(1): 53–68. http://dx.doi.org/10.1680/geot.1987.37.1.53.
Jung J.K., O'Rourke T.D., and Olson, N.A. 2013. Lateral soil-pipe interaction in dry and partially saturated sand. *J. Geotech. and Geoenviron. Eng.*, ASCE 139(12): 2028-2036. doi: 10.1061/(ASCE)GT.1943-5606.0000960.
Kausel, E. 2010. Early history of soil-structure interaction. *Soil Dynamics and Earthquake Eng.*, 30(9): 822–832. https://doi.org/10.1016/j.soildyn.2009.11.001.
Kézdi, Á. 1957. Bearing Capacity of Piles and Pile Groups. *Proc.* 4th. ICSMFE, Budapest, Hungary: 46-51.
Khalili, N., and Khabbaz, M.H. 1998. A unique relationship for χ for the determination of the shear strength of unsaturated soils. *Géotechnique* 48(5): 681-687, http://dx.doi.org/10.1680/geot.1998.48.5.681.
Khari, M., Kassin, K.A., and Adnan, A. 2013. An experimental study on pile spacing effects under lateral loading in sand. The Scientific World Journal, 2013. http://dx.doi.org/10.1155/2013/734292.
Khosravi, A., and McCartney, J. S. 2011. Resonant column test for unsaturated soils with suction-saturation control. *Geotech. Test. J.*, ASTM 34(6): 730–739. https://doi.org/10.1520/GTJ103102.
Kouretzis, G.P., Krabbenhoft, K., Sheng, D., and Sloan, S.W. 2014. Soil-buried pipeline interaction for vertical downwards relative offset. *Can. Geotech. J.* 51: 1087–1094. doi: 10.1139/cgj-2014-0029.
Khoury, C.N., Miller, G.A., and Hatami, K. 2011. Unsaturated soil-geotextile interface behavior. *Geotextiles Geomembranes*, 29(1): 17-28.
Klar, A., and Marshall, A.M. 2015. Linear elastic tunnel pipeline interaction: The existence and consequence of volume loss equality. *Géotechnique* 65(9): 788-792. http://dx.doi.org/10.1680/geot.14.P.173.
Khosravi, A., and McCartney, J. S. 2011. Resonant column test for unsaturated soils with suction-saturation control. *Geotech. Test. J.*, ASTM 34(6): 730–739. https://doi.org/10.1520/GTJ103102.
Lee, S.H. and Chung, C.K. 2005. An experimental study of the interaction of vertically loaded pile groups in sand. *Can. Geotech. J.*, 42(5):1485-1493. https://doi.org/10.1139/t05-068.
Lee, K.M., Rowe, R.K., and Lo, K.Y. 1992. Subsidence owing to tunnelling. I. Estimating the gap parameter. *Can. Geotech. J.* 29(6): 924-940. doi: 10.1139/t92-104.
Leonards, G.A., and Roy, M.B. 1976. Predicting performance of pipe culverts buried in soil. Joint Highway Research project, report No. JHRP-76-15.
Liangtong, Z. 2003. Field and laboratory study of an unsaturated expansive soil associated with rain-induced slope instability. Ph.D. thesis, Department of Civil Engineering, The Hong

Kong University of Science and Technology, Hong Kong.
Lings, M.L., and Dietz, M.S. 2004. An improved direct shear apparatus for sand. *Géotechnique* 54(4): 45–256. doi: 10.1680/geot.2004.54.4.245.
Lins, Y., and Schanz, T. 2005. Determination of hydro-mechanical properties of sand. Unsaturated Soils: Experimental studies, *Edited by* T. Schanz. Springer, Berlin: 15-32. doi: 10.1007/3-540-26736-0_2.
Lu, N., Godt, J., and Wu, D.T. 2010. A closed-form equation for effective stress in unsaturated soil. Water Resources Research, 46, W05515. doi: 10.1029/2009WR008646.
Lu, N., Kim, T.H., Sture, S., and Likos, W.J. 2009. Tensile strength of unsaturated sand. *J. Eng. Mechanics*, ASCE, doi: 10.1061/_ASCE_EM.1943-7889.0000054.
Lu, N., and Kaya, M. 2014. A drying cake method for measuring suction-stress characterisitics curve, soil-water-retention curve, and hydraulic conductivity function. *Geotech. Test. J.*, ASTM 36(1): 46-56. doi:10.1520/GTJ20120097.
Lu, N., and Kaya, M. 2014. Power law for elastic moduli of unsaturated soil. *J. Geotech. and Geoenviron. Eng.* 140(1): 46-56. doi: 10.1061/(ASCE)GT.1943-5606.0000990.
Marston, A., and Anderson, A.O. 1913. The theory of loads on pipes in ditches and test of cement and clay drain tile and sewer pipe. Bulletin 31, Iowa State College of Agriculture and Mechanic Arts.
McDowell, G.R. and Bolton, M.D. 2000. Effect of particle size distribution on pile tip resistance in calcareous sand in the geotechnical centrifuge. *Granular matter* 2(4): 179-187.
Meyerhof, G.G. 1976. Bearing capacity and settlement of pile foundations. The Eleventh Terzaghi Lecture, *J. of Geotech. Engrg. Div.*, ***ASCE***, 102(GT3): 195-228. Discussions in 103(GT3 and GT4), Closure in 103(GT9).
Meyerhof, G.G. 1995. Development of geotechnical limit state design. *Can. Geotech. J.* 32(1), 128–136. https://doi.org/10.1139/t95-010.
Meyerhof, G.G. 1983. Scale effects of ultimate pile capacity. *J. Geotech. Eng. Div.*, ASCE, 109(6): 797-806.
Miao, L., Liu, S., and Lai, Y. 2002. Research of soil-water characteristics and shear strength features of Nanyang expansive soil. *Engineering Geology* 65(4): 261–267. doi: 10.1016/S0013-7952(01)00136-3.
Mills, R. 2016. Risky routes: Energy transit in the Middle East. Brookings Institution, Washington DC, USA. https://www.brookings.edu/wp-content/uploads/2016/07/en-energy-transit-security-mills-2.pdf.
Mohamed, F.M.O. 2014. Bearing capacity and settlement behaviour of footings subjected to static and seismic loading conditions in unsaturated sandy soils. Ph.D. thesis, University of Ottawa, Ottawa, Canada.
Mohamed, F.M.O. and Vanapalli, S.K. 2006. Laboratory investigations for the measurement of the bearing capacity of an unsaturated coarse-grained soil, Proc. 59th Can. Geotech. Conf., Vancouver, BC, Canada: 219-226.
Mohamed, F.M.O. and Vanapalli, S.K. and Saatcioglu, M. 2013. Generalized Schmertmann's

equation for settlement estimation of shallow footings in saturated and unsaturated sands. *Geomech. and Eng.* 5(4): 343-362. doi: 10.12989/gae.2013.5.4.343

Moser, A. P. 2001. *Buried pipe design*. 2nd ed. McGraw-Hill, USA. doi: 10.1036/0071418016.

Murthy, V.N.S. 2002. *Geotechnical engineering: Principles and practices of soil mechanics and foundation engineering.* Marcel Dekker, Inc. New York.

National Energy Board Pipeline Damage Prevention (NEBPDP). 2016. Guidance notes – National Energy Board Regulations for Pipeline Damage Prevention. National Energy Board Pipeline Damage Prevention Regulations – Authorizations, Report, June 2016. Available from https://www.neb-one.gc.ca/bts/ctrg/gnnb/dmgprvntnrgltn/2016dmgprvntnrgdgn-eng.html. [accessed 18 August 2017].

New York City. 2014. *New York City Building Code*. Available from: https://www1.nyc.gov/site/buildings/codes/2014-construction-codes.page#bldgs. [Accessed July 18, 2018].

Ng, P.C.F. 1994. Behaviour of buried pipelines subjected to external loading. Ph.D. thesis, University of Sheffield, Sheffield, United Kingdom.

Ng, C.W.W., Xu, J., and Yung, S.Y. 2009. Effects of wetting-drying and stress ratio on anisotropic stiffness of an unsaturated soil at very small strains. *Can. Geotech. J.* 46(9): 1062–1076. doi: 10.1139/T09-043.

Ng, C.W.W., and Yung, S.Y. 2008. Determination of anisotropic shear stiffness of an unsaturated decomposed soil. *Géotechnique* 58(1): 23-35. doi: 10.1680/geot.2008.58.1.23.

Obadina, T. 1999. Harnessing abundant gas reserves: Nigeria alone could provide the power needs of all West Africa. Africa Recovery 13(1), pp.16.

Oh, W.T., and Vanapalli, S.K. 2009. A simple method to estimate the bearing capacity of unsaturated fine-grained soils. *Proc*. 62nd Can. Geotech. Conf., Halifax, N.S., 20-24 September 2009.

Oh, W.T., and Vanapalli, S.K. 2011. Modelling the applied vertical stress and settlement relationship of shallow foundations in saturated and unsaturated sands. *Can. Geotech. J.* 48: 425-438.

Oh, W.T., and Vanapalli, S.K. 2013. Interpreting the bearing capacity of unsaturated fine-grained soils using modified effective and total stress approaches. *Int. J. Geomech.* 13(6): 769-778. doi: 10.1061/(ASCE)GM.1943-5622.0000263.

Oh, W.T. and Vanapalli, S.K. 2018. Modeling the stress versus settlement behavior of shallow foundations in unsaturated cohesive soils extending the modified total stress approach. *Soils and Foundations* 58: 382–397. https://doi.org/10.1016/j.sandf.2018.02.008.

Oh, W.T., Vanapalli, S.K., and Puppala A.J. 2009. Semi-empirical model for the prediction of modulus of elasticity for unsaturated soils. *Can. Geotech. J.* 46: 903-914. doi: 10.1139/T09-030.

Oloo, S.Y., Fredlund, D. G., and Gan, J. K. M. 1997. Bearing capacity of unpaved roads. *Can. Geotech. J.* 34: 398-407.

Olson, N.A. 2009. Soil performance for large-scale soil-pipeline tests. Ph.D. thesis, Cornell University, NY, USA.

O'Neill, M.W., Ghazzaly, O.I. and Ha, H.B. 1977. Analysis of three-dimensional pile groups with nonlinear soil response and pile-soil-pile interaction. *Proc*. 9th Annual OTC, Houston Paper OTC 2838: 245-256.

Ontario Provincial Standard Specification (OPSS) 401. 2013. Construction specification for trenching, backfilling, and compacting. Ministry of Transportation, Ontario, Canada.

Ontario Provincial Standard Specification (OPSS) 421. 2013. Construction specification for pipe culvert installation in open cut. Ministry of Transportation, Ontario, Canada.

Organization of the Petroleum Exporting Countries (OPEC). 2015. OPEC Annual statistical bulletin. 50th edition, Vienna, Austria.

O'Reilly, M.P., and New, B.M. 1982. Settlements above tunnels in the United Kingdom - their magnitude and prediction. Tunnelling '82, London Institute of Mining and Metallurgy: 173–181.

O'Rourke, T.D. 2010. Geohazards and large, geographically distributed systems. *Géotechnique* 60(7): 505-543. doi: 10.1680/geot.2010.60.7.505.

O'Rourke, T.D., Jezerski, J.M., Olson, N.A., Bonneau, A.L., Palmer, M.C., Stewart, H.E., O'Rourke, M.J. and Abdoun, T. 2008. Geotechnics of pipeline system response to earthquakes. Proc. Geotech. Earthquake Eng. and Soil Dynamics IV (GEESD), 18-22 May 2008, ASCE, Sacramento, CA, pp. 1-38.

Organization of the Petroleum Exporting Countries (OPEC). 2015. OPEC Annual statistical bulletin. 50th edition, Vienna, Austria.

Perez-Valdivia, C. 2009. Groundwater in the Canadian prairies: Trends and long-term variability. M.Sc. thesis, University of Regina, Regina, Saskatchewan, Canada.

Pipeline Research Council International (PRCI). 2009. Guidelines for constructing natural gas and liquid hydrocarbon pipelines through areas prone to landslide and subsidence hazards. Report prepared for the Design, Material, and Construction committee of Pipeline Research Council International, Inc.

Potts, D.M. and Zdravković, L. 1999. *Finite Element Analysis in Geotechnical Engineering: Theory*. 1st ed., Thomas Telford, London, UK.

Potts, D.M., and Zdravković, L. 2001. *Finite element analysis in geotechnical engineering: Application*. 1st ed., Thomas Telford, London, UK.

Poulos, H.G. 1989. Pile behaviour-theory and application. *Géotechnique* 39(3): 365-415. https://doi.org/10.1680/geot.1989.39.3.365.

Prakash, S. and Sharma, H.D. 1990. *Pile foundation in engineering*. John Wiley & Sons, Inc.

PRCI. 2009. Guidelines for constructing natural gas and liquid hydrocarbon pipelines through areas prone to landslide and subsidence hazards. Report prepared for the Design, Material, and Construction committee of Pipeline Research Council International (PRCI), Inc.

Qi, S. and Vanapalli, S.K. 2015. Hydro-mechanical coupling effect on surficial layer stability of unsaturated expansive soil slopes. *Comp. and Geotech.* 70: 68 – 82. doi:

10.1016/j.compgeo.2015.07.006.
Rajapakse, R. 2008. *Pile design and construction rules of thumb*. Elsevier Inc.
Rahardjo, H., Melinda, F., Leong, E.C., and Rezaur, R.B. 2011. Stiffness of a compacted residual soil. *Engineering Geology*, 120: 60–67. doi:10.1016/j.enggeo.2011.04.006.
Ravichandran, N. Krishnapillai, S.H. and Machmer, B. 2013. A Novel procedure for physical modeling of unsaturated soil-pile system using geotechnical centrifuge. *J. Earth Sci. and Geotech. Eng.* 3(1):119-134.
Revier, R. W. 2015. *Oil and gas pipeline integrity and safety handbook*. John Wiley & Sons Inc., Hoboken, New Jersey, USA.
Rivin, E.I. 2010. *Handbook on Stiffness & Damping in Mechanical Design*. ASME, New York, USA. doi: 10.1115/1.802939.
Robert, D.J., Soga, K., and O`Rourke, T.D. 2016. Pipelines subjected to fault movement in dry and unsaturated soil. *Int. J. Geomech.* doi: 10.1061/(ASCE)GM.1943-5622.0000548.
Rogers, C.D.F. and O'Reilly, M.P. 1991. Ground movements associated with pipe installation and tunnelling. Proc. 10th Europ. Conf. on Soil Mech. Found. Eng., Florence, Italy, 2: 907-10.
Rojas, J.C., Salinas, L.M., and Sejas, C. 2007. Plate-load test on an unsaturated lean clay. Experimental unsaturated soil mechanics, *Edited by* T. Schanz. Springer, Berlin: 445 – 452. doi: 10.1007/3-540-69873-6_44.
Roy, K., Hawlader, B., Kenny, S., and Moore, I. 2015. Effects of post-peak softening behavior of dense sand on lateral and upward displacement of buried pipelines. Proc. ASME 34th Int. Conf. on Ocean, Offshore and Arctic Eng. OMAE2015, St. John's. NL. May 31 - June 5, 2015. OMAE2015-42138.
Roy, K., Hawlader, B., Kenny, S., and Moore, I. 2016. Finite element modeling of lateral pipeline-soil interaction in dense sand. *Can. Geotech. J.* 53: 490-504. doi: 10.1139/cgj-2015-0171.
Rumsey, P.B., Cooper, I., and Kyrou, K. 1982. Ground movement and pipe strain associated with trench excavation. In Restoration of Sewerage System. ICE publications, Thomas Telford, London, UK, pp. 105-115, http://dx.doi.org/10.1680/ross.01459.0014.
Rowe, P.W. 1962. The stress dilatancy relation for static equilibrium of an assembly of particles in contact. Proc. Royal Society of London, Series A, 269, pp. 500–527, doi: 10.1098/rspa.1962.0193.
Rowe, P.W. 1969. The relation between the shear strength of sands in triaxial compression, plane strain and direct shear. *Géotechnique* 19(1): 75–86, doi: 10.1680/geot.1969.19.1.75.
Saadeldin, R., Hu, Y., and Henni, A. 2015. Numerical analysis of buried pipes under field geo-environmental conditions. *Int. J. Geo-Eng.* 6(1). doi: 10.1186/s40703-015-0005-4.
Sadrekarimi, A. and Olson, S.M. 2013. Residual state of sands. *J. Geoenviron. Eng.* 140(4), doi:10.1061/(ASCE)GT.1943-5606.0001054.
Sales, M.M., Prezzi, M., Salgado, R., Choi, Y.S., and Lee, J. 2017. Load-settlement behaviour of model pile groups in sand under vertical load. *J. of Civil Eng. and Management*, 23(8): 1148-1163. https://doi.org/10.3846/13923730.2017.1396559.
Sawangsuriya, A., Edil, T.B. and Bosscher, P.J. 2009. Modulus-suction-moisture relationship for

compacted soils in postcompaction state. *J. Geotech. and Geoenviron. Eng.* 135(10):1390-1403, doi: 10.1061/(ASCE)GT.1943-5606.0000108.

Scarpelli, G., Sakellariadi, E., and Furlani, G. 2003. Evaluation of soil-pipeline longitudinal forces. *Rivista Italiana di Geotecnica* 4(3): 24-41.

Schanz, T., and Alabdullah, J. 2007. Testing unsaturated soil for plane strain conditions: A new double wall biaxial device. Experimental unsaturated soil mechanics, *Edited by* T. Schanz. Springer, Berlin: 169-178. doi: 10.1007/3-540-69873-6_16.

Schanz, T., Vermeer, A., and Bonnier, P. 1999. The hardening soil model: formulation and verification. Beyond 2000 in Computational Geotechnics-10 Years PLAXIS. Amsterdam Netherlands 1820 March 1999, 281.

Schuettpelz, C.C., Fratta, D., and Edil, T.B. 2010. Mechanistic corrections for determining the resilient modulus of base course materials based on elastic wave measurements. *J. Geotech.and Geoenviron. Eng.* 136(8), 1086–1094.

Seed, H.B., and Reese, L.C. 1957. The action of soft clay along friction piles. *Transactions*, ASCE, 122:731-754.

Sheikhtaheri, M. 2014. Experimental and numerical modelling studies for interpreting and estimating the P-δ behavior of single piles in unsaturated sands, M.Sc. thesis, Department of Civil Engineering, University of Ottawa, Ottawa, Canada.

Sherif, M.A., Tsuchiya, C., and Ishibashi, I. 1977. Saturation effects on initial soil liquefaction. *J. Geotech. Eng. Div.* 103(8): 914-917.

Sivakumar, V., Sivakumar, R., Boyd, J., and Mackinnon, P. 2010. Mechanical behaviour of unsaturated kaolin (with isotropic and anisotropic stress history). Part 2: Performance under shear loading. *Géotechnique* 60(8): 595-609. http://dx.doi.org/10.1680/geot.8.P.008.

Skempton, A.W. 1959. Cast-in-situ bored piles in London clay. *Géotechnique* (9): 153-173.

Spangler, M.G. 1941. The structural design of flexible pipe culverts. Iowa Engineering Experiment Station, Bulletin 153. Ames, Iowa.

Stevens, P. 2003. Cross border oil and gas pipelines: Problems and prospects. ESMAP Technical paper 035. Joint UNDP/World Bank, ESMAP, Washington DC, U.S.

Suleiman, M.T. 2002. The structural performance of flexible pipes. Ph.D. thesis, Iowa State University, Iowa, USA.

Sun, R. 2010. Bearing capacity and settlement behavior of unsaturated soil from model footing tests, M.Sc. thesis, Department of Civil Engineering, University of Ottawa, Ottawa, Canada.

Sun, S. and Xu, H. 2007. Determining the shear strength of unsaturated silt. Experimental unsaturated soil mechanics, *Edited by* T. Schanz. Springer, Berlin: 195-206. doi: 10.1007/3-540-69873-6_19.

Symons, I.F., Chard, B., and Carder, D.R. 1982. Ground movements caused by deep trench construction. In Restoration of Sewerage System. ICE publications, Thomas Telford, London, UK, pp. 87–104. http://dx.doi.org/10.1680/ross.01459.0013.

Terzaghi, K. 1925. Erdbaumechanik auf bodenphysikalisher grundlage. Deuticke, Vienna.

Terzaghi, K. 1936. Relation between soil mechanics and foundation engineering: Presidential

address. Proceedings, First Int. Conf. on Soil Mech. Found. Eng, Boston, 3: 13–18.
Terzaghi, K. 1943. *Theoretical soil mechanics.* Wiley, New York.
Taylan, Z.N. 2013. Experimental and numerical modeling studies for interpreting and estimating the δ behavior of single piles in unsaturated soils. Ph.D. Thesis, Graduate School of Science Engineering and Technology, Istanbul Technical University, Istanbul, Turkey.
Taylor, R.N., Rose, A.V. and Gorasia, R.J. 2013. Pile and pile group capacity: Some findings from centrifuge tests. *Int. J. of Geo-Engineering*, 5(2): 5-15.
Toll, D.G. 1990. A framework for unsaturated soil behavior. *Géotechnique* 40(1): 31–44. http://dx.doi.org/10.1680/geot.1990.40.1.31.
Tsukamoto, Y., Kawabe, S., Matsumoto, J., and Hagiwara, S. 2014. Cyclic resistance of two unsaturated silty sands against soil liquefaction. *Soils and Foundations* 54(6): 1094–1103. http://dx.doi.org/10.1016/j.sandf.2014.11.005.
Uzuoka, R., Sento, N., Kazama, M., and Unno, T. 2005, Landslides during the earthquakes on May 26 and July 26, 2003 in Miyagi, Japan. *Soils and Foundations* 45(4): 149–163.
Vanapalli, S. K. 2009. Shear strength of unsaturated soils and its applications in geotechnical engineering practice. Proc. 4th Asia-Pacific Conf. on Unsaturated Soils, Newcastle, New South Wales, Australia: 579-598.
Vanapalli, S.K., Eigenbrod, K.D., Taylan, Z.N., Catana, C., Oh, W.T. and Garven, E. 2010. A technique for estimating the shaft resistance of test piles in unsaturated soils. Fifth Int. Conf. Unsaturated Soils, UNSAT 2010, September 6-8, Vol. 2:1209-1216, Barcelona, Spain.
Vanapalli, S.K., Fredlund, D.G., and Pufahl, D.E. 1997. Comparison of saturated-unsaturated shear strength and hydraulic conductivity behavior of a compacted sandy-clay till. *In* Proc. 50th Can. Geotech. Conf., Ottawa, ON, 20-22 October 1997.
Vanapalli, S.K., Fredlund, D.G., and Pufahl, D.E. 1996b. The relationship between the soil-water characteristic curve and the unsaturated shear strength of compacted glacial till. *Geotech. Test. J.*, ASTM 19(2): 259-268.
Vanapalli, S.K., Fredlund, D.G., and Pufahl, D.E. 1999. The Influence of Soil Structure and Stress History on the Soil-Water Characteristics of a Compacted Till. *Géotechnique* 49(2):143–159, http://dx.doi.org/10.1680/geot.1999.49.2.143.
Vanapalli, S.K., Fredlund, D.G., Pufahl, D.E. and Clifton, A.W. 1996a. Model for the prediction of shear strength with respect to soil suction. *Can. Geotech. J.* 33: 379-392, doi: 10.1139/t96-060.
Vanapalli, S.K., and Mohamed, F.M.O. 2007. Bearing capacity of model footings in unsaturated soils. Experimental unsaturated soil mechanics, *Edited by* T. Schanz. Springer, Berlin: 483–493. doi: 10.1007/3-540-69873-6_48.
Vanapalli, S.K., Nicotera, M.V., and Sharma, R.S. 2008. Axis translation and negative water column for suction control. *Geotech. and Geolog. Eng.* 26: 645–660, doi: 10.1007/s10706-008-9206-3.
Vanapalli, S.K., and Oh, W.T. 2010. A model for predicting the modulus of elasticity of unsaturated soils using the soil-water characteristic curve. *Int. J. Geotech. Eng.* 4(4): 425–

433. doi:10.3328/IJGE.2010.04.04.425-433.
Vanapalli, S.K., and Oh, W.T. 2013. Interpretation of the bearing capacity of unsaturated fine-grained soil using the modified effective and modified total stress approaches. *Int. J. Geomech.*, ASCE, 13(6):769-778. doi: 10.1061/(ASCE)GM.1943-5622.0000263.
Vanapalli, S.K., Oh, W.T., and Puppala, A.J. 2007. Determination of the bearing capacity of unsaturated soils under undrained loading condition. Proc. 60th Can. Geotech. Conf., October 21-24: 1002-1009, Ottawa, Canada.
Vanapalli, S.K., Sillers, W.S., and Fredlund, M.D. 1998. The meaning and relevance of residual state to unsaturated soils. Proc. 51st. Can. Geotech. Conf., Edmonton, AB. October 4-7, 1998.
Vanapalli, S.K., and Taylan, Z.N. 2011. Estimation of the shaft capacity of model piles in a compacted fine-grained unsaturated soil. Proc. 14th Pan-Am Conf. on Soil Mech. Geotech. Eng., Toronto, Canada.
Vanapalli, S.K., and Taylan, Z.N. 2012. Design of single piles using the mechanics of unsaturated soils. *Int. J. GEOMATE* 2(1): 197–204.
van Genuchten, M.T. 1980. A closed-form equation for predicting the hydraulic conductivity of unsaturated soils. *Soil Science Society of America Journal* 44(5): 892-898.
Vesić, A.S. 1963. Bearing capacity of deep foundations in sand. *National Academy of Sciences,* National *Research Council, Highway Research Record*, 39:112-153.
Vesić, A. S. 1969. Experiments with Instrumented Pile Groups in Sand. *Performance of Deep Foundations,* Lundgren, R. and D'Appolonia, E., Ed., ASTM International, West Conshohocken, PA, STP 444: 177-222. https://doi.org/10.1520/STP47286S.
Vesić, A.S. 1977. *Design of Pile Foundations*. Transportation Research Board, National Research Council, Washington D.C. USA.
Vo, T., and Russell, A.R. 2016. Bearing capacity of strip footings on unsaturated soils by the slip line theory. *Comp. and Geotech.* 74: 122-131. doi: 10.1016/j.compgeo.2015.12.016.
Watkins, R.K., and Anderson, L.R. 2000. *Structural mechanics of buried pipes*. CRC Press, New York.
Wehnert, M. and Vermeer, P.A. 2004. Numerical analyses of load tests on bored piles. Proc. 9th Symp. on Numerical Models in Geomech. – NUMOG IX, Ottawa, Canada: 505-511.
Wu, S., Gray, D.H. and Richart, F.E. 1984. Capillary effect on dynamic modulus of sand and silts. *J. Geotech. Eng.* 110(9):1188-1203.
Wuttke, F., Kafle, B., Lins, Y., and Schanz, T. 2013. Macroelement for statically loaded shallow strip foundation resting on unsaturated soil. *Int. J. Geomech.* ASCE, 13: 557–564, doi: 10.1061/(ASCE)GM.1943-5622.0000254.
Wijewickreme, D., Karimian, H., and Honegger, D. 2009. Response of buried steel pipelines subjected to relative axial soil movement. *Can. Geotech. J.* 46: 735–752. doi: 10.1139/T09-019.
Wong, T.T., Fredlund, D.G., and Krahn, J. 1998. A numerical study of coupled consolidation in unsaturated soils. *Can. Geotech. J.* 35: 926 – 937. doi: 10.1139/t98-065.
Yasufuku, N. and Hyde A.F.L. 1995. Pile End-Bearing Capacity in Crushable Sands,

Géotechnique 54(4): 663-676.

Yimsiri, S., Soga, K., Yoshizaki, K., Dasari, G.R., and O'Rourke, T.D. 2004. Lateral and upward soil-pipeline interactions in sand for deep embedment conditions. *J. Geotech. and Geoenviron. Eng.*, ASCE 130(8): 830–846. doi: 10.1061/(ASCE)1090-0241(2004)130:8(830).

Yoshimi, Y., Tanaka, K., and Tokimatsu, K. 1989. Liquefaction resistance of a partially saturated sand. *Soils and Foundations* 29(3): 157–162.

Zhang, C., Nguyen, G.D. and Eivav, I. 2012. The End-Bearing Capacity of Piles Penetrating into Crushable Soils, *Géotechnique* 63(5): 341-354.

Zhao, Q., Kuraoka, S., Baker, T.H.W., Masson, P., Gu, J-F., Boudreau, S., and Brousseau, R. 1998. Durability and performance of gravity pipes: A state-of-the-art literature review. National Research Council of Canada (NRC), Ottawa, Canada.

Zhang, B., Muraleetharan, K.K., and Liu, C. 2016. Liquefaction of unsaturated sands. *Int. J. Geomech.* ASCE. doi: 10.1061/(ASCE)GM.1943-5622.0000605.